DNA ADSORPTION ON SILICA, ALUMINA AND HYDROXYAPATITE AND IMAGING OF DNA BY ATOMIC FORCE MICROSCOPY

A Thesis Submitted to
the Graduate School of Engineering and Sciences of
Izmir Institute of Technology
in Partial Fulfillment of the Requirements for the Degree of

DOCTOR OF PHILOSOPHY

in Chemical Engineering

by
SENEM YETGİN
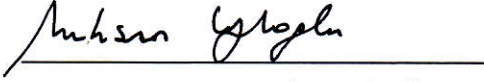
January, 2013
IZMIR

We approve the thesis of **Senem YETGİN**

Examining Committee Members:

_____
Prof. Dr. Devrim BALKÖSE
Department of Chemical Engineering, Izmir Institute of Technology
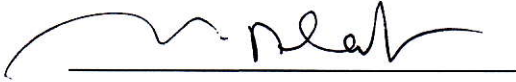
_____
Prof. Dr. Muhsin ÇİFTÇİOĞLU
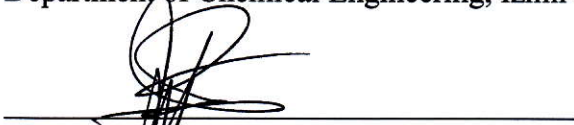Department of Chemistry Department, Izmir Institute of Technology

_____
Prof. Dr. Mehmet Şengün ÖZSÖZ
Department of Biomedical Engineering, Katip Çelebi University

_____
Prof. Dr. Mehmet POLAT
Department of Chemical Engineering, Izmir Institute of Technology

_____
Assoc. Prof. Dr. Mustafa Muammer DEMİR
Department of Chemistry Department, Izmir Institute of Technology

9 January 2013

_____
Prof. Dr. Devrim BALKÖSE
Supervisor, Department of Chemical Engineering, Izmir Institute of Technology

_____
Prof. Dr. Fehime ÖZKAN
Head of the Department of
Chemical Engineering

_____
Prof. Dr. Tuğrul ŞENGER
Dean of the Graduate School of
Engineering and Sciences

ACKNOWLEDGEMENT

ABSTRACT

DNA ADSORPTION ON SILICA, ALUMINA AND HYDROXYAPATITE AND IMAGING OF DNA BY ATOMIC FORCE MICROSCOPY

The scope of the study is to investigate calf thymus DNA adsorption process on solid powders such as silica, alumina and hydroxyapatite (HAP) to improve DNA solid phase extraction efficiency and to visiulize DNA adsorption by atomic force microscopy (AFM). The equilibrium and kinetics of the DNA adsorption were investigated in batch adsorption on a commercial silica gel and a synthesized silica aerogel, commercial alumina and HAP powders from aqueous DNA solution. Commercial DNA extraction kit adsorbents were also characterized and used for adsorption. Adsorbed DNA was imaged in ambient air on flat surfaces of mica, silica and alumina wafers and HAP particles coated glass surfaces and a HAP pellet surface by AFM. Effects of ambient air, nitrogen flow and freeze drying methods on DNA morphology on the releted surfaces were also investigated.

Adsorption of DNA on silica, alumina and HAP increased with the decrease of pH from 9.0 to 2.0. Enhancements of the adsorption capacities of adsorbents were obtained with the addition of $MgCl_2$. It was found that the Van der Waals and the hydrogen bonds rather than the surface charge were the cause of the adsorption. The adsorption isotherms of DNA on silica, alumina and HAP were fitted to Langmuir model in pH range 2-9. The adsorption kinetics obeyed pseudo second order model.

The sharpest image of DNA by AFM was obtained by freeze drying method on alumina surface. Dispersed DNA in water was adsorbed on the surfaces not as single molecules but as supercoils consisting of many molecules.

ÖZET

SİLİKA, ALÜMİNA VE HİDROKSİAPATİTE DNA ADSORPSİYONU VE DNA'NIN ATOMİK KUVVET MİKROSKOPU İLE GÖRÜNTÜLENMESİ

Bu tez DNA katı yüzey ile saflaştırma verimini arttırmak için DNA nın silica, alumina ve hidroksi apatit (HAP) tozlarına adsorpsiyon sürecinin araştırılması ve DNA adsorpsiyonunun atomic kuvvet mikroskopu (AFM) ile görsel olarak incelenmesini kapsar. DNA nın sulu çözeltilerden ticari silikajel, alumina ve HAP tozlarına adsorpsiyon dengesi ve kinetiği araştırılmıştır. Sentezlenmiş bir silica aerojel ve iki adet ticari DNA saflaştırma kiti adsorbenti de karakterize edilmiş ve adsorpsiyonda kullanılmıştır. Mika, silika ve alumina plaka düz yüzeyleri, HAP ile kaplanmış cam ve HAP pellet yüzeyleri üzerine adsorplanmış DNA nın AFM ile görüntüsü alınmıştır. Ortam havasında, azot akımı altında ve dondurarak kurutma tekniklerinin ilgili yüzeylerdeki DNA morfolojisine etkisi araştırılmıştır.

Silika, alumina ve HAP üzerine DNA adsorpsiyonu pH'ın 9.0'dan 2.0'a düşmesiyle artmıştır.Adsorbentlere adsorpsiyon kapasitesi $MgCl_2$ katılması ile arttırılmıştır. Yüzey yükünden çok Van der Walls ve hidrojen bağlarının adsopsiyona neden olduğu bulunmuştur. Silika, alümina ve hidroksiapatit için adsorpsiyon izotermleri Langmuir modeline daha iyi uyum sağlamıştır. Adsorpsiyon kinetiği yalancı ikinci derece kinetiğine daha fazla uymaktadır.

AFM ile en iyi görüntü dondurularak alumina yüzeyde kurutulmuş DNA için elde edilmiştir. Su içinde çözünen DNA nın yüzeylerde tekli moleküller olarak değil birçok molekülden oluşan superkoiller halinde adsorplandığı bulunmuştur.

dedicated to my father
Safder YETGİN

my mother,
Zehra Sevcan YETGİN

my brother,
Serdar YETGİN

TABLE OF CONTENTS

LIST OF TABLES

LIST OF FIGURES

CHAPTER 1

INTRODUCTION

After the discovery of the deoxyribonucleic acid (DNA) double helix by Watson and Crick, our knowledge about the structure of DNA increased. DNA is generally placed inside the cell and the molecule is in a tightly packaged form called as chromosome. Scientists are using the special properties of DNA structure, including its ability to store information in the double helix, for new applications in science and biomedical research. These studies required pure DNA for downstream processes. Otherwise additional chemicals coming from cell have negative effect on scientific research. For example undesired substances in cell lysates can reduce PCR efficiency. Therefore investigation of the DNA purification techniques and their improvement is very important. Finding more effective adsorbents or development of higher surface area material are the main solutions of solid phase DNA extraction method. Additionally DNA has been considered as a highly specific functional material for electrically conductive material and for network fabrication. Therefore DNA is an important and promising molecule, not only due to its genetic function, but also a molecular scaffold usage for nanotechnology and nanostructure. DNA interaction with surfaces and imaging DNA on the surfaces are also important. Atomic Force Microscopy (AFM) is the promising analysis method for this purpose

An appropriate technique does change based on the application, sample size, source and followed application. In spite of the numerous purification method there is no certain purification method for all DNA species; genomic from eukariotic and prokaryotic cells, plasmid or mitochondrial DNA.

There are three main purification methods: organic, inorganic and solid phase extraction. All extraction or purification DNA methods are generally time-consuming. Organic and inorganic purification methods require the use of toxic and hazardous reagents. When organic and inorganic purification methods were compared with solid phase extraction (SPE), solid extraction techniques become favorable. SPE can be performed by commercial kits. They should serve quick and reliable procedure. Additionally used solids in these kits should also be effective. Solid material adsorption

capacity must be high and selectively adsorb DNA in lysed solution. The efficiency of the method is described by the yield and purity of the DNA, not just the accessibility. Adsorption depends on adsorptive species, solid surface, concentration and solid material. Attention on solid phase material has been increasing day by day.

Silica is the mainly used material in solid phase extraction method. Glass which is a form of silica, was proposed first in 1979 for purifying DNA from agarose gels (Vogelstein and Gillespie 1979).

Nowadays DNA can be considered as a naturally occurring and highly specific useful biopolymer. Therefore DNA film and networks have possibility of serving as biomaterials for medical, engineering, environmental applications (Kanno et al., 2000) and recently nanowire or nanodevice applications (Tseng et al., 2011)

Knowing the structure of DNA gave scientists opportunity of approaching into how genetics works and made the improvement in molecular biology and DNA technology possible. Moreover, the structure of DNA had a huge advantage on our understanding of gene function and DNA replication in cells. For this purpose DNA should be highly purified. DNA purification techniques previously focused on soil samples to figure out DNA extraction from soils, chemical evolution of life and influence of genetically modified organism. Then isolation or purification of DNA from biological samples, natural habitat or from reaction mixtures is of extreme importance when considering the success of the following process of molecular applications such as polymerase chain reaction (PCR), DNA cloning, DNA sequencing and DNA hybridization (Yu et al. 2008).

To solve the DNA purification problem less chemical should be used. Increased purification productivity means spending less time for purifying DNA and more time developing experiments and analyzing data. Mainly modern DNA purification process is based on adsorption of DNA onto a solid surface. Therefore higher adsorption capacity is desired for purification. Furthermore adsorption on solid surface increases the DNA's resistance of hybridization enzyme degradation.

DNA interactions with surfaces can be repulsive, or attractive (Douarche et. al., 2008). Attractive interactions lead to adsorption. DNA adsorption onto solid surface is forced by hydrogen bonding or through electrostatic interactions because of the negatively charged structure of DNA.

The aim of the present study is to investigate the interaction of DNA with different materials and kinetics of DNA adsorption on different solid surfaces. The

scope of the study is to analyze DNA adsorption onto silica, alumina and biocompatible nano sized hydroxyapatite surfaces and to figure out the surface interaction by atomic force microscopy. The increase in DNA adsorption capacity on the selected solid surfaces is another subject of the thesis.

In Chapter 2, DNA, DNA isolation methods in biology and DNA metal interactions are introduced. DNA analysis methods are also defined. Besides them, recent studies related to the DNA adsorption and control mechanism are reviewed. In Chapter 3, selected adsorbents are summarized, the synthesis of silica aerogel (by supercritical ethanol drying of silica alcogel) sol gel method is explained. Chapter 4 includes the equilibrium and kinetics adsorption of DNA. Imaging details of DNA by atomic force microscope (AFM) are explained in Chapter 5. Chapter 6 introduces silica, alumina and hydroxyapatite adsorbents used in the adsorption of DNA. Methods of studying thermodynamic and kinetics of DNA adsorption and experimental procedure of synthesis and the preparation of a silica aerogel are reported. This chapter also explains the characterization techniques for all adsorbents, as well. Results and discussion of this study is in Chapter 7. The conclusions are presented in Chapter 8.

CHAPTER 2

DNA

2.1. Deoxyribonucleic Acid (DNA)

DNA is a biopolymer generally occurring in the central region of the living cell (termed as nucleus) which contains genetic information of living organism -chemical structure that forms chromosomes. A cell has thousands of genes, so DNA molecules are usually very big. The structure of DNA was first determined by James Dewey Watson and Francis Harry Compton Crick who are the two molecular biologists by using unpublished data from Maurice Wilkins and Rosalind Franklin. In the words of Watson and Crick: "It has not escaped our notice that the specific pairing that we have postulated immediately suggests a possible copying mechanism for the genetic material" (Watson and Crick 1953). After that they and their friend Maurice Wilkins were awarded the 1962 Nobel Prize for Physiology or Medicine, for their discoveries concerning the molecular structure of nucleic acids and its significance for information transfer in living material.

Before DNA structure was defined constructional units of DNA had already been defined by Phoebus A. T. Levene (Fitzgerald-Hayes and Reichsman 2010). He found that DNA is constructed from nucleotide units which are a five-carbon sugar, which could be either ribose (in RNA) or deoxyribose (in DNA); phosphate, a chemical group derived from phosphoric acid molecules; and four different compounds containing nitrogen that only specific pairs of bases can bond together. These pairs are: adenine (purine) with thymine (pyrimidine), and guanine (purine) with cytosine (pyrimidine). Also these four different nitrogen containing bases: are described as capital letters such as; adenine (A), guanine (G), cytosine (C), and thymine (T). As a conclusion genetic material of all life is made of only six components in DNA shown in Figure 2. 1 This essential building block of DNA molecule is called as "*nucleotide*" as seen in Figure 2. 2.

The nature of the hydrogen bond imposes a limitation on the types of bases that can pair. Adenine normally pairs only with thymine through two hydrogen bonds, and

cytosine normally pairs only with guanine through three hydrogen bonds. Because three hydrogen bonds form between C and G and only two hydrogen bonds form between A and T, G-C pair is stronger than A-T pairing. The specificity of the base pairing means that there is an A on one strand there must be a T in the corresponding strand as corresponding position. Where there is a G on one strand, C must be on the other. As a result the two polynucleotite strands of the DNA molecule are not identical, but complementary.

Chemical complementarily plays a key role in designing new structures and materials. For example, the bases of adenine can form pairs with thymine, but not guanine and cytosine in a DNA double helix. DNA is like a twisted ladder or structure of DNA and is illustrated by a double helix. The double helical structure of DNA (dsDNA) consists of two strands where the sugar and phosphate are the rails, and the base pairs are the rungs. The rails run in opposite orientation to each other
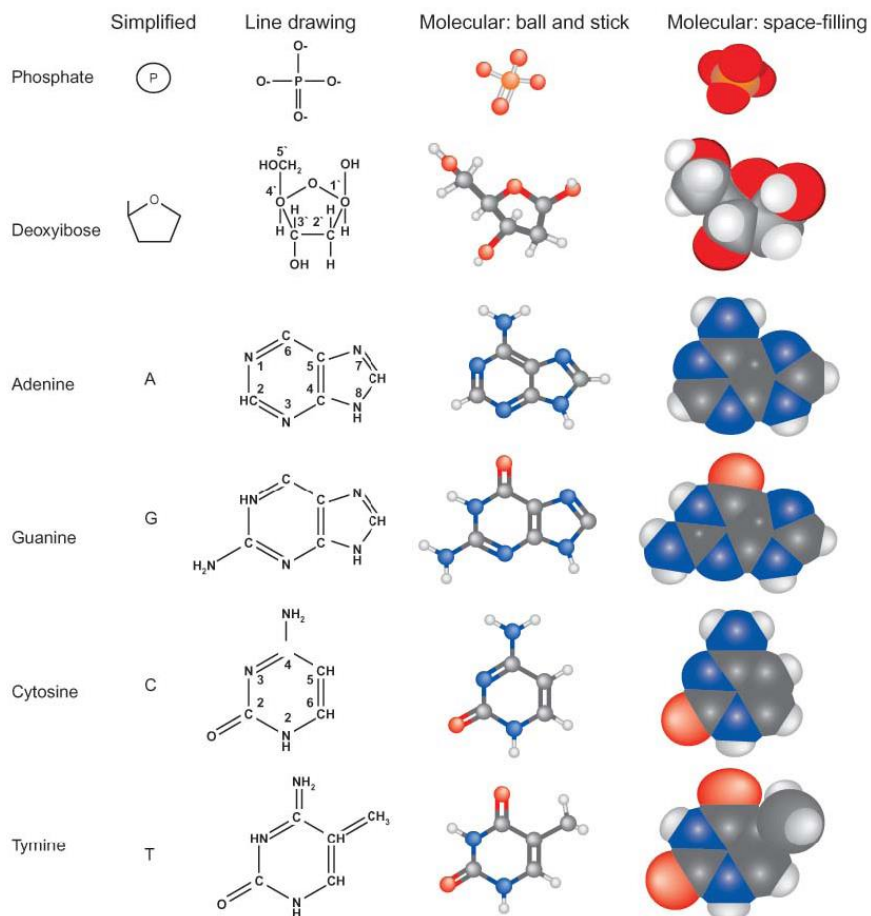
Figure 2. 1 Fundamental components of nucleic acids.
(Source:Fitzgerald-Hayes and Reichsman 2010)
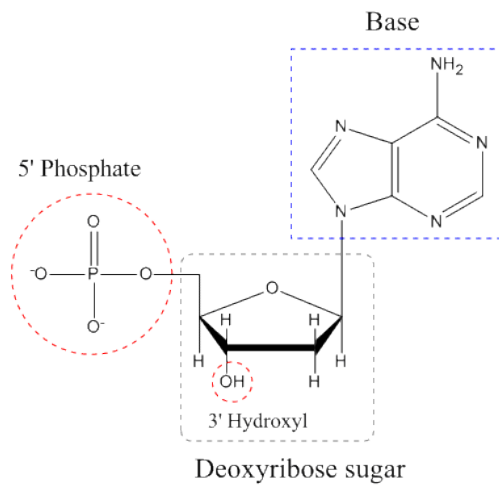
Figure 2. 2. Basic representation of a nucleotide
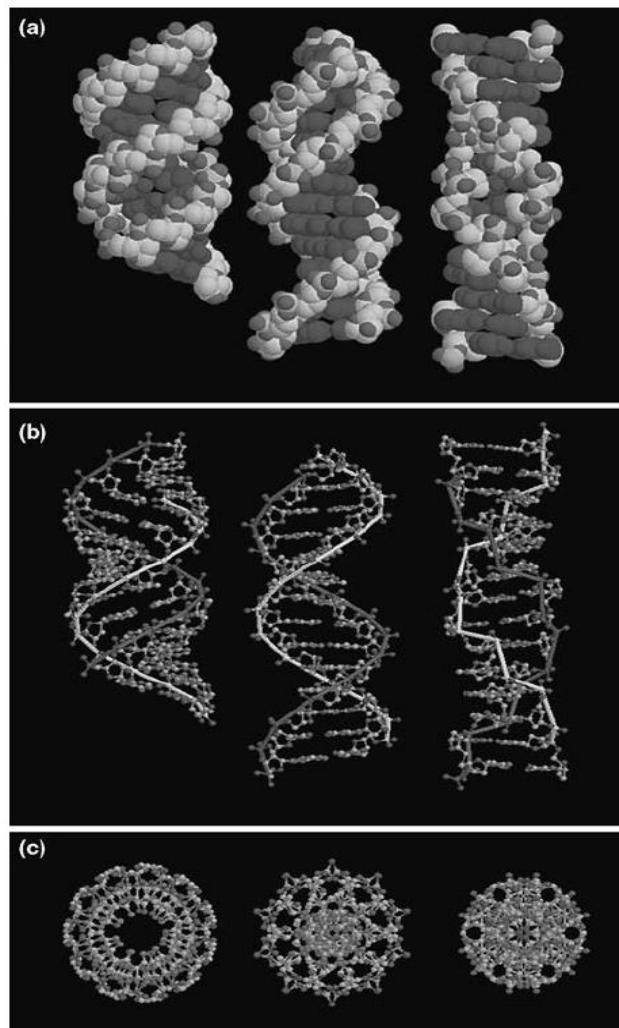
Figure 2.3.   Secondary structures of (from left to right) A-form, B-form, and Z-form of DNA. (left to right)Space-filling model (a) and "ball-and-stick" representation with the phosphate backbones highlighted in a side (b) and top (c) view (Biochem 2010)

On the outside of the helix structure, there is a space between the turns of the phosphate groups; these are termed grooves. There are three types of DNA double helices, i.e., A-type, B-type, and Z-type. These three DNA conformations are shown in Figure 2. 3 and their some properties listed in Table 2. 1 Figure 2. 2. Basic representation of a nucleotideThe Watson-Crick structure is also referred to as B form DNA, or B-DNA. Kistner et al., (2008) reported that DNA is in mainly in the B form in aqueous solution. The right-handed B-type helix is the typical structure and is the most stable structure under physiological conditions. DNA molecules in the B-form (native form) are helical with a diameter of about 2.0 nm. The B-type double helix is relatively sequence independent. DNA assumes the A-form upon dehydration. When electronic repulsions between the phosphate groups are reduced DNA is complexed with oppositely charged species. The Z-form differs from the other two forms by presenting a left-handed helical sense. This form has one more base pairs per turn and a rise of 0.38 nm per base pair. In physiological conditions Z-DNA is less stable than the B-DNA due to the electrostatic repulsions between the phosphate groups that are closer together in the Z-form (Dias and Lindman, 2008)

Because of the asymmetry in the base pairs, the grooves have unequal width. For the B-form, the narrower is called minor groove and the wider is termed the major groove. The latter is easily accessible to proteins.

Table 2. 1. Structural Characteristics of the A, B, and Z Forms of DNA
(Source: Nelson and Lenginher 2005)

	A-Form	B-Form	Z-Form
Helical sense	Right-Handed	Right-Handed	Left-Handed
Diameter	~2.6 nm	~2.0 nm	~1.8 nm
bp per helical turn	11.6	10.5	11.6
Helix rise per bp	0.26 nm	0.34 nm	0.37 nm
Charge density e-/ nm	0.077	0.059	0.054

DNA is negatively charged because of the phosphate diesters on the backbone of DNA. This sugar-phosphate backbone is strong acids, building duplex DNA a strong polyelectrolyte carrying negative charges per base pair at nearly all solution pH (Melzak et al 1996).

When the phosphate group of DNA is dissolved in water, it releases a proton and the remaining group becomes negatively charged. For DNA at normal conditions (pH=7 and NaCl concentration of 0.15 M) thermal denaturation occurs between temperatures 67 °C and 110 °C (which are the temperatures for A-T and C-G unbinding, respectively) (Grosberg and Khokhlov 1994). On the other hand, denaturation or melting temperature (Tm) is related to double-stranded (dsDNA) decomposition to single-stranded DNA (ssDNA).

With the combination with enzymes and proteins DNA has gained some properties, such as self–assembly, self-multiplication, self-repair, self-degradation, redundancy, self-diagnosis, learning and prediction/notification (Marx et al 1994). Also interaction between other molecules is a fundamental issue in life sciences, which is related to mutation of genes, action mechanism of DNA-targeted drugs, and biosensors. DNA chips and DNA microarrays are used in molecular biology, pharmaceutical industry and clinical research to identify presence of specific biological targets (Stoliar et al., 2009). A common principle of a biosensor/biochip is that ''detector molecules'' are attached/immobilized on a solid surface in such a way that a specific signal is obtained from the sensor when the detector molecules selectively bind to the biomolecules they are designed to detect. Conductivity of DNA has a different story. For a long time DNA has been thought to be an insulator (Pablo et al., 2000), and only recently have some experiments suggested that this might not be true. DNA was reported to be a very good conductor (Tran et al., 2000) and most surprisingly there exists only one report of superconducting behavior for a 16 μm long λ-DNA by Kasumov et al (2001).

For example electrochemical DNA sensors are based on the immobilization of a single-chain DNA strand onto an electrode and the measurement of changes in electrical parameters which is caused by the hybridization of DNA. These types of bio-recognition can be performed when the pre-coated sensor is exposed to blood or urine samples or their extracts. Therefore DNA is the first and the most important requirement in carrying out a genetic analysis, such as mutation or disease detection. For instance acquired immunodeficiency syndrome (AIDS) can be easily defined through human

immunodeficiency virus (HIV) detection by selective DNA adsorption on glass bead on urine samples from patients without protein and other substances influence (Buffone et al.,1991).

DNA-targeted drugs and gene therapy in other words drug delivery are the current study of the pharmaceutical industry. The medical professions increasingly desire the ability to deliver drugs to a specific organ or area of the body; the "magic bullet" approach. This can be useful to reduce the size of dose needed to control and to reduce the damage caused by drug toxicity to health.

To understand the adsorption mechanism of DNA first its structure, physical and chemical properties should be defined. The main role of DNA molecules is the long-term storage of information

2.2. Calf Thymus DNA

Calf thymus DNA has been known as highly polymerized "polydisperse", "fibrous preparation", "containing low amount of RNA and proteins (Porsch et al., 2009). Its molecular weight (M_w) was mentioned as 8.3×10^6 (Tanigawa et al., 1996) and 6×10^6 g / mol as determined by multiangle laser light scattering (Sundaresan et al., 2008).

It is usual in the case of large DNA molecules; the DNA can be often cut into smaller fragments using a DNA restriction endonuclease (or restriction enzyme). It is suggested that high molecular weight DNA sample like calf thymus can be divided short length of fragments with ultrasonic treatment procedure without any change of their double-helical conformation. Ultrasonication is able to degrade DNA in aqueous solution preparing DNA fragments in vitro. This solution may be needed in preparation of higher concentrations of DNA faced difficulty in dissolution and reach desired homogeneity.

<center>(a)   (b)</center>
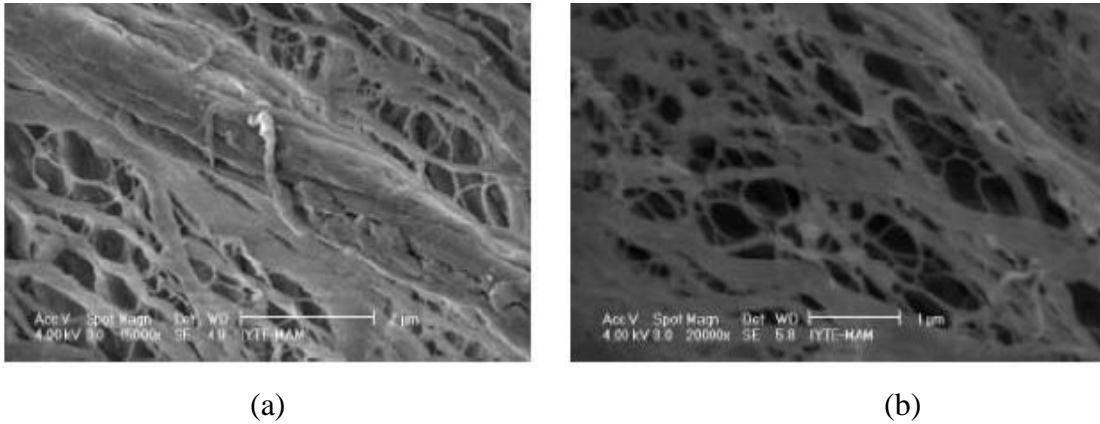
<center>Figure 2. 4 SEM micrographs of DNA at a) *N*=15000×, b) *N*=20000×</center>

Scanning electron microscopy (SEM) images of calf thymus DNA are illustrated in Figure 2. 4 (Balkose et al., 2008). According to this illustration calf thymus DNA has 0.1–0.5 μm diameter fibers and highly polymerized.

Digestion of DNA with Restriction Enzymes

Digestion of DNA with restriction endonucleases is the first step in many gene manipulation projects. A restriction enzyme (or restriction endonuclease) is an enzyme that cuts DNA at specific nucleotide sequences they call also "molecular scissors" (Goodsell 2002). Restriction enzymes distinguish a specific sequence of nucleotides and produce a double-stranded cut in the DNA. Their main role is to protect themselves from attack by viruses -foreign DNA's- especially bacteriophage DNA. It is known that each restriction enzyme identifies specific 4-base (tetramer), 5-base (pentamer), or 6-base (hexamer) sites located on the received DNA, and make double-stranded cuts. During restriction, the endonuclease must cut each of the strands to generate a double-strand cut. Actually cutting process is the result of hydrolysis, a reaction in which water is added across a bond, thereby breaking DNA.

Each enzyme is named after the bacterium from which was isolated using a naming system based on bacterial genus, species and strain. For instance EcoRI; "E" Escherichia (genus), "co" coli (species), "R" RY13 (strain), "I" First (identified order of identification in the bacterium)(Biochem 2010)

Sonication of Genomic DNA

Some references has suggest that high molecular weight DNA sample like calf thymus can be divided little more fragments with ultrasonic treatment procedure without their double-helical conformation being changed. Ultrasonication is able to degrade DNA in aqueous solution preparing DNA fragments in vitro. This solution might be needed in case of preparation of higher concentrations of DNA faced difficulty in dissolution and reaching the desired homogeneity.

Ultrasonic degradation of DNA in solution is performed by breaking hydrogen bonds and by single-strand and double-strand break of the DNA helix. Two mechanisms are mainly reasons of breaking: cavitation and a thermal or mechanical effect. This method is an alternative of degrading the DNA helix instead of highly specific fragmentation which can be obtained by restriction endonucleases. In other words end of the ultrasonication process DNA fragments does not known without extra agarose jel modification.

2.3. DNA Isolation Methods

Nucleic acid extraction was first adapted by Friedrich Miescher in 1869 (Tan and Yiap 2009). He got sufficient result with leucocytes, which obtained from the collected surgical bandages, after lymph nodes cell collection try. He first figured out DNA precipitation under acidic condition while dissolved after base addition. As a result DNA was obtained from cell.

DNA isolation and purification methods technology has enhanced day by day. For instance DNA has become even more important with the new technology of cloning, criminal science, mutation of genes, action mechanism of DNA-targeted drugs and biosensor. Therefore isolation of a sufficient amount of high quality DNA must be available for these kinds of applications. The selection of an appropriate DNA extraction method plays a critical role in this regard. First of all sample type and sizes are important and define selection of extraction protocol. DNA can be extracted from whole blood, serum, saliva, urine, stool, cerebral spinal fluid, tissues, and cells (Price et al., 2009). Success of DNA extraction results depend strongly on the selected protocols

and the amount of the sample. For example Hui and coworkers exposed that 1 ng DNA can be obtained per microliter of blood (Huie et al., 2007).

DNA purification is the extraction of DNA from inside of the cell -what ever it is- and purification from this media. The separation of DNA from cellular components can be divided into four stages; disruption, lysis, removal of proteins and contaminants and purification of DNA. It is also not possible to control what passes through the cell membrane. After disruption and lysis of cells all components (protein, DNA, lipid) are mixed together; protein, DNA, lipid and others. Removal of proteins is typically achieved by digestion with proteinase K. It is active against a broad spectrum of native proteins, before extracting with solvents, followed by DNA purification methods. DNA extraction procedure has some essential factors. Success of DNA purification depends on maximize DNA recovery, remove inhibitors, remove or inhibit nucleases, maximize the quality of DNA.

There are three main methods to use in DNA extraction organic, inorganic and solid phase extraction. They have been used in DNA purification. For example phenol and chloroform is classified in organic extraction method. Using material such as detergents, ethylenediamine tetraacetic acid (EDTA), acetic acid or salt define inorganic extraction method. Immobilization onto solid particle, beads or column is named solid phase extraction method. The advantages and disadvantages of these methods have been summarized in Table 2. 2. Comparison consistency, cost, specific DNA target and low protein binding are positive sides of a technique while time, many handling steps, expensive equipment are the negative sides.

Table 2. 2. Comparison of advantages and disadvantageous of nucleic acid extraction techniques (Source: Pierre et al., 2009)

Technique	Advantages	Disadvantages
CsCl	Isolate specific form of DNaA and RNA from cells	Time intensive, many handling steps, bulky, expensive equipment required
Phenol-chloroform	Reliable for most people comfortable technique	Toxicity, many handling steps
Chaotropic binding(silica)	Consistent, well characterized	PCR inhibiting reagents required
Commercial system	Low cost, reliable, consistent	Large elution volume is incompatible with microfluidic devices
Electrostatic binding (chitosan,aluminum oxide,aminosilane)	PCR compatible, no organics, chitosan has low protein binding	High protein binding (some), some elution buffers incompatible with PCR, must be low salt samples
Affinity gel	Target to specific sequence, possible to perform PCR in gel	Only isolates specific targets; must know target sequence

Salting out (Miller et al., 1988, Platero et al., 2007), solvent extraction by phenol-chloroform extraction (Psidifi et al 2010,Platero et al 2007, Rivero et al 2006), binding of the DNA to a solid-phase support either by anion-exchange or by silica technology (Psidifi et al 2010) are some of the methods used extensively. Commercially available DNA isolation kit based on silica technology is solid phase extraction method and nucleic acid binding to silica beads is the basis for many automated extraction systems. From engineering point of view, the choice of a method depends on many factors such as the required quantity and molecular weight of the DNA, the purity required for downstream applications, and the time and cost of purification.

In salting out procedure, salt (usually sodium chloride, potassium acetate or ammonium acetate are used) is associated with charged groups of DNA and finally precipitated proteins are removed by centrifugation, then DNA remains in the supernatants. Also this method is less toxic than phenol-chloroform method (Rivero et

al 2006). Phenol-chloroform separation is based on the solubility difference of the nucleic acids, proteins, and lipids in these organic solvents. This method has both advantageous and disadvantageous. High purity DNA can be obtained by this method. On the other hand it requires laborious procedures including several centrifugations. This extra manipulation greatly increases the potential of contamination. Another is that the toxicity of these solvents, especially phenol. On the other hand adsorption on solid support is a low cost and nontoxic purification method. This method simply does not require salt or toxic chemical like phenol.

2.4. DNA –Metal and Metal Ion Interaction

Electron conductivity is an important parameter in nanotechnology. DNA is a biopolymer and its electron conductivity gains unique application area for DNA. For instance the development of DNA biosensors is inspired by electron conductivity of DNA (Bixon et al., 1999). DNA can be transferred to M-DNA by certain divalent cations from B-DNA form (Wettig et al., 2003) at high pH values ($7.5 - 9.0$) (Hadjiliadis and Sletten 2009). Metal ions affect the stability of DNA structures and they are concerned in the formation of alternative structures such as triplexes and quadruplexes. It is obvious that not only the conformation but also other properties of the DNA, such as electrical conductivity, can be strongly affected by its interactions with metal ions.

Metal ion-DNA interactions are also important for DNA replication and transcription in vivo, and can be exploited for the development of DNA-targeted drugs and bioensors. Alkali and alkaline earth metal cations (mainly Na^+, K^+, Mg^{2+} and Ca^{2+}) are present in human body in millimolar concentrations and bind to DNA electrostatically, usually mediated by water. They become toxic if the concentrations exceed the natural levels. Their depletion may also cause diseases. For example, deficiency of iron, magnesium or calcium may cause anemia, cardiovascular diseases or osteoporosis, respectively.

DNA directly or indirectly can be attached to metal ions through hydrogen bonding of the coordinating water molecules surrounding the metal ions (Anastassopoulou 2003). It is claimed that metal binding maybe the cause of the base pair hydrogen bonding destruction and destabilizes the double helix.

Interactions between metal complexes and oligonucleotides structure of DNA is mainly explained by the electrostatic attraction through cationic complex and the anionic phosphate backbone. More scientifically the interaction type can be listed in three main parts. The first is the covalent interaction between the Lewis acidic metal and the nucleic acid Lewis bases, such as nucleophilic guanine N7 residues the second interaction occurs through intercalation of a small molecule between stacked base pairs of the double helix structure and the third one is the simple electrostatic, occurring between a cationic complex and the anionic phosphate backbone (Hadjiliadis and Sletten 2009).

The interaction among double helical DNA and ions, specifically mono- and divalent metal cations was investigated extensively during the past 30 years. Franchi and coworkers studied adsorption of single- or double-stranded- nucleic acids on their clay minerals (Franchi et al., 2002). They figured out a model that explains adsorption in presence of cations, which is also called as "*cation bridge*" adsorption model. Double and single strand DNA adsorption onto negatively charged surface was presented in Figure 2.5 and Figure 2.6 respectively. This mechanism is also explained by "double layer depletion". Higher amount of cation is related to the double-layer overlap
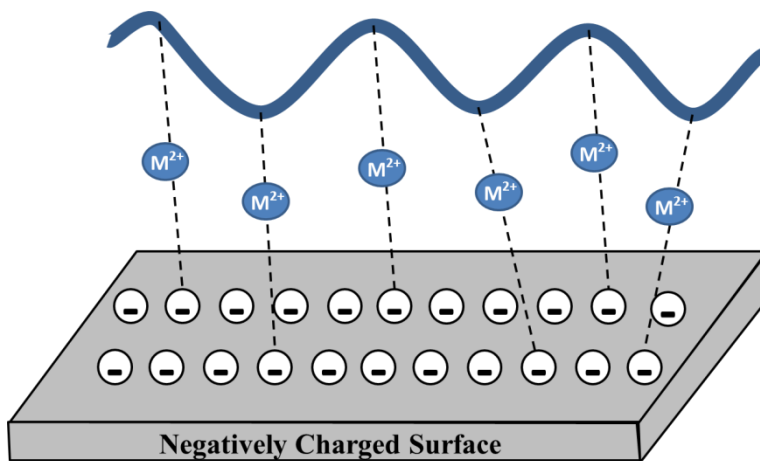
Figure 2.5. Adsorption of single-stranded polynucleotides on negatively charged surface
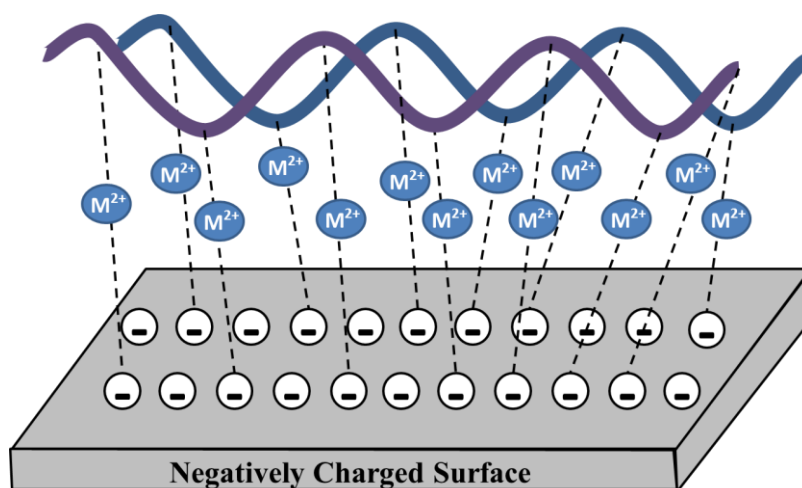
Figure 2.6. Adsorption of double -stranded polynucleotides on negatively charged surface

Moreover they concluded that during the adsorption process double strand DNA needed more metal concentration than single strand DNA as shown in Figure 2.5 and Figure 2.6. These positively charged metal ions interact directly or indirectly with sites characterized by high electron density or negatively charged residues of DNA. According to the same study, the divalent cations are more efficient than the monovalent cations.

2.5. DNA Analysis

DNA concentration analysis is done traditionally by UV visible spectrometer. Nowadays surface plasmon resonance, quartz crystal microbalance have been used which are based on electroanalytical methods. Electroanalytical methods are important for the investigation of nucleic acids and several reports have appeared concerning the electrochemistry of DNA and RNA and metal complex–nucleic acid interaction. Electroactivity of DNA was first discovered by Palecek (1960). Recently, several studies have described the use of metal complexes for the recognition of double stranded nucleic acids and have established promising DNA hybridization sensors based on cyclic voltametry, electrogenerated chemiluminescence and the quartz crystal microbalance. Cyclic voltammetry (CV) is one of the most popular techniques to characterize the redox behavior of compounds and to elucidate the kinetics of electrode

reactions. Surface plasmon resonance (SPR) allows for real time monitoring of binding between nucleic acid target and probe on the surface of a gold coated prism. SPR-based instruments use an optical method to measure the refractive index near (within ~300 nm) a sensor surface. SPR is also useful for measuring the affinity, enthalpy, stoichiometry, and kinetics and activation energy of an interaction (Van der Merve 2003). Quartz crystal microbalance (QCM) has found due to its natural ability to monitor analytes in real time a wide range of applications in areas of food, environmental and clinical analysis since its discovery. QCM biosensors have also been developed widely, and their theory and applications have been described in a review article (O'Sullivan and Guilbault 1999) and in a research article that reported the three basic concepts of QCM; mass, viscosity, and viscoelastic changes (Muramatsu et al 2002). Fawcett et al. (1988) were the first to describe a piezoelectric crystal (PZ) biosensor for DNA by immobilizing single stranded DNA on anti-quartz crystals and detecting the mass change after hybridization. Aslanoglu et al. (1998) adsorbed DNA onto a QCM and studied the metal complex binding projection of the immobilized DNA by cyclic voltammetry (CV) and QCM. The results of the two techniques were comparable. Caruso et al (1997) showed the suitability of the QCM for in-situ detection of hybridization of a complementary 30 unit DNA oligonucleotide by with avidin-immobilized biotin-DNA and PAH-immobilized BS1-SH.

CHAPTER 3

ADSORBENTS FOR DNA SEPARATIONS

Adsorption DNA purification technique is widely used for DNA biological analysis. The main parameters affecting the adsorption process are its size, shape, polarity, and chemical structure of the substance wanted to be removed. DNA is a biopolymer and it structurally depends on nucleotide sequence and has been known to bind many classes of molecules alumina, clay, and silica, including single-walled carbon nanotube (SWNT) as biosensor (Zhao and Johnson.2007), metals, organic and bioorganic molecules such as drugs.

Under most environmental conditions, DNA molecules are defined negatively-charged, and they can easily adsorbed to positively-charged surfaces such as the edges of clay minerals (Khanna et al., 1998), as well as to negatively-charged surfaces such as the surfaces of clays by electrostatic bridges with the water of hydration of charged cations (Lorenz and Wackernagel, 1994; Paget and Simonet 1994).

It should be noted that DNA double helix form has been affected by physical adsorption of the DNA on a surface, which also influences its denaturation (Allahverdyan et al., 2009).

Some composites were also reported as DNA adsorbents such as polypyrrole (PPy)-silica monocomposite particles (Saoudi et al., 1997), polymers and hydrogels (Şenel et al., 2003)

Polypyrole conducts polymer stable and biocompatible compared to other polymers (Kumar et al.,2011). Its good thermal and mechanical stability let its use in biological areas such as biosensor design. Composite form of it with DNA absorbable material make them acceptable for DNA adsorption. Therefore polypyrrole–silica nanocomposites (untreated and amine or carboxylic powder acid functionalized) were studied at neutral pH in sodium phosphate buffer by Saoudi and coworkers. (Saoudi et al., 1997). DNA adsorption was measured to be 32 and 22 mg/g for the aminated silica sol and for the aminated PPy-silica particles respectively and 6.5 mg/g for the carboxylated particles.

DNA adsorption is not applied only for purification of DNA, but also therapies of autoimmune diseases. DNA-immobilized supports such as polymeric adsorbent have been used. Amount of immobilized DNA on the material is directly related to antibody removal rate for instance poly-L-lysine immobilize poly(2-hydroxyethyl methacrylate) (pHEMA) membrane (Şenel et al.,2003). At 4 ºC from phosphate-buffered salt solution maximum DNA adsorption was obtained as 5849 mg/m^2.
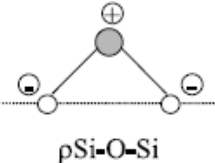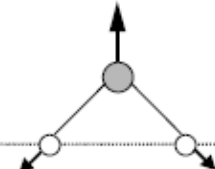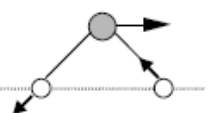
3.1. Silica –Alumina-Hydroxyapatite

3.1.1. Silica

Silica is one of the commonly used adsorbents and support materials for scientific research. It is mainly found in soil material (Nawrocki 1997). Adsorption of DNA onto soil, variable-charged minerals, humic substance, and organo-mineral complexes are the most frequently used materials understanding the DNA extraction from soil as model solid surfaces. DNA of various organisms has an advantage to adjust its activity and susceptibility to biodegradation. Saeki et al (2008) also emphasized that the presence of oxide minerals in soil enhance DNA adsorption. Silica is one of them. Higher number of cross-linking sites on the surface of silica enables it higher attachment rate occurred by hydroxyl groups that easily form hydrogen bonding with amine groups Table 3. 1 shows the main silica band related to fourier transform infrared spectroscopy (FTIR). However it is reported that perfect silica surface such as quartz has no free surface hydroxyl groups (Vandeventer et al.,2012). On the other hand acid treatment of silica is hydrolyze the surface, increases the concentration of surface silanol groups (Nawrocki 1997). Silica is also known for having high thermal resistance, which was necessary when undergoing modification with a coupling agent. The peak band at 3400 cm^{-1} is related to the νO–H mode of residual silanol (Si–OH) groups and of adsorbed water hydrogen bonds (Fidalgo and Ilharco 2005). In other words this wavenumber is relevant to the –OH vibrations of molecular water that is physically adsorbed in the network. This band mostly reflects silanol groups. Low intensity of the peak at 1.630 cm^{-1} is also related to bending water vibration (Estella et al., 2008).

The weak band near 970 cm^{-1} was assigned to the oscillating oxygen atoms in the silica network, including silanol groups and broken Si–O–Si bridges (Estella et al., 2008). The 1080 cm^{-1} wavenumber has been related to Si-O-Si bond tensile strain.

Table 3. 1. Assignments of the main infrared bands in the spectra of Silica.

Wavenumber (cm^{-1})	Assignment	Schematic Representation	Reference
~460	ρSi-O-Si	ρSi-O-Si	Fidalgo and Ilharco 2001
800	v_aSi-O-Si		Fidalgo and Ilharco 2001
950	Si-OH stretching vibration		Fidalgo and Ilharco 2001
~1080	asymmetric stretching vibration of the Si–O bond		Fidalgo and Ilharco 2001 Fidalgo and Ilharco 2005
1600	bending vibration of H$_2$O δH–O–H mode		Balkose et al., 2008 Fidalgo and Ilharco 2005
3400	-OH stretching		Balkose et al., 2008

Nucleic acids are readily adsorbed on silica and on a glass surface under chaotropic solution conditions (Boom et al. 1990, Buffone et al 1991). DNA adsorption by silica was extensively investigated (Melzak et al 1996; Mao et al., 1994; Fujiwara et al 2005). Silica offers a quick and less chemical purification. Therefore silica, the most commonly used matrix for solid-phase extraction, was shown to effectively bind DNA in 1979 when it was used to purify DNA from agarose gels (Vogelstein and Gillespie 1979). Silica is extensively used in DNA purification as commercial kits. Silica-based kits are the most common method of nucleic acid purification for PCR. A typical spin column comprises a nearly 5 mm diameter and 1 mm thick glass fiber disc (membrane), or other form of silica, filled in a polypropylene tube (Kim et al.,2010). Spin column was designed to allow centrifugation or vacuum suction to facilitate flow through the porous silica membrane. Silica based DNA extraction kits are widespread, produced by companies such as Clontech (Nucleo Spin), Mo Bio Laboratories (UltraClean BloodSpin), Qiagen (QiaAmp), Promega (Wizard), Epoch Biolabs (EconoSpin) and Sigma Aldrich (GenElute). Promega products are available for plasmid, genomic and fragment/PCR product purification. Promega has sold and supported silica-based DNA purification systems for nearly two decades.

According to some studies, DNA molecules bind to OH groups on the edge of phyllosilicates such as montmorillonite (Lorenz and Wackemagel 1987; Paget et al., 1992) as seen in Figure 3. 1(a) and (b). DNA adsorption in soils using montmorillonite as adsorptive has been investigated by several researchers (Khanna and Strotzgy 1992, Creccio et al.; 2005, Pietramellara et al., 2001). Adsorption mechanism in Figure 3. 1 (c) represents DNA molecules associated with the surface, which negatively charged materials via a bridging of cations (Khanna and Strotzgy 1992; Paget et al.1992). Divalent cations like Mg^{2+} and Ca^{2+} support binding about 100-times greater than monovalent cations like Na^+, K^+, and NH^{+4} (Lorenz and Wackernagel 1987; Franchi et al. 2003) According to Figure 3. 1 (d) DNA molecules directly bind to solid organic surface. On the contrary Saeki et al. (2009) proved that organic matter addition decreased the adsorption capacity of DNA on the soil material.
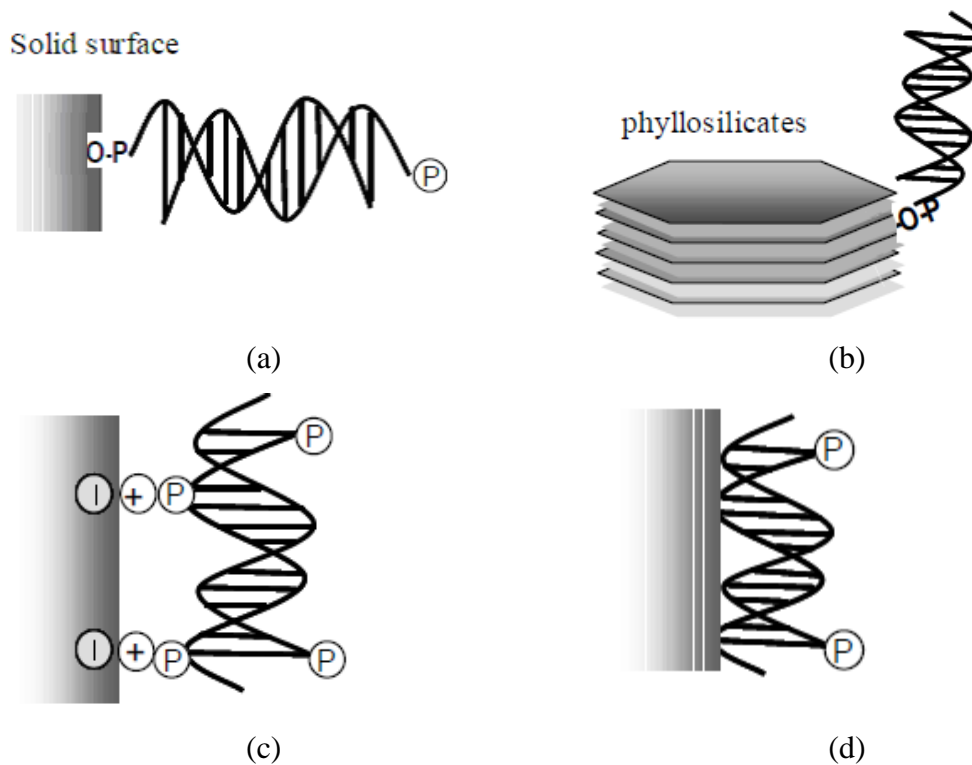
Figure 3. 1. Conceptual figures of DNA adsorptions
(Source: Saeki and Sakai, 2009 with permission)

DNA adsorption by silica was controlled by three effects (i) weak electrostatic repulsion forces, (ii) dehydration, and (iii) hydrogen bond formation (Melzak et al 1996). The presence of a monovalent cation such as Na^+ neutralizes the negative charges on the phosphate backbone of DNA, reducing the electrostatic barrier between DNA and silica. Therefore DNA adsorption capacity is increased.

Mao et al. (1994) have also indicated that it is possible the formation of hydrogen bonds between the phosphate group in DNA and the silanol group on the surface of silica (Figure 3. 2). This hydrogen bond formation has a weak and additive effect on adsorption. Melzak et al. (1996) reported that intermolecular electrostatic forces between DNA and silica surface strongly disfavors adsorption at low ionic strength. The adsorption capacity as a function of ionic strength can be explained by electrostatic double-layer repulsion between the DNA and the natural organic matter (NOM) layer (Nguyen and Elimelech 2007). In Table 3.2. effects of pH, ionic strength and phosphate ions on Salmon sperm DNA (average size of 1000 bp) adsorption on different solid surfaces are shown.
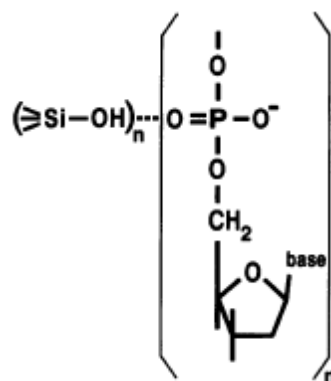
Figure 3. 2. Proposed binding of DNA to silanol groups on the silica surface
(Source: Mao et al., 1994).

Table 3. 2. Comparison of DNA adsorption on variety of minerals
(Source: Saeki et al., 2010)

	DNA adsorption average (%)	Standard deviation SD	n	pH	Ionic strength (mol /dm^3)
Montmorillinite	6.1	2.2	3	6.9	0.16-0.18
Kaolinite	36.7	4.1	3	6.8	0.16-0.17
Silica	16.6	2.1	4	6.7-7.1	0.16-0.17
Goethite	86.1	1.9	4	6.9	0.17-0.18
Gibbsite	54	3.1	3	6.9	0.17-0.18
Synthetic allophane	30.5	1.4	3	6.8	0.14-0.18
Naturel allophane	49.5	2.9	3	6.7-7.0	0.17-0.18

Solid weight: 10 mg, Solution volume: 1.0 cm^3., Initial DNA concentration: 100 ng cm^{-3}. Background: 0.1 M NaCl. Reaction time: 2 h, n: number of the analysis

According to the results, silica adsorption capacity of DNA was found to be greater than that of montmorillonite. The solution chemistry and the type of surface will influence the amount of DNA adsorbed.

Consequently there are other important situations where both adsorption and denaturation of DNA occur simultaneously. For example adsorption of plasmid and chromosomal DNA on microcrystalline silica surface and the effect of ionic strength, temperature, pH, DNA size and conformation on the adsorption phenomenon were

reported by Melzak et al.(1996). Adsorption isotherm results pointed out those three effects, (1) shielded intermolecular electrostatic forces, (2) dehydration of the DNA and silica surfaces, and (3) intermolecular hydrogen bond formation in the DNA–silica contact layer. These three effects mentioned above make the dominant contributions to the overall driving force for adsorption. For instance adsorption of DNA from Bacillus subtilis, calf thymus and salmon sperm on montmorillonite, kaolinite and silica increased with an increase of ionic strength or a decrease of pH (Melzak et al., 1996)

Adsorption of DNA onto bare silica under high ionic strength and chaotic solution conditions is supported (Breadmore et al 2003). High ionic strength serves to protect the negative surface, reducing the electrostatic repulsion between the negative DNA and the surface of the silica, while the mono and divalent salt dehydrates the silica surface and DNA, thus promoting hydrogen bonding between the DNA molecules and the protonated silanol groups.

Solberg and Landry (2006) focused on with mesoporous silica material to find its gene therapy potential. Ammonium ion containing chemicals was found to be 2-3 times more effective in crosslink between DNA and mesoporous silica surface than mono or divalent cations

Adsorbed DNA was 100 times more resistant against DNase I than was DNA free in solution. Khanna and Stotzky (1992) reported that the protective effect of clays – montmorillonite (M) and kaolinite-(K)-against the activity of nucleases did not eliminate the transforming ability of bound DNA. In order to determine Clay-DNA complexes X-ray diffractometry (X-RD) and transmission (TEM) and scanning (SEM) electron microscopy were used. The results figured out possible place of the DNA bound and the adsorption process.

SEM images showed that the binding of this DNA was mainly on the edges of M and K, although some binding was also apparent on the planar surfaces (Khanna et al., 1998). Extension from the edges of the clays enables the unbound end of DNA to interact with receptor sites on competent cells and result in their transformation; and binding on clays alters the electron distribution and/or conformation of DNA, which reduces its hydrolysis by nucleases. In Table 3.3. different surfaces used in DNA adsorption are listed.

Table 3. 3. DNA Adsorption onto Different Surfaces

Adsorbent	DNA Type	Ref.
Glass	Escherichia coli DNA human spleen DNA	Vogelstein and Gillespie 1979
Silica particles or diatoms	DNA and RNA from, e.g., human serum and urine	Boom et al. 1990
PolymerizedPoly-L-lactic Acid Film Surface	Plasmid DNA	Jiang et al.,2007
Positively charged Amidine functionalised polystyrene microspheres	Double stranded DNA extracted from herring	Alison et al., 2007
Chemically synthesized polypyrrole powders	Calf thymus	Saoudi et al.,1997
Soil	Calf thymus DNA	Ogram et al., 1994
N-methylpyridinium terminated gold	(type XIV from herring testes)	Aslanoğlu et al., 1998
Silica beads were packed into glass microchips	PCR-amplifiable DNA	Breadmore et al.,2003

Recently, there has been an increasing interest in methodology of DNA extraction the synthesis of microchip and biosensor. Silica solid phase is also most commonly and easily adaptable to microdevices. Because standard procedures are time consuming, microdevices are preferable. Price et al (2009) reviewed DNA microchips. They concluded that DNA purification by microchips is related to the availability of equipment, reagents and sample, as well as the balance between speed, extraction efficiency, and quality.

5×10^{-7} dm^3 bed volume filled silica resin was used in a microchip DNA purification device by Tian et al. (2000). Sol gel derived silica adsorption was used in DNA purification on microchips under chaotropic conditions and was described in many studies. Breadmore et al.(2003) used a tetraethoxyorthosilicate-based sol-gel to

immobilize the silica beads in a microdevice, and also showed effective extraction of DNA from only 0.2 µL of whole blood sample. Figure 3. 3 shows the microchip channel filled with silica beads which was immobilized with sol−gel method. They improved DNA purification from blood in less than 15 min. However silica beads size was not provided.

(a) (b) (c)
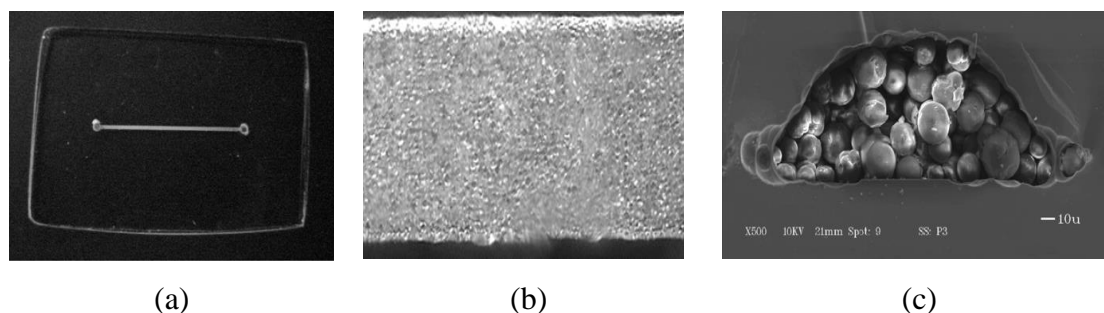
Figure 3. 3. Microchip packed with silica particles (a) 1× magnification; (b) 10× magnification; (c) cross section of packed channel at 500× magnification.(Source: Breadmore et al, 2003 with permission of the American Chemical Society.)

Different oxide forms of iron are used in the studies in biological applications that focus on magnetic bioseparation, biological labeling and diagnostics contrast enhancement agents for magnetic resonance imaging, tumor hyperthermia and drug-carrier design (Souza et al., 2010). Magnetic particles are also used in DNA purification method. Magnetic separation is also a good way to shorten both adsorption and separation steps. In DNA purification method magnetic silica microspheres are used. They consist of magnetic nanoparticles uniformly dispersed in a silica matrix where there are large amounts of hydroxyl groups on their surfaces. These groups interaction efficiency can be enhanced with silanol, epoxide, diol, and carboxyl groups. Chao et al. tested over 100 ng/µl concentrated calf thymus DNA adsorption behavior onto silica coated magnetic particle with modified surfaces (2007). As a result surface modified magnetic particles are promising materials to DNA purification.

3.1.2. Silica Aerogels

Aerogels have been used in a wide range of applications as listed in Table 3.4. such as catalytic supports, thermal insulation in solar window systems, acoustic barriers, supercapacitors, refrigerators, hydrophobic adsorbents for non-polar compounds, Cerenkov radiation detector media in high energy physics, or inertial confinement fusion targets for thermonuclear fusion reactions (Pierre and Pajonk 2002; Estella et al., 2008). Ru et al (2010) studied drying of silica aerogels and xerogels by conventional and CO_2 and ethanol supercritical drying (SCD) methods.

Table 3. 4. Identification of aerogel properties and features, with their applications

Property	Features	Applications
Thermal conductivity	✓ Best insulating solid ✓ Transparent ✓ High temperature ✓ Lightweight	✓ architectural and appliance insulation, portable coolers, transport vehicles, pipes, cryogenic, skylights ✓ space vehicles and probes, casting molds
Density/porosity	✓ lightest synthetic solid ✓ homogeneous ✓ high specific surf. area ✓ multiple compositions	✓ catalysts, sorbers, sensors, fuel storage, ion exchange ✓ targets for ICF, X-ray lasers
Optical	✓ low refractive index solid ✓ transparent ✓ multiple compositions	✓ Cherenkov detectors, lightweight optics, lightguides, special effect optics
Acoustic	✓ lowest sound speed	✓ impedance matchers for transducers, range finders, speakers
Mechanical	✓ elastic ✓ lightweight	✓ energy absorber, hypervelocity particle trap
Electrical	✓ lowest dielectric constant ✓ high dielectric strength ✓ high surface area	dielectrics for ICs, spacers for vacuum electrodes, vacuum display spacers, capacitors

Silica is one of the most frequently used inorganic simple oxides. In recent years, silica aerogels have been investigated increasingly due to their unusual properties. Therefore their potential has applications in wide variety of technological areas. Silica aerogel is a nanostructured material with high specific surface area, high

porosity, low density, low dielectric constant and applicable heat insulation properties (Dorcheh and Abbasi, 2008). For instance it was reported by several studies that aerogel has high specific surface area between 500–1200 m^2/g, high porosity 80–99.8%, low density ~0.003 g/cm^3, high thermal insulation value 0.005 W/mK, ultra-low dielectric constant k = 1.0–2.0 and low index of refraction nearly 1.05. Table 3.5. provides an overview of the most important physical properties of silica aerogels.

Table 3. 5. The overview of the most important physical properties of silica aerogels. (Source: Dorcheh and Abbasi, 2008).

Property	Value	Comments
Apparent density g/cm^3	0.003–0.35	Most common density is ~0.1
Internal surface area	600–1000m^2/g	
%Solids	0.13–15%	
Mean pore diameter	~20nm	Typically 5% (95% free space) As determined by BET method
Primary particle diameter	2–5nm	Determined by electron microscopy
Refractive index	1.0–1.08	
Coefficient of thermal expansion	2.0–4.0×10^{-6}	Determined using ultrasonic methods
Dielectric Constant	~1.1	For a density of 0.1 g/cm^3
Sound velocity	100 m/s	For a density of 0.07 g/cm^3

Silica aerogels, which are synthesized through the association of a chemical step, called as "sol– gel" chemistry. Physical step is a particular way of drying the wet gel at supercritical conditions which are discussed in a broader view in the following chapter.

3.1.2.1. The Sol-Gel Process

The sol-gel process is a wet-chemical technique widely used for producing promising materials in scientific areas such as material science and ceramic engineering. Special property of sol –gel method is its capability to convert the molecular precursor to the product. It makes possible to control the process and structural composition. This method is used primarily for the fabrication of materials (typically metal oxides) starting from a colloidal solution (sol). Sol is a colloidal suspension which consists of particles having sizes less than 1000 nm. Thus, the gravitational force become negligible and short time forces such as wander walls and surface charge forces are the main forces acting on the particles. A gel is described as a solid molecular three-dimensional network that included a liquid network of the same size and shape. Chemical step has three general reversible reactions: hydrolysis-esterification, alcohol condensation-alcoholysis, and water condensation-hydrolysis as indicated in Figure 3. 4. In the first reversible reaction, alkoxide grups (OR) are replaced with hydroxyl groups (OH). Then condensation reaction occurs rather than hydrolysis or alcoholysis.

Hydrolysis and Esterification:
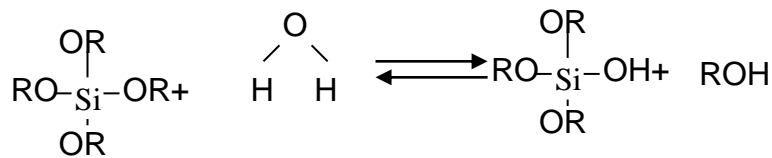
Alcohol Condensation and Alcoholysis:
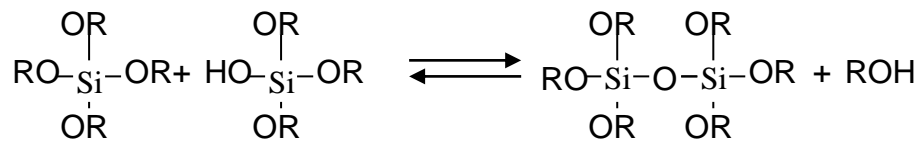
Water Condensation and Hydrolysis :
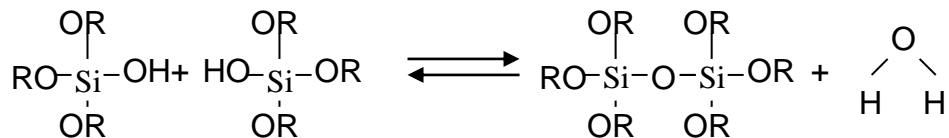
Figure 3. 4. Hydrolysis and condensation for silicon alkoxides
(Source: Brinker and Scherer, 1990)

These reversible reaction rates define the generally assumed product structures. According to this relative slow hydrolysis and fast condensation rates are resulted as controlled precipitation. In Table 3.6. expected products from different reaction rates are shown.

Table 3.6. Expected product of sol-gel process
(Source:Pierre 1998)

Hydrolysis rate	Condensation rate	Results
Slow	Slow	Colloids/sols
Fast	Slow	Polymeric sols/gels
Fast	Fast	Colloidal gels or precipitate
Slow	Fast	Controlled precipitation

Hydrolysis starts with water. However water and alkoxysilanes such as tetraethoxysilane (TEOS) and tetramethoxysilane (TMOS) are partially immiscible as shown in Figure 3. 5. Additional solvent is needed to homogenize the mixture. Therefore alcohols, acetone, dioxane, tetrahydrofurane are the solvents added to this mixture.

In the sol–gel process, a sol is first formed by mechanically mixing a liquid alkoxysilane precursor, such asTEOS, deionized water, a solvent and an acid or alkaline catalyst at ambient conditions. During this step, the alkoxysilane groups are transformed to silanol groups by acid catalyzed.

Several important papers have investigated the significance of the chemical parameters such as the nature of the starting alkoxide (Dorcheh and Abbasi 2008, Alie et al., 2002), the hydrolysis ratio (water:alkoxide molar ratio) the co-solvent (Brinker and Scherer, 1990), and the catalysis conditions that determine the kinetics and mechanisms of the hydrolysis and condensation reactions (Fidelgo et al.,2003). Some attention has also been devoted to the influence of the processing factors such as the reaction temperature, the ageing period and conditions, the washing solvent and the drying conditions.
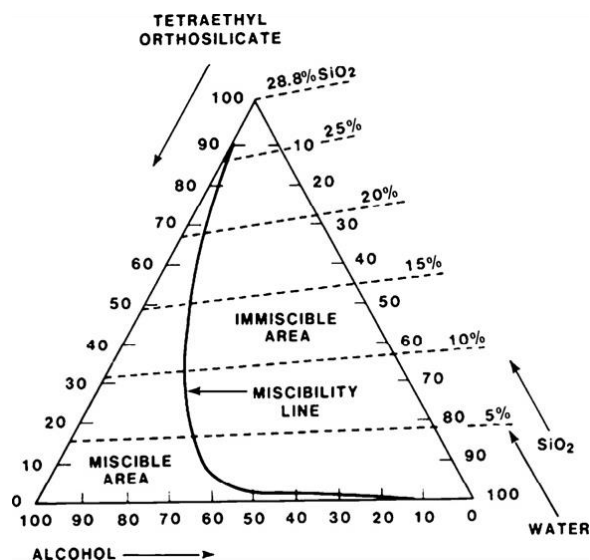
Figure 3. 5. Ternary phase diagram of the system TEOS–ethanol–water at 25 °C.

3.1.2.2. Gel and Gelation

A gel is composed of solid and liquid phases which are independent of each other. A wet gel was prepared by two-step process which was developed Brinker et al. (1990). The first step involves acid (hydrochloric) catalysis of the hydrolysis of tetraethyl ortosilicate (TEOS). The second step involves condensation polymerization of the silanol groups resulting from the hydrolysis reaction. The condensation reaction is reserved by the acid added in the first step; thus the second step includes the addition of ammonium hydroxide to neutralize acid.

3.1.2.3. Drying of the Gels

Three main routes are commonly used for drying (Bisson et al., 2003):

1. Freeze-drying (which needs to avoid the triple point)

2. Evaporation (which implies crossing the liquid–gas equilibrium curve)

3. Supercritical drying (SCD) (which needed to avoid the critical point)

Depending on the drying process, gel is named differently. Drying of the gel is a critical step. A xerogel is the result of that liquid evaporation at ambient temperature and pressure (it often retains the same form as the original gel with up to 90% shrinkage).
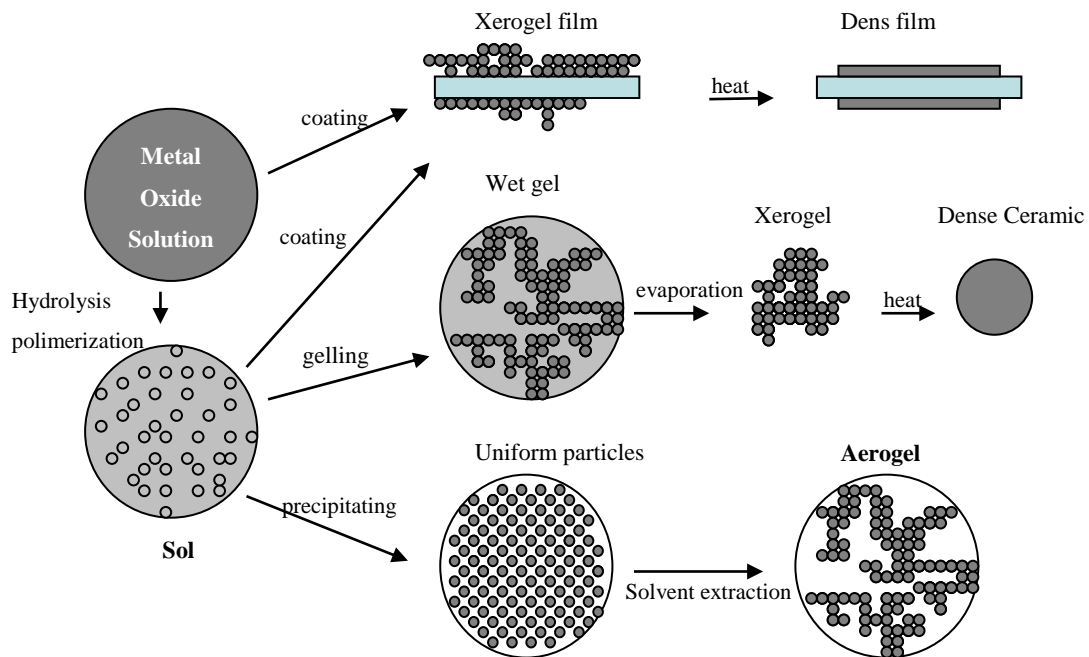
Figure 3. 6. Overview of sol-gel process steps
(Source: Adapted by Brinker and Scherer 1990)

An aerogel is the result of the removal of the liquid part without damaging the solid structure (often by supercritical removal). During SCD, especially under high pressure and high temperature, not only drying but also supercritical extraction and the chemical reaction of alcogel component occurs. This drying process discovered by Kistler in 1931, involves removal of the solvent from wet gel (Land et al. 2001). This process preserves the texture of the dry material. In practice it strongly reduces the pore collapse. Supercritical drying is consisted in heating a gel in a device like autoclave, until the pressure and temperature exceeded the critical temperature T_c and critical pressure P_c of the liquid entrapped in the gel pores. Aerogel shows very high surface area and important nanoporosity. This is provided by the absence of capillary forces. The surface forces attracting the liquid and solid phases were not present, since only the gas phase and the solid existed above critical temperature.   Shrinkage of the gels during

drying is driven by the capillary pressure, P, which can be represented by Eqn.3.1. Capillary force can also be measured by contact angle as represented in Eqn. 3.2.

$$P = \frac{\gamma_{LV}}{(r_P - \delta)} \quad\quad (3.1)$$

$$P = \frac{2\gamma x Cos\theta}{r_p} \quad\quad (3.2)$$

where γ_{lv} is the surface tension of the pore liquid, r_p is the pore radius, which can be represented by Eqn. 3.3, δ is the thickness of a surface adsorbed layer (Brinker and Shere 1990).

$$r_P = \frac{2V_p}{S_p} \quad\quad (3.3.)$$

where V_p and S_p are pore volume and surface area, respectively. When liquid evaporates from the pores of a gel became concave (meniscus) liquid / vapor forms as seen in Figure 3. 7 . At the moment that the liquid/vapor meniscus enters a pore, the walls will be covered with a film of adsorbed liquid and then capillary pressure will increase according to Equation 3.1 attracting the walls of the capillary closer to each other

(a)   (b)
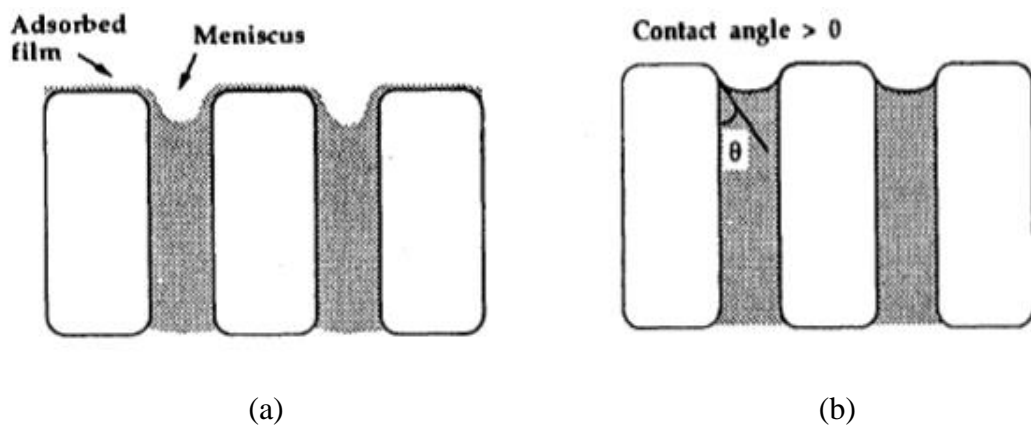
Figure 3. 7. Distribution of liquid at surface of drying porous body, when liquid is (a) spreading (contact angle $\theta=0°$) or (b) wetting but nonspreading ($90°> \theta \, 0°$)

By transforming the solvent into a supercritical fluid, the surface tension disappears along with the capillary pressure gradient built up in the pore walls, avoiding the potential collapse of the pore volume due to the capillary force. Supercritical drying in organic solvents which are usually alcohols due to the preparation conditions, leaves the pores without damaging and the resulting materials are generally hydrophobic since their surfaces are covered with alkoxy groups (Pierre and Pajonk 2002).

It is important that during SCD mass transport and heat transfer occur simultaneously. Therefore homogenizer solvent should be selected carefully. The most commonly used supercritical fluids and their properties are given in Table 3.7. Supercritical fluids (SCF) are highly compressed gases which combine properties of gases and liquids in same conditions. Figure 3. 8 is the phase diagram of a pure substance in a two coordinate system: P pressure, (P) and temperature, (T). For every substance, there is a value of T and P where liquid phase and gaseous phase have the same density. They are the coordinates of the so called critical point, which ends the liquid-vapor coexistence curve. The area corresponding to temperature and pressure beyond the critical point coordinated is the supercritical region. The fluid in this region is called as a SCF. Subra and Justin have reported that SCF can transfer heat and mass better than gases do.
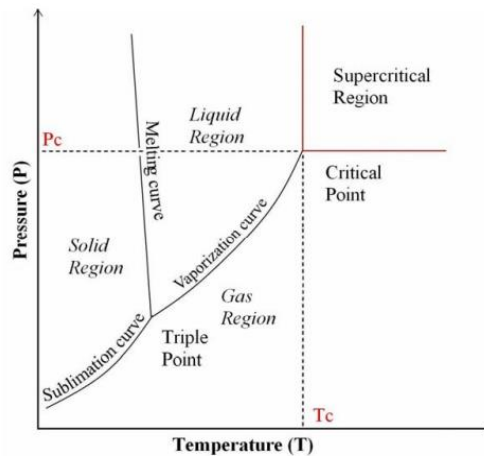
Figure 3. 8. P-T plane phase diagram of a pure substance.

Table 3. 7. Properties of some supercritical fluids
(Source: Pierre and Pajonk, 2002)

Fluid	Formula	Critical Constant	
		Pressure (MPa)	Temperature (C°)
Carbon Dioxide	CO_2	7.36	31.1
Freon 116	CF_3CF_3	2.97	19.7
Ethanol	C_2H_5OH	6.36	243
Methanol	CH_3OH	7.93	240
Nitrous Oxide	N_2O	7.24	36.4
Acetone	$(CH_3)_2O$	4.66	235
Water	H_2O	22	374

3.1.3 Aluminium Oxide -Alumina

Alumina also called aluminium oxide is the only solid oxide form of aluminium. It has the chemical formula Al_2O_3. It is commonly referred to as alumina (α-alumina), or corundum which is the naturally occurring alumina. Alumina materials have been technologically significant ceramic materials throughout human history. Type of α alumina has hexagonal close packed while γ signifies cubic close packed crystalline form. In a hexagonal unit cell, the sides that provide depth and width to the cell are equal, and are at an angle of 120 degrees to each other. c is at angles of 90 degrees to sides "a" and "b. The hexagonal parameters for α -Al_2O_3 are c = 1.297 nm and a = 0.475 nm, with c/a = 2.73 (Levin and Brandon 1998). X'Pert graphic and identity software of XRD pattern and obtained data for alumina were listed in Table 3.8.

Table 3. 8. XRD data of Alumina

Identity		JCPDS (PDF)[*] number	Observed 2θ	JCPDS # (75-1865) 2θ
Name	Formula			
			25.6	25.546
			35.14	35.105
			37.74	37.734
Aluminium Oxide	Al_2O_3	75-1865	41.65	41.619
Aluminium Oxide	Al_2O_3	75-1862	43.36	43.302
Aluminium Oxide	Al_2O_3	05-0712	52.64	52.486
Aluminium Oxide	Al_2O_3	75-1863	57.45	57.423
Aluminium Oxide	Al_2O_3	78-2426	59.73	59.670
Corundum	Al_2O_3	74-0323	61.35	61.056
Corundum	Al_2O_3	42-1468	66.40	66.434
			68.19	68.126
			76.70	70.756

(left side, spanning rows) **Alumina**

*PDF: Powder Diffraction File

α phase alumina called also corundum is the only thermodynamically stable oxide of aluminium and is the final produt of the calcination process. Calcination order can be define as follow: Gibbsite→boehmite (γ-AlOOH)→γ-alumina(γ-Al_2O_3)→δ-alumina(δ-Al_2O_3)→θ-alumina(θ-Al_2O_3)→α-alumina. Metastable Al_2O_3 phases calcination procedure toward stable α- alumina were listed in Table 3.9. based on starting structure. Zeta potential measurement was identified that the α-alumina has isoelectric point at nearly pH 9.1 (Polat et al., 2006).

Alumina has a melting point nearly 2000 °C. Therefore it is used as insulator or refractory material. It is used in orthopedic and dental implants surgery (Hench, 1998). Furthermore it is used catalytic support material in reaction engineering.

Table 3.9 . Structures and the Sequences of Phase Transformations toward the Stable α Al$_2$O$_3$ Phase (Source: Levin and Brandon 1998)

Approximate Packing of Oxygen for the Metastable Al$_2$O$_3$ Structures

---

α - AlOOH(diaspore) $\xrightarrow{700\text{-}800\,^0\text{C}} \overset{hc}{\alpha - Al_2O_3}$

γ - Al(OH)$_3$(gibbsite) $\xrightarrow{150\text{-}300\,^0\text{C}} \chi \xrightarrow{650\text{-}750\,^0\text{C}} \kappa \xrightarrow{1000\,^0\text{C}} \alpha - Al_2O_3$

$5Al_2O_3.H_2O$(tohdite) $\xrightarrow{700\text{-}800\,^0\text{C}} \kappa^I \xrightarrow{750\,^0\text{C}} \kappa \xrightarrow{9000\,^0\text{C}} \alpha - Al_2O_3$

Vapor(CVD) $\longrightarrow \kappa \longrightarrow \alpha - Al_2O_3$

γ - AlOOH(boehmite) $\xrightarrow{300\text{-}500\,^0\text{C}} \gamma \xrightarrow{700\text{-}80\emptyset\text{C}} \overset{fcc}{\delta} \xrightarrow{900\text{-}1000\,^0\text{C}} \theta \xrightarrow{1000\text{-}110\emptyset\text{C}} \alpha - Al_2O_3$

$\propto$ -Al(OH)$_3$(bayarite) $\xrightarrow{200\text{-}300\,^0\text{C}} \eta \xrightarrow{600\text{-}80\emptyset\text{C}} \overset{fcc}{\theta} \xrightarrow{1000\text{-}1100\,^0\text{C}} \alpha - Al_2O_3$

Amorphous(anodic film) $\rightarrow \gamma \rightarrow \delta \rightarrow \theta \rightarrow \alpha - Al_2O_3$

Melt $\rightarrow \gamma \rightarrow \delta, \theta \rightarrow \alpha - Al_2O_3$

Alumina is also classified as non bioactive material (Ohgushi and Caplan 1999). It has been used in orthopedic surgery because of its high biocompatibility (Karlsson et al., 2003). Its adsorption capacity of DNA was studied and already published by Chattoraj and Upadhyay in 1968 and reported as review by Chattoraj and Mitra (2009). Alumina has been also tested on DNA and RNA purification. DNA and RNA were also denaturized with heat and acid presence. Values of the point of adsorption per kg of DNA (or per mole of nucleotide) were obtained versus volume of the solution per kg of DNA (or per mole of nucleotide). The average value of molecular weight of nucleotide was taken as 330 in this calculation. The DNA concentration of the supernatant has been estimated at 260 nm UV device. Each curve was found to fit Langmuir equation in linear form. Therefore authors concluded that denaturized DNA and RNA adsorbed by alumina more than native form of them. Alumina was adsorbed 0.25mg and 0.75 mg amount of DNA and RNA respectively at pH 6.5 with maximum 10 mg /cm^3 concentration.

3.1.4. Hydroxyapatite (HAP)

Hydroxyapatite's (HAP) chemical formula is Ca_{10} $(PO_4)6(OH)_2$ which is the main mineral element of teeth and bones and belong to calcium phosphates family. Different techniques are used for HAP powder production. HAP's morphology, stoichiometry and level of crystalinity change with preparation technique, which define biomaterial phase thermal stability, mechanical stability and dissolution behavior. HAP has lattice parameters a=b=0.934 nm, c=0.687 nm, $\alpha=\beta=90º$, $\gamma=120º$ and hexagonal crystal structure with the space group P63/m (Peroos, et al. 2006) Ca/P ratio is an important ratio which defines calcium phosphate mineral such as acidity and solubility(Vallet-Regi and Calbet 2004).

HAP has also been confirmed with literature based on X'Pert graphic and identity software of XRD pattern and obtained data are listed in Table 3.10. Joint Committee on Powder Diffraction Standards (JCPDS) numbers which are known to identity of the x-ray powder diffraction patterns were also obtained by this software

Table 3. 10. XRD data of HAP
(Source: JCPDS number 09-0432 by Wu et al., 2007)

Identity		JCPDS (PDF)* number	Observed 2θ	JCPDS # (09-0432) 2θ
Name	**Formula**			
Hydroxyapatite	$Ca_5 (PO_4)_3(OH)$	09-0432	10.79	10.820
Apatite	$Ca_{9.93}(P_{5.84}B_{0.16}O_{24})$	80-0537	16.90	16.741
			21.70	21.819
			22.77	22.902
			25.77	25.879
			28.05	28.126
			28.79	28.966
			31.64	31.773
			32.05	32.196
			32.78	32.902
			39.05	39.204
			40.27	40.452
			41.82	42.029
			46.54	46.711
			49.30	49.467
			50.29	50.490
			63.15	63.011
			63.88	64.078

(Left side vertical label: **Hydroxyapatite**)

*PDF: Powder Diffraction File

Lower Ca/P ratio represents larger acidity and solubility of the mixture, for example Ca/P < 1. These properties change while increasing the Ca/P ratio to the value of 1.67. In Different Ca/P ratios have been listed with their formulation in Table 3.11. Tetracalcium Phosphate ($Ca_4P_2O_9$), Amorphous calcium Phosphate, α-Tricalcium Phosphate ($Ca_3(PO_4)_2$), β-Tricalcium Phosphate ($Ca_3(PO_4)_2$), and Hydroxyapatite ($Ca_{10}(PO_4)6(OH)_2$) are the members of calcium phosphates.

Table 3. 11. Various calcium phosphates with their respective Ca/P atomic ratios
(Source: Vallet-Regi and Calbet 2004)

Ca/P	Name	Formula	Acronym
2.0	Tetracalcium phosphate	$Ca_4O(PO_4)_2$	TetCP
1.67	Hydroxyapatite	$Ca_{10}O(PO_4)_6(OH)_2$	OHAp
	Amorphous calcium phosphate	$Ca_{10-x}H_{2x}(PO_4)_6(OH)_2$	ACP
1.50	Tricalcium phosphate (α,β,γ)	$Ca_3(PO_4)_2$	TCP
1.33	Octacalcium phosphate	$Ca_8H_2(PO_4)_6.5H_2O$	OCP
1.0	Dicalcium phosphate dihydrate	$CaHPO_4.2H_2O$	DCPD
1.0	Dicalcium phosphate	$CaHPO_4$	DCPA
1.0	Calcium pyrophosphate (α,β,γ)	$Ca_2P_2O_7$	CPP
1.0	Calcium pyrophosphate dihydrate	$Ca_2P_2O_7.2H_2O$	CPPD
0.7	Heptacalcium phosphate	$Ca_7(P_5O_{16})_2$	HCP
0.67	Tetracalcium dihydrogen phosphate	$Ca_4H_2P_6O_{20}$	TDHP
0.5	Monocalcium phosphate monohydrate	$Ca(H_2PO_4)_2.H_2O$	MCPM
0.5	Calcium metaphosphate (α,β,γ)	$Ca(PO_3)_2$	CMP

HAP has been used clinically for many years. HAP has good biocompatibility in bone contact as its chemical composition is similar to that of bone material. HAP shows excellent biocompatibility with hard tissues and also with skin and muscle tissues (Hench, 1991). Synthetic hydroxyapatite is a very important biomaterial used for several applications in medicine either as a bulk ceramic, implant coating materials, ceramic coating or as one of the components of composites.

Porous HAP was used for cell loading. Ohgushi and Caplan (1999) applied HAP for cell loading, drug carrier for controlled drug released based on adsorption /desorption properties (Komlev et al 2002), most extensively for hard tissue scaffolds, affinity chromatography analysis for DNA binding for protein purification (Gadgil et al., 2001), and the separation of ssDNA and dsDNA by chromatography (Chen et. al., 2007) or both of them like plasmid DNA and protein adsorption (Schmoeger et. al., 2010). This can be explained by positively charged pairs of calcium ions and six negatively charged oxygen atoms which are associated with triplets of crystalline phosphates placed onto the surface. It is possible that amino and guanidinyl groups of

proteins can attached to phosphate ions of hydroxyapatite, DNA's phosphate part can attach to calcium ions.

HAP has osteogenic cell proliferation capacity onto implant surface therefore should be investigated of surface interaction on coated material or smooth surface. Therefore coating is main usage area of HAP. In practice HAP surface can be formed on either HAP thin film or HAP pellet forms (Şimsek 2002). Sol-gel deposition technique is well a known film formation procedure. Sol or particulate sol can be used. The final form can be obtained by dip or spin coating. In dipping process substrate such as inert glass film is contact with the dip solution for a few seconds. HAP pellet can be prepared from powder form. For instance Şimsek (2002) compacted HAP powder in a stainless steel die 1cm internal diameter under 160 MPa pressure. All pellets were sintered different temperatures between 800-1300 ^{o}C for 2 hours. The sol–gel approach affords conditions for the synthesis of HAP films. HAP film can also be prepared directly from sol or indirectly from particulate sol solutions. Ozcan and Çiftçioğlu (2010) prepared particulate sol route hydroxyapatite thin film.

CHAPTER 4

ADSORPTION OF DNA

Adsorption is one of the most widely useful techniques for removal of pollutants from contaminated media or required substance in solution. Several parameters effect on adsorption process therefore understanding adsorption mechanism is challenge work during on it.

Solid phase extraction method is one of the useful extraction techniques for DNA purification based on adsorption. Immobilization onto solid particle, beads or column is named solid phase extraction method. DNA is negatively charged biopolymer. This charge defines interaction possibilities with surface. DNA can be attached positively charged surface easily. DNA interaction with surfaces is illustrated in Figure 4.1.
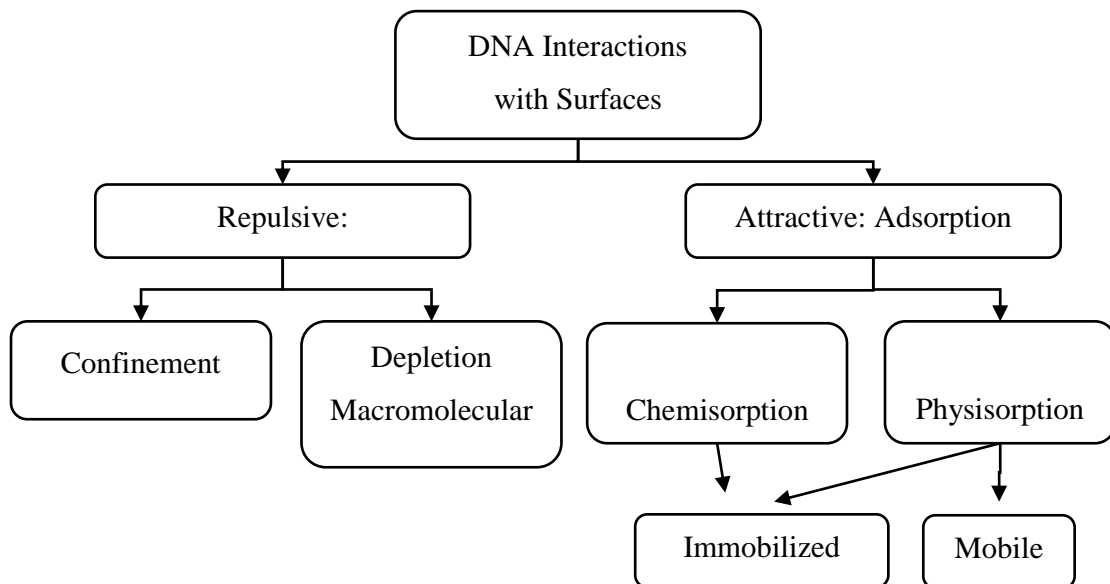
Figure 4. 1.Surface science of DNA
(Source : Douarche et. al., 2008).

Attraction of DNA might be repulsive or attractive. The adsorption phenomenon depends on the interaction between the surface of the adsorbent and the adsorbed

species. Attractive interactions lead to adsorption. The interaction may be due to: chemical bonding, hydrogen bonding, hydrophobic bonding, Van der waals force and electrostatic interaction (Parida et al., 2006). DNA adsorbed at the silica surface depend on solution pH, ionic strength, electrolyte type and valency and conformation of DNA (linear, plasmid, supercoiled). (Lorenz and Wackemagel 1987, Romanowski et al.,1991, Melzak et al.,1996, Allemand,et al.,1997)

Surface charge is one of the important parameter to understand electrostatic interaction between DNA and solid surface. In the double helix structure, the bases exist in a highly hydrophobic environment inside the helix, while the outer, negatively charged backbone allows the dsDNA molecule to interact freely with the hydrophilic environment. General idea is about DNA that does not adsorbed by same charged surface due to the electrostatic repulsion. It is reported that based on the physicochemical circumstance DNA has superior adsorption onto different hydrophilic and hydrophobic, inorganic and organic solid surface because of its surface active characteristic (Chattoraj and Mitra 2009).

DNA is surface active due to its preferential adsorption from solution to different hydrophilic and hydrophobic, inorganic and organic solid surfaces depending upon physicochemical conditions.

Adsorption process is defined by isotherm. The adsorption isotherm is the relationship that shows the distribution of adsorbate between the adsorbed phase and the solution phase at equilibrium. Adsorption isotherms are essential for the description of how adsorbate concentration interacts with adsorbents and are useful in optimizing their use. Therefore, empirical equations are important for adsorption data interpretation and predictions. The Langmuir and Freundlich are the most frequently used models used in data evaluation.

Possible electrostatic and hydrophobic mechanisms for the adsorption of DNA in solutions containing monovalent salt are discussed and compared to the observations in divalent salt (Chattoraj and Mitra 2009). Also other parameters that effect DNA adsorption have been classified as; base composition, ionic strength, pH, DNA chain length, and DNA concentration (Dias and Lindman, 2008).

4.1. Sorption Isotherm Method-Adsorption Equilibria

A wide variety of other adsorption models have been formulated over the years. Freundlich, Langmuir, and Brunauer-Emmett-Teller (BET) are the most useful models figure out adsorption profile despite the fact they are old adsorption models. These fundamental adsorption equation's general equilibrium constants were analyzed on the basis of equilibrium concentration. Langmuir and Freundlich differs in that while Langmuir expression explains monolayer adsorption process Freundlich can explain multilayer adsorption process. BET equation is a theoretical expression of adsorption is commonly used in the gas phase adsorption process for finding the monolayer adsorption capacity of an adsorbent.

The adsorption isotherm is the relationship that shows the distribution of adsorbate between the adsorbed phase and the solution phase at equilibrium. Adsorption isotherms are essential for the description of how adsorbate concentration interacts with adsorbents and are useful in optimizing their use. Therefore, empirical equations are important for the adsorption data, interpretation and predictions.

Langmuir Model:

The Langmuir equation is based on a kinetic approach and assumes a uniform surface, a single layer of adsorbed material at constant temperature. The model is useful when there is no strong specific interaction between the surface and the adsorbate. Thus single adsorbed layer forms and no multi-layer adsorption occurs. It also assumes that the surface is homogeneous (Iqbal and Ashiq 2006) and adsorption energy is constant over all sites. Adsorption occurs at specific homogeneous sites within the adsorbents and there is no interaction between the sorbate molecules that are bound to the next active sites The Langmuir equation has the form:

$$q_e = \frac{Q°bC_e}{1 + bC_e} \qquad (4.1)$$

where q_e is the amount adsorbed at equilibrium, C_e is the equilibrium concentration, b and Q^0 are Langmuir coefficients related to the energy of adsorption and the maximum

adsorption capacity respectively. Langmuir equation can be described by the linearized form as follows:

$$\frac{1}{q_e} = \frac{1}{Q^\circ} + \frac{1}{bQ^\circ C_e}$$ (4.2)

The linear Langmuir plot can be obtained by plotting $1/q_e$ versus $1/C_e$. The coefficients Q° and b can be evaluated from the intercept and slope, respectively.

Freundlich Model:

The Freundlich model is an empirical equation, which assumes that the adsorbent has a heterogeneous surface composed of adsorption sites with different adsorption potentials and energy. The model equation is as follows:

$$q_e = K_f C_e^{1/n}$$ (4.3)

where q_e is amount adsorbed at equilibrium and C_e is the equilibrium concentration. K_f and n are equilibrium constants (temperature dependent) related to adsorption capacity and intensity, respectively. Graphically, a plot of q_e versus C_e gives the adsorption isotherm. The linearized form of Freundlich sorption isotherm is:

$$\log q_e = \log K_f + \frac{1}{n}\log C_e$$ (4.4)

A plot of log q_e versus log C_e gives a linear graph. The coefficients K_f and n can be calculated from the intercept and slope respectively.

The dimension of K_f depends on the value C_e while the exponent "n" is dimensionless. Adsorbent total adsorption capacity increases result as K_f parameter increases. The n value might vary along adsorption process and is related to the adsorption efficiency and also to the energy of adsorption.

Dubinin–Radushkevich model

Dubinin-Radushkevich (D-R) equation is widely used for description of adsorption in microporous materials,where adsorption process follows a pore-filling mechanism. Instead of surface layering, in pore filling mechanism the chemical potential is a function of adsorbed amount. Dubinin-Radushkevich equation can be represented in Equation 4.5 (Do, 1998). This model is based on the assumptions of a change in the potential energy between the adsorbate and adsorbent phases and a characteristic energy of a given solid. Adsorption energy value has a clue about the type of sorption whether it is physical or chemical.

The linear plot of ln qe versus ε^2 are used to define sorption energy constant (K) and maximum adsorption capacity based on D–R isotherm (qm), respectively. Then adsorption energy (E) is obtained by the use of sorption energy constant with Equation 4.7. Units of the isotherm formula parameters are Ce (ng/µL), qm is the maximum adsorption capacity based on D–R isotherm (µg/g) and K is the constant related to the sorption energy (mol^2/kJ^2) therefore E has kJ/mol unit. If the this value is lover than 8 kJ/mol adsorption is defined physical. Between the value of 8 to 16 kJ/mol sorption is chemicaly controlled (Erdoğan and Ulkü 2012).

$$q_e = q_m e^{\left(-K\varepsilon^2\right)} \tag{4.5}$$

$$\varepsilon = RT\left(1 + \frac{1}{C_e}\right) \tag{4.6}$$

$$E = \frac{1}{\sqrt{2K}} \tag{4.7}$$

,

where ε is Polanyi potential, R is the gas constant (8.314×10^{-3} kJ/mol K) and T is the temperature (K),where E is the mean adsorption energy (kJ/mol)

4.2. Sorption Kinetic Models-Adsorption Kinetic

Adsorption is one of the most widely used techniques to remove of pollutants from contaminated media or required substance in solution. Several system variables should be considered. For instance initial concentration, sorbent particle size, solution temperature, solution pH and agitation have a greater effect on the sorption of solutes in reaction controlled sorption processes. As a result the correlation coefficients between experimental and theoretical data will provide the 'best fit' model. Some kinetic models are involved adsorption reaction models reaction; the pseudo first-order equation, the pseudo second-order equation or diffusion model; the Elovich equation and intraparticle diffusion model.

Sorption rate is described by three main series of resistances due to external mass transfer, intraparticle diffusion and reaction. The first one occurs through transport of adsorbate molecules from the bulk solution to the adsorbent external surface. The second is the diffusion of the adsorbate from the external surface into the pores of the adsorbent. Figure 4. 2 shows the adsorption kinetics steps, which effect adsorption phenomena.
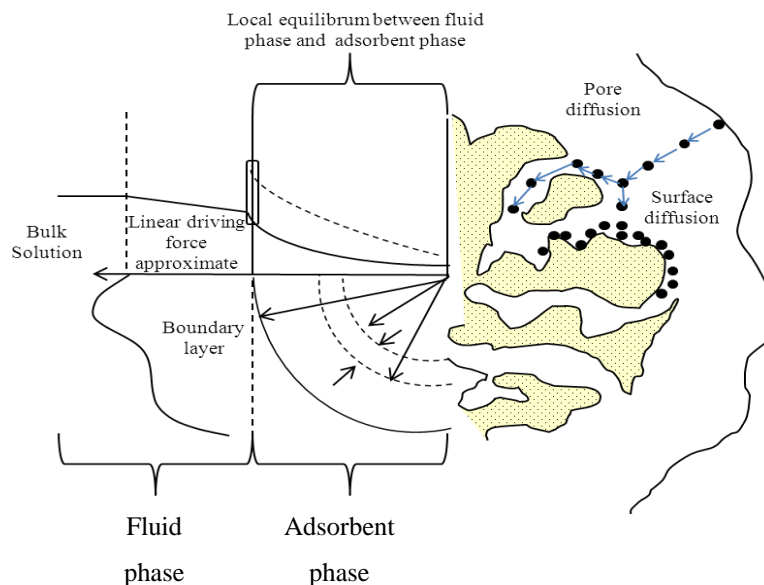
Figure 4. 2. Adsorption kinetic steps.

When adsorption is performed, thermodynamic and kinetic parts should be involved to get more details about its performance and mechanisms (Qiu et al., 2009). To determine the kinetic performance of a given adsorbent has great significance for the small application as much as adsorption capacity of used adsorbent. The cost and performance of a product or the mode of application are the concerns in controlling the efficiency of this process. Therefore the sorption capacity and required contact time are the two most important parameters.

Adsorption is not only to remove substance from solution but also is a fundamental parts of a reaction mechanism. Reaction mechanism requires the adsorption of each reactant on the catalysis surface. Therefore adsorption kinetic is important. Chemical kinetics is a useful way of describing the reaction pathway and time needed to reach equilibrium. In other words in kinetics analysis, the solute uptake rate, which determines the residence time required for completion of adsorption reaction, may be established. The dependence of the sorption kinetics on the physical and chemical characteristics of the adsorbent is obvious and affects the mechanism. Numerous studies were carried out in formulating a general expression to analyze the kinetics of adsorption on solid surfaces for the liquid-solid adsorption system. Adsorption rate covers a series of resistance resulted from diffusion and reaction steps

4.2.1 Reaction Models:

The Pseudo First-Order Equation

Scientists have proposed mathematical models to describe adsorption data, which can generally be classified as adsorption reaction models and adsorption diffusion models. In 1898, Lagergren presented the first order rate equation for the adsorption of ocalic acid and malonic acid onto charcoal (Lagergren, 1898). Lagergren kinetics equation may have been the first one in describing the adsorption of liquid-solid systems based on solid capacity. Lagergren rate equation is one of the most widely used sorption rate equations for the sorption of a solute from a liquid solution. It is represented (Ho and Mckay 1999) in the following formula.

$$\frac{dq_t}{dt} = k(q_e - q_t) \qquad (4.8)$$

where: q_t is the adsorption capacity at time "t", q_e is the adsorption capacity at equilibrium and k_l is the rate constant of pseudo first-order adsorption.

It can be linearized after taking integration and applying boundary conditions for t = 0 to t = t. The integrated form becomes:

$$\log(q_e - q_t) = \log(q_e) - \frac{k_l}{2.303}t \qquad (4.9)$$

When the log $(q_e - q_t)$ versus t plot is drawn, the slope gives the $k_l/2.303$ and the intercept gives the log q_e. This model assumes that the rate of change of adsorbate uptake with time is related to the difference in saturation concentration and the amount of solid uptake with time (Erdoğan and Ülkü 2012).

The Pseudo Second-Order Equation

A pseudo second-order model describing the adsorbtion kinetic may be expressed in the following form;

$$\frac{dq}{dt} = K_2(q_e - q)^2 \qquad (4.10)$$

where, q_e: adsorbate amount per unit weight of adsorbent amount at equilibrium, K_2: the rate constant of pseudo second-order adsorptionIt can be linearized by taking integration and applying the initial conditions.

$$\frac{t}{q} = \frac{1}{K_2 q_e^2} + \frac{1}{q_e}t \qquad (4.11)$$

If t/q vs. t is plotted, slope gives the $1/q_e$ and the intercept gives the $1/K_2q_e^2$. This model assumes that the sorption process is a pseudo-chemical reaction process. The driving force is difference between the average solid concentration and the equilibrium concentration. Also the overall sorption rate is proportional to the square of the driving force (Erdoğan and Ülkü 2012).

4.2.2. Diffusion Models

Adsorption and desorption rate in porous material is generally defined transport within the pore structure rather than surface kinetic (Ruthven, 1984). Diffusion models derived from Fick's law of mass transport as represented in equation (4.12). It is important that in this equation mass transport not only depends on concentration. Because it is known that for any transport mechanism true driving force gradient of the chemical potential (μ). The adsorption process only be independent of the adsorbate concentration in case of thermodynamically ideal system (Ruthven, 1984))

$$F = -D\frac{\partial C}{\partial x} \tag{4.12}$$

Adsorption process includes fluid film diffusion, intraparticular diffusion and mass action. Mass action can be neglected because of high rate for kinetic study in physisorption processes. Consequently, adsorption process is predominantly controlled by film diffusion or intraparticular diffusion.

Adsorption kinetics is described by many models: The two-resistance models such as the film-solid model, the film-pore model and the branched pore model, give detailed analysis of the adsorption dynamics.

Distinction of kinetic and diffusion control mechanism generally is not simple. It is a general idea that if system reaches equilibrium within three hours, the process is usually kinetic controlled. If process takes place above 24 hours it is diffusion controlled. Either diffusion or kinetic control adsorption equilibria when the duration of the process between 3 to 24 hours. A more suitable quantitative approach to distinguishing between kinetic and diffusion rate control can be performed by the square root of contact time analysis according to equation

However, these models include complex partial differential equations solution and their solution needs computer programs aid and extensive computer time (Malash and El-Khaiary 2010). Mathews and Webber (1976) intraparticle-diffusion models are the two most widely used models for studying the mechanism of the adsorption without complex solution and computer program.

External mass transfer-Mathew–Weber Model.

This model assumes that only external film diffusion is the driving force main during the initial sorption period and controls the sorption process. In other words the film diffusion controls the adsorbate uptake rate in the initial stages, followed by particle diffusion in the latter stages. The model equation is given formula in equation 4.13.

$$\ln \frac{C_t}{C_0} = -k_f St \tag{4.13}$$

where C_t is the concentration of adsorbate in the solution at time t, C_0 is the initial concentration of adsorbet in the solution, k_f is the external mass transfer coefficient (m/s), t is the time, S is the surface area for mass transfer (m^{-1}). The initial slope of the linear plot of $\ln C_t$ /C_0 versus t is used in the determination of the external mass transfer coefficient (k_f).

Intraparticle diffusion-Weber–Morris Model.

This model was derived from the Fick's second law. According to this the effects of the external mass transfer resistance can be ignored, the direction of the diffusion is radial and the intraparticle diffusivity is constant. This model was used to calculate the intraparticle diffusion rate constant. The model equation is given below

$$q_t = k_d t^{0.5} \tag{4.14}$$

A plot of the amount of adsorbed, qt, against the square root of time, $t^{0.5}$, gives a straight line plot of slope k_d, a diffusional rate parameter. This straight line, passing through the origin, indicates intraparticle diffusion control (Ho et al.,2000). It can be seen from eqn. (4.14) that if intraparticle-diffusion is the rate limiting step, then a plot of q versus t $^{0.5}$ will give a straight line with a slope that equals k_d and an intercept equal to zero.

$$\frac{q_t}{q_0} = \frac{6}{\sqrt{\pi}} \left(\frac{D_t}{r^2} \right)^{1/2} \tag{4.15}$$

Micropore Diffusion

For a spherical particle at constant surface concentration for short time and long time periods can be written in Equation 4.16. and Equation 4.18 respectively. Definition of the formula of Equation 4.18 comes from derivation of Equation 4.17

$$\frac{m_t}{m_\infty} = 6\left(\frac{D_t}{r^2}\right)^{1/2}\left[\frac{1}{\sqrt{\pi}} + 2\sum_{n=1}^{\infty} ierfc\left(\frac{nr_c}{\sqrt{D_c t}}\right) - 3\frac{D_c t}{r_c^2}\right] \tag{4.16}$$

$$\frac{\partial_q}{\partial_t} = D\left[\frac{\partial^2 q}{\partial r^2} + \frac{2}{r}\frac{\partial q}{\partial r}\right] \tag{4.17}$$

$$\frac{m_t}{m_\infty} = 1 - \frac{6}{\pi^2}\exp\left[-\frac{\pi^2 D_c t}{r_c^2}\right] \tag{4.18}$$

In literature a variety of studies focused on developing a formula to be used in analyzing the kinetics of adsorption on solid surface. To identify the exact mechanism it is necessary to carry out experiments. Therefore to determine DNA adsorption kinetics requires adsorption experiments.

DNA adsorption onto silica coated natural organic matter (NOM) surface kinetic was found 120 mg/dm^3 supercoiled and the linear plasmid DNA by QCM-D Chen and Nyugen (2007). Their result also revealed that adsorption took place within 20 for Ca and 40 minutes for Mg^{2+} cations. Just 7 mM Na$^+$ ion positively affects DNA adsorption capacity both divalent cations present. They concluded that adsorption was mainly controlled by specific bridging between the DNA phosphate groups and NOM carboxyl groups. Additionally same group was report that kinetics of DNA adsorption to NOM-coated silica surfaces depend on ionic strength and that DNA adsorption is significant at moderately high ionic strength (Nguyen and Elimelech, 2007). Adsorption kinetic measurements were performed by quartz crystal microbalance device which is sensitive for any little change the amount mass.

DNA adsorption kinetics model was reported by Vandeventer et al (2012) onto silica surface. Their model schematic representation can be seen in Figure 4.3. According to the study, DNA can loosely or tightly bound to available silica surface sites.
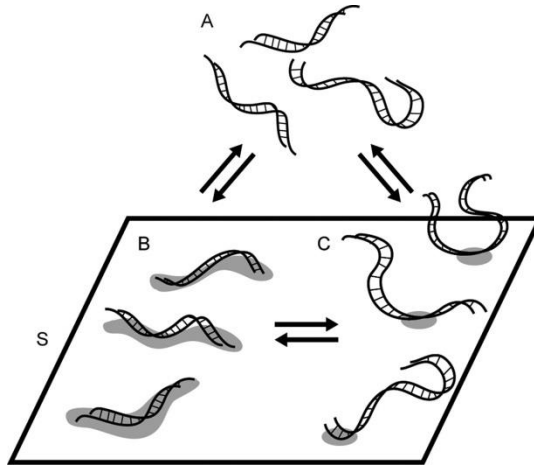
Figure 4.3 Kinetic model representation of DNA adsorption to Silica
(Source: Vandeventer et al.2012 Reuse with the permission)

"A" represents bulk DNA in solution, and "S" denotes the available surface binding sites. "B" and "C" represent DNA tightly and loosely bound to the surface through multiple binding sites or a single binding site, respectively. Assumed adsorption pathway is given in equations from 4.19 to 4.21.

$$A+nS \underset{k_2}{\overset{k_1}{\rightleftharpoons}} B \tag{4.19}$$

$$B \underset{k_4}{\overset{k_3}{\rightleftharpoons}} C+(n- \tag{4.20}$$

$$A+S \underset{k_6}{\overset{k_5}{\rightleftharpoons}} C \tag{4.21}$$
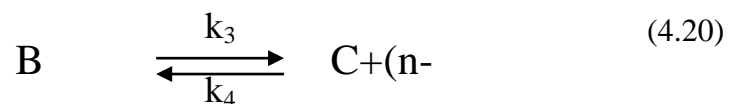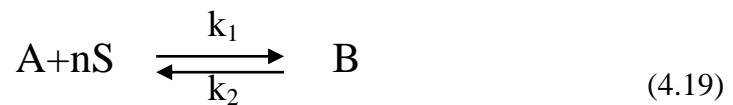
Experiments were performed with Sigma Aldrich silica particles and MagPrep silica particles (MagPrep silica particles (70912) from Merck) as a function of time by using different buffer solution at pH 5 such as in 6 M sodium perchlorate (SP), acetic acid containing 400 mM K+ (AA), glycine containing 400 mM KCl (GL), or sodium citrate containing 400 mM KCl

MagPrep beads and Sigma Aldrich silica particle were used different amounts. 250 µg magnetic beads loaded tubes were filled with 100 ng/µL salmon sperm DNA in 150 µL of the buffer under investigation. Aldrich silica was used 3-6 mg amount 200 ng/µL salmon sperm DNA for experiments using SP buffer or 80 ng/µL for all other buffers. Figure 4. 4 (a) represents DNA adsorbed by silica (mass per unit area) at pH 5 with different buffer solution (grey: MagPrep,white: Sigma Aldrich silica particles). Sodium perclorate buffer solution has great effect on DNA adsorption both two type silica material. It is obvious because the MagPrep particles have been optimized for DNA extraction and may have additional surface modifications. Nevertheless magnetic bead and silica particle show the same trend with respect to buffer type. On the other hand the same figure indicated that buffer ions play a role in the DNA adsorption process further than simply adjusting the pH.

(a)   (b)
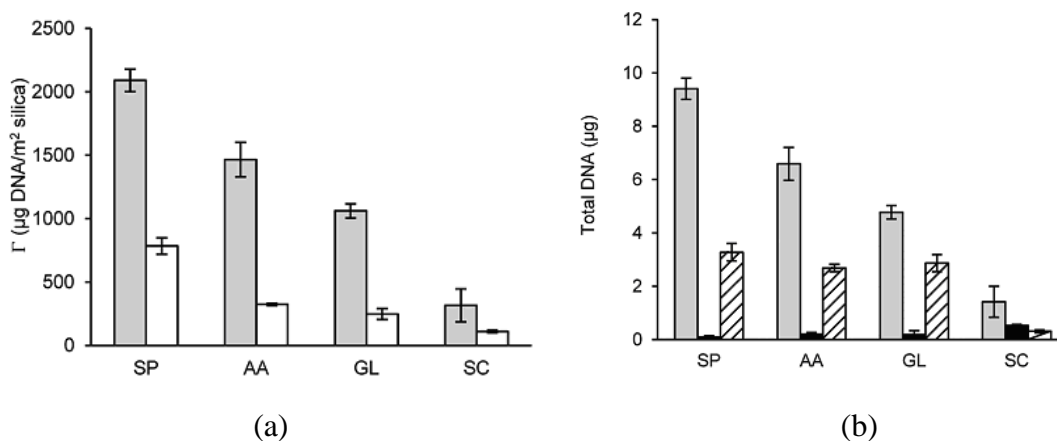
Figure 4. 4. (a) DNA adsorbed to silica (mass per unit area) at pH 5 (b) Total DNA adsorbed to 250 µg of MagPrep Silica particles as a function of buffer (gray);

CHAPTER 5

DNA IMAGE ON SOLID SURFACES BY ATOMIC FORCE MICROSCOPY (AFM)

5.1. Atomic Force Microscopy (AFM)

High resolution imaging by atomic force microscopy (AFM) of biomolecules such as DNA, proteins or cell membranes has been the main motivations of biological research. It is well known that scanning tunneling microscopy (STM) has inspired AFM because of its limitation. STM is just available for conducting materials not insulators and biomolecules. AFM imaging lets perform single-molecule experiments with DNA and proteins that helping us answer questions about biological function that would be difficult or impossible to address in bulk experiment. Single and double stranded DNA and DNA protein complex DNA condensation for gene therapy, single-molecule mechanics, and DNA-protein interaction Yaneva et al., 1997, Kasas et. al., 1997, van Noort et al., 1998 are the some of the study subjected biomolecules with AFM. Because of its essential role in biology DNA has been studied extensively by AFM. Understanding the mechanisms of DNA replication and transcription again AFM is addressed (Klinov et al.2007).

Atomic force microscope (AFM) was discovered by Binnig et al in 1986. This device could be addressed only to conductive or semi–conductive materials. This technique is now widely used since it does not require conductive specimens and it is suitable for almost all kind of surfaces. One of the main advantages of AFM over other ultra-high resolution microscopy techniques (e.g. SEM , TEM) is that sample preparation is relatively simple and does not involve casting with a metal coating (as required for electron microscopy), hence AFM measurements can be made to reflect directly the natural surface of the specimen. Another advantage of AFM over SEM is that a sample can be prepared without staining the DNA. Moreover, rinsing with water and drying the sample can be avoided by imaging in solution.

The main difficulty of AFM imaging is that this technique requires perfect surface cleaning Perfect sample preparation is required, which can influence the sample image under air or liquid.

AFM becomes powerful tool understand surface morphology and surface properties. Depending on the situation, forces that are measured in AFM include mechanical contact force, Van der Waals forces, capillary forces, chemical bonding, electrostatic forces which are classified into long-range forces and short range forces.

After invention of this technique high resolution images of DNA, proteins and polymers have been obtained in air and liquids (Anselmetti et al.,1994, Bustamante and Keller 1995, Möller et al., 1999, Paulo and Gacia 2000) Most importantly, biological structures can be observed in their original form in buffer solution. The ability of microorganisms to attach to solid substrates by means of extracellular polymeric substances may also be exploited for AFM studies, but the resolution remains limited Atomic force microscopy (AFM) provides a means to image many biological structures.

AFM instrument is included three essentially parts: A piezoelectric scanner, a probe which consist of very sharp tip (that could ends with only few atoms), an electronic system consisting of a computer that records signals and sets up the parameters for the experiments and a controller that is able to detect signals from the microscope, allows for the movement of the sample, and realize the feedback.

The probe (tip) interacts physically with the sample. This provides information about the topography and the mechanical properties of the surface. There are two materials commonly used for AFM cantilevers: silicon nitride ($Si_3 N_4$) and silicon (Si) (Eaton and West, 2010)
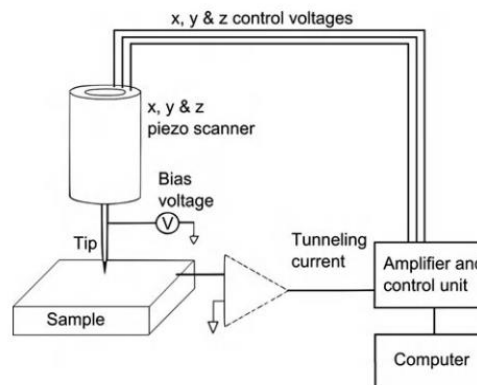
Figure 5. 1. Simplified schematic of a scanning tunnelling microscope
(Source: Eaton and West 2010)

The deflection of the cantilever Δx is proportional to the force acting on the tip, via Hook's law is represented in Equation (5.1) where k is the spring constant of the cantilever.

$$F = -k.\Delta x \qquad (5.1)$$

The AFM can operate in a number of modes, depending on the application. The choice of mode depends on the nature of the sample of interest and the degree of the clearness of the image is required. In general, possible imaging modes are divided into two parts: static (also called contact) modes and a variety of dynamic (tapping) mode. Contact mode imaging is so called because the tip remains in contact with the sample at during measurement. As a result, the probe–sample interaction occurs in the repulsive regime as illustrated in Figure 5. 2. Consequently the sample and the tip interactions are illustrated in Figure 5. 3.
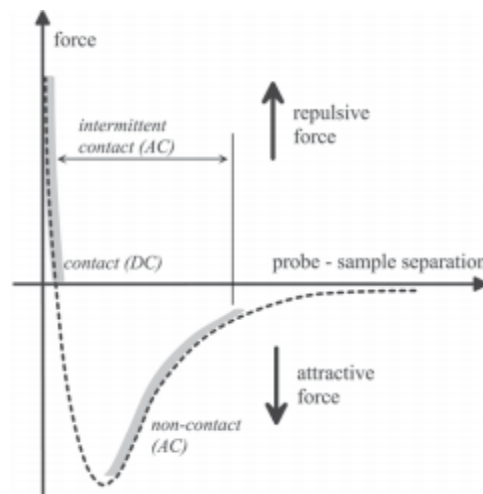
Figure 5. 2. Idealized plot of the forces between tip and sample, highlighting where typical imaging modes are operative. (Source: Ricci and Braga 2004)

In other words, in contact-mode AFM, the tip is always touching the sample. The followings are the important requirements for contact-mode:

➢ Because of the repulsive force between tip and the sample, the sample may be damaged or surface properties can be changed by the scanning process

- On the other hand, the tip could also be damaged or changed by the scanning process.
- For the period of contact between the tip and the sample surface of the sample may affect by tip as mentioned. Therefore technique can be sensitive to the nature of the sample. Operating modes some properties were listen in Table 5. 1

In tapping mode, tip–sample interactions are very small and good vertical resolution can be obtained, but lateral resolution is lower than in other mode. The greatest disadvantage is that it cannot be used in liquid environment, just only for dry samples (Ricci and Braga 2004). However tapping mode is useful mode which does not destroy the molecules even after several scans (Delain et al., 1992)
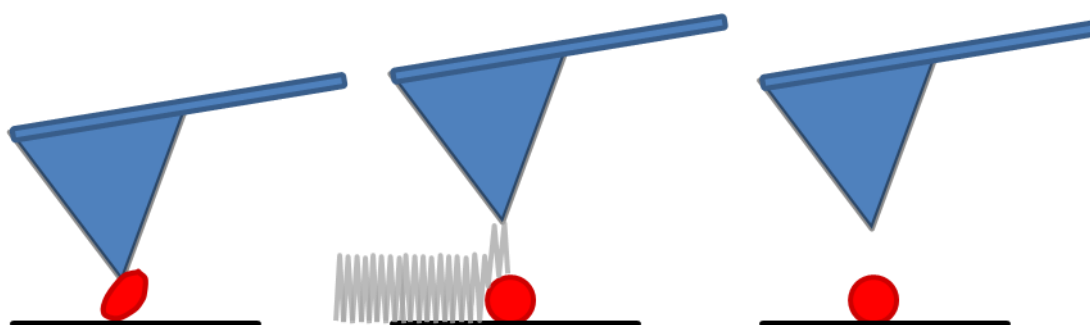
Figure 5. 3. Operating modes of AFM a) Contact b) Tapping c) Non-contact modes

Table 5. 1 Properties of the different operation modes in AFM.
(Source Clemente and Gloystein 2008)

	Operation modes		
	Contact	**Tapping**	**Non-contact**
tip loading force	low → high	low	low
contact with sample surface	yes	periodical	no
manipulation of sample	yes	yes	no
contamination of AFM tip	yes	yes	no

Tip is the heart of the device. Its relation between surfaces defines every detail on image procedure. As tip and surface come close to each other, attractive van der Waals interactions begin to force the probe to the surface. During this contact, the net interaction becomes repulsive as electron shells in atoms in the opposing surfaces repel each other. In Figure 5. 2. , the repulsive forces are shown as being positive and attractive forces negative. From a physical point of view, it is possible to make a distinction between the two modes depending on the sign of the forces involved in the interaction between tip and sample, that is might be attractive or repulsive.

5.2. Substrates Used in AFM Experiments

Preparing samples for AFM supported material seems to be not important but if it has an interaction with sample it would change everything. Therefore, it is important for acceptable sample preparation due to good results. This is particularly important for high-resolution work, and looking at individual molecules in particular, for which an atomically flat substrate is usually required. The first problem is choice a suitable substrate (Eaton and West 2010).

To be able to examine biological structures in their original form, these must be well attached to a solid substrate to resist the forces applied by the scanning tip. Smoot surface is the condition for sample holder. Glass silicon oxide mica and silicon wafers (Lyubchenko et al., 2011) have been proved to be excellent substrates.

Muscovite mica, $KAl_2 (OH)_2AlSi_3O_{10}$ is a nonconducting layered mineral offer excellent property being substrate. The mica surface has silicon, oxygen, and aluminum atoms surrounding hydroxyl groups that are near below the surface (Hansma et al., 1996).

Mica is the most frequently used substrate for imaging biological specimens, including double-stranded DNA, DNA–protein complexes, protein arrays, densely packed proteins, supported lipid films and animal cells. Because mica can be easily prepared for imaging by cleaving the top layer off with tape. It is atomically flat, clean after cleavage, easy to cut to desire sizes, relatively inexpensive, negatively charged and can be modified to make the surface positive. Mica is useful as an AFM substrate because it is atomically flat, with a layer height of 0.37 ± 0.02 nm (Xu et al., 2010). Washing can be made in concentrated acidic solution followed by ultrasonication in

water solutions. On the other hand Delain and coworkers concluded that mica pretreatment, both soaking in $MgCl_2$, ultrasonic cleaning, washing or the use of a glow-discharge, was considered unnecessary for the binding of DNA onto the mica surface (Delain et al 1992).

Mica, glass can also be modified with silane molecules, bringing new chemical functions at the surface for further covalent modification. Silanization is the famous name of modification. Alternatively, various substrates have been reacted with 3-aminopropyltriethoxysilane (APTES) to generate quarternary amines to which DNA could be bound efficiently to be imaged in air, propanol, and water (Lyubchenko et al., 1993). Also "*cationic liposome*" was used by Safinya et al (1998). This material is mainly used for gene therapy applications and has two main advantages. The first one cationic liposome is known to have similar characteristics of viruses by being efficient chemical carriers of genes (DNA sections) for delivery in cells the second is they are models of studies of DNA condensation phases in two dimensions.

5.3. Imaging Media

AFM can be worked under air or aqueous media. In order to eliminate capillary forces and also to reduce the effect of surface forces, biological sample analysis is carried out generally under liquid condition. There are two reasons. The first is that the force applied by the tip to the surface can be decreased by a factor of 10-100 compared to the force applied in air as the meniscus force is not present (Weisenhorn et al., 1989). The second, for many applications, water is the natural environment. Biological materials for instance often denature if not kept in electrolyte solution. However media serves additional interaction also most biological sample become mobile in presence of water.

Hansma is focus on DNA imaging by atomic force microscopy. According to her about 15% of published articles on AFM of DNA explain studies involving imaging under aqueous solutions (Hansma H.G., 2001). As a result image DNA under air is common. Nevertheless it is not simulated the normal condition of DNA native form.

Table 5. 2. Average superhelix dimensions of p1868 plasmid
(Source :Rippe et al 1997)

	Air	Water	Air&Water
Length of superhelix axis (nm)	246 ± 23	252 ± 22	249 ± 23
Number of nodes n	4.7 ± 1.9	3.7 ± 1.3	4.2 ± 1.7
Number of end loops "E"	2.0 ± 0.0	2.0 ± 0.0	2.0 ± 0.0
Superhelix radius "r" (nm)	11.6 ± 4.4	13.6 ± 4.5	12.5 ± 4.7
Superhelix diameter "D" (nm)	26 ±9	30± 9	27 ± 9
Interstrand distance "z" (nm)	21 ± 9	25± 9	23 ± 9
Superhelix pitch "P" (nm)	95 ± 45	122 ± 54	107 ± 51
Pitch angle α (degree)	52 ± 8	55± 8	54 ± 8

If consider imaging in aqueous media scan rate become important parameter. Since the DNA molecules are highly mobile AFM images resolution is generally fuzzy. To be able to observe moving DNA appropriately at a high scan rate can be adapted, but it is not an easy charge. It is essential to select appropriate vibration frequency of the cantilever for successfully imaging biomolecules in liquid Scan rate should be enough to sense the topography and to allow the z feedback of the AFM. Furthermore, the scan rate is limited by the piezotube time response and/or the resonance frequency of the AFM cantilever (Pastre´et al., 2005). Liquid environment provides strong and higher friction rate than image under air condition. This is a crucial if DNA/ligand complexes is subjected since strong friction for imaging is favorable, which will be discussed in imaging DNA part.

On the other hand it is reported that when DNA is dried onto mica, the amount of DNA bound to the mica is considerably higher while the DNA solution contains salts of a divalent or other multivalent inorganic cation, as compared with DNA in water (Hansma et al., 1996). Spermidine is one of the multivalent cation. It is a chemical that has polyamine bonds and thus used as fixation agents for AFM (Hamon et al., 2007). Although at submillimolar concentration, spermidine can persuade a strong DNA adsorption and can still be effective at high NaCl concentration (up to 300 mM).

5.4 Sample Drying

Biomaterial containing solution is generally transferred on to AFM substrate as a drop. Some surface dynamic and different types of dissolved molecules play role on it. Fang et al. (2006) were studied evaporation kinetics of droplets containing DNA, as a function of DNA concentration by confocal fluorescence microscopy at 25°C 36 ±2% humidity. Volume size of the sample was 2 µl of 1xTE buffer (10 mM Tris, 1 mM EDTA) drops containing 0.5, 25 and 500 µg/ cm^3 λ-DNA. Figure 5. 4. is displays their findings.
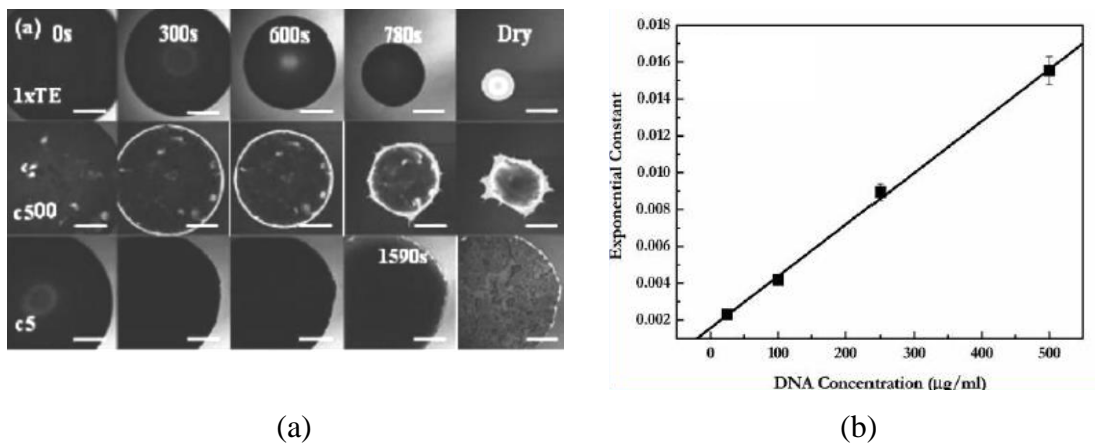

(a)   (b)

Figure 5. 4. (a) Top view confocal images of 2 µL drops evaporating on OTS at 25 °C and 1 atm. The scale bar on the images represents 400 µm. (b) The ring intensity exponential constant for drops with different DNA concentrations (with the permission)

As a result DNA concentration effect on drying kinetics was revealed. Results show that the concentrated DNA is localized at the edges (c500). This is called "coffee ring effect"

Investigated sample can be dried by different methods such as under air, nitrogen flow regime by forced mass transfer, freeze drying procedures under vacuum condition. Drying under ambient condition is the easy and chosen way for preparation of AFM sample for tapping and contact modes.

Surface-tension can be reduced by freeze-drying in vacuum, a technique often applied in electron microscopy. Freeze-dried biomacromolecules samples keep their hydration layer so they remain stable but at end of the drying they do not affect ambient pressure directly. Freeze-drying is certainly the best procedure for dehydrating

biomacromolecules, freeze-dried samples have to be stabilized for observation at ambient pressure (Engel A, 1991).

Samples are generally immobilized onto surface when imaged under air, because sample is dried with substrate. If not it would have some problems. AFM working principle is includes atomic level interactions such aselectrical and van Der Walls.

It is reported that air-dried supramolecular structures covering the surface orderly might be distorted except DNA or the bacterial hexagonally packed intermediate (HPI) layer (Engel A., 1991). They keep their native 3D structure extraordinarily during dehydration in air.

Generally a sample is investigated in drop size onto the proper surface in tapping mode. It is very important that dropped sample must be dried completely to prevent the AFM tip from any sticking problem. Therefore the immobilization of the sample on a suitable substrate is an indispensable requirement for AFM analysis.

For instance Fang et al were investigated evaporation kinetics of droplets containing DNA as a function of DNA concentration (2006). According to their report drop size drying of complex molecules DNA, proteins and long chain polymers might be more complex than expected because structure of the molecules in the drop can be affected by the salt concentration, the self-organization with other molecules or the surface interaction.

5.5. Imaging DNA

Adsorption of DNA on particulate surfaces could be explained by examining morphology of DNA on flat surfaces by AFM Recent explanations of the semiconducting properties of DNA molecules propose that they may be used for the nano-electronic devices in the future. DNA has been considered as a highly specific functional material for electric conductive material and for network fabrication (Brun and Hariman 1992; Murphy et al., 1993; Tabata et al., 2003).

The first reliable AFM imaging of long DNA molecules was made in the laboratory of Bustamante (Bustamante et al., 1992). In this approach, the mica surface was treated with Mg^{2+} to increase the affinity of negatively charged mica surface to DNA. As a result, the DNA molecules were held in place strongly enough to permit reliable imaging by AFM. Later studies showed that metal cations such as Co^{2+}, La^{3+},

and Zr [4+] can be used for mica pretreatment to obtain images of DNA (Thundat et al., 1992). Other experiments showed that pretreatment of mica with cations is not necessary (Bezanilla et al., 1995; Bustamante and Rivetti, 1996; Hansma and Laney 1996). However adsorption of the DNA is not clearly understood, concerning the respective role of divalent and monovalent ions concentrations and the effect of mica pretreatment by various cations.

Surprisingly, one of the commonly used substrates for AFM imaging of DNA or RNA is negatively charged mica (Thunante and Rivetti 1996, Hansma and Laney 1996). Since DNA is normally negatively charged due to its phosphate groups in the backbone. Divalent cations are used to link them to the negatively charged mica surface. It was found that DNA could tightly bind to mica with suitable solution concentrations of Ni^{+2} and, Co^{2+}, or Zn^{2+} ions. Mica has been determined to be a very good substrate for imaging DNA in that it is extremely flat (on the scale of the DNA molecule) and DNA binds to it in common buffer solutions (Allen, 1997).

Adsorption on mica surface was investigated based on diffusion of the DNA by Pastre´et al.(2005). They have estimated DNA bonding is effected Rouse dynamic which was described by Maier and Radler before (2000)

$$D = \frac{k_b T}{\zeta N} \qquad (5.2)$$

where ζ is the friction, N is the number of DNA bp, and $k_b T$ is the thermal energy. Previously the self-diffusion constant of free linear DNA in buffer solution was reported as D=10[-12] m²/s for a 1,444 bp DNA (Smite et al. 1996). According to rouse dynamic formulated in Eqn (5.2) the measured friction ζ per bp for the molecules on cationic membrane was about 8.310[-11] Ns/m giving D= 3.10[-14] m²/s for a 1,.440 bp "freely" moving DNA molecule. This is a hydrodynamic consideration observed for cationic membranes, which is not enough in the case of divalent cation presence. Cations cause higher friction comes from electronic interaction between DNA and mica. Diffusion is carried out by jumping of divalent cation available on mica from one site to one other.

E_{move} is assumed the energy barrier required to induce one "jump" of a divalent counterion.

$$E_{Barrier} = \left(n - n^{'}\right)E_{Move} \qquad (5.3)$$

$$E_{Move} = k_b T\left[\frac{l_b}{d}e^{-d/\lambda_D} - \frac{4l_b}{\sqrt{d^2+b^2}}e^{-\left(\sqrt{d^2+b^{2/\lambda_D}}\right)} + \frac{4l_b}{\sqrt{d^2+b^2}}e^{-\left(\sqrt{d^2+b^{2/\lambda_D}}\right)}...\right] \qquad (5.4)$$

$$E_{Barrier} = \left(n-n^{'}\right)k_b T\left[\frac{l_b}{d}e^{-d/\lambda_D} - \frac{4l_b}{\sqrt{d^2+b^2}}e^{-\left(\sqrt{d^2+b^{2/\lambda_D}}\right)} + \frac{4l_b}{\sqrt{d^2+b^2}}e^{-\left(\sqrt{d^2+b^{2/\lambda_D}}\right)}...\right] \qquad (5.5)$$

where l_b is reported the Bjerrum length known as the distance which the electrostatic energy of two elementary charges is equal to $k_B T$, b is distance of separation between two mica sites (about 1 nm), and λ_D (in nanometers) is the Debye length that depends on the ionic strength "I" which is given in equation (5.6).

Equation (5.5) explains the diffusion is enhanced by a high ionic strength; λ_D is inversely proportional with, ionic strength. This consideration was proved y Pie´trement et al. in 2003.

$$\lambda_D = \frac{0.33}{\sqrt{I}} \qquad (5.6)$$

$$D = D_0 e^{\left(-E_{barrier}/k_b T\right)} \qquad (5.7)$$

$$D = D_0 e^{-\left(n-n^{'}\right)\left(E_{barrier}/k_b T\right)} \qquad (5.8)$$

Relation between $E_{Barrier}$ and friction can be generated by equaling Eqn (5.2) and Eqn (5.8), which is represented below.

$$D = D_0 e^{(-E_{barrier}/k_b T)} = \frac{k_b T}{\zeta N} \tag{5.9}$$

Additionally diffusion was related to the number of divalent cations per base pairs that participate to the counterion correlations (n − nⁱ) (Pastre´et al.2005). Therefore theoretical and experimental evidence are consistent to those transition metal cations (Ni $^{2+}$, Cu $^{2+}$. . .), for which DNA molecules bind strongly to mica.

Nevertheless, other divalent metal ions such as Mg^{2+}, Ca^{2+}, Cd^{2+}, or Hg^{2+} cannot bind DNA to mica tightly or cannot bind DNA (Hansma and Laney 1996) They provided a reasonable explanation for these observations. The ions with large ionic radii cannot fit into the mica cavities and therefore cannot bind DNA to mica. Namely the divalent metal ions react with the hydroxyl groups in the ''cavities'' of mica surface. However, narrow ionic strength conditions are often required for adsorption, suggesting a more complex mechanism. Also the adsorption of plasmid DNA molecules onto untreated cleaved mica instead of treated one, from a solution containing Mg^{2+} or Ca^{2+} was identified as easy and repeatable (Delain et al., 1992).

Feng et al (2008) reported that four single strands of calf thymus DNA were self-assembled to a network structure having 2.2 ± 0.01 nm height on mica surface in 2008.
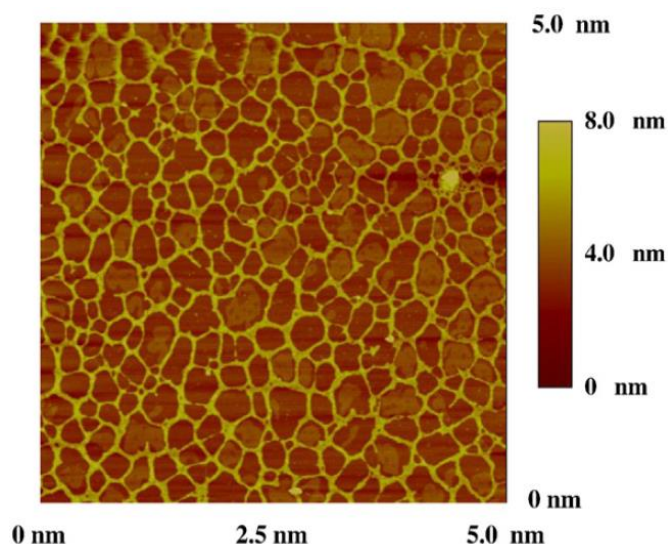
Figure 5. 5. AFM images of DNA networks adsorbed on mica surface from 100 ng DNA/µL solution (Source: Feng et al., 2008, reproduced with permission)

This study aims at imaging highly polymerized calf thymus DNA in air media on bare mica substrates that were not surface functionalized in order to elucidate the effect of the immersion time in water to mechanism of adsorption of DNA on particulate surfaces. Figure 5. 5 displays studied calf thymus DNA networks on mica surface. According to Figure 5. 6 AFM images of DNA molecules obtained at various developing times in water after the preadsorbed DNA network structure mica plate (Figure 5. 5) was dipped into the water. According to this study immersion time is effected transitions from network structure to rod like structure, and to stretched wormlike coil. In Table 5. 3 the studies related with DNA imaging by AFM were listed.
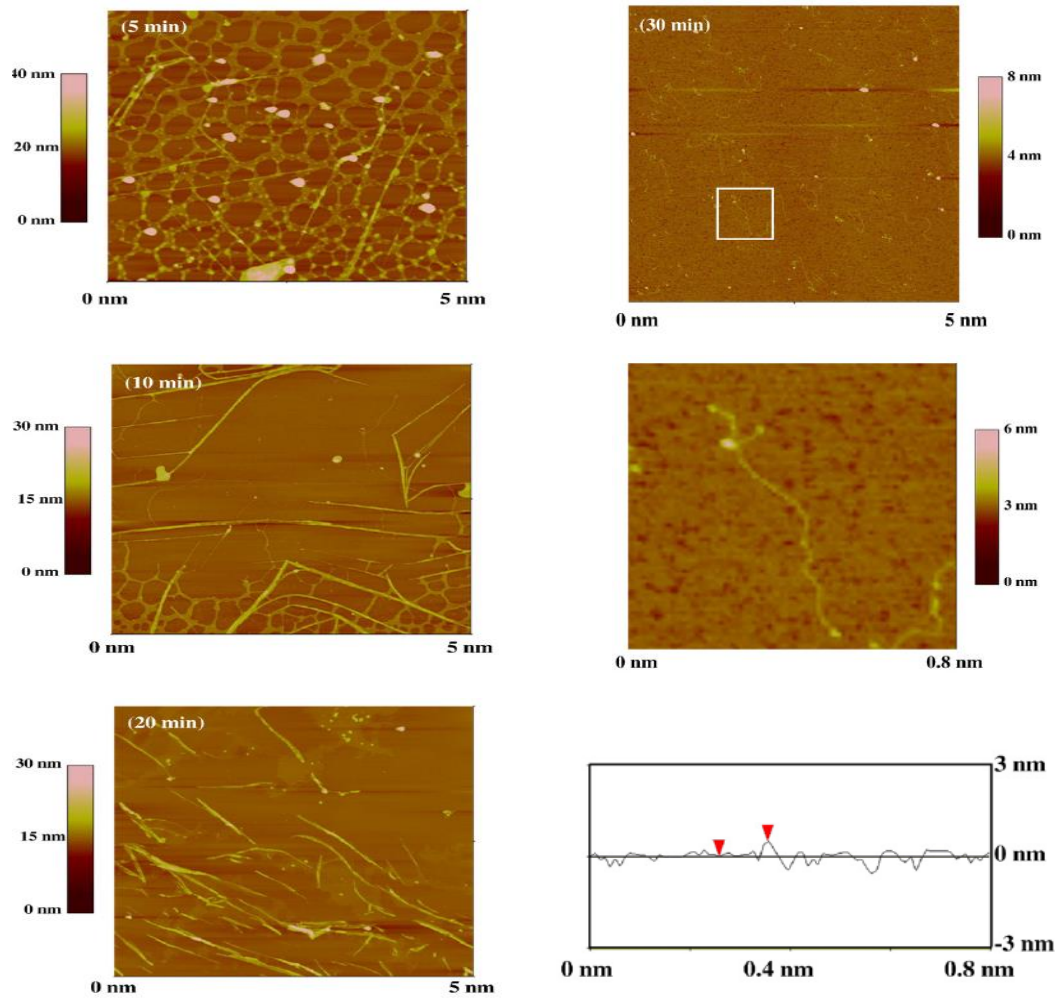
Figure 5. 6. DNA molecules adsorbed on mica surface by dipping into the water for 5, 10, 20, 30 min; higher resolution image of the sample dipped for 30 min and cross section analysis of a segment containing a DNA strand (Source: Feng et al.,2008 reproduced with permission) .

Table 5. 3 Literature Search about DNA Imaging by AFM generally on Tapping mode

Reference	DNA Type	Conc.	Buffer	Substrate	Sample size	Modification	Drying method	Media	*RH %	Scan Rate&Tip
Bustamante, et al.,1992	plasmid	10 $\mu g/cm^3$	TE	Mica	few microliters	Soaked 33 mM magnesium acetate	Nitrogen flow	air	30-60	Si_3N_4
Delain et al.,1992	Plasmids&protein	0.5 $\mu g/cm^3$	Tris (80μM, pH 7.5)	Mica	3-5 μl	$Mg2^+,Ca^{2+}$ (0 to 2 mM)	rinsed with uranyl acetate solution	-	-	Si_3N_4
Bensimon et al.,1994	λ DNA	250 ng/μl	MES (50mM pH 5.5)	glass	5 μl	Silanazition-protein coat				
Hansma and Laney,1996	500 bp	-	water	Mica	25 μL	1 mM **$MC1_2$:Ni, Co, Zn, Mn, Cd or Hg.	air	air & water	-	Si_3N_4 7.3 Hz
Hansma et al.,1996	Short dsDNA&ssDNA , λ DNA	100 ng/μl	HEPES–Mg,TE buffer,water	Silicon wafers-mica	1 μl	-	Compressed air& desiccator over P_2O_5.	-	-	-

* Relative Humidity, **M represent given divalent cations　　　　　　　　　　　　　　　　　　**(continue on the next page)**

Table 5. 3. (cont.)

Reference	DNA Type	Conc.	Buffer	Substrate	Sample size	Modification	Drying method	Media	*RH %	Scan Rate&Tip
Allen et al.,1997	PstI- 7.5 kb	1–10 ng/µl	TE	Mica	1–2 µl	$MgCl_2$	rinsed with water and dried with N_2	air	5–25	5 Hz.
Dunlap et al., 1997	plasmids	40 ng/µl		Mica	10 µl	poly-L-ornithine coated	N_2 flow	air & water	-	Silicon- Si_3N_4 tips 1–2.5 Hz.
Li et al.,1998	λ DNA	1 ng/µl	pH 5.5-7		5 µl		N_2 flow		-	
Fang and. Hoh 1998	λ DNA- 3850 bp plasmid	-	water	Silicon-mica	20 µl	APTES silanization	compressed air	air	-	Silicon 3–5 Hz.
Shlyakhtenko et al.,1999	plasmid	0.5 µg/cm^3	TE	Mica	10 µl	APTES silanization	rinsed with water and dried with argon	air	-	TESP silicon

* Relative Humidity, **M represent given divalent cations **(continue on the next page)**

Table 5. 3. (cont.)

Reference	DNA Type	Conc.	Buffer	Substrate	Sample size	Modification	Drying method	Media	*RH %	Scan Rate&Tip
Gad et al.,2000	500 bp	-	-	Mica	-	amino silanization-heterobifunctional cross-linker	rinsed with water and dried with air	-	-	-
Umemura et al.,2001	supercoiled RFI ds DNA	10 µg/cm^3	TE pH 8.0	Mica	10 µl	APTES silanization	dried using an aspirator.	air	-	TESP
Bussiek et al.,2003	Supercoiled&Linear 2497 bp	0.5 nM	HEPES (10mM,pH 8.0)	Mica	20 µl	polylysine (PL)-coating	rinsed with water and dried with N$_2$, or not	air & water	-	Si$_3$N$_4$ 2-3 Hz
Pie´trement et al.2003	1,444 bp plasmid DNA/Ethidium bromide	0.2 µg/cm^3	Tris- MgCl$_2$ (10 mM pH 7.5)	Mica	5 µl	NiCl$_2$ pretreated mica or not	-	water	-	Si$_3$N$_4$ 5 Hz

* Relative Humidity, **M represent given divalent cations

Table 5. 3. (cont.)

Reference	DNA Type	Conc.	Buffer	Substrate	Sample size	Modification	Drying method	Media	*RH %	Scan Rate&Tip
Pastre´et al.,2005	1,444 bp plasmid DNA/Ethidium bromide	0.2 µg/cm^3	Tris- MgCl$_2$ (10 mM pH 7.5	Mica	5 µl	NiCl$_2$ pretreated mica or not	-	water	-	10 Hz
Hamon et al.2007	ssDNA–E. coli	2 µg/cm^3	Tris (20mM pH 7.5)	Mica	5- µl	NaCl, MgCl$_2$ or spermidine	rinsed with 0.02% diluted uranyl acetate solution	filter paper	-	1.5 Hz
Klinov et al.2007	duplex & triplex DNA	1–2 nM	Tris-acetate (2 mM pH 7.0)	highly oriented pyrolitic graphite (HOPG)	10 µl	Graphite modifier (GM) solution	N$_2$ flow	water		Si tip
Wu et al.2004	pBR322/pstI - 4361bp	60-260 ng/ µl	water (pH 7.0)	Glass, sapphire,mica, titanate	6-12 µl	Na$_2$HPO$_4$ solution	-	Air	-	1-2 Hz Si$_3$N$_4$ Contact mode
Song et al.,2009	Plasmid DNA pBR 322 (4363 bp)	6 ng/ µl	Tris–HCl (10 mM pH 7.6)	Mica	20 µL	MB or Co(phen)$_3^{3+}$		Air	-	silicon
Profio et al.,2010	Calf Thymus	-	-	Mica	25 µL	CTAB and CTBAB	dry for 24 h in a drybox containing silica gel	Air	-	-

* Relative Humidity, **M represent given divalent cations

CHAPTER 6

MATERIAL METHODS

6.1   Material

6.1.1. Materials

Calf thymus DNA was used and supplied by Sigma Aldrich (D1501) and it is used in adsorption experiments and AFM imaging. As adsorbent, alumina (Al_2O_3), silica (SiO_2), and hydroxyapatite (HAP) ($Ca_{10}(PO_4)_6(OH)_2$) were used. Silica (Sigma Aldrich-Silicagel, Grade 7744 pore size 60Å,70-230 mesh), alumina was obtained from Seydişehir-Turkey and hydroxyapatite were supplied Sigma Aldrich (23093-6). Silica ground by an agate mortar was used for adsorption equilibrium and kinetics of DNA from solutions. Also commercially DNA purification kit of Fermentas K0513 Silica Bead DNA Gel Extraction Kit and Fermantas K0503 GeneJET™ Spin Column were used.

Silica aerogel was prepared by controlled hydrolysis and condensation reactions of and Tetraethyl-orthosilicate (TEOS). The specifications of chemicals utilized for preparation of sols is given in Table 6. 1

Table 6. 1 Properties of used materials for silica aerogel and xerogel preparation.

Materials	Abbreviation	Specifications
TEOS-	$Si(OC_2H_5)_4$	98%, M=208.3, d=0.934 g/cm^3 (Aldrich)
Ethyl alcohol	C_2H_5OH	99.8%, M=46.07, d=0.79 g/cm^3 (Riedel)
Ammonium-hydroxide	NH_4OH	28-30% NH_3 M=35.05, d=0.9 g/cm^3 (Aldrich)
Hydrochloric acid-	HCl	37% M=36.46,d=1.9 g/cm^3 (Merck)

Thin film HAP preparation materials are HAP powder, deionized water, dispersing agent Dolapix 64 (Carboxylic acid preparation-Zschimmer-Schwarz, d = 1.20 g/cm³) and 1.00 N NH_4OH.

AFM images were taken onto Ted Pella 9.9-mm-diameter mica, silica and alumina wafer surfaces with both surface polished c plane (0001) which were taken from CS analytic company. Another alumina surface with polished alumina surface (0001) by MTI Corporation is tested for AFM image technique .

Wafers and glass substrate were cleaned differently. Solvent for needed to clean bioinert glass slide are listed in Table 6. 2.

Table 6. 2 Materials used in this study for the AFM glass substrate cleaning

Materials	Abbreviation	Specifications
Acetone	$(CH_3)_2CO$	99%, M=58.08, d=0.79 g/cm3 (Merck)
2-propanol	C_3H_8O	≤100%, M=60.1, d=0.786 g/cm3 (Merck)
Ethyl alcohol	C_2H_5OH	99.9%, M=46.07, d=0.79 g/cm3 (Merck)
Sodium Hydroxide	NaOH	≤100%, M=40, d=2.13 g/cm3 (Merck)
Deionized water	H_2O	Milli-Q Ultrapure water

6.1.2. Preparation of Buffer Solutions

DNA stock solutions were prepared in different range of pH (2-9) adjusted buffer solutions according to the biochemistry and molecular biology sense of scientists (Fasman, 1992). All the buffer solutions were prepared with ultrapure water obtained from Milli-Q Ultrapure Water Purification system in 0.01M ionic strength. After that buffer solutions were autoclaved at 121 ºC to prevent bacteriological negative effect on adsorption and analysis.

100 ng/µl Calf thymus DNA stock solutions were prepared in each buffer solution. DNA 10- 100 ng/µl range concentrations in the buffer at a given pH have been prepared by diluting the stock solution with the same buffer solution. After that, buffer solutions were autoclaved at 121 ºC to prevent bacteriological negative effect on

adsorption and analysis. Features of the buffer solutions are listed in Table 6. 3 at 0.001 M ionic strength.

Table 6. 3.Buffer Types and Ionic Strength

pH	Ionic Strength	Buffer Type
2	0.001 M	Glycin -HCl
3	0.001 M	Potassium hydrogen phthalate -HCl
4	0.001 M	Potassium hydrogen phthalate -HCl
5	0.001 M	Acetate
6	0.001 M	Acetate
7	0.001 M	Phosphate Buffer
8	0.001 M	Phosphate Buffer
9	0.001 M	Phosphate Buffer

6.1.3. Measurement of DNA Concentration

Calf Thymus DNA concentration was measured firstly by UV spectrophotometer (Perkin Elmer Model No: Lambda 45). This device requires at least 1.5 cm^3 of sample for each run of the scan. However, working with this amount of solution sample is a limitation. Because of this the calf Thymus DNA concentration was measured by the UV spectroscopy with NanoDrop ND-1000 (NanoDrop Technologies Inc., Wilmington, DE, USA). NanoDrop is a full-spectrum spectrophotometer that required just 2 µl samples for each run. Its working principle is surface tension. Surface tension holds the sample via two plate surface. Additionally this device eliminates the essential usage of a quartz cell during the UV measurement. Analysis made by UV on scan mode lasts for 5-10 second via Nano Drop for full spectrum. It is fast and has high accuracy and precision. Concentration of DNA is determined from the difference in absorbance readings at 260 nm with calibration curves. Quality of DNA can also be

evaluated by the 260/280 nm ratio. If the ratio 260/280 is close to 2, it indicates that DNA is sufficiently free from the protein.

6.1.4. Calibration and NanoDrop Sample Preparation

Six-point calibration curves of the DNA were prepared using calf thymus DNA in pre-defined pH buffer solutions. Stock solutions were diluted in the same buffer solution to obtain 10, 20, 40, 60, 80 and 100 ng/µl of DNA concentration. These ranges were obtained for three adsorbents set in 1.5 cm^3 of sample volume. Calibrations were performed with the three DNA having the same concentration range. Therefore, each calibration point was repeated three times. The correlation coefficients (R^2) were found to be greater than 0.915 for used pH levels. Some of the calibration graphs are illustrated in Appendix A.

6.2 Method

6.2.1 Characterization of Materials -Fresh and Used Adsorbents

The characterization of adsorbent materials is of great importance to understand the properties of the received and produced adsorbents and to determine the structure as well as the morphology of the used particles.

The characterization part of the present study included the determination of pore size, surface area, morphology, thermal stability and chemical composition. The adsorbents used in this study were characterized using Scanning Electron Microscopy (SEM), X-Ray diffraction (XRD), Fourier Transform Infrared spectroscopy (FTIR), elemental analysis (EDX), X Ray fluorescence spectroscopy (XRF), physical adsorption of nitrogen techniques, zeta potential measurements and thermo gravimetric analysis (TGA). Used adsorbents were characterized by SEM only. Commercially available spin column and silica bead were also characterized using SEM, FTIR, and EDX analytical methods.

6.2.1.1. X-Ray Powder Diffraction (XRD)

Philips X'Pert Pro diffractometer was used to investigate phase structure of the adsorbents and crystalline form of the component present in the adsorbent samples. The operating conditions were 45 kV and 40 mA. Cu K_α radiation, $\lambda = 0.154$ nm. The registrations were performed in the range over 2θ values of 5°-70° with a scan speed of 0.06^o/s. The data were collected with X'Pert data collector. The collected data were analyzed by X'Pert Graphics & Identify software

6.2.1.2. Fourier Transform Infrared Spectroscopy (FTIR)

FT-IR spectroscopy is used to obtain information about functional groups present in a material using the transmission technique. The range of the wavenumber used in this study was between 400 and 4000cm^{-1}. KBr disc method was used to obtain the pellets. Adsorbent KBr pellets were prepared by mixing 4.0 mg of silica ,alumina or HAP powder and 196 mg of KBr in an agate mortar and pressing the mixture under 8 tons force. Shimadzu 8601 FTIR spectrophotometer was used to obtain the spectra.

6.2.1.3. Scanning Electron Microscopy (SEM)

Scanning electron microscope (SEM) images were taken by Philips SFEG 30S and FEI Qanta 250 FEG instruments. Images are used for identifying the morphology of the adsorbents before and after adsorption.

6.2.1.4. Physical Adsorption of Nitrogen

Specific surface area, pore diameter and pore volume of the adsorbent, silica aerogel, silica xerogel and commercial silica bead DNA extraction kit were obtained by using the physical adsorption of nitrogen technique at 77 K, using Micromeritics ASAP 2010. Pore size analysis of mesoporous materials from adsorption isotherms is a specific technique based on capillary condensation, evaporation and associated hysteresis phenomena (Thomness et al., 2006) of the adsorbed gases such as nitrogen (N_2).

6.2.1.5. Elemental Analysis

Elemental analyses were done by XRF and EDX methods. XRF analyses were carried out by using Spectro IQ II on the opaque surfaces of the pellets obtained from the powder to determine the elements present in the adsorbents. EDX method was used just for the commercial Fermentas spin column kit K0503 analysis.

6.2.1.6. Thermogravimetric Analysis (TGA)

TGA and DTA analyses gave information about the dehydration, thermal stability properties, water content and types of water within the sample structure. The samples (10-15 mg) were loaded into an alumina pan and heated from room temperature to 600 °C at 10 °C min^{-1} under N$_2$ flow of 40 cm^3 min^{-1}.

6.2.1.7. Atomic Force Microscopy (AFM)

Surfaces that are used in DNA imaging by AFM should be previously characterized. The surface roughnesses of mica, silica, two different alumina wafers, HAP thin film and pellets surface were measured by Digital Instruments MMSPM Nanoscope IV in the tapping mode.

6.2.1.8. Particle Size Analysis

Dynamic light scattering (DLS) was used to determine the particle size distribution of HAP particle and DNA solutions were tested by the zeta sizer (Malvern 3000 HS) for particle size distribution and zeta potential.

Particle sizes of DNA at pH 7 and nanosized HAP samples were determined using by particle size analyzer (Malvern Mastersizer 2000). Silica and alumina particle size were determined by the help of SEM images using Scandium software available in Material Science Centre.

6.2.1.9. Characterization of DNA

Charges on solid surfaces change with the pH of the aqueous solutions. DNA molecule is negatively charged due to the phosphate groups when the pH is above the isoelectric point. Therefore, surface charge influences adsorption phenomena in that surface charge changes electrolytic interaction.

Characterization of the calf thymus was performed by surface charge measurements. DNA solutions having different pH values have been tested by zeta sizer (Malvern 3000 HS) for zeta potential and particle size distribution of the DNA. The refractive index of DNA was considered to be 1.5 (Wu et al., 2004). This value is general for polymeric material and measurements done at 0.001M ionic strength.

Raw calf thymus DNA was investigated by SEM and adsorbed DNA on the adsorbents dried after adsorption process were investigated by SEM.

6.2.2 Adsorption Experiments

Before the adsorption experiment all adsorbents were dried at 120 ºC for 18 hours under vacuum. Buffer solutions equilibriated with adsorbents were used as blank control in UV analysis. $1.5cm^3$ buffer solution was equilibrated with 0.0075g of adsorbent and UV spectrum of the supernatant was taken as the blank. The DNA concentration has been estimated at 260 nm using a standard curve obtained by measuring absorbance of a series of solutions of known DNA concentrations by spectrophotometric method. This method was applied using NanoDrop 2000 (Thermo Scientific ND 1000) spectrophotometer. 10-20-40-60-80-100 ng/μl DNA solutions were prepared for obtaining the calibration curve. Stock solution of DNA (100 ng/μl) were diluted with pH buffer solutions to obtain the 10-100 ng/μl concentration range. Subsequently 0.0075mg of adsorbent (SiO_2, Al_2O_3 and HA) were added to the $1.5 cm^3$ DNA solutions to get a solid to liquid ratio 5 g/dm^3 and DNA concentration of the supernatant was measured after incubation at 100-200 rpm by Fine PCR mixer incubator at 25^oC for 24 hours.

6.2.3 Adsorption Kinetics

0.008mg of adsorbent (SiO_2, Al_2O_3 or HAP) was added to the 1.6 cm^3 100ng/µl DNA concentration solutions to keep a solid to liquid ratio 5 g/dm^3. Kinetic measurements were carried out at 25 °C under constant stirred conditions for a maximum of three hours by Fine PCR mixer incubator. 2-4µl supernatant sample were taken each time interval. Separated samples were stored in clean eppendorf tubes until analyses. Data were collected for each pH with respect to time.

6.2.4 Data Collection

Adsorbents could be added after calibration and the same solution can be used for adsorption process because nanodrop device just requires 2µl sample volume for analysis. All calf thymus DNA concentrations were measured from supernatant part of the retain DNA concentration after equilibrium and kinetics data collection. Samples were measured with UV spectrophotometer technique with NanoDrop 2000 (Thermo) after centrifugation at 15,000 g (Nüve NF800R) at 20 °C for 15 minutes. If sample concentration could not be measured after analysis sample were kept to storage in refrigerator at +4 °C

Initially DNA UV spectrum analysis's accuracy and precision enhancement was considered with using special dye ethidium bromide. This option was cancelled because of some restriction of using ethidium bromide to providing for health protection against DNA form change. And using cyber green give expected booster effect on analysis. 1.6 fold of the normal spectrum band intensity has been obtained by cyber green. This dye is known to be intercalating dye for real-time polymer chain reaction (PCR) applications (Giglio et al., 2003). It is to bind the double stranded DNA and identify PCR product that accumulates during the PCR. However absorbance range has not been as low to be not identified. Therefore this type of addition was not required so far.

Data obtained were analyzed by the nonlinear regression method which is performed using the Solver Add-In function to Microsoft® ExcelTM. By selecting the options button in the Solver tool box, it is possible to modify the maximum number of iterations, maximum run time, percent tolerance, precision, and approach criteria. This is performed by minimizing the sum of squared deviations, SSE, by numerical

optimization techniques. The numerical function for minimization is given below formula. Deviation is expressed difference between experimental data (q_{exp}) and model estimated (q_{est}) value.

$$SSE = \sum_{i=1}^{N} \left(q_{exp} - q_{est}\right)^2 \qquad (6.1)$$

A common practice in research is to fit the experimental data to several models, then perform some kind of test to compare and decide which model fits the data better. Based on the choice of the "best model", conclusions about the difficult mechanism of the system are often available. The most popular tool for model comparison is the coefficient of determination, R^2. It is the square of the correlation coefficient, r, between the dependent variable and the regression-predicted value of the dependent variable. In other words, R^2 is the fraction of the total variance of the dependent variable that is explained by the model's equation.

6.2.5. Induction of DNA Chain Breakages

Calf thymus DNA has a high molecular weight. To be able to investigate single strand or small size of DNA, calf thymus was treated by two different methods. Sonication and restriction enzyme methods were applied to 100ng/µl calf thymus DNA solution. DNA solutions were prepared in ultra pure water and Tris EDTA (TE) buffers. In first try three sonication periods; 10-30-90 second and three enzyme contact time 5, 10,20,30 and 60 minutes were selected for each 10 µl DNA solutions. In enzyme restriction parts of the study 1 µl EcoRI was used. The DNA molar mass was determined following electrophoresis on 1% agarose gel prepared with 100 ml Tris base- acetic acid- EDTA. Buffer-(TAE) mixed with 1g Agarose. It was then poured into the gel casting tray and left to cool and set. The gel was placed into the electrophoresis apparatus and filled with the same buffer and a very small amount ethidium bromide. Then the samples were run on gel at 100V for 1 hour. After electrophoresis the gel was illuminated with an ultraviolet lamp because the process was available imagining the polymerised gel under different time intervals. After that, 100 V voltage was applied to

the gel placed in the electrophoresis platform for four more hours. Gel was illuminated again totally 5 hours later after start.

After electrophoresis, all samples were compared with 1kb DNA Ladder (Thermo Scientific Gene Ruler #SM0313).

6.2.6. Preparation of Silica Alcogels and Silica Aerogel

Silica aerogel was prepared having the aim of having high surface area and reasonable pore diameter for adsorption of our calf thymus DNA sample. Then it was characterized through nitrogen adsorption techniques.

Silica aerogel prepared by a two steps sol gel procedure. First step, hydrochloric acid was used as an acid catalyst of the hydrolysis. Tetraethylorthosilicate (TEOS). TEOS, ethanol (EtOH), distilled water and hydrochloric acid were mixed in a 250 cm^3 glass bottle at a molar ratio of $1:6:4:10^{-3}$ and led to be stirred for 30 min, and a hydrolysis solution was obtained. In the second step, ammonia, as a base catalyst, was added drop-wise into the solution resulting from the first step, at the molar ratio of TEOS: NH_4OH equals to $1:10^{-2}$. A white precipitate was seen immediately. The mixture was further stirred for 2 min, and then kept for gelation. The set gel is called the alcogel and contained some amount of water. The alcogel was washed several times with ethanol. The aim of this part is remove excess water inside the alco gel structure. This part can be named as "*washing*". A measured volume of ethanol was added to the wet alco gel gel that was inside the glass bottle and kept there until next washing time. Previously 10 cm^3 ethanol had been used for washing but it did not remove the water as high as expected. Increasing the volume of ethanol (40 cm^3) gave better result for removal the water which was controlled by UV absorbance analysis. The washing procedure was repeated several times.

The % water content present in ethanol used in washing process. Various mixtures of water in ethanol were used to plot a calibration curve shown in Figure 6. 3 to determine the water present in ethanol after supercritical drying. 50 cm^3 of ethanol solutions with 0.5, 1, 2, 3 and 4 % H_2O were prepared and 100 mg $CoCl_2.6H_2O$ was added to each solution. Subsequently the spectra of the solutions were taken between 400-700 nm and absorbance values at 650 nm were recorded. High regression coefficient indicated very accurate water concentration measurement. After each

washing step water content of ethanol phase was measured by $CoCl_2.6H_2O$ addition and then water diffusion coefficient in alcogel was calculated.

If there is diffusion controlled mass transfer graph of the fraction of water diffused versus square root of time should be linear.

$$\frac{M_t}{M_\infty} = \frac{4}{L}\sqrt{\frac{D_{AB}t}{\pi}}$$
(6.2.)

D_{AB} is the water diffusion coefficient in wet gel, "t" is the time and "L" is the thickness of the wet gel. After preparation of silica and the washing procedure wet gel was dried by two methods: ethanol supercritical drying (SCD) and normal condition drying. Therefore samples can be named as aerogel and xerogel as respectively based on drying method. SCD was carried out above super critical temperature shown in Figure 6. 1. . During the procedure temperature and pressure data were collected to be able to check critical point was exceeded or not. Ethanol critical point is crossing of P_c (6.36 atm) and T_c(243 ºC) in Figure 6. 1 and as listed in Table 3. .
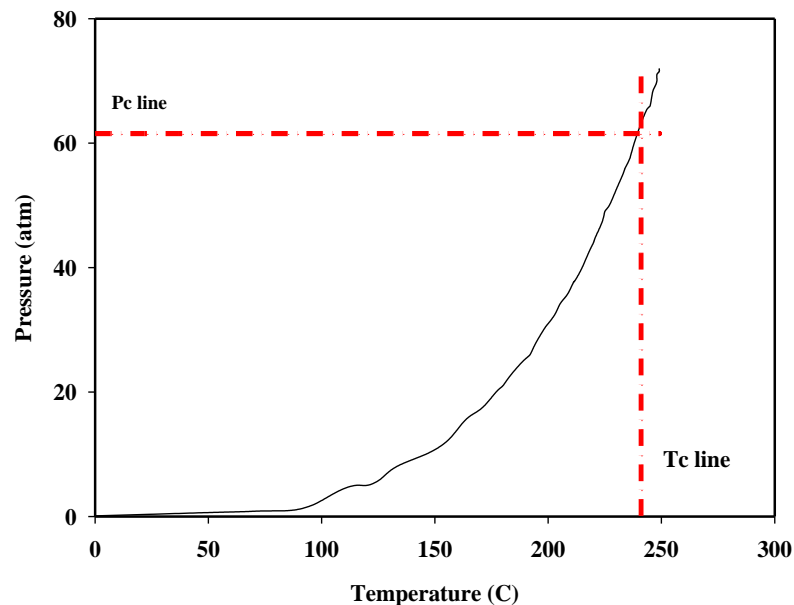
Figure 6. 1. Pressure-Temperature relation of ethanol in closed reactor.

Before heating the system, nitrogen gas was passed through the system to remove oxygen in the reactor and pipelines. The supercritical pressure of ethanol (6.36 MPa) was achieved by heating the system to 250 °C and 72 bar. In a typical experiment, approximately 5.0 g of wet solid and 100 cm3 ethanol was placed in the reactor as shown in Figure 6. 2. The system was heated up to 250°C and 72 MPa. When the supercritical pressure was reached, the heating system was shot off and the valve between the two vessels was opened to release ethanol into the second reactor. The reactor system was allowed to cool to room temperature. The ethanol phase was analyzed for water content (Figure 6.3.) and the silica aerogel in the reactor was characterized.
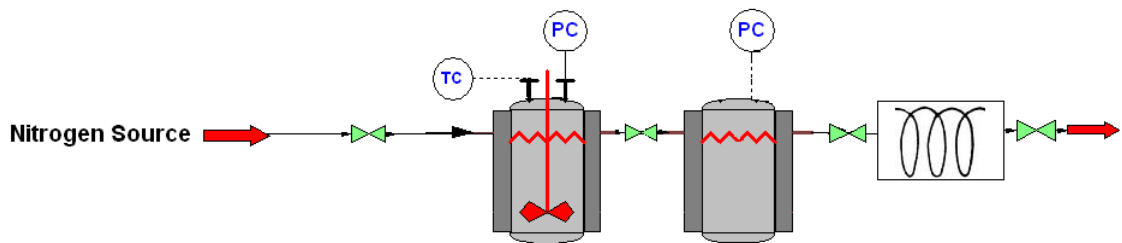
Figure 6. 2 Schematic representation of supercritical ethanol drying system
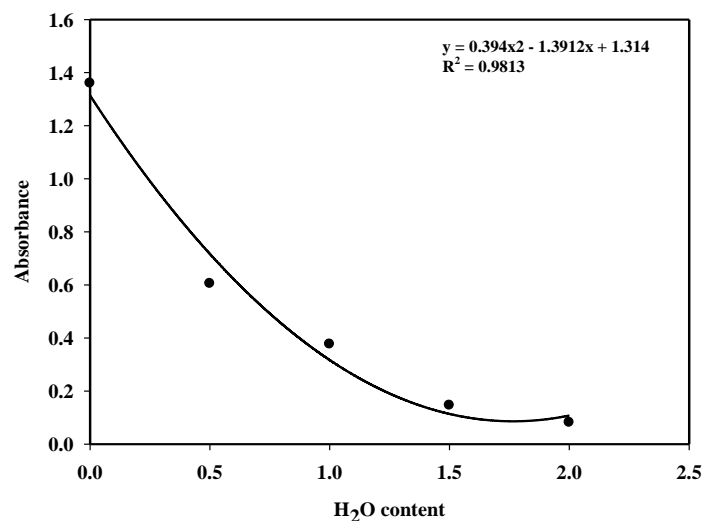
Figure 6. 3 Calibration curve of water % in wet gel

6.2.7 AFM Analysis

6.2.7.1 Surface Cleaning

Clean surface condition is inevitable for reproducibility of the AFM imaging measurements. Therefore clean study and preparation is important.

The first problem is to select an appropriate substrate. Indeed, to observe biological structures in their native state, these must be well attached to a smooth solid surface to resist against forces applied by the scanning tip. Surface must be clean as possible as to decrease extra resistance and forces. In this part just included only HA coated sample preparation which is selected as preliminary AFM image surface.

Surfaces were cleaned prior to the AFM measurements, using a large variety of methods. Every sample was polished with a nitrogen flux in order to remove contaminants such as dust or other impurities; chemical washings of the specimens were then performed to avoid organic contamination or in order to prepare the surface for functionalization. Common solvents used in during the experiments were acetone, ethyl alcohol, 2-propanol, 1 M sodium hydroxide ultra pure water as with this order and time requirements: acetone- 15 min(30°C), 2-propanol- 15 min (30°C), Ethanol- 15 min (30°C), NaOH (1M)- 15 min (30°C), deionized water- 20 minutes × 5 times (30°C)

The glass substrates were cleaned according to a main procedure. Transsonic 660/H Elma 300W ultrasonic bath cleaner was used through all cleaning process to remove hydrophobic and hydrophilic contamination on substrates.

Silica and alumina wafers were just cleaned by ethyl alcohol (EtOH) and deionized water least 15 min in ultrasonic bath. The surfaces must be cleaned to make them flat with a uniform oxide layer. The surface and all equipment were exposed to the short range UV light for 20 minutes at each solvent changing time. Mica disc just was exposed to the UV light for each analysis after it had been cleaved from the top layer off with a skotch tape. Then nitrogen gas was applied to all substrates surfaces in order to avoid dust contamination of substrate.

6.2.7.2. Hydroxyapatite Surface Preparation

6.2.7.2.1. Thin Film Preparation

Thin film coatings of hydroxyapatite were achieved by dip coating of bioinert glass slide substrates with suspension having dispersed HAP powder. The suspensions of HAP powders were prepared in deionized water. The HA powder content of the suspensions was 15 %. Hydroxyapatite sol was stabilized with Dolapix CE 64 (approximately 10 drops), and adjusted pH=9.4-10.0 by 1.00 N NH_4OH (Ozcan and Çiftçioğlu 2010). Dolapix CE 64 (sodium diisooctylsulfosuccinate; $C_{20}H_{38}O_7S$, MW=422.58) was added as a dispersing agent. Ultrasonic treatment (30 kHz) was applied to the suspension for 2 hours. Particulate HAP layers were coated on bioinert glass slide substrates by dip coating technique with a withdrawing speed of 100 mm/min and with dipping time of 5 seconds. The substrates were coated up to 1, 2 and 5 layers. Each coating was repeated after 30 min drying time in ambient conditions.

6.2.7.2.2. Pellet Preparation

A sufficient amount of HAP powder was weighed to obtain a pellet having a thickness enough for polishing its surface. Then HAP powders were compacted in a 1 cm diameter stainless steel die under 25 MPa. Pellets were sintered at 1300 °C by Carbolite RHF 1600 high temperature furnace. The temperature program was 10 °C/min up to 400 °C. After 400 °C furnace temperature increased 4 °C/min rate until 1300 °C. Then the pellets were kept in the furnace so that their temperature can cool down to room temperature. After that surface of the pellets were polished with 3μm diamond solution to obtain smooth surfaces for AFM measurements in order to investigate DNA behavior onto smooth HAP surface. The surface roughness of the pure HAP pellet compacts were reduced by polishing.

6.2.7.3. DNA Solution Peparation for AFM Imaging

AFM images were taken in mainly two different DNA solutions: one was in TE buffer and the other was just in ultrapure water. Calf thymus DNA was dissolved in water and TE buffer to a concentration of 100 ng /μL. A solution of DNA in TE buffer (10 mM Tris, 1 mM EDTA) was used as DNA solution media. The molar fraction of salt to water in pure 1 x TE buffer solution was referred to be less than 1/10 000 (Fang et al., 2006). Thus, according to the dilute solution theory, 1 x TE buffer was considered as dilute solution, which means that it has similar behavior as pure water. To prepare a DNA sample, 2μl of 100ng/μl of calf thymus DNA was deposited onto freshly cleaved mica (already glued on a steel disc), silica and alumina wafers. The sample volume was selected to be 2 μL to avoid the overflow.

Also DNA dissolved in ethanol and dried on the surfaces was investigated. Same DNA concentration was used (100 ng/ μL) for this purpose. Ethanol is reducing the water activity. In the presence of ethanol, using AFM was also tested. It is known that the B−A transition is higher with the increase of the concentration of ethanol (Fang et al 1999) also persistence lengths decrease linearly as the concentration of ethanol increases.

10 ng/μL DNA solution was also used to observe the DNA concentration effect on imaging of DNA.

6.2.7.4. Sample Drying Procedures

DNA solution dropped surface substrates were dried at 25 °C in a closed Stuart Orbital incubator (SI500) at least for 15 hours. Besides this drying technique, other known drying techniques such as forced convection drying with nitrogen flow regime, freeze drying and drying in ethanol athmosphere were used.

Nitrogen flow regime forced drying procedure was carried out for surface of mica and silica, alumina wafers. 2μl of 100ng/μl of calf thymus DNA was placed onto the surface. The sample first was incubated at room temperature then compressed nitrogen gas applied to the sample with the direction of the gas flow was at nearly an angle of ~ 45º as illustrated in Figure 6. 4 . Distance between gas source and the sample were carefully controlled to drive stable condition through the interface. The gas stream

was kept in the same condition for more minutes to be sure the sample completely dried after the drop was disappeared.

Figure 6. 4 Schematic diagram of the drop size DNA nitrogen flow regime drying procedure

DNA solutions were dropped mica and alumina, silica wafers. Substrates were placed in vials containing 1 cm^3 frozen water. Freeze drying was done using Labconco FreeZone-4.5 at the temperature of -51 °C, and under vacuum until the water and dropped sample was completely dried.

DNA aqueous solution dried in ethanol vapor atmosphere was also examined.

6.2.7.5. AFM Imaging

The AFM, Digital Instruments MMSPM Nanoscope IV was used in the tapping mode to obtain the 2 and 3-dimensional surface topology, and phase information of the HAP coated glass, HAP pellets, mica and silica, alumina wafer surfaces in air using Veeco RTESP tips. The typical tapping frequency was 263-291 kHz, and the scanning rate was 1.0 Hz. The images of dried DNA on the surfaces were examined under the same conditions. Data were examined with Nanoscope software with measuring the section analysis. Distributions of obtained vertical distance of the DNA assemblies were fitted with Gaussian distribution as seen in Equation 6.3. μ is the mean of distribution, σ variance of distribution

$$y = \frac{1}{\sigma\sqrt{2\pi}} e^{-\left(\frac{y-\mu}{2\sigma^2}\right)^2}$$

(6.3)

CHAPTER 7

RESULTS and DISCUSSION

7.1. Characterization of Adsorbents

7.1.1 X-Ray Diffraction

Adsorbents were investigated about mineralogical content and crystalline form by X-Ray diffraction (XRD) method. XRD patterns of silica alumina HAP powders adsorbents and HAP pellet are shown in Figure 7.1, Figure 7. 2, Figure 7. 3 and Figure 7. 4 respectively. Silica sample has shown completely amorphous structure as seen in Figure 7. 1 which present amorphous structure main characteristic peaks through 2θ values (broad peak at 2θ 24°).
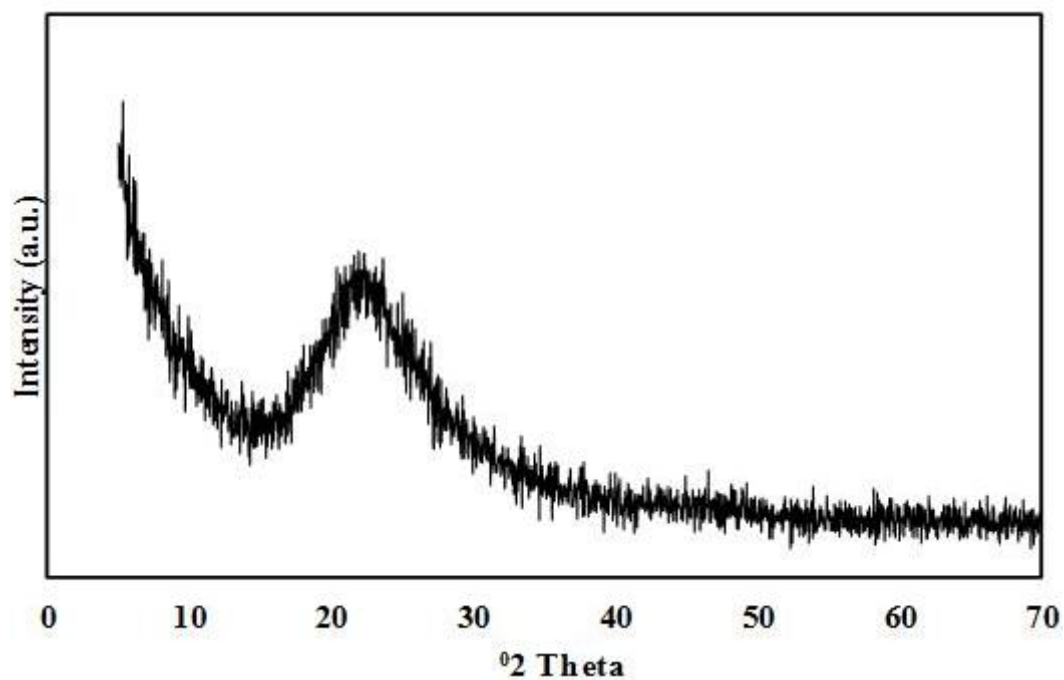
Figure 7. 1. XRD pattern of Silica

On the other hand alumina and HAP have characteristic peaks of their patterns which are given in Table 3.8 and Table 3. 10
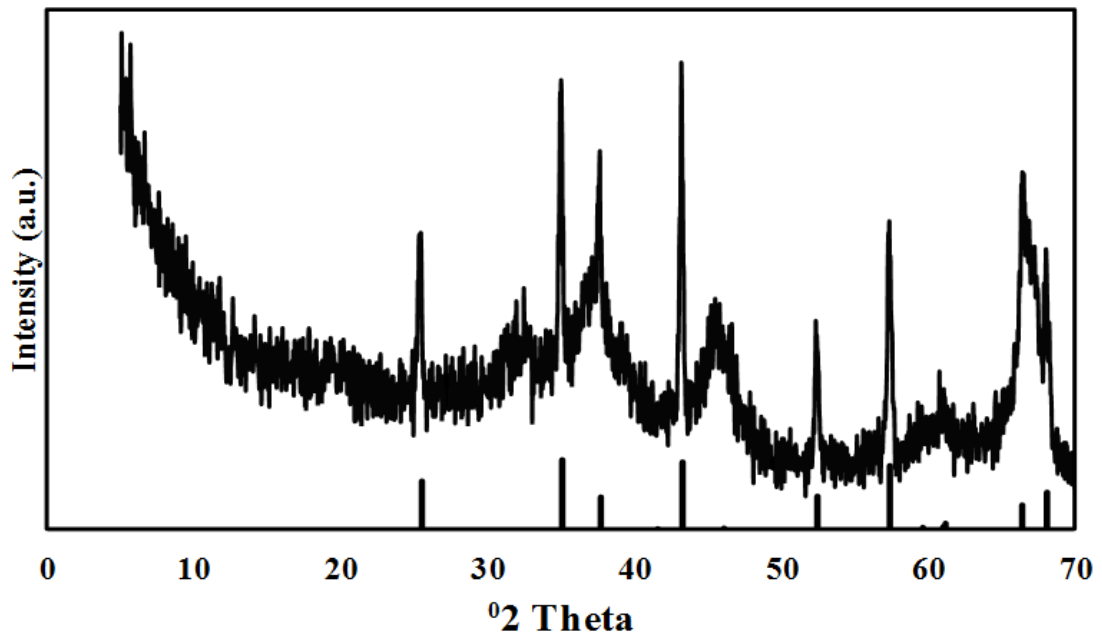
Figure 7. 2.XRD pattern of Alumina
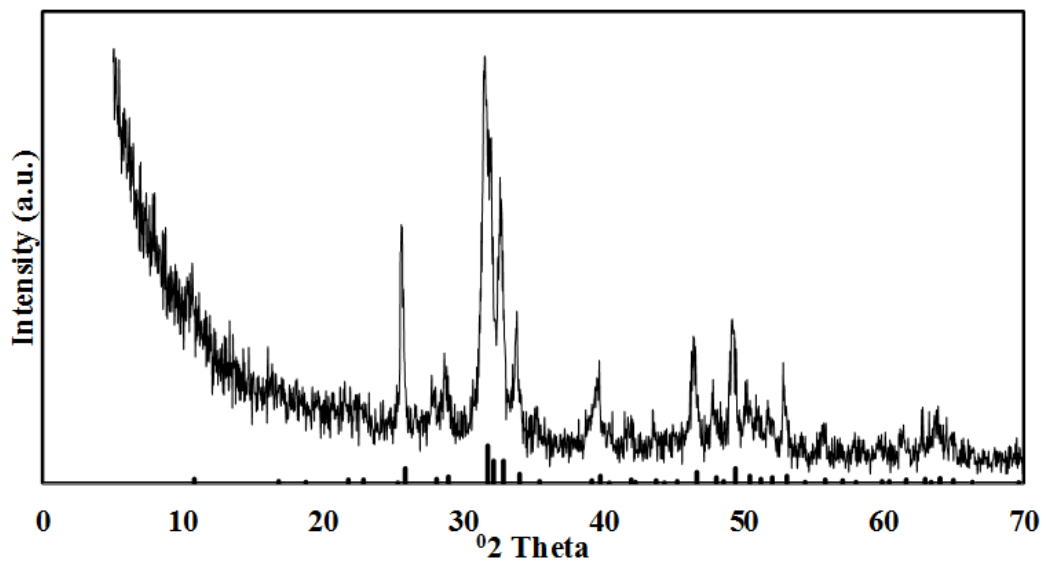
Figure 7. 3. XRD pattern of HAP
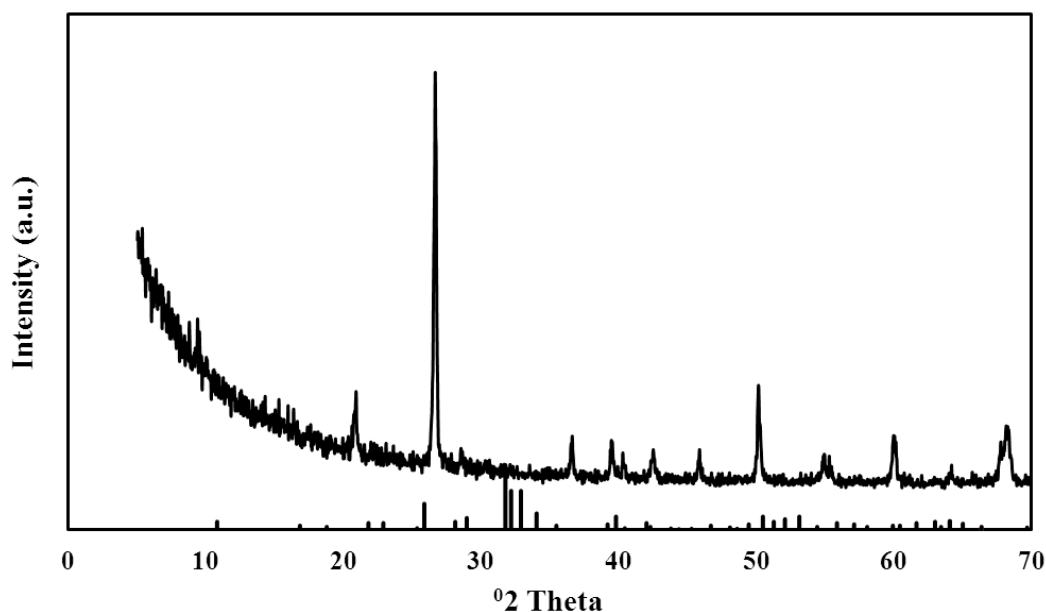
Figure 7. 4.XRD pattern of HAP Pellet

Alumina and HAP adsorbents have also been confirmed with literature based on X'Pert graphic and identity software of XRD pattern. Identity results include alumina and corundum for alumina sample. Observed and known - which has the most relative score -2θ values compared. These peaks of alumina correspond for aluminum oxide (JCPDS, file 75-1865). Same procedure also carried out for calcium phosphate hydroxide (hydroxyapatite) pattern which has JCPDS number 09-0432 (Wu et al., 2007). There is consistency of alumina and HAP sample diffractions pattern with literature. Figure 7. 4 indicates prepared HAP pellet is transformed to the calcium tri phosphate with JSPDS file 09-169 after high temperature sintering.

7.1.2. Fourier Transform Infrared Spectroscopy

Infrared spectroscopy (FTIR) is a widely used technique for investigating chemical structure of a substance. Analysis of the IR spectra has given important information on the microstructure these can be considered as the material fingerprint.
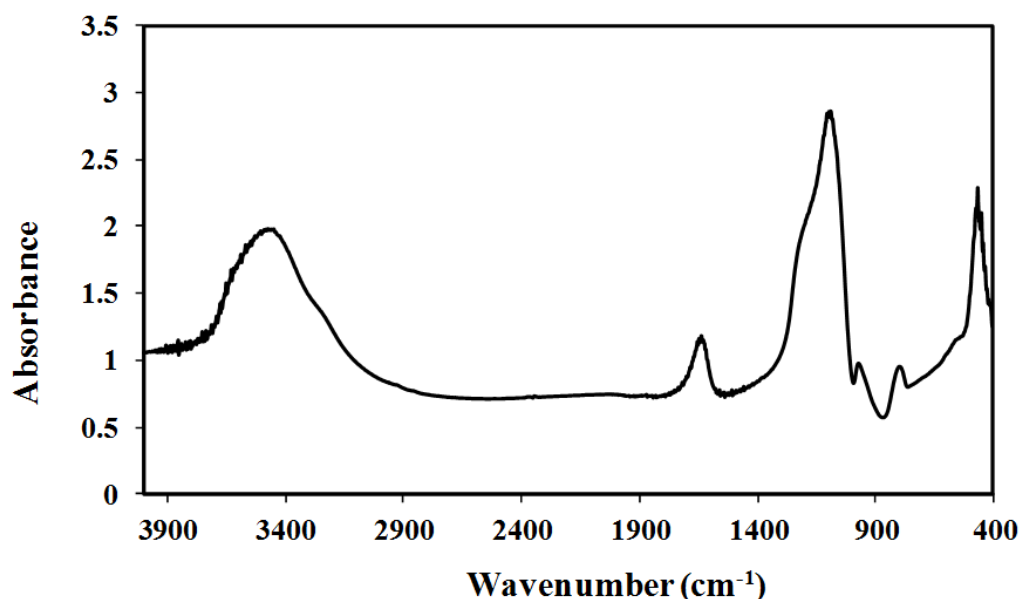
Figure 7. 5. Fourier Transform Infrared Spectrum of Silica

FTIR spectrum of commercial silica is seen in Figure 7.5. The presence of water can be observed from the band at 1640 cm^{-1}, assigned to the δH–O–H mode. (Fidalgo and Ilharco 2005). The peak at 3400 cm^{-1} is related to the νO–H mode of residual silanol (Si–OH) groups and of adsorbed water hydrogen bonds (Fidalgo and Ilharco 2005). In other words this wavenumber is relevant to the –OH vibrations of molecular water that is physically adsorbed in the network. This band mostly reflects silanol groups when the peak at 1630 cm^{-1} related to bending water vibration has low intensity (Estella et al., 2008). The weak band near 970 cm^{-1} was assigned to the oscillating oxygen atoms in the silica network, including silanol groups and broken Si–O–Si bridges (Estella et al., 2008). The peak at 1080 cm^{-1} wavenumber has been related Si-O-Si bond stretching.

The FTIR spectrum of alumina shown in Figure 7.6 had peaks related with water (at 1600 cm^{-1}) and OH groups(3464 cm^{-1}) and Al-O stretching vibrations (1014 cm^{-1}).
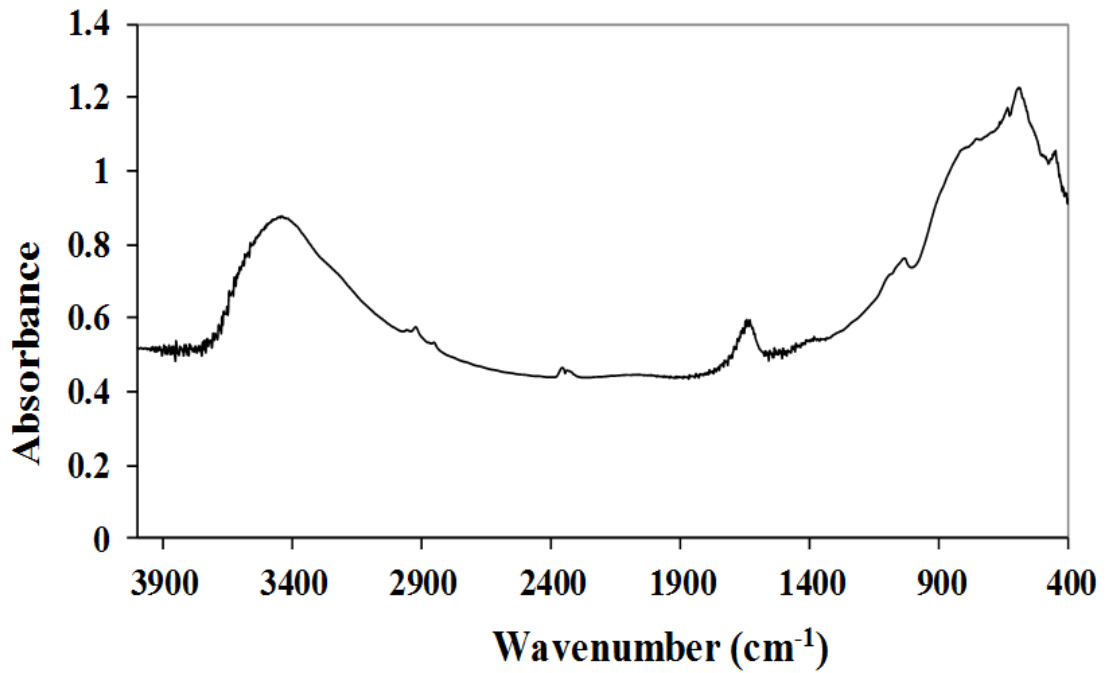
Figure 7. 6 Fourier Infrared Spectrum of Alumina
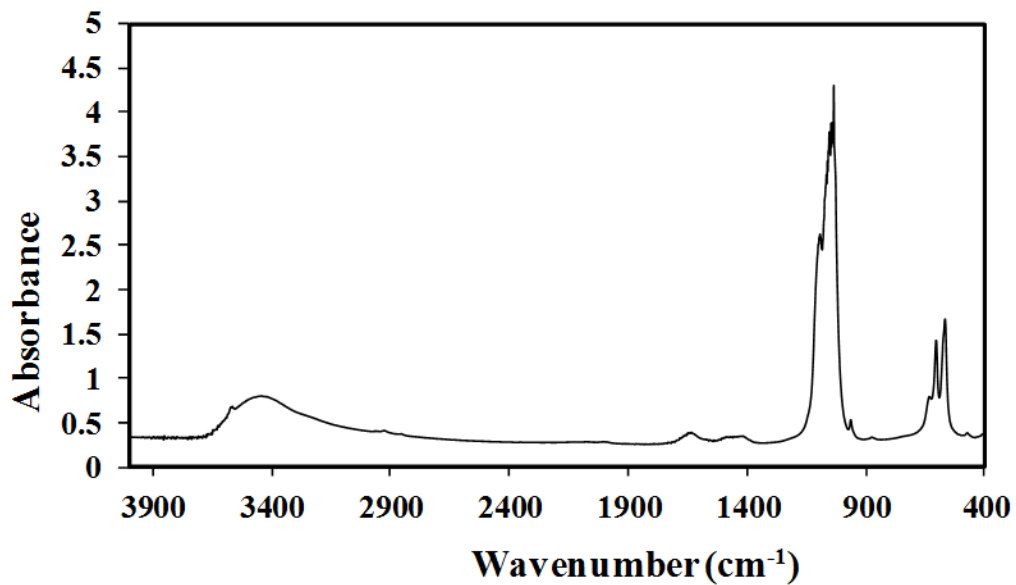
Figure 7. 7 Fourier Transform Infrared Spectrum of HAP

Hydroxyapatite FTIR spectrum is shown in Figure 7. 7. Bands in 3400 and 1600 cm^{-1} again represent the OH stretching and water bending vibration respectively. The bands at 1092 cm^{-1} and about 1040 cm^{-1} were assigned to the components of the triply degenerated asymmetric P-O stretching mode (Slosarczyk et al., 1996). The bands at 601 cm^{-1} and 571 cm^{-1} are related to components of the triply degenerate O-P-O bending mode and the bands in the range 462-474 cm^{-1} are also connected to the components of the doubly degenerate O-P-O bending mode (Fowler, 1974). Figure 7. 8 a shows commercial Fermantas K0503 GeneJET™ Spin Column FTIR spectrum. This material has peaks around 1080 and 460 cm^{-1}, asymmetric stretching vibration of the Si–O bond and ρSi-O-Si. The peak at 1350 cm^{-1} can be attributed to the B-O vibration. It does not contain water since no band was present around 1600 cm$^{-1.}$ The FTIR spectrum of the spin column adsorbent indicated that it was made out of borosilicate glass. Figure 7. 8. b shows the infrared spectrum of Fermantas K0513 GeneJET™ silica bead. This silica did not have any OH groups since there was not a peak at 3400 cm^{-1}. It has peaks around 1049 for cm^{-1} asymmetric stretching vibration of the Si–O bond. However the bonds at 796 cm^{-1}, 776 cm^{-1} and 692 cm^{-1} indicated that it was crystalline silica, quartz (Francis et al, 2009).
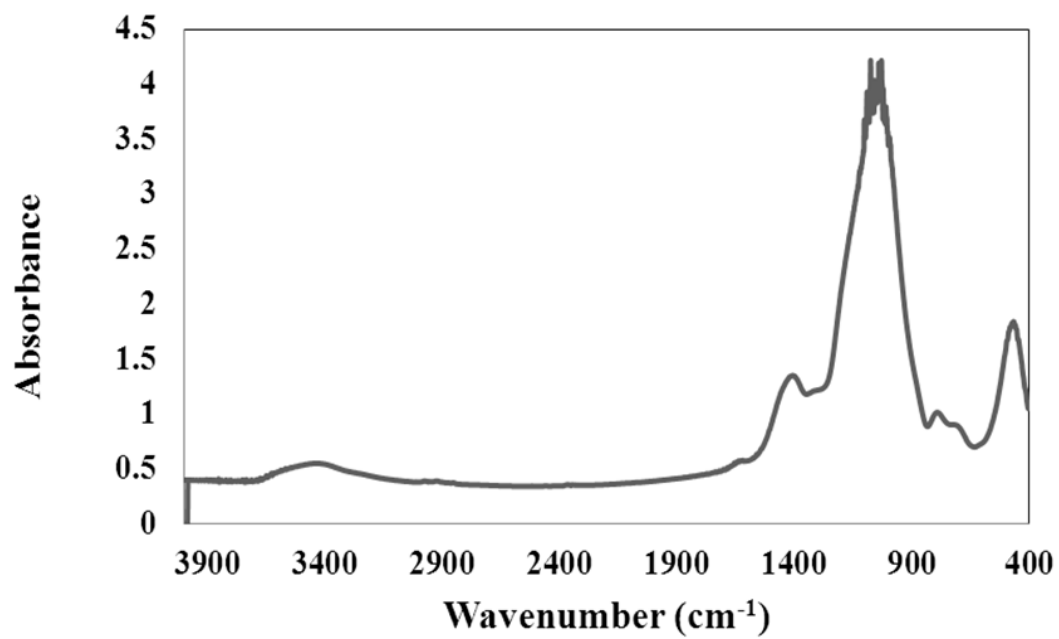
(a)
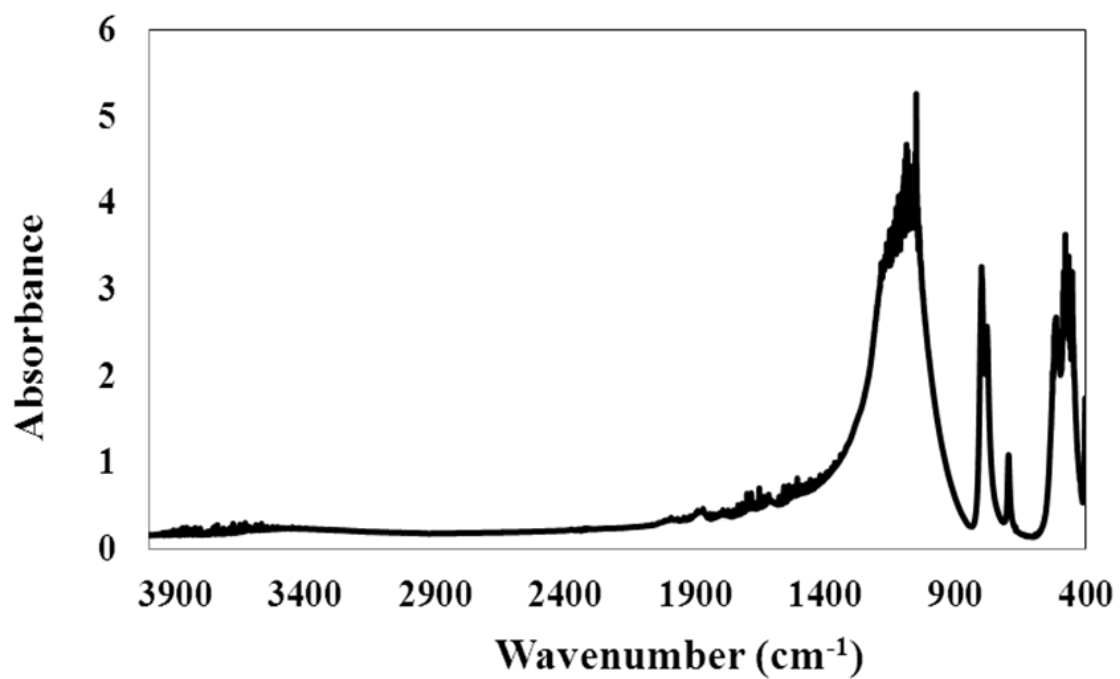
(b)

Figure 7. 8 Fourier Transform Infrared Spectrum of Fermentas a. Spin Column b. Silica
    bead

7.1.3. Elemental Composition of Adsorbents

X-ray Fluorescence (XRF) Analysis

Elemental analyses of the adsorbents were performed by XRF. The elemental compositions were displays in Appendix A, for silica, alumina and HAP respectively. Main determined element concentrations in % mass are listed in

Table 7.1. According to this table silica and alumina show expected results and HAP has Ca/P mass ratio of 2.71 and mole ratio of 1.67. There is a consistency between hydroxyapatite (Ca/P ratio:1.67) (Şahin E. 2006).

Moreover oxides for of the adsorbents elemental analysis result were listed in Table 7.2. Represented composition graphs are in Appendix A

Table 7.1 Main Elements (%mass) of Silica Alumina and Hydroxyapatite (HAP)

	Na	Mg	Al	Si	P	Ca	Fe	Cu
Silica	0.02	0.55	0.46	37.75	0.02	0.13	0.09	0.28
Alumina	1.11	1.16	43.61	0.001	0.01	0.06	0.09	0.25
HAP	0.21	0.27	0.66	0.68	9.84	26.69	0.08	0.23

Table 7.2 Composition of Adsorbents Reported in Oxide form by XRF

	Na_2O	MgO	Al_2O_3	SiO_2	P_2O_5	CaO	Fe_2O_3	CuO
Silica	<0.02	0.91	0.86	80.77	0.05	0.179	0.13	0.3
Alumina	1.494	1.927	82.38	<0.0021	0.0277	0.0837	0.134	0.306
HAP	0.28	0.454	1.25	1.451	22.54	37.35	0.1204	0.292

EDX Analysis of Adsorbent of the Spin Column and Silica Bead

Commercial DNA extraction kit (Fermantas K0503) of spin column is a kind of membrane. Chemical analysis of the samples taken from the top and bottom of the membrane was made by EDX technique. Average percent of mass of elements are represented in Table 7. 3. The results indicate that spin column DNA extraction kit is consisted of mainly silica and oxygen elements together with sodium, Al, K, Ca and Ba. The small peak observed before N in Figure 7.9 belonged to B element indicating that the spin colum is made out of borosilicate glass. The elemental analysis of the silica bead reported Table 7.2 indicated that it was pure silica.
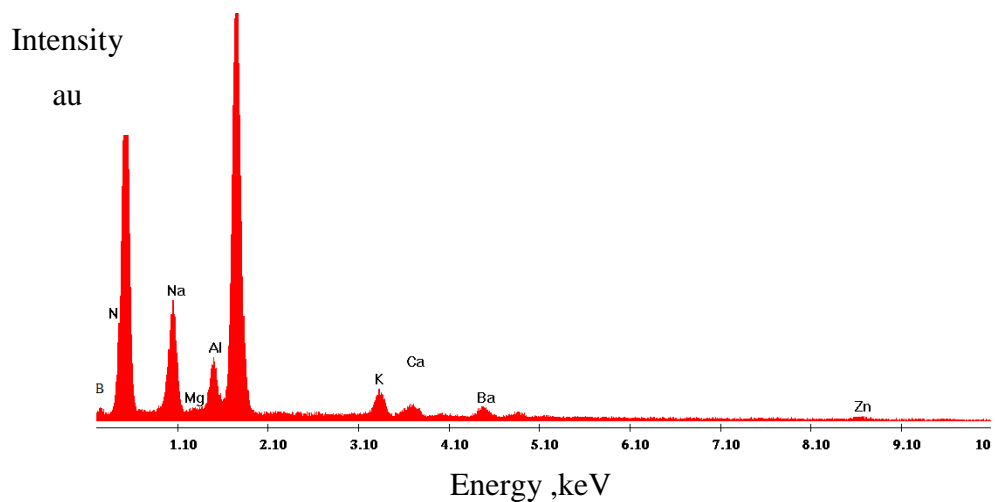
(a)
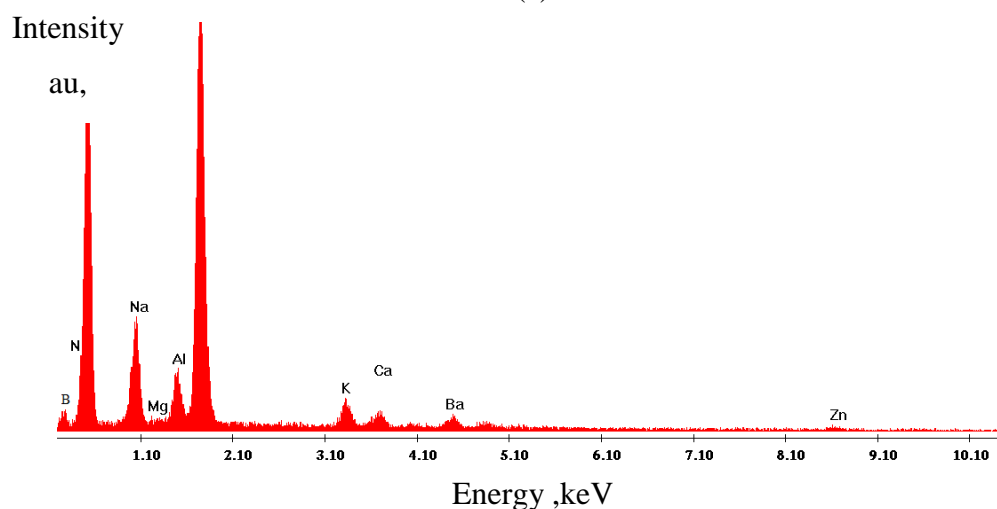
(b)

Figure 7. 9. EDX results of Spin column a) top and b) bottom parts

Table 7. 3. Elemental Analysis of Spin column adsorbent's top and bottom surfaces and the silica bead

	Average % Mass of elements									
Sample	Si	Al	N	O	Na	Mg	K	Ca	Ba	Zn
Spin column Top	25.2	2.9	4.2	34.4	7.7	0.5	3.48	1.09	1.30	2.30
Spin Column Bottom	25.4	3.1	3.7	35.0	7.6	0.5	3.42	1.19	1.17	2.31
Silica bead	40.6	0	0	60.4	0	0	0	0	0	0

7.1.4. Thermal Analysis of Adsorbents

The TGA curve obtained for silica, alumina and HAP are shown in Figure 7.10. Figure 7.11. and Figure 7.12. respectively. The samples were heated up to 1300 °C at a heating rate of 10 °C/min, and were kept at this temperature until constant weight was attained. Silica contained nearly 5% water as bound-OH groups. Alumina has 2.5 % H_2O and HAP 10 % bound of OH groups.
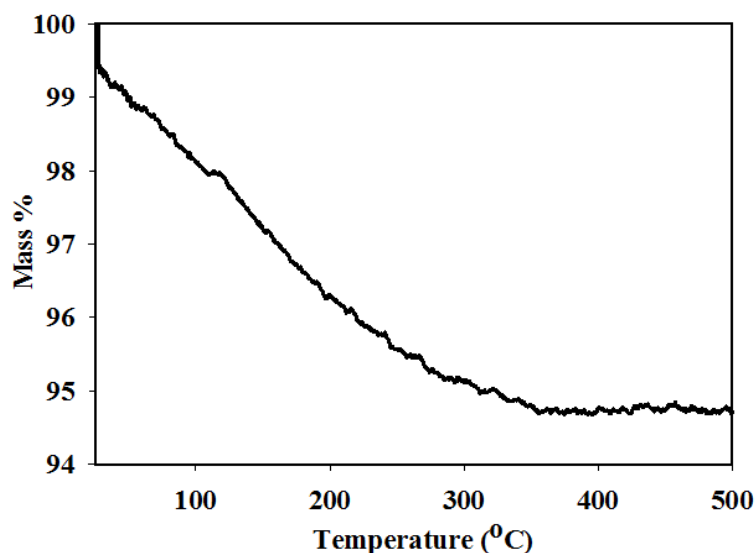
Figure 7. 10. TGA thermogram of Silica
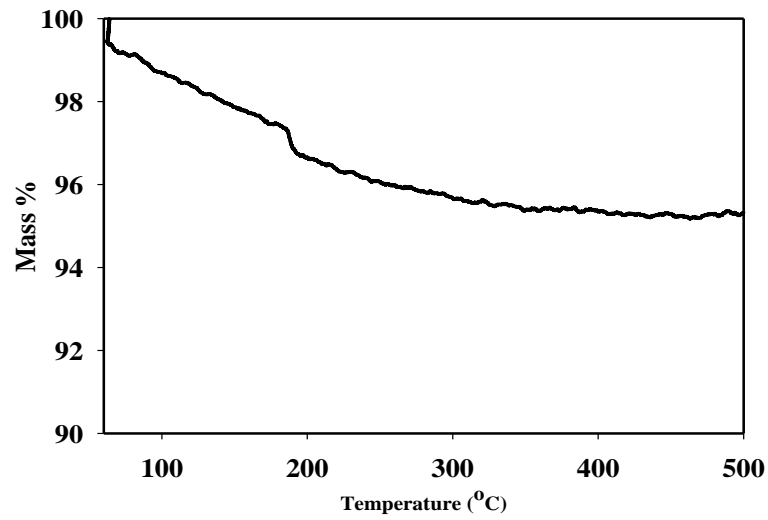
Figure 7. 11 TGA thermogram of Alumina
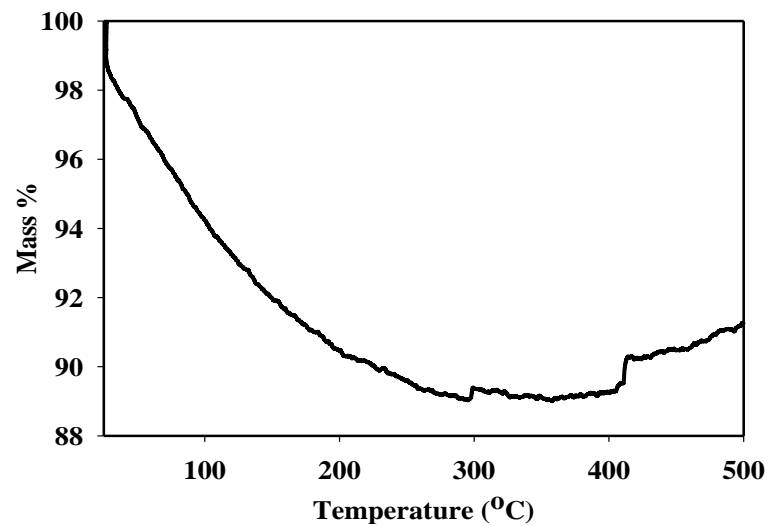
Figure 7. 12. TGA thermogram of HAP

7.1.5. Morphology of the Adsorbents

Silica morphology was investigated scanning electron microscopy technique with different magnifications as represented in Figure 7.13. Silica has very uniform structure and at high magnification surface shown to be very flat. Figure 7.13. (d) also used to measurement of particle size distribution as will mentioned in the related part of the report.
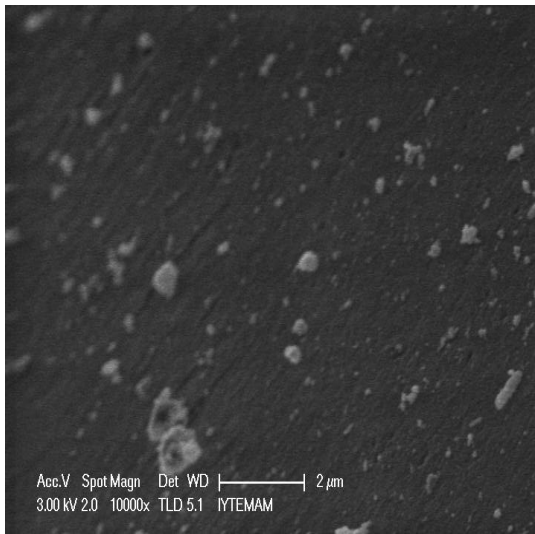
(a)
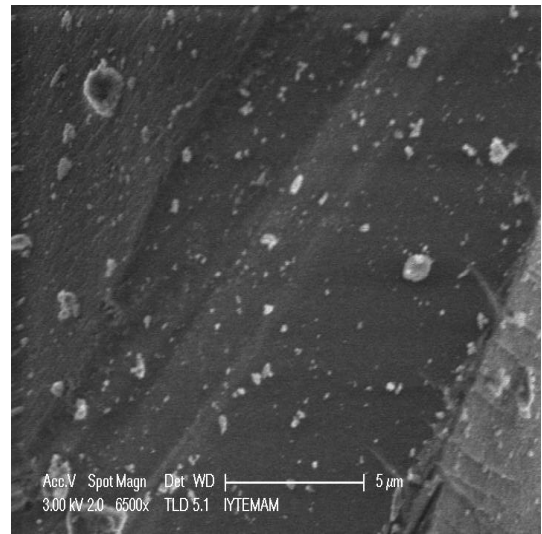
(b)
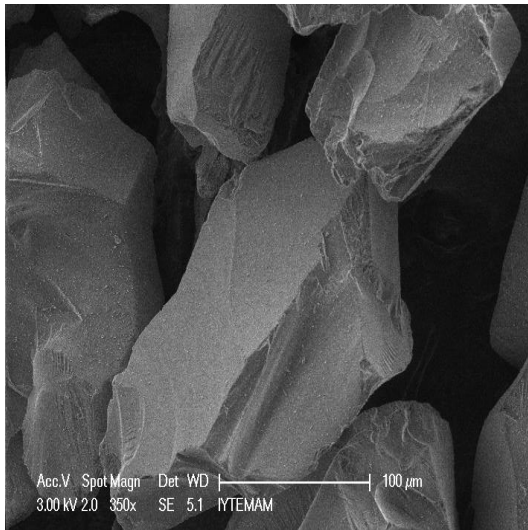
(c)
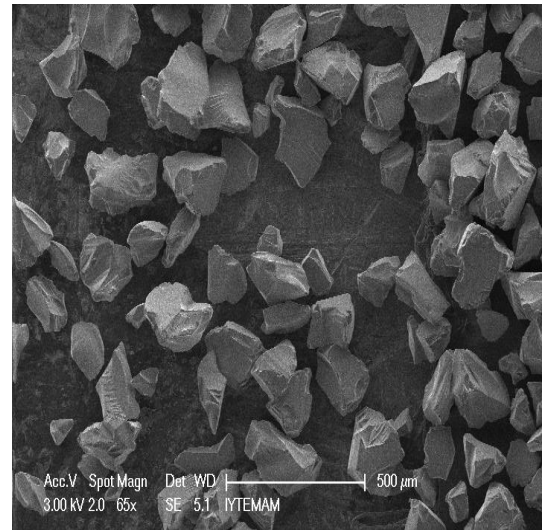
(d)

Figure 7. 13. SEM images of Silica with Secondary Electron Detector (SE); a) 10000 X b) 6500 X c) 350 X d)65 X magnification
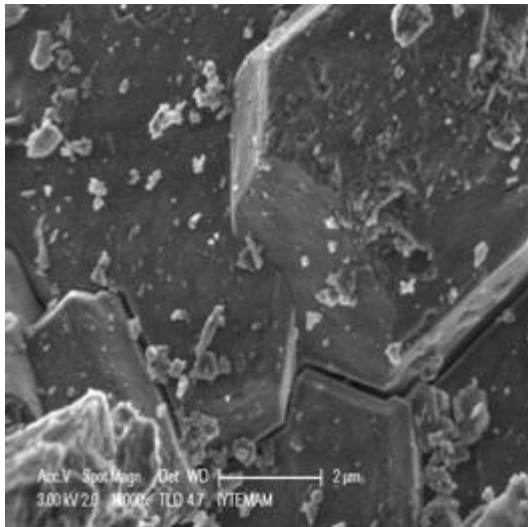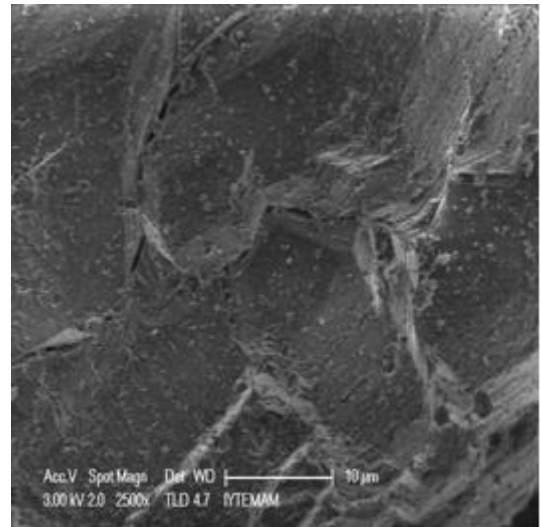
(a)   (b)
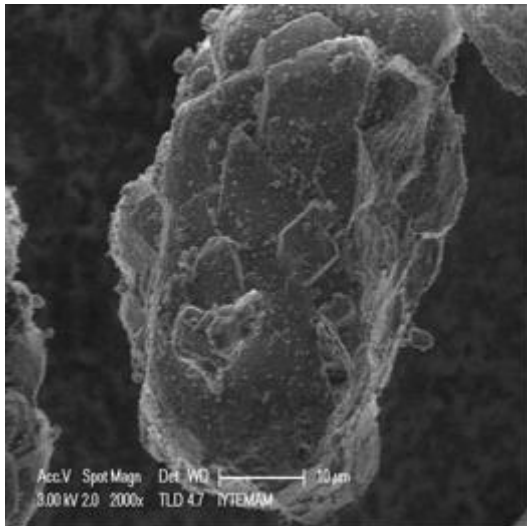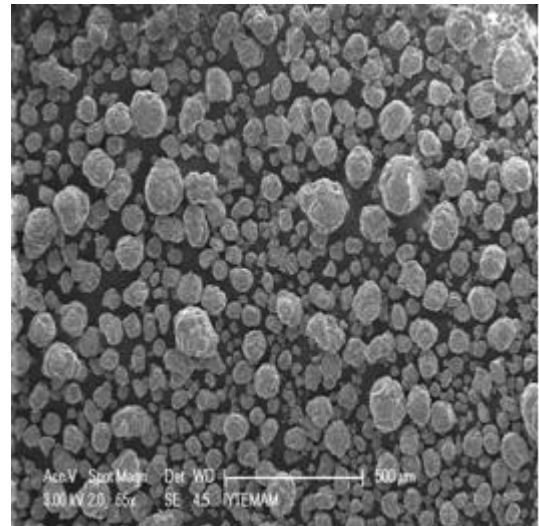
(c)   (d)

Figure 7.14. SEM images of Alumina with Secondary Electron Detector (SE); a) 12000
X b) 2500 X c) 2000 X d)65 X magnification

Alumina SEM images are shown in Figure 7.14. Particle has some has a regular plate like crystals structure. Figure 7.14. (d) again will used in the Alumina particle size distribution measurements.

SEM images of HAP in Figure 7.15. showed that it had nanosized particles. Figure 7.16. showed that spin column adsorbent was in fiber form and a silica bead commercial kit has a particulate structure as seen Figure 7.17.
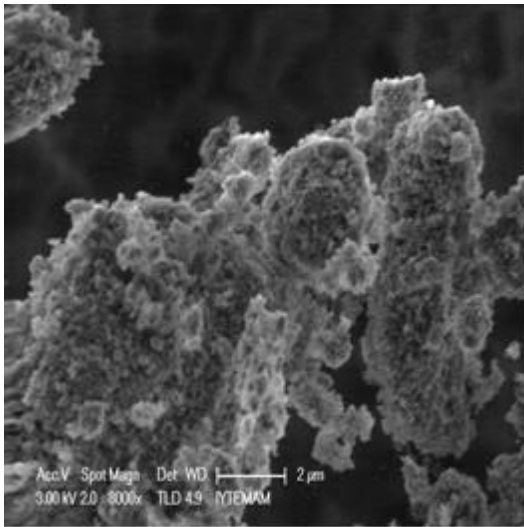
(a)
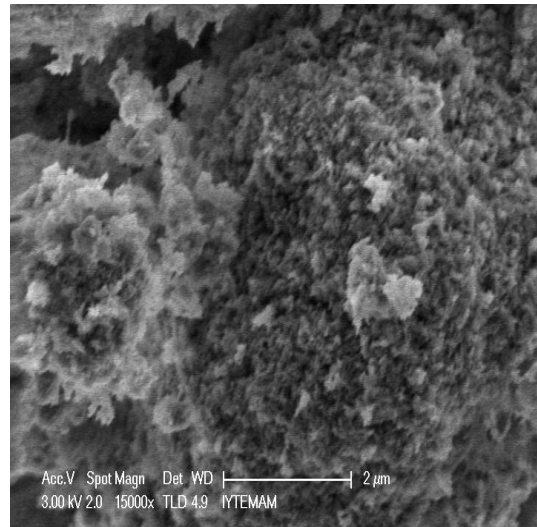
(b)
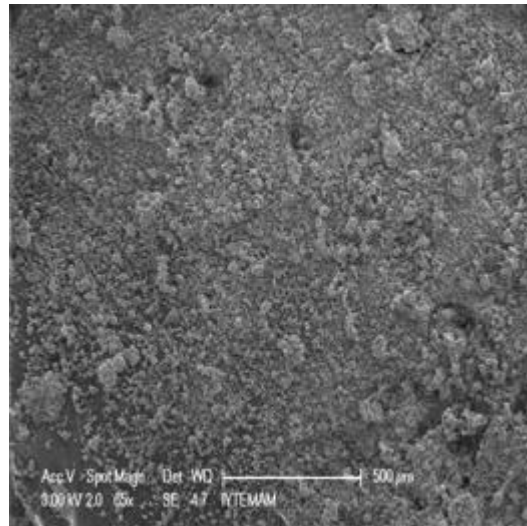
(c)

Figure 7. 15. SEM images of HAP at different magnifications
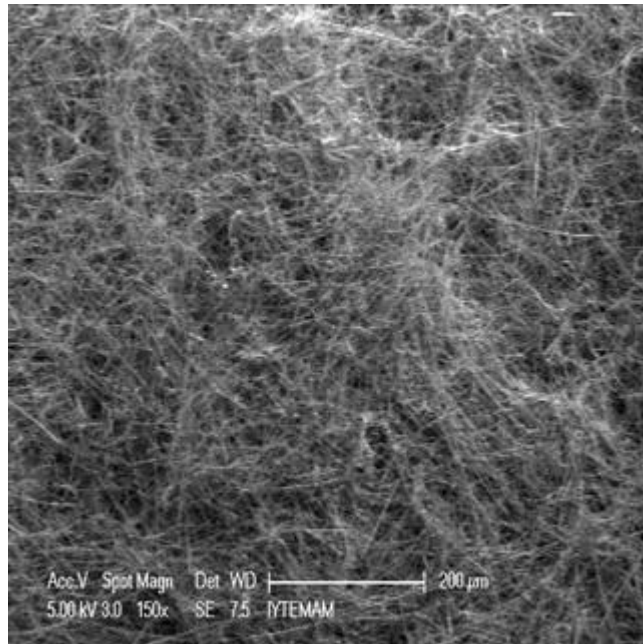
(a)
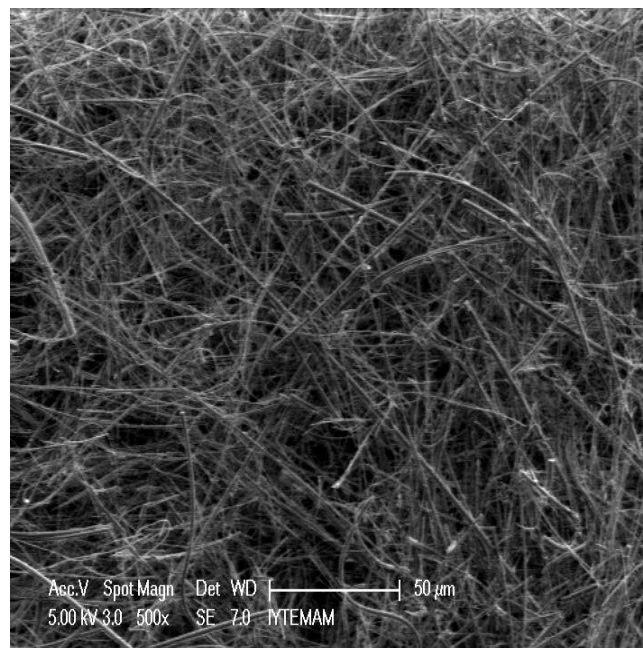
(b)

Figure 7.16. SEM images of (a) ,(b) Spin Column Adsorbent at different magnifications
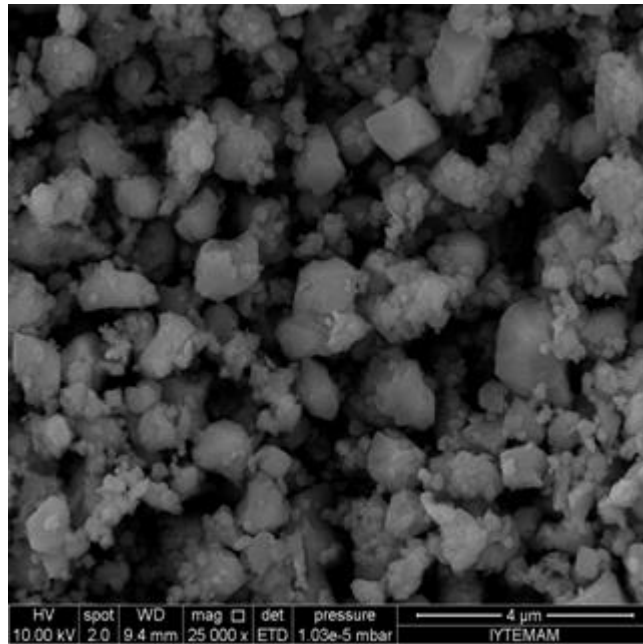
(a)
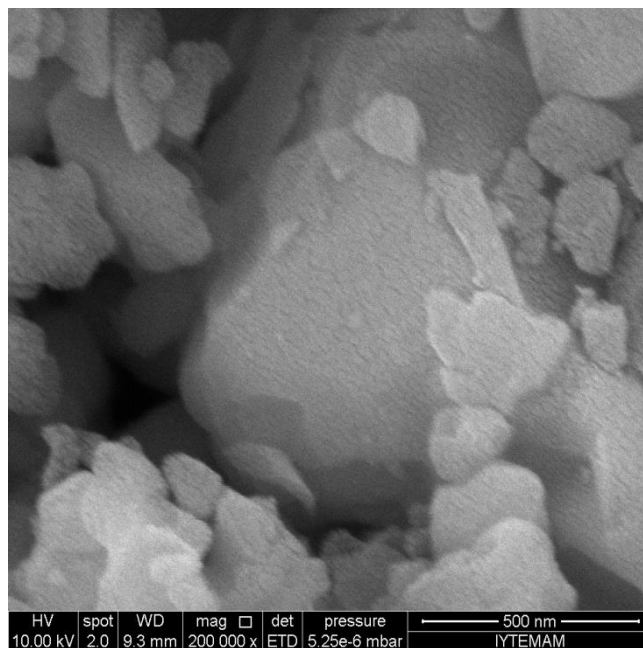
(b)

Figure 7.17. SEM images of Silica bead commercial kit adsorbent at different magnifications

7.1.6. Nitrogen Adsorption

The adsorption isotherms of N_2 adsorption at 77 K are shown for silica, Fermentas silica bead, alumina and HAP in Figure 7.18. a, b, Figure 7.19 and 7.20. respectively. Silica, alumina and hydroxyapatite isotherms were of the Type IV of the UIPAC classification. Hysteresis loop formed by adsorption/desorption isotherms due to condensation and evaporation of liquid nitrogen from mesopores and depends upon the shape and size of pores (Greeg and Sing , 1982). Hysteresis cycle was commonly observed for materials with interrelated pore networks with different size and shape. The isotherms of silica, alumina and hydroxyapatite have hysteresis loops, which are consistent with the presence of mesopores. Relative pressure of (P/P_0) if greater than 0.6 is associated with capillary condensation in mesopores, which is characteristic of type IV isotherms (Ru et al., 2010). Single point, BET and Langmuir surface areas, average pore diameter, total pore volume, micropore volume of the adsorbents are listed in Table 7.4.
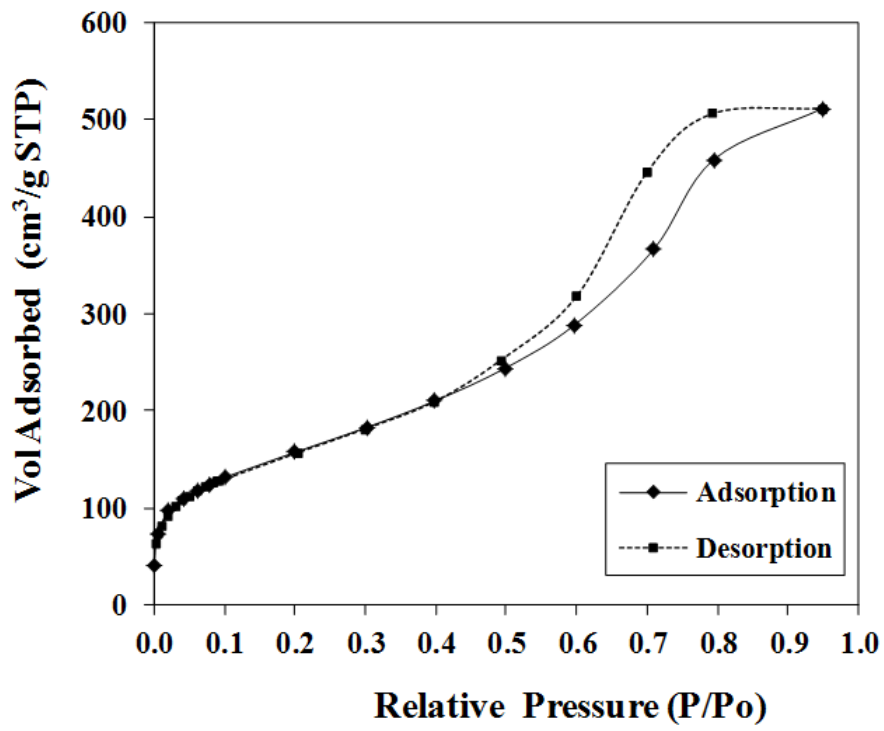
(a)
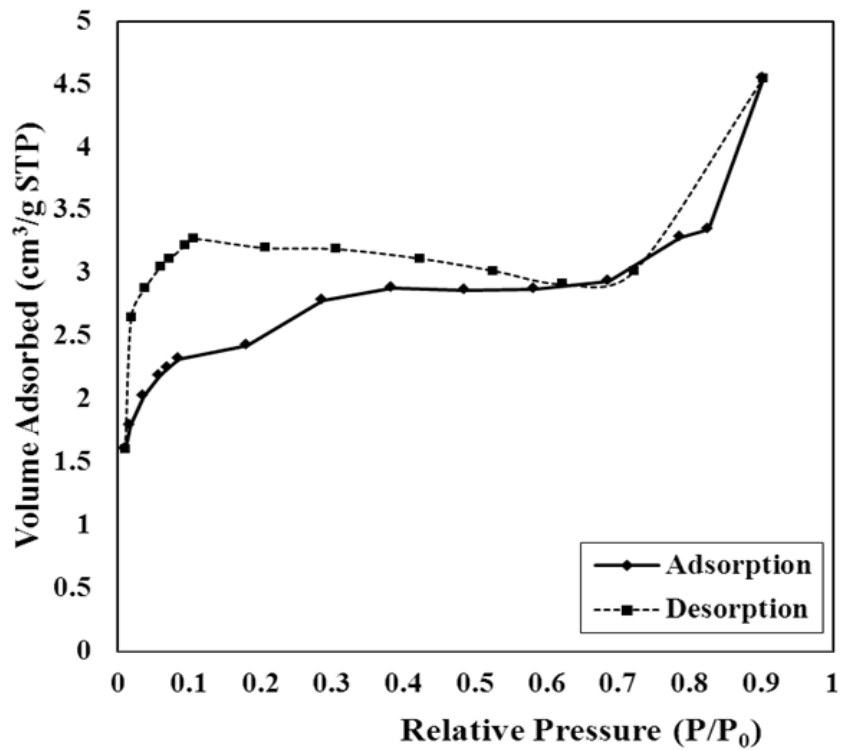
(b)

Figure 7. 18. Nitrogen adsorption and desorption isotherms of a. Silica b. Fermentas
Silica bead at 77 K
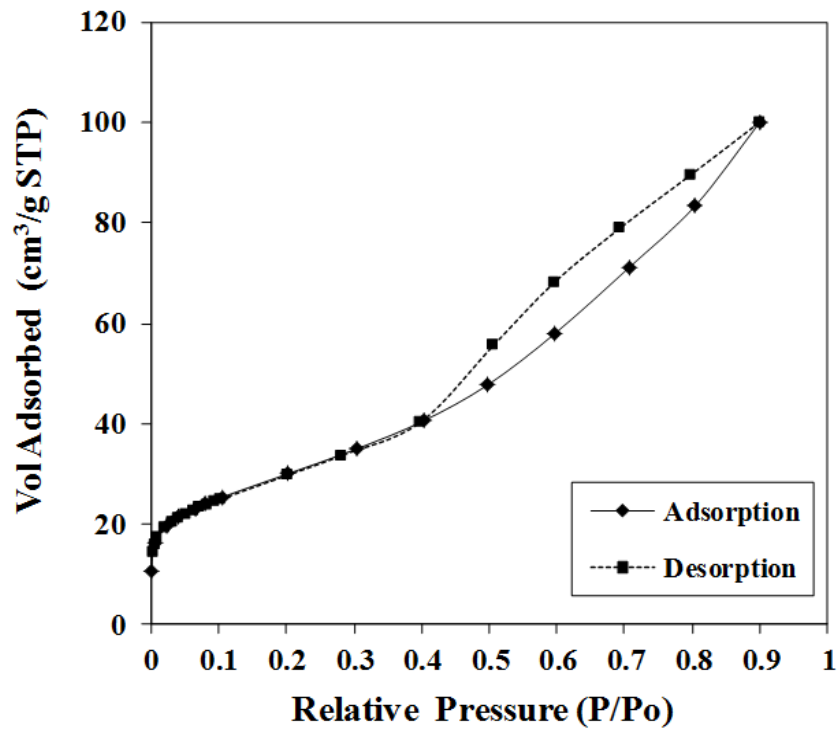
Figure 7.19. Nitrogen adsorption and desorption isotherms of Alumina at 77 K
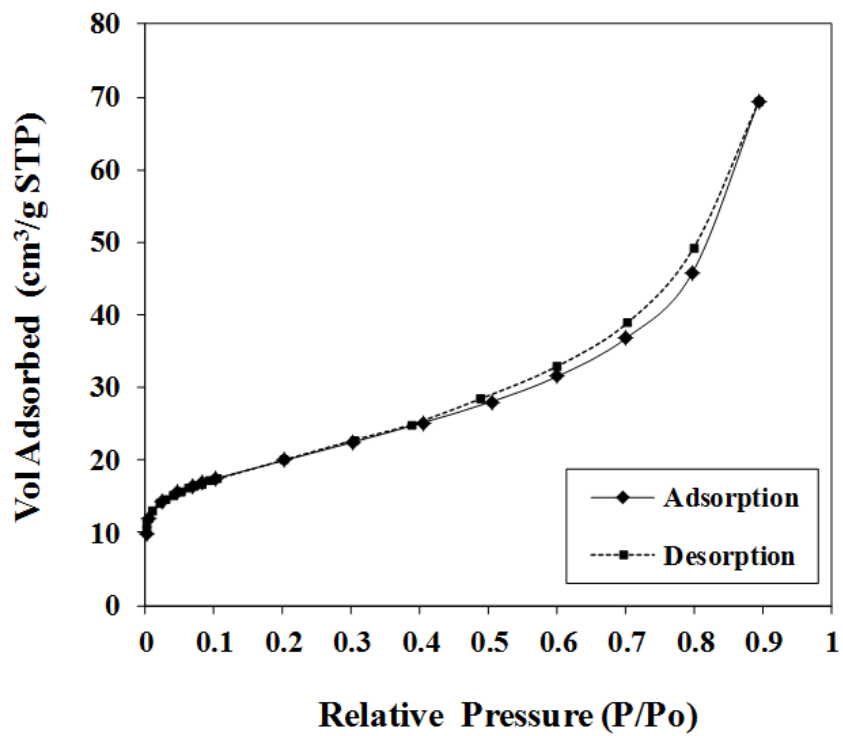
Figure 7. 20 . Nitrogen adsorption and desorption isotherms of HAP

Table 7. 4 Surface Characteristics of the Adsorbents

Properties	Silica	Fermantas Silica Bead	Alumina	HAP
Single Point Surface Area (m^2/g)	556	10	106	68
BET Surface Area (m^2/g)	571	9	108	69
Langmuir Surface Area (m^2/g)	787	14	148	96
Average Pore Diameter (nm) (4V/A by BET)	5.5	0.11	5.7	6.2
Single Point Total Pore Volume (cm^3/g)	0.79	0.006	0.16	0.11
Max Micropore Volume (cm^3/g)	0.20	0.003	0.04	0.03

According to these data silica had the highest surface area, total pore volume and maximum micropore volume compared to alumina and HAP. Nitrogen adsorption analysis for Fermentas K0513 silica bead showed that it has 10 m^2/g single point surface are, 9 m^2/ g BET surface area and 0.1nm average pore diameter. Its total pore volume is close to zero (0.006 cm^3/g), indicating that it was a nonporous powder.

7.1.7 Particle Size Distribution Measurements

Adsorbent particle size distribution could only be performed for silica and alumina sample by the help of SEM images using Scandium software available in Material Science Centre. Figure 7. 21. (a) (b) show the particle size distribution of silica and alumina respectively. They have nearly uniform particle size distribution. Average particle size of silica and alumina were measured with eqn (7.1) Results were found to be as 162 and 59 µm for silica and alumina respectively.

$$\text{Average particle size} = \sum \left(\frac{frequency}{\text{number of total measurement}} \text{interval range} \right) \qquad (7.1)$$
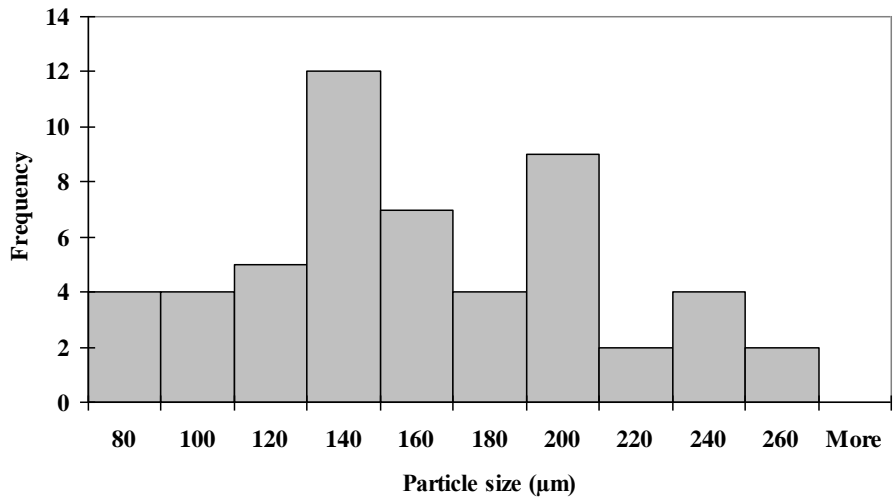
(a)
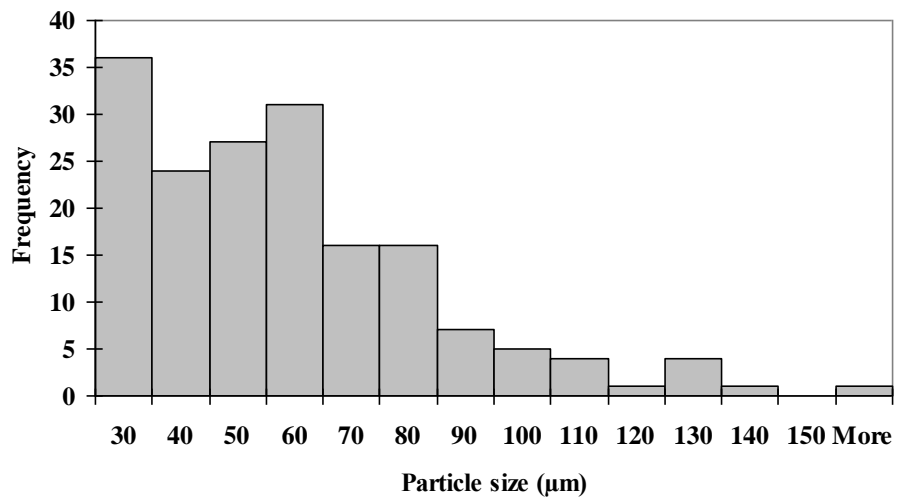
(b)

Figure 7. 21. Particle Size Distribution of (a) Silica and (b) Alumina
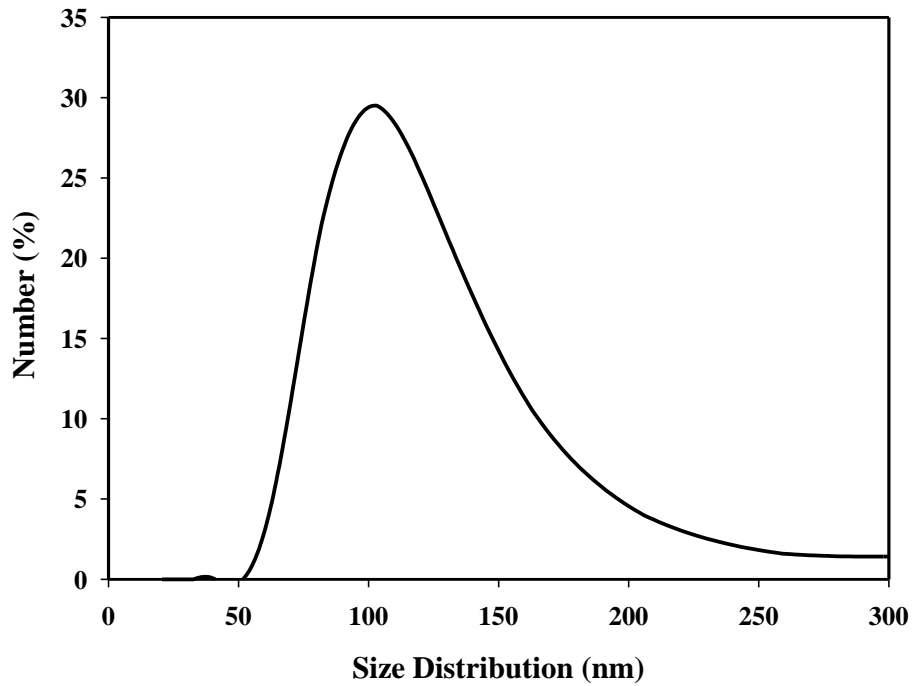
Figure 7.22. Number particle size distributions obtained for HAP.

Hydroxyapatite shows nanosized particle distribution as seen by its SEM images in Figure 7.15. Size distribution of HAP can be done appropriate analysis method of zetasizer. The average number particle size distributions obtained from the four repeat measurements was plotted in Figure 7.22. HAP has a mean number -weighted diameter of 102 nm.

7.2. Characterization of DNA

7.2.1. Zeta Potential

Some special studies have been focus on the DNA isoelectric point (IEP). The isoelectric point of DNA from different sources is reported about to be pH 5.0 (Cai et al., 2006, Stotzky 2000). Zeta potential measurements showed calf thymus DNA solutions have isoelectric point near the pH 2 value. Figure 7.23 and Figure 7.24 displays initial zeta potential distribution measurements at pH2.2, pH4, pH5,and pH7. After that zeta potential measurement were repeated pH values of 2 to 9.
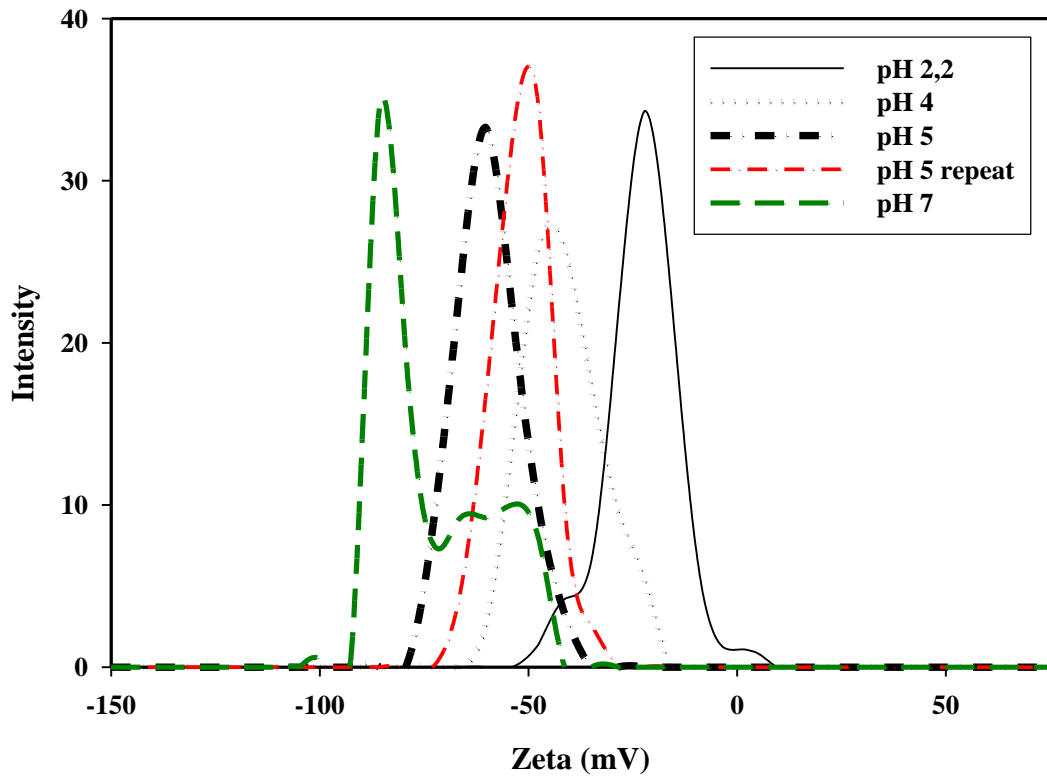
Figure 7. 23. Zeta potential distribution of calf thymus at different pH values
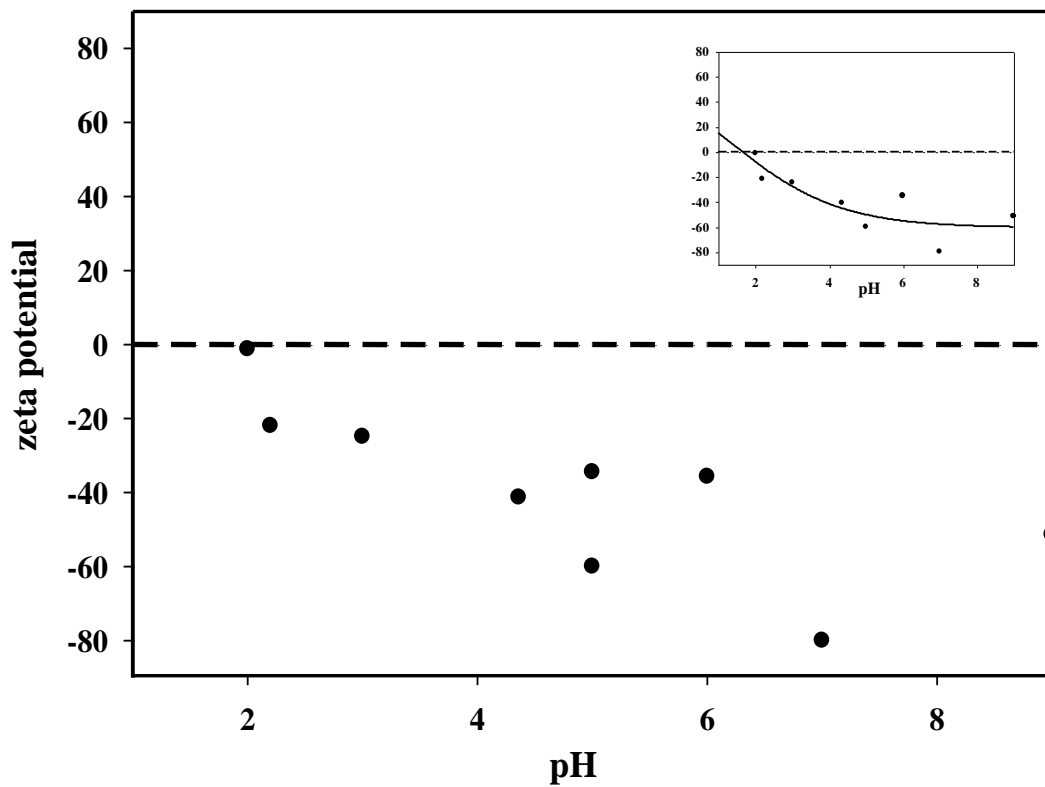
Figure 7. 24. Change of the average zeta potential of calf thymus DNA with pH

The zeta potential distribution curves were obtained and shown in Figure 7.23. The average zeta potential values of calf thymus DNA versus pH values are shown in Figure 7.24. Zeta potential measurements define isoelectric point (IEP) of the calf thymus DNA material that has been used as DNA source. IEP is defined as the pH where the surface will carry no charge. By the help of obtained potential distribution data based on different pH values of the buffer solution highly polymerized calf thymus DNA isoelectric point was found less than pH 2. This is value is found to be lower than the value reported for different DNA molecules by previous workers. These studies have been focus on the DNA IEP. The isoelectric point of DNA from different sources is reported about to be pH 5.0 (Caie et al., 2006, Chargaff and Davidson 1955).

Isoelectric point is considered as one of the important factors affecting the adsorption profile in aqueous solution. For instance adsorption of recognized component for biosensor application is related with the strong electrostatic interactions in electrochemical DNA biosensor. Consequently isoelectric point (IEP) of both phases became important. Therefore different isoelectric point definition for DNA is important at low ionic strength.

7.2.2. Particle Size distribution of DNA

Size characterization of the DNA was made by dynamic light-scattering (DLS) measurements using the Zetasizer. Before the analysis calf thymus DNA solution with 100 ng/μl concentration was softly shaken to be able to get a homogenous DNA sample stock solution in pH 7 phosphate buffer solution (ionic strength is 0.001M). The volume and number particle size distributions of DNA in the solution are shown in Figure 7.25. DNA average particle size in water was determined to be 500 nm assuming their shape is spherical by zeta sizer. The size of the calf thymus was calculated from its molar mass $8.6x \ 10^6$ reported by Tanigawa et al.(1996) close to the this value as 600 nm.
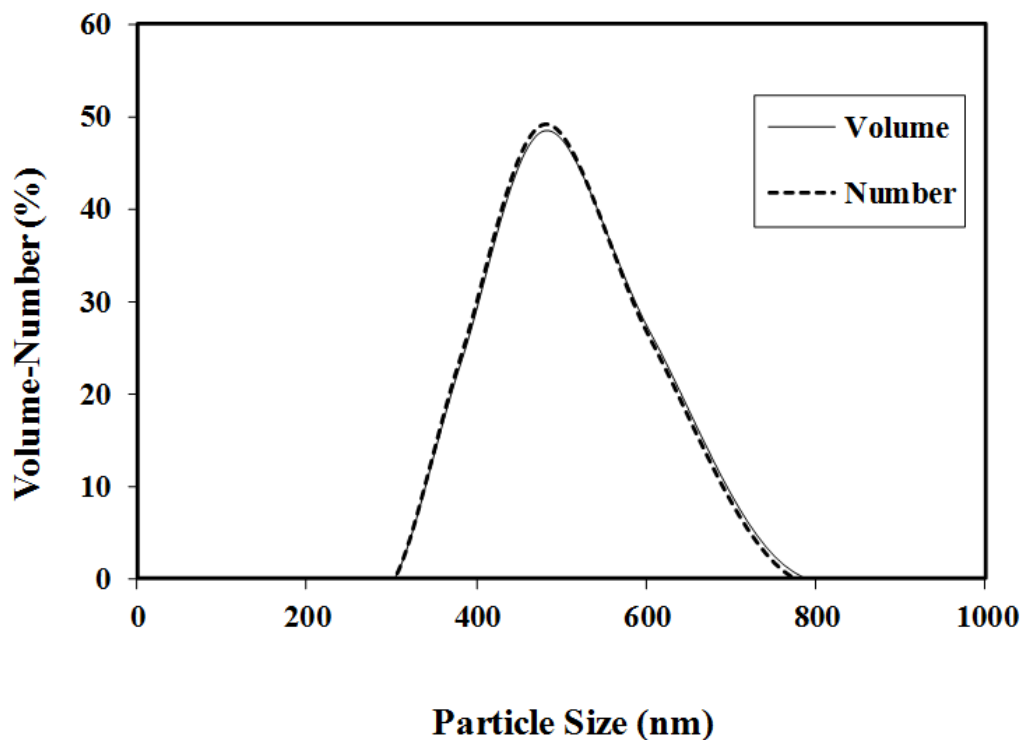
Figure 7. 25. Volume and Number particle size distributions obtained for DNA

7.2.3. Morphology of DNA

Calf thymus DNA images as shown in Figure 7.26. Figures can be comparable at same magnification range. Especially details inside the circle in Figure 7.26. (e) can be seen in Figure 7.26. (f). As a result calf thymus DNA sample has a very polymerized complex structure. DNA has nearly 5μm diameter fibers Figure 7.26. (d) and in Figure 7.26. (f) it has nearly 2μm diameter fibers.
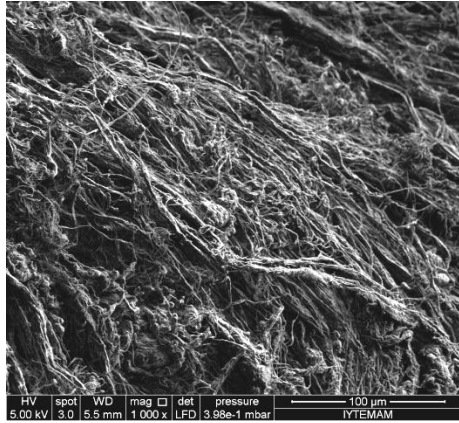
(a)
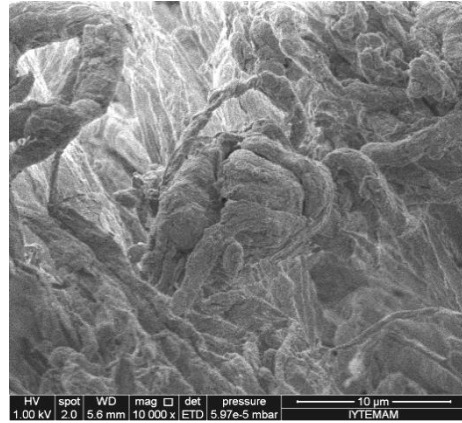
(b)
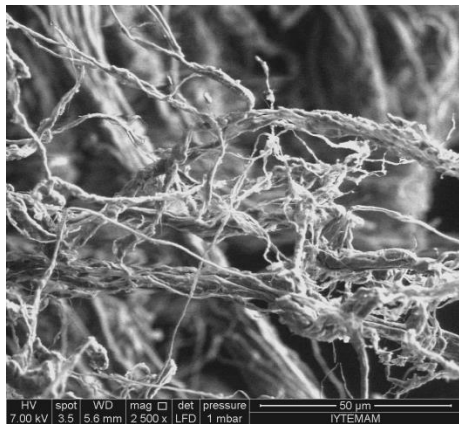
(c)
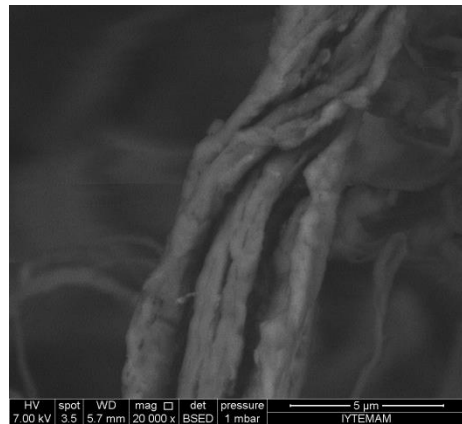
(d)

(e)
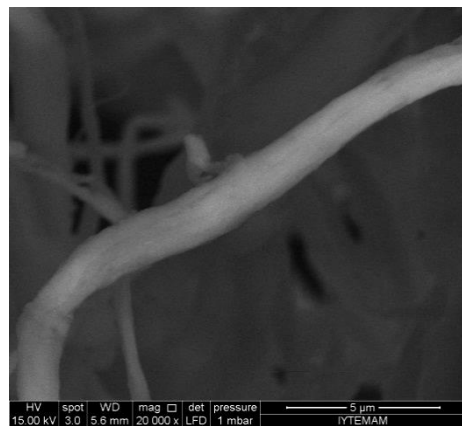
(f)

Figure 7. 26 SEM images of Calf Thymus DNA at different magnification a) 1000x b)
10,000x c) 2,500x d) 20,000x e) 2000x f) 20,000x

7.2.4. Calf thymus DNA Chain Breaking

In enzyme restriction parts of the study 1 µl EcoRI was used. Fragment size determination is typically performed by comparison to commercially available DNA markers containing linear DNA fragments of the known length which one chosen 1kb DNA Ladder (Thermo Scientific Gene Ruler #SM0313) in this study. After 1 hour electrophoresis the gel was illuminated with an ultraviolet lamp. After that the gel was placed into electrophoresis, platform again and voltage was applied for 4 more hours. The gel was illuminated again totally 5 hours later after the start of the experiment.

The samples were placed with the given order into agarose gel inside the. 1× TBE buffer as seen in Figure 7.27 (a); marker, 100ng/µl calf thymus DNA in water, 100ng/µl calf thymus DNA in TE buffer, 100ng/µl calf thymus in water with enzyme treated for 5, 10 and 20 minutes respectively followed by calf thymus in TE with enzyme treated for 5, 10 and 20 minutes.

(a)   (b)
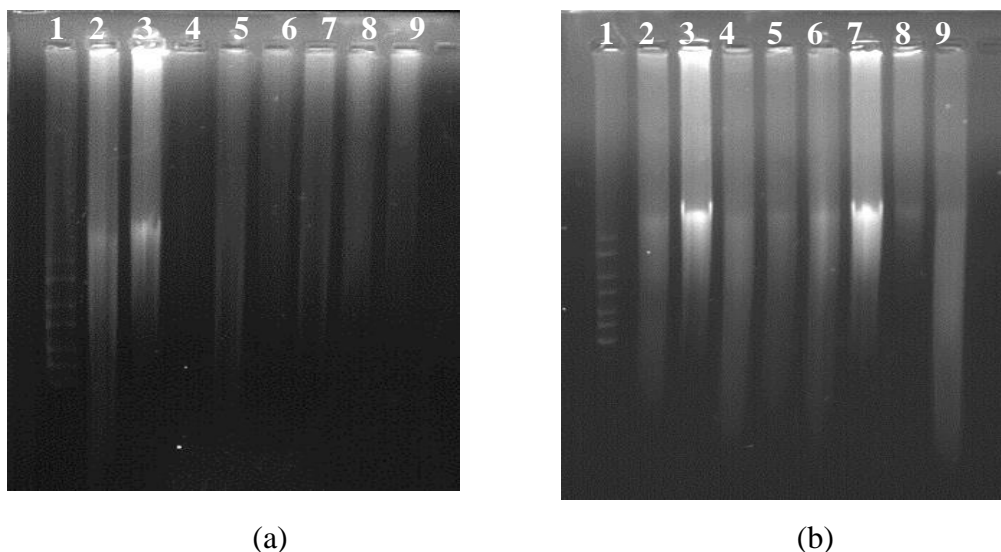
Figure 7. 27. Illuminated gel after 1 hour of electrophoresis with an ultraviolet lamp;
    a. (1) DNA marker,(2) DNA in water, (3) DNA in TE, (4) enzyme treated DNA in water for 5 min, (5) 10 min, (6) 20 min (7) enzyme treated DNA in TE buffer for 5 min(8) 10 min (9) 20min
    b. (1) DNA marker, (2)DNA in water, (3) DNA in TE, (4) sonicated DNA in water for 10 s, (5) 30 s,(6) 90 s (7) sonication treated in TE buffer for 10 s (8) 30 s, (9) 90 s.

(a)   (b)
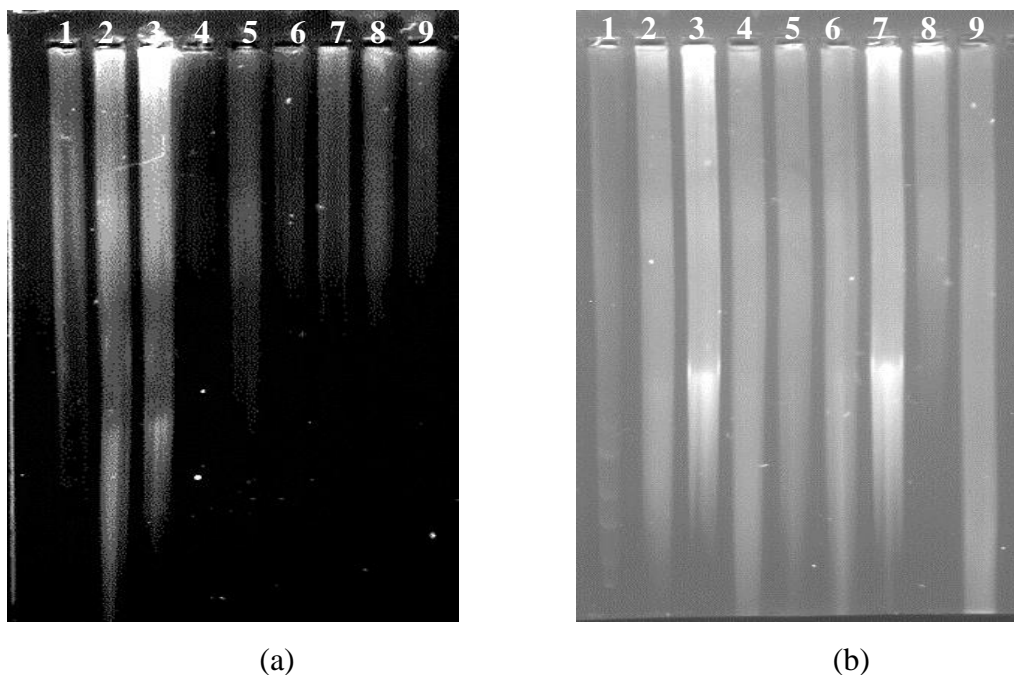
Figure 7. 28. Illuminated gel after 5 hour of electrophoresis with an ultraviolet lamp;

    a. DNA marker,(2) DNA in water, (3) DNA in TE, (4) enzyme treatedDNA in water for 5 min, (5) 10 min, (6) 20 min (7) enzyme treated DNA in TE buffer for 5 min(8) 10 min (9) 20min

    b. (1) DNA marker, (2)DNA in water, (3) DNA in TE, (4) sonicated DNA in water for 10 s, (5) 30 s,(6) 90 s (7) sonication treated in TE buffer for 10 s (8) 30 s, (9) 90 s.

Sonication effect as seen in Figure 7.27. (b). marker, 100ng/µl calf thymus DNA in water, 100ng/µl calf thymus DNA in TE buffer, 100ng/µl calf thymus in water with sonicated for 10, 30 and 90 seconds respectively followed by calf thymus in TE with enzyme treated for 10, 30 and 90 seconds.According to Figure 7.28. not only the marker but also samples were not seen properly. Illumination of 3 rd line is in (a) part which represents enzyme restriction desired situation, but does not fit the marker. The other trial of calf thymus DNA digestion was repeated two more times just with enzyme restriction method for 30 min and 1 hour to be able to optimize enzyme incubation time and the operation time in 50 ml 1% agarose gel.. As seen in Figure 7.29. first five wells of the gel were filled with the marker.Then, calf thymus DNA which treated with enzyme in water and TE buffer for 30 minutes and 60 minutes were placed in the wells.

Gel electrophoresis of calf thymus DNA digested with EcoRI restriction enzymes confirmed that enzyme restriction methods were more effective than sonication for selected sonication times.
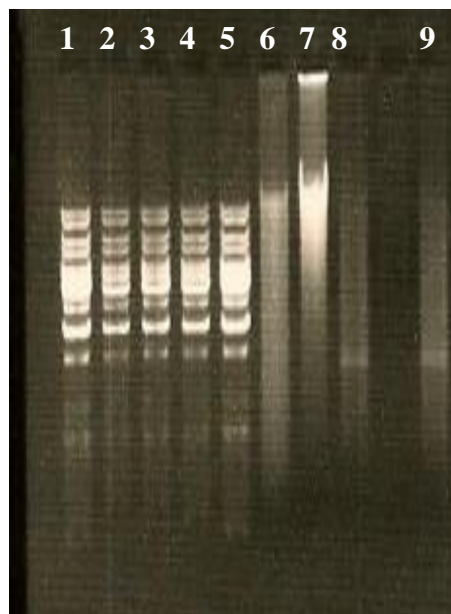
Figure 7. 29. Illuminated gel after 30 min electrophoresis for enzyme restriction part with an ultraviolet lamp, first 5 wells (1-5) were filled with marker, 60 minutes enzyme treated calf thymus DNA (6) in water (7) in TE, 30 minutes enzyme treated calf thymus DNA(8) in water , (9) in TE

A defined base pair size (700 bp) of calf thymus DNA was cut from well 6 by removing agarose gel and DNA in the gel was extracted with Fermentas K0513 Silica Bead DNA Gel Extraction Kit. After all procedure were completed the concentration of DNA was measured using Nanodrop spectrophometer and 19.5 ng/µl 700 bp calf thymus DNAwas obtained.

7.3. Adsorption Experiments

Adsorption experiments were done at different pH values from pH 2 to pH 9. The adsorbents were added to DNA solutions. The mixtures were centrifuged at 20,000 g (Nüve NF800R) after adsorption. The retained DNA concentrations in supernatants were measured with UV spectrophotometer technique with NanoDrop 2000 (Thermo). Initially DNA UV spectrum analysis's accuracy and precision enhancement was

considered with using special dye ethidium bromide. This option was cancelled because of some restriction of using ethidium bromide to provide health protection. Using Cyber Green gave expected booster effect on UV analysis as shown Figure 7.30. 1.6 fold intensity of the normal spectrum band has been obtained by Cyber Green. This dye is known to be an intercalating dye for real-time polymer chain reaction (PCR) applications (Giglio et al., 2003). It is to bind the double stranded DNA and identify PCR product that accumulates during the PCR. However absorbance range in the present study has not been as low to be not identified. Therefore this type of addition was not made in futher analysis.
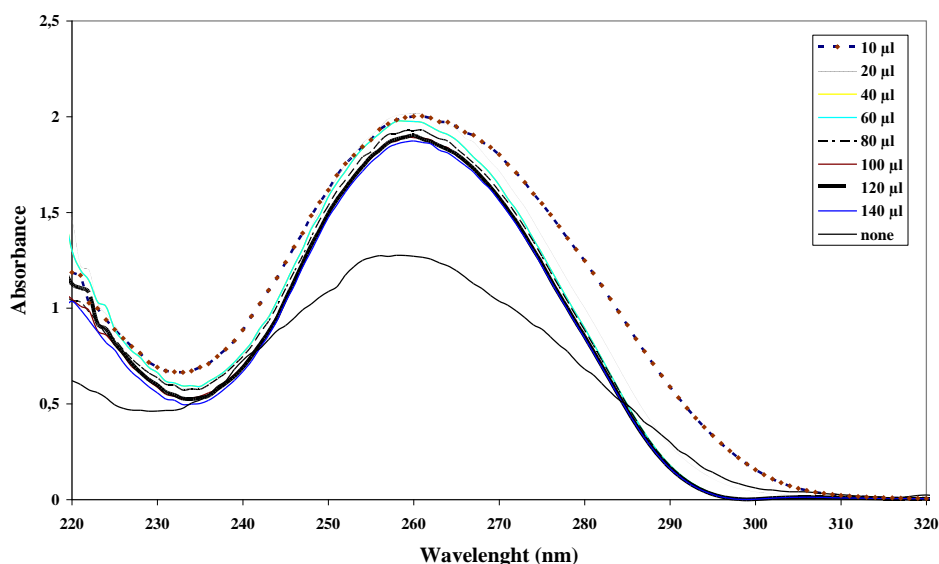
Figure 7. 30. Cyber Green addition effect on full UV spectrum band

UV spectrum required an auto zero based on solvent of the sample. Consequently UV device had been calibrated with buffer solution before each adsorption set. Previously some spectrum oscillations were defined. It was the most challenge work of initial of the experimental part. Reason was identified as buffer adsorption on silica alumina and HAP adsorbents individually or adsorbent dissolution into buffer. After that autozero was performed using adsorbent treated buffer solutions without calf thymus DNA for each pH. In Figure 7.31. the spectra of the supernatants of buffer solutions equilibriated with adsorbents are seen. Pure water was used for autozeroing in these spectra. For instance at pH 2 adsorbents release and adsorb something that affects the UV full spectrum shown in

Figure 7. 31. a. Similarly at pH 5 and pH 6 adsorbents adsorb buffer solution as shown Figure 7. 31. b and c respectively. Adsorbents adsorb the buffer solution materials or dissolve in buffer solution to UV active materials

(a)

(b)

(c)
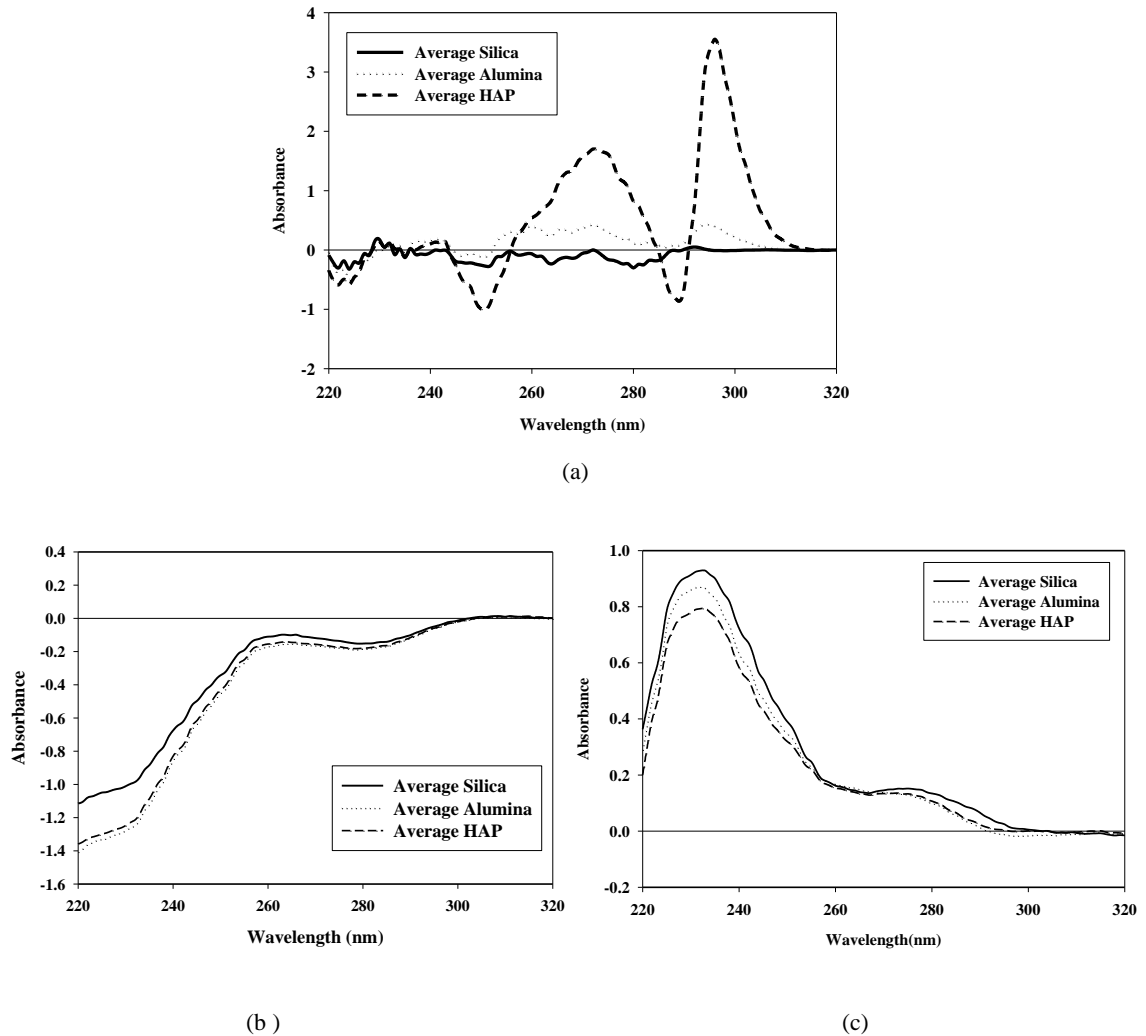
Figure 7. 31. UV spectra of supernatanst in contact with adsorbents showing a) pH 2, b) pH 5 c) pH 6

HAP dissolves at pH 2 more than silica and alumina as seen in Figure 7.31 . HAP is known the most stable calcium phosphate salt but its crystal structure changes under acidic condition. Equilibrated samples were analyzed as described previously. Full spectrums of the samples were obtained and DNA concentrations were calculated based on calibration curves. Adsorbed and non-adsorbed DNA concentrations were figured out.

7.3.1. Sorption Isotherm

Then data were analyzed for equilibrium DNA concentration versus adsorbed DNA concentration. Figure 7.32. to Figure 7. 42. show adsorption isotherms of silica alumina and HAP at different pH values. 0.5 mM and 20mM Mg Cl2 addition onto batch adsorption experiments at pH 5 results are shown in Figure 7. 43. and Figure 7.44. According to these figures divalent cation addition positively affected DNA adsorption as expected because of the cation bridge effect.
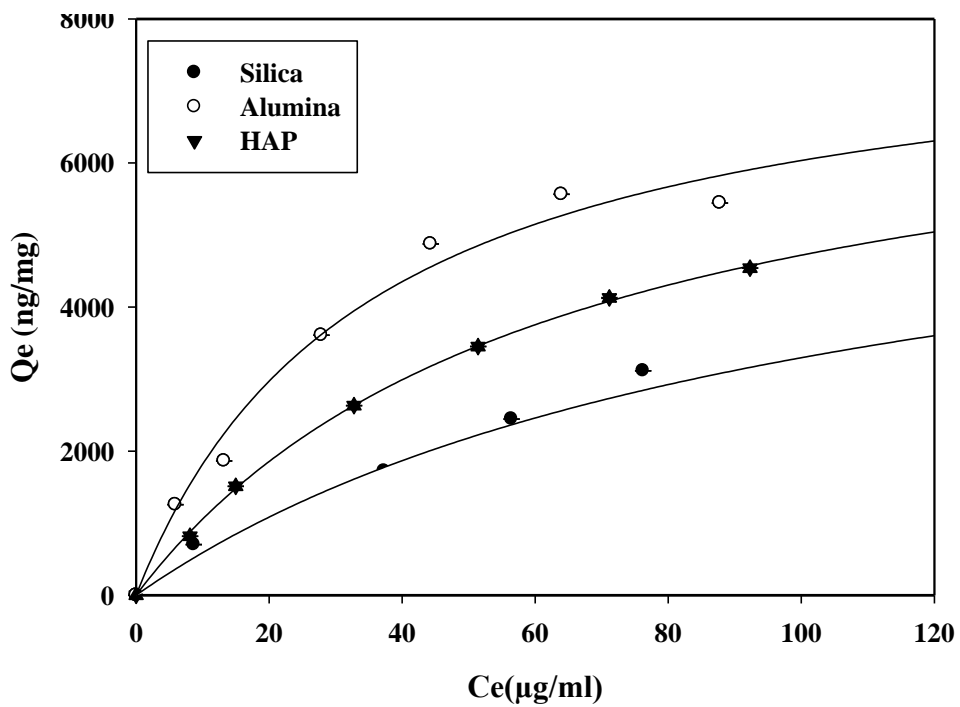
Figure 7.32. DNA adsorption on Silica, Alumina, and HAP at pH 2
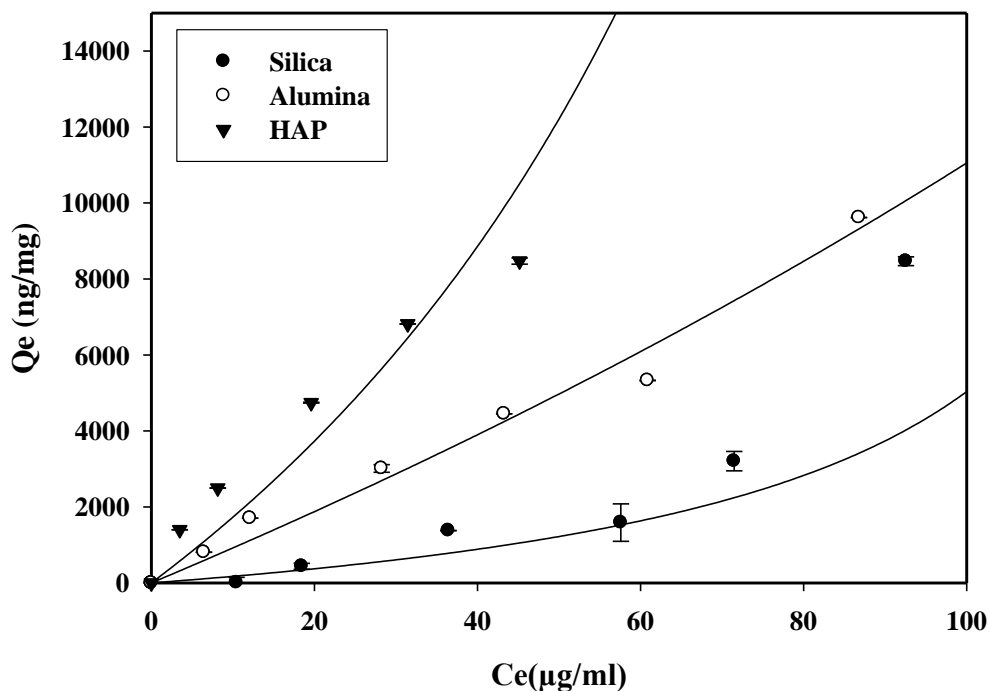
Figure 7. 33. DNA adsorption on Silica, Alumina, and HAP at pH 3

Adsorption isotherms did not reach the equilibrium value for all three of the adsorbents at pH 3. These buffer solutions were prepared by potassium hydrogen phthalate –HCl complex. It is obtained that buffer solution chemical composition has effect on adsorption. DNA was well known to be adsorbed by sand at low pH value (Lorenz and Wackemagel 1987). These pH values are near the IEP of DNA which is found near the pH 2 value.

The initial slope is near infinite for HAP at solution pH 4 seen in Figure 7. 34. This is indicated a high affinity of DNA for the HAP surface at this acetate buffer pH.
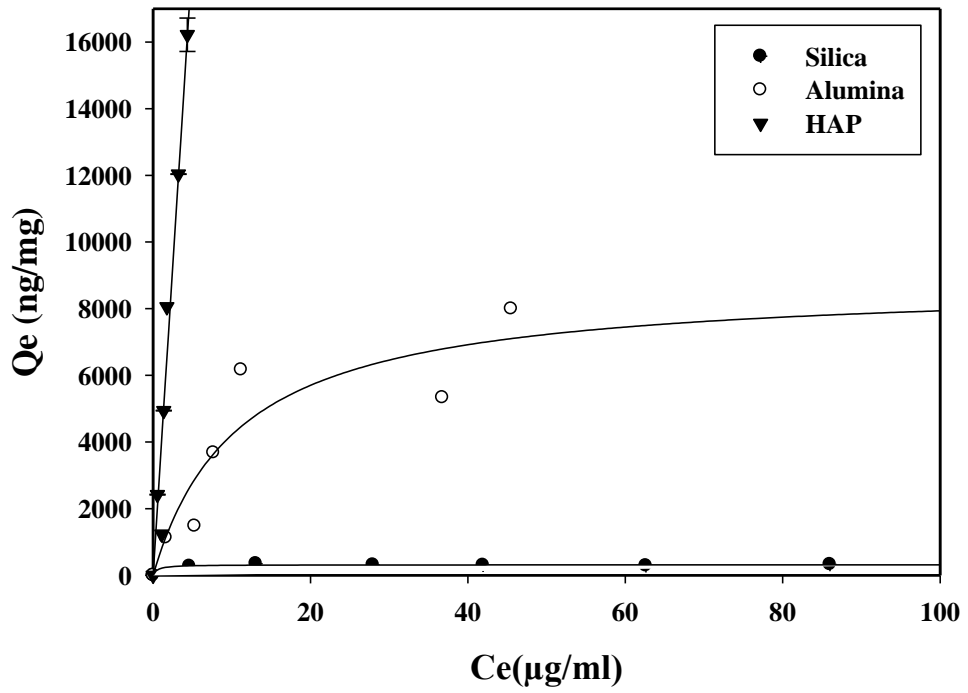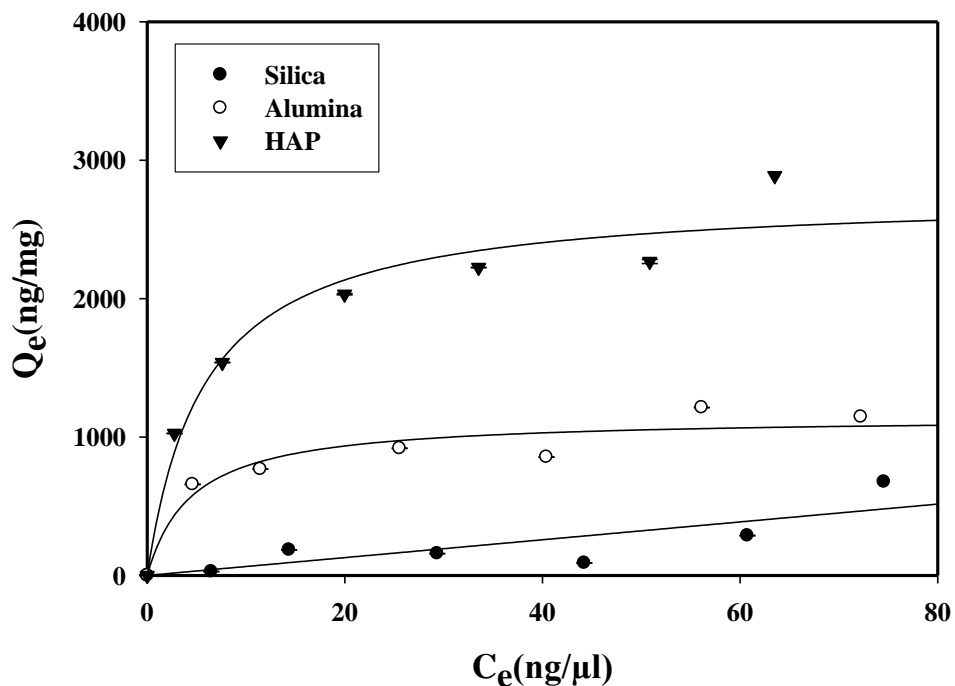
Figure 7. 34. DNA adsorption on Silica, Alumina, and HAP at pH 4
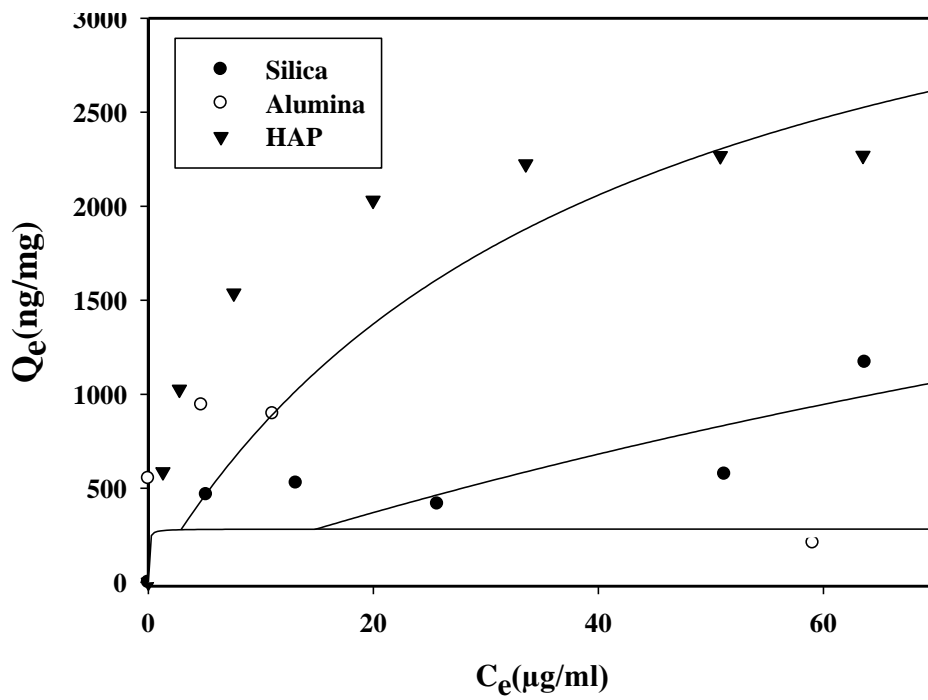
Figure 7. 35 . DNA adsorption on Silica, Alumina, and HA at pH 5
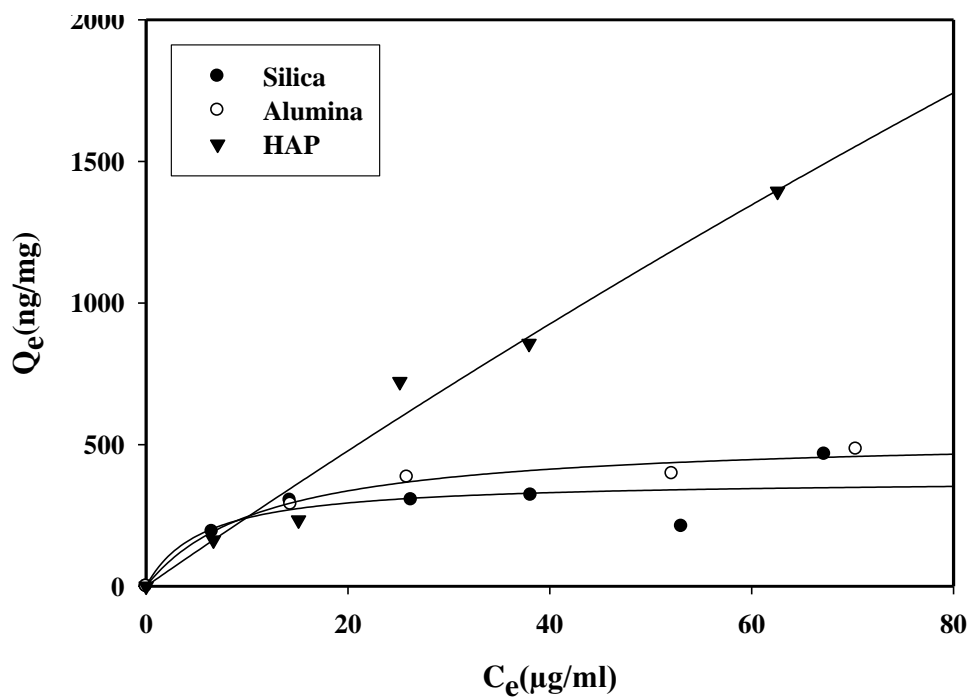
Figure 7. 36. DNA adsorption on Silica, Alumina, and HAP at pH 6
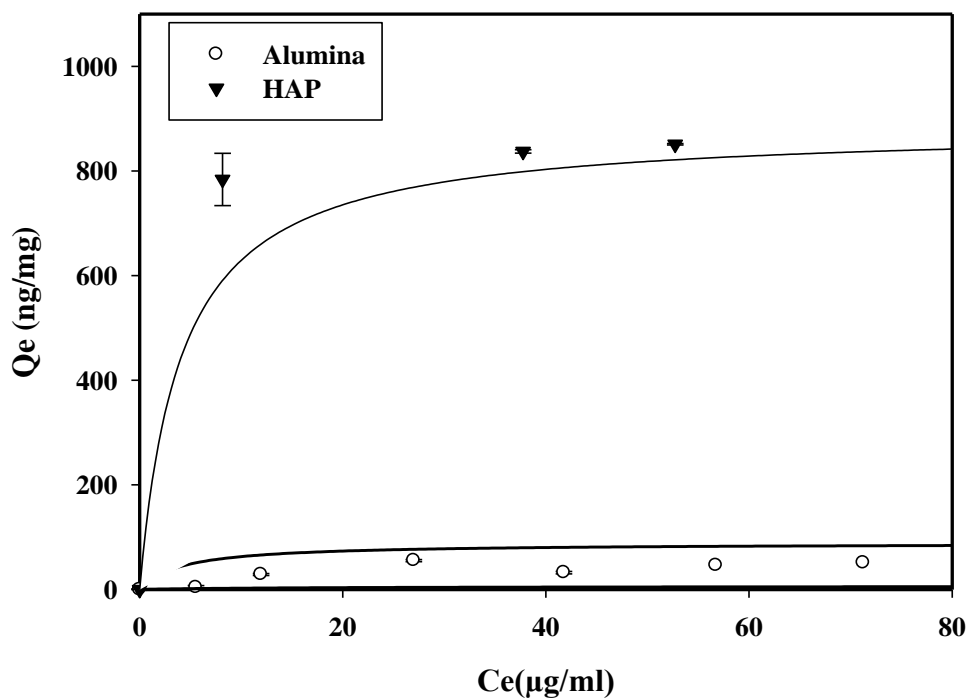
Figure 7. 37. DNA adsorption on Silica, Alumina, and HAP at pH 7.4
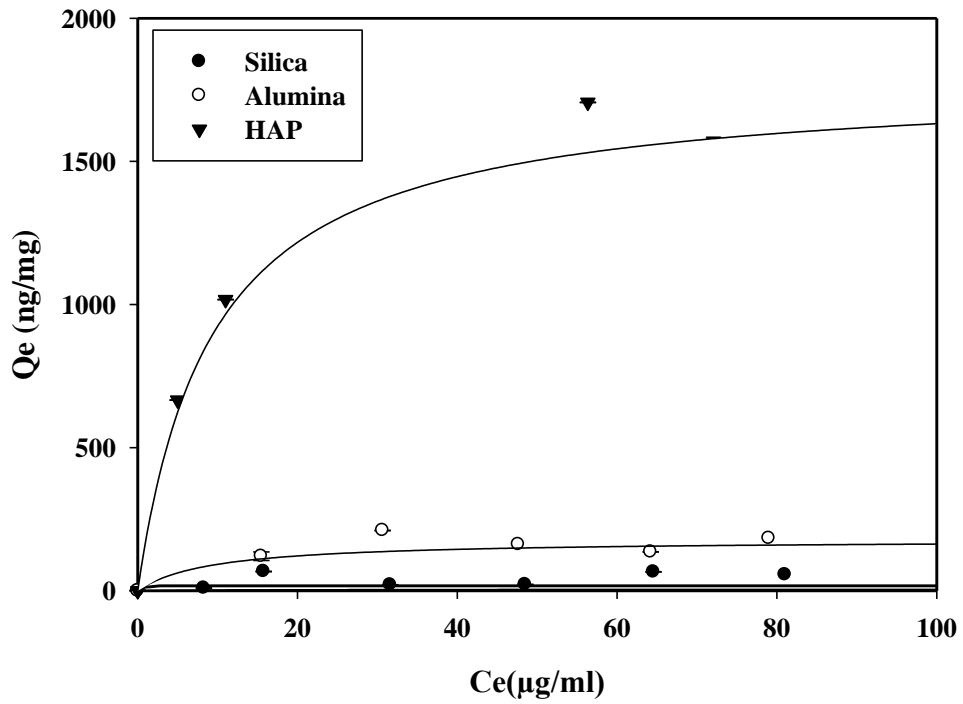
Figure 7. 38. DNA adsorption on Silica, Alumina, and HAP at pH 8
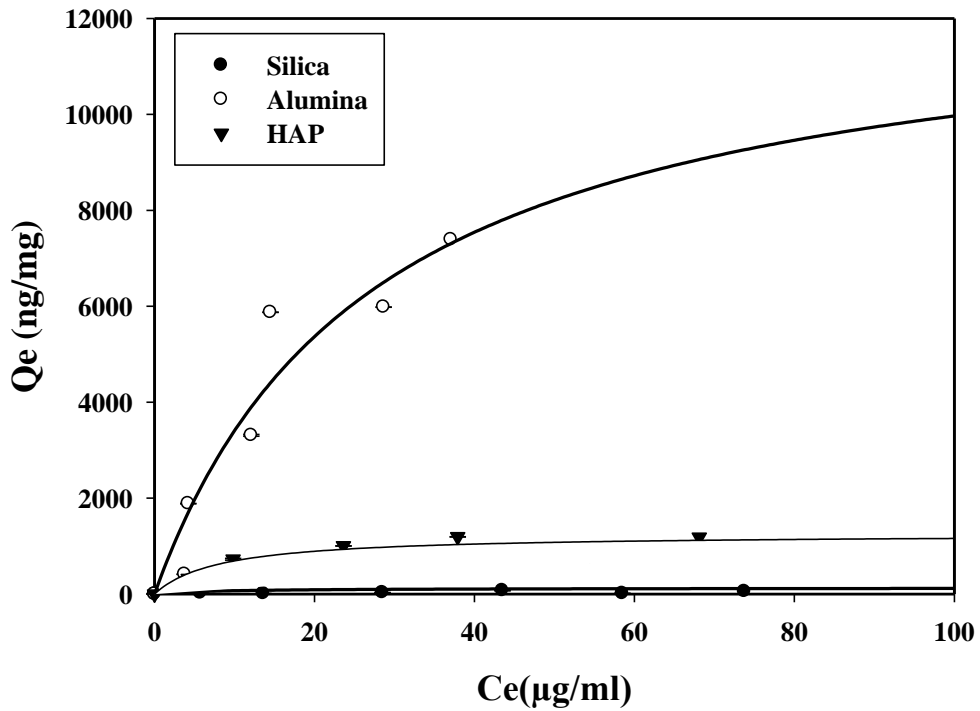
Figure 7. 39. DNA adsorption on Silica, Alumina, and HAP at pH 9
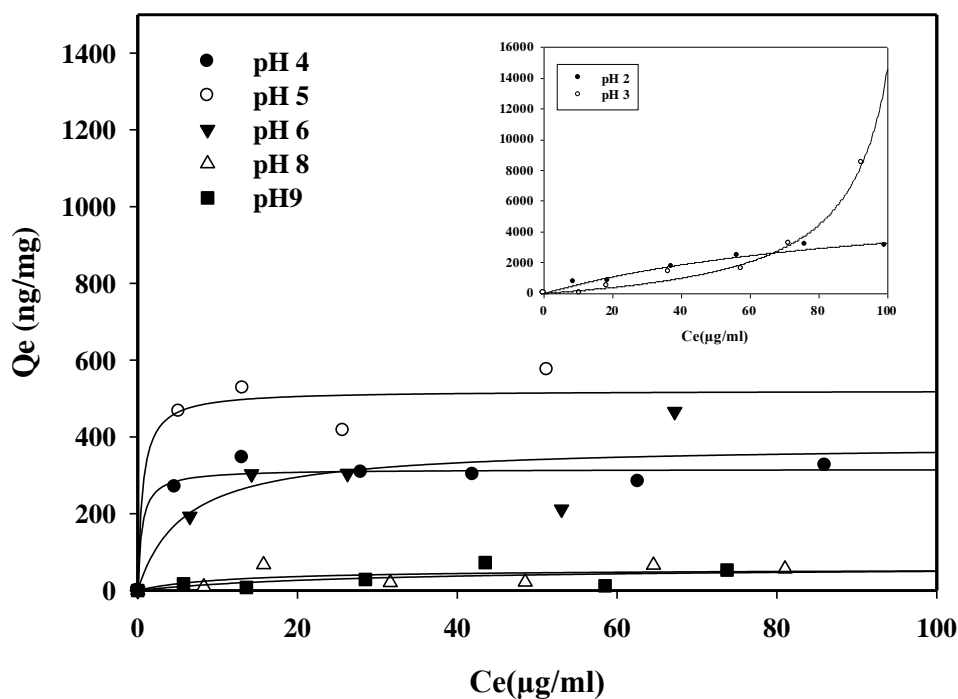
Figure 7. 40. DNA adsorption on Silica at different pH values

Because silica has a point of zero charge near pH 3.0, the SiO_2 coating substrate is negatively charged at the studied pH (4.0 and 9.0). DNA is also not stable at pH2 and pH3 very close to DNA isoelectric point which was verified DNA characterization part.

The increase calf thymus DNA adsorption capacity on silica while decreasing solution pH is consistent with the related loss of negative charge and increase in hydroxyl groups on the silica surface. This proves and indicates that, electrostatic forces are a real driving force for adsorption.
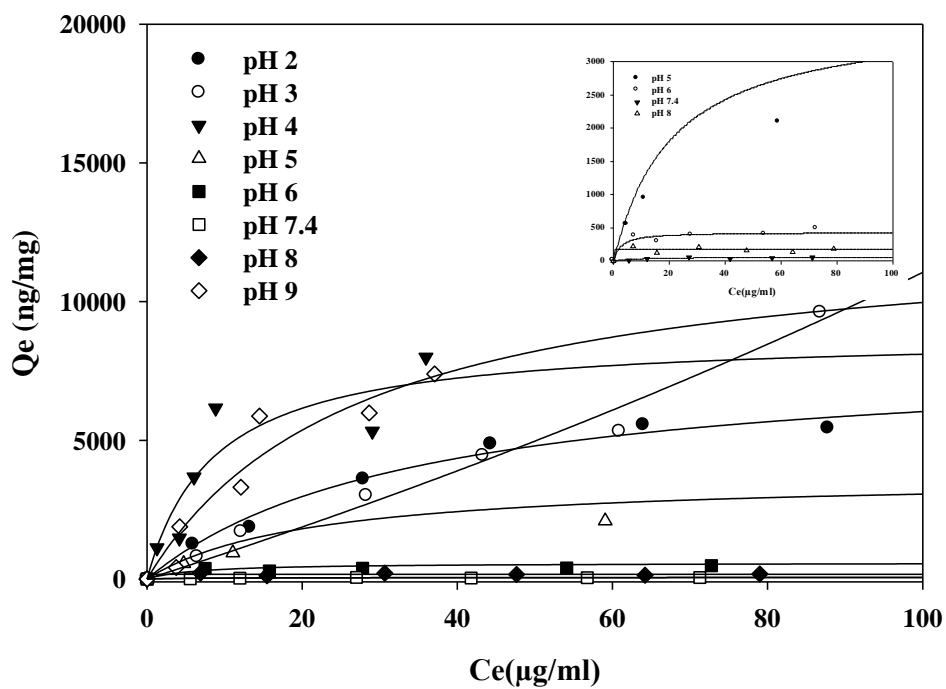
Figure 7. 41. DNA adsorption on Alumina at different pH values
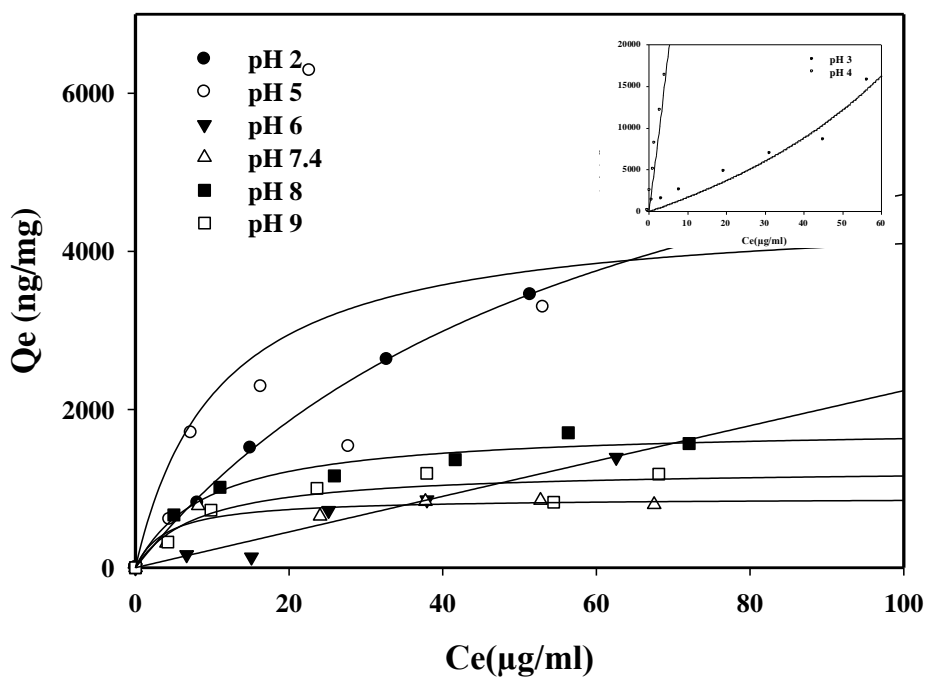
Figure 7. 42 DNA adsorption on HAP at different pH values

Charging of solid surfaces in aqueous environments changes with the pH of the aqueous solutions. DNA molecule is negatively charged due to phosphate groups when the pH is above the isoelectric point. Therefore surface charge influences inevitably to adsorption phenomena in considering electronic interaction. Therefore pH 5 is the optimum value that figure out other parameters influence on adsorption process, which is away from DNA isoelectric point (pH 2) so DNA is stable. Structural or chemical properties might impact on DNA purification method. Cation addition was also tested by adding $MgCl_2$ into the DNA stock solution. 0.5 and 20mM $MgCl_2$ were tested. Adsorption isotherms about this situation are shown in Figure 7.43.and Figure 7.44.respectively. Consequently adsorption capacities of adsorbents were enhanced. Mg ions help the DNA adsorption onto the surface as a bridge. Each adsorbent reach the equilibrium state clearly. Approximately 3 mg /g adsorption capacity of HAP is greater than that of fine organic clay minerals and montmorillonite (1 mg /g) reported by Cai et al. (2006) for 0.5 mM $MgCl_2$ concentration with 25 g/dm^3 solid to liquid ratio. However at 20 mM $MgCl_2$ concentration clay minerals DNA adsorption capacities were greater than that of HAP. It should be considered that their initial concentration is 200 µg salmon sperm DNA in 400 µl tris buffer, which is higher than this study's initial concentration.

Figure 7. 43 DNA adsorption on Silica, Alumina, and HAP at pH 5 with 0.5mM $MgCl_2$
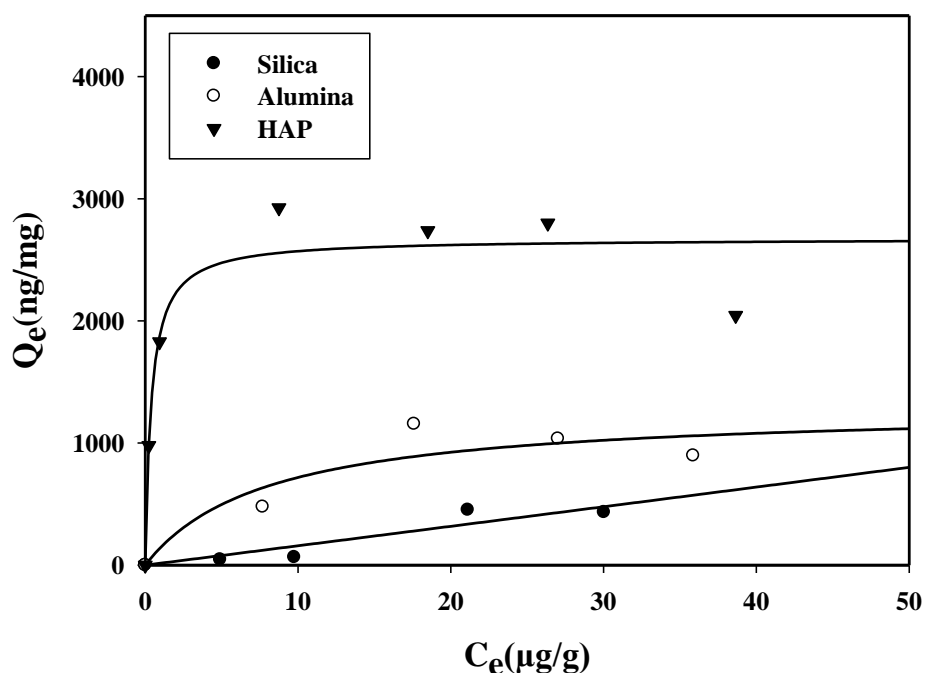
Figure 7. 44. DNA adsorption on Silica, Alumina, and HAP at pH 5 with 20mM MgCl$_2$

Sorption isotherms data can be transformed to the Langmuir and Freundlich plots. The Langmuir plots yielded two important parameters: Langmuir monolayer capacity, Q$_o$, giving the amount of DNA required to occupy all the available sites in unit mass of the adsorbent and the Langmuir equilibrium parameter, b, related to the equilibrium constant. According to nonlinear modelling of data silica alumina and HAP isotherm adsorption capacity is high at low pH value of buffers such as pH 2, pH 3 and pH 4 which are Potassium hydrogen phthalate –HCl and glycine –HCl buffers. Figure 7.45. Figure 7.46. show Langmuir plots o the data. The Freundlich plots are shown in Figure 7.47. and Figure 7.48 Also regression coefficients were not different for Langmuir and Freundlich models. On the other hand MgCl$_2$ addition decreases the freundlich model regression coefficient dramatically (Figure 7.49.)

As a summary Table 7.5 shows Langmuir and Freundlich model constants and their regression coefficients. In Figure 7.49. the adsorption capacities of the adsorbents at different pH values are shown. HAP has always higher adsorption capacity than silica and alumina. The results indicate that there is significant potential for the removal of DNA from aqueous solution using HAP as an adsorbent. Nano sized HAP is a promising DNA purification adsorbent. DNA's phosphate part can easily be attracted to calcium ions of hydroxyapatite.

MgCl$_2$ addition experiment data were used to plot Langmuir and Freundlich models. The Freundlih model plots are seen in Figure 7.49. Except silica; they theoretically obeyed the Freundlich model with smaller regression coefficients as reported in Table 7.5. However negative Langmuir model adsorption capacities for silica indicated the adsorption did not fit to Langmuir model. Increasing divalent cation molarity from 0.5 to 20 mM enhanced the adsorption capacity of DNA on silica (Figure 7.50).
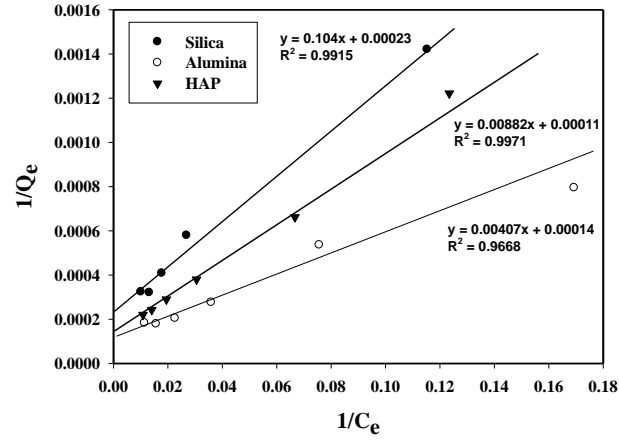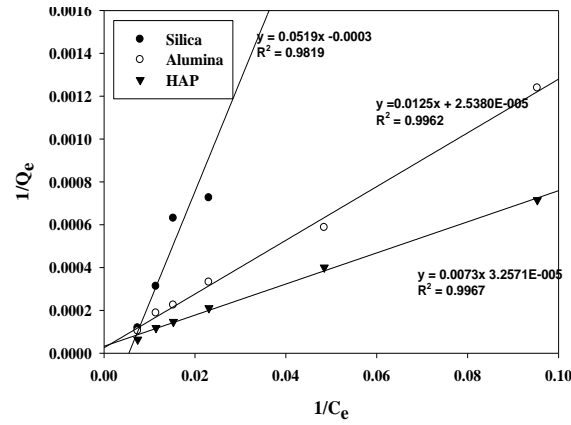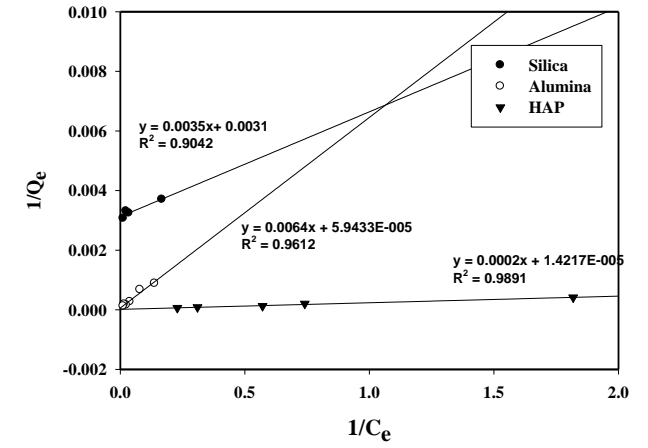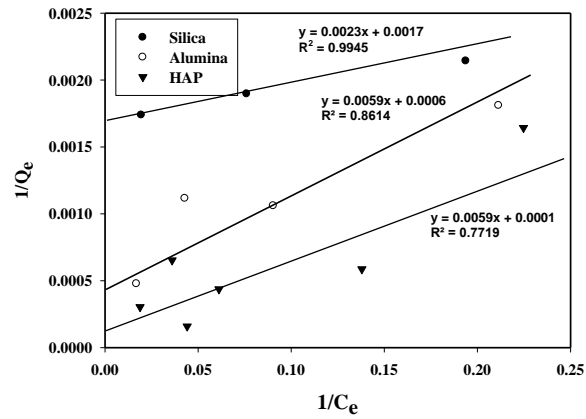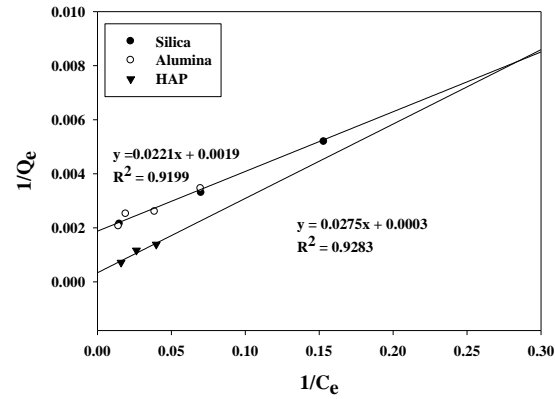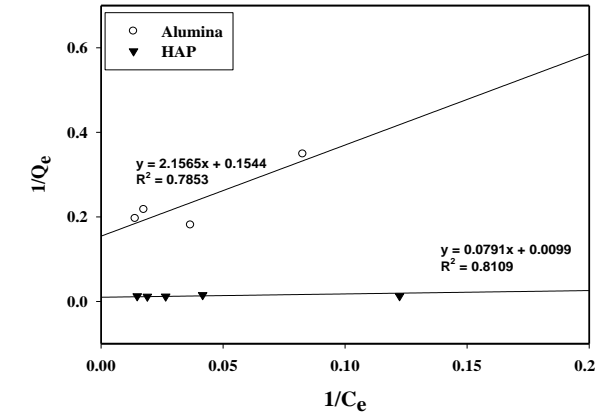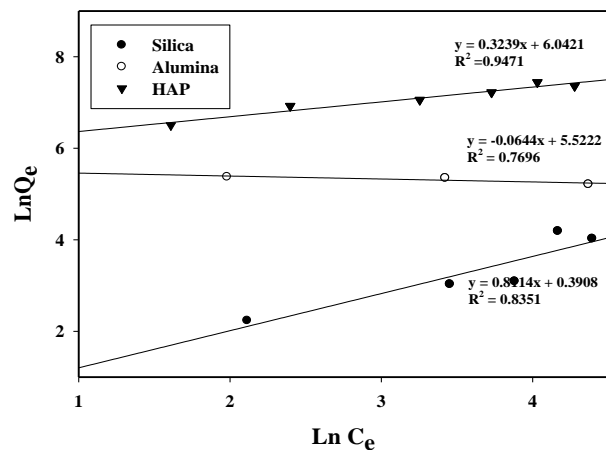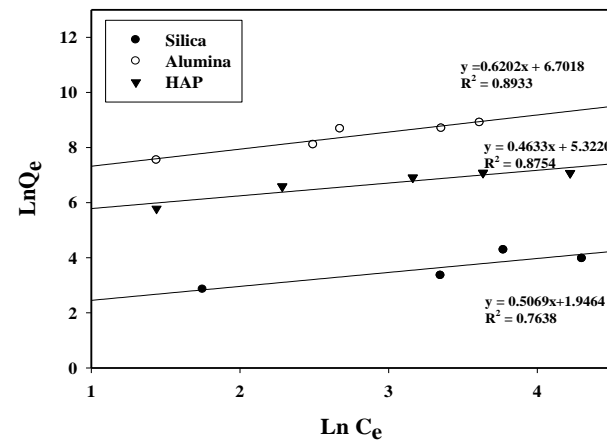
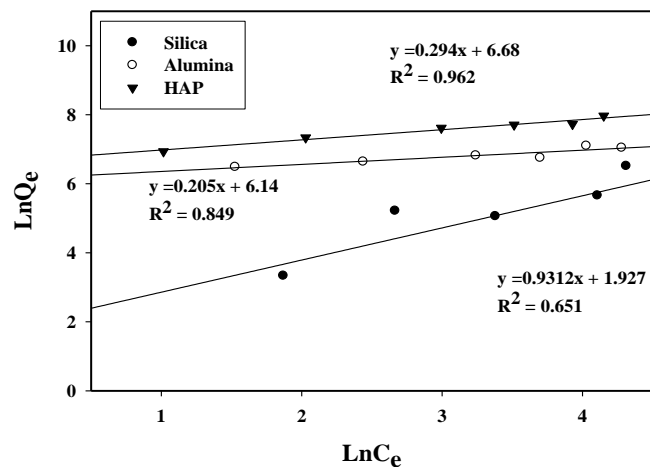Figure 7. 45. Langmuir plots DNA adsorption on Silica, Alumina, and HAP (a) pH 2, (b)pH 3, (c) pH 4 (d) pH5 (e) pH 6 (f) pH 7.4
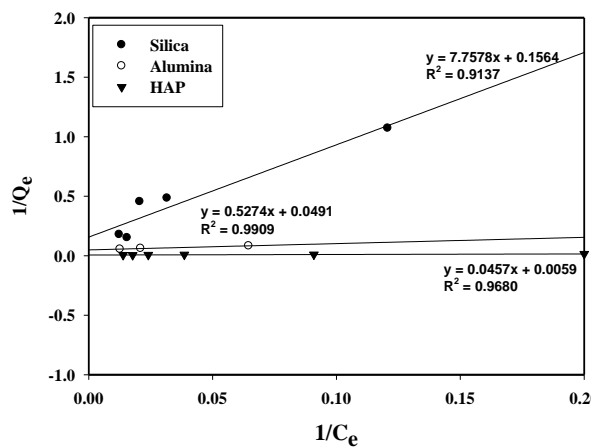
(a)
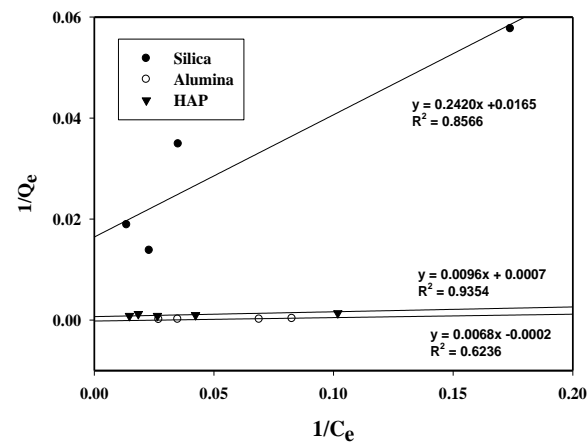
(b)
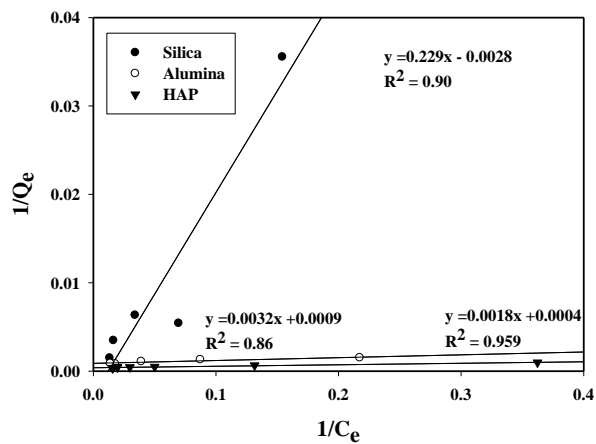
(c)
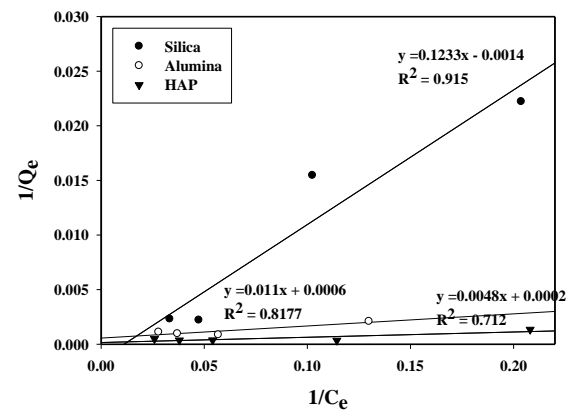
(d)

Figure 7. 46. Langmuir plots DNA adsorption on Silica, Alumina, and HAP at (a) pH 8 (b) pH 9 (c) pH 5 with 0.5mM MgCl$_2$ (d) pH 5 with 20mM MgCl$_2$
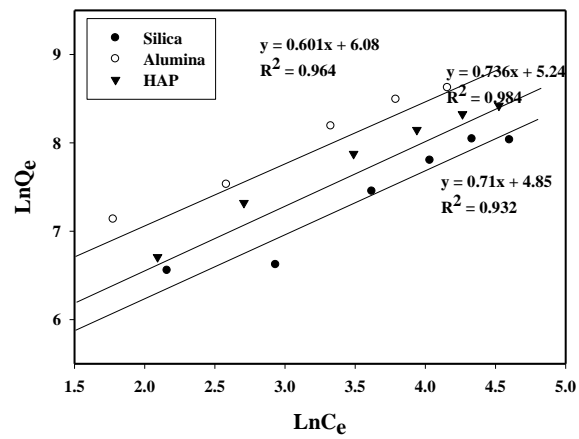
(a)
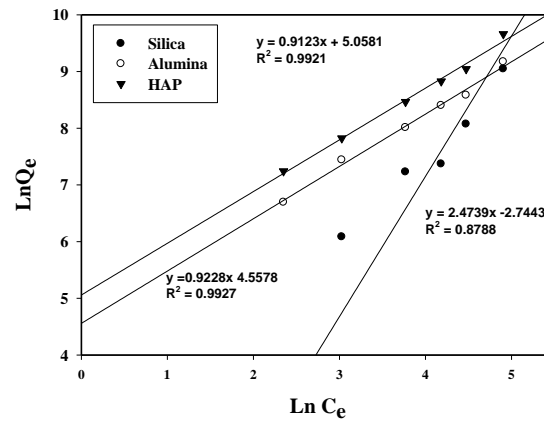
(b)
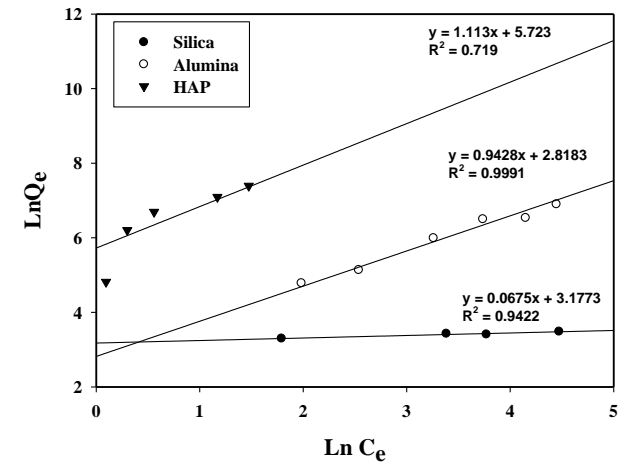
(c)
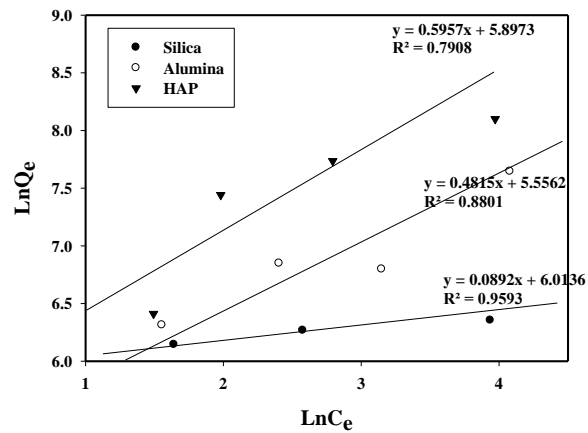
(d)
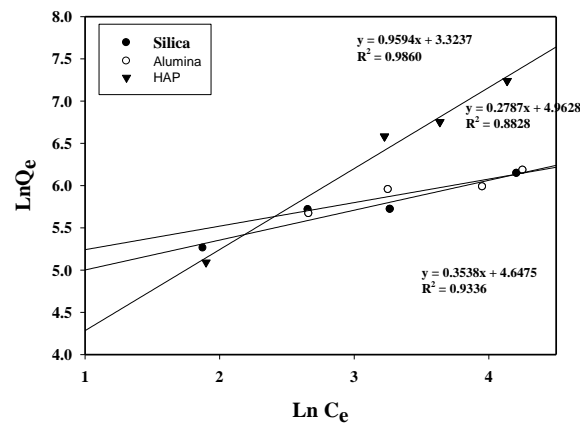
(e)
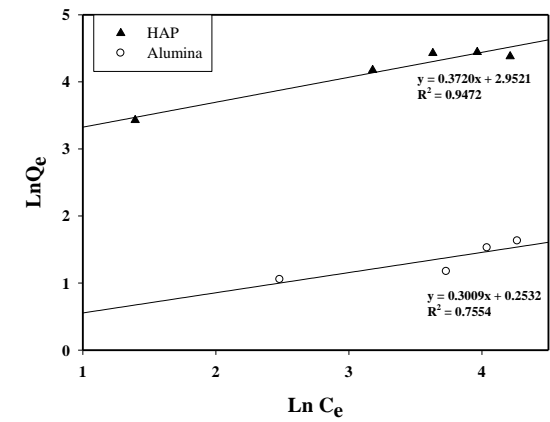
(f)

Figure 7. 47. Freundlich plots for DNA adsorption on Silica, Alumina , and HAP at(a) pH 2, (b)pH 3, (c) pH 4 (d) pH 5 (e) pH 6 (f) pH 7.4
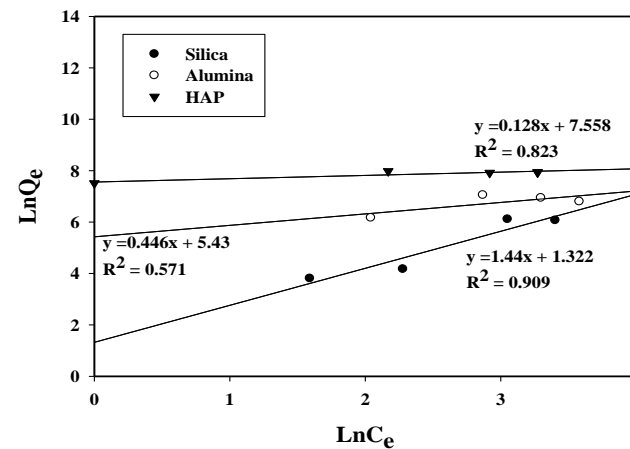
(a) pH 8

(b)pH 9

(c)

(d)

Figure 7. 48 Freundlich plots for DNA Adsorption on Silica, Alumina , and HAP at (a)pH 8 (b) pH 9 (c) pH 5 with 0.5 mM MgCl$_2$ (d) pH 5 with 20 mM MgCl$_2$

Table 7. 5 Parameters of Langmuir and Freundlich Models for Calf Thymus DNA
Adsorption Isotherms

| pH	Adsorbent	Langmuir			Freundlich		
		R^2	Q_0	b	R^2	K_f	n
2	Silica	0.992	4347.8	0.0022	0.932	127.7	1.41
	Alumina	0.967	7142.8	0.0344	0.964	437.03	1.66
	HAP	0.997	9090.9	0.0125	0.984	188.67	1.35
3	Silica	0.982	-3333	-0.0058	0.878	0.064	0.404
	Alumina	0.996	40000	0.0019	0.993	95.37	1.083
	HAP	0.997	30703	0.0045	0.992	157.3	1.096
4	Silica	0.909	76.16	0.3730	0.942	23.98	14.81
	Alumina	0.909	16826	0.0093	0.997	16.74	1.06
	HAP	0.999	70338	0.0711	0.72	305.8	0.89
5	Silica	0.995	584.79	0.747	0.959	408.9	11.21
	Alumina	0.861	172.4	0.988	0.88	258.8	2.07
	HAP	0.772	8333	0.0201	0.79	364.1	1.68
6	Silica	0.912	524.1	0.094	0.934	104.3	2.83
	Alumina	0.912	524.1	0.094	0.883	142.9	3.59
	HAP	0.928	3333	0.011	0.986	27.7	1.04
7.4	Silica	-	-	-			
	Alumina	0.785	6.48	0.072	0.776	1.288	3.32
	HAP	0.811	101	0.125	0.947	19.15	2.668
8	Silica	0.914	6.39	0.201	0.835	1.47	1.232
	Alumina	0.991	20.37	0.093	0.769	250.1	-15.52
	HAP	0.968	169.49	0.129	0.947	420.8	3.087
9	Silica	0.857	60.79	0.068	0.764	7.0	1.973
	Alumina	0.624	-5000	-0.029	0.893	813.8	1.612
	HAP	0.936	1449.2	0.072	0.875	204.8	2.158
pH 5 & 0.5 mM $MgCl_2$	Silica	0.9	-357.1-	-0.012-	0.651	6.86	1.07
	Alumina	0.86	1111	0.281	0.849	464	4.89
	HAP	0.959	2500	0.222	0.962	796.3	3.40
pH 5 & 20 mM $MgCl_2$	Silica	0.915	-714.2	-0.011	0.909	464.1	4.87
	Alumina	0.817	1666.7	0.055	0.571	228.14	2.24
	HAP	0.712	5000	0.042	0.823	2335	7.8
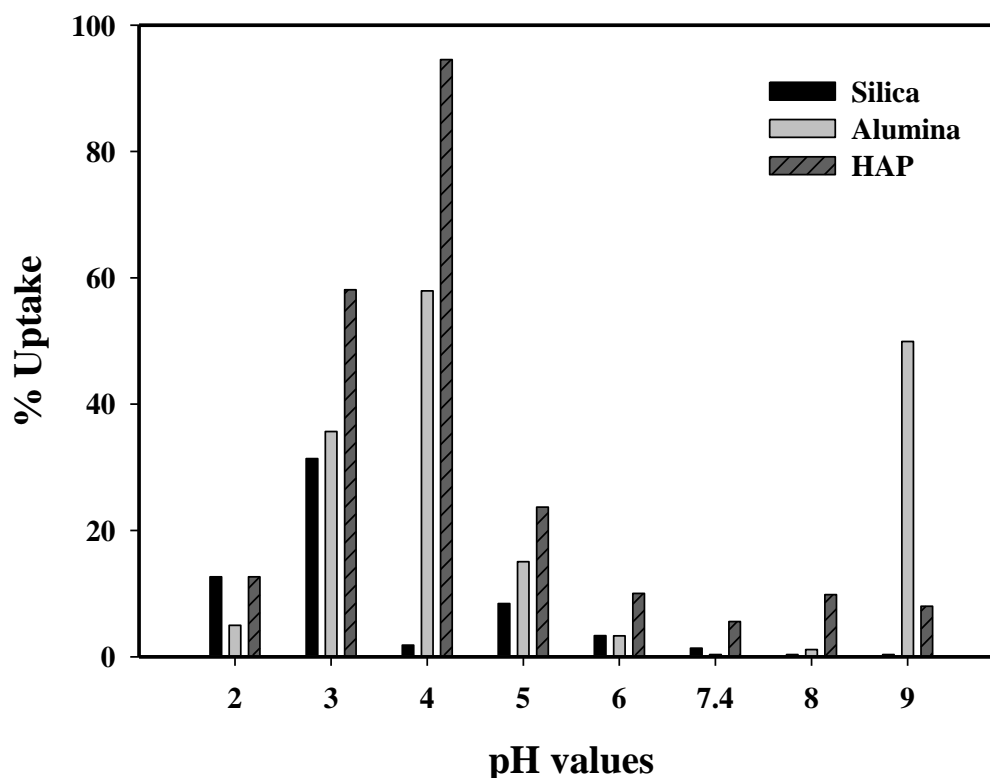
Figure 7. 49. Calf thymus DNA removal % by Silica Alumina and HAP versus pH
values

The isoelectric point of DNA was found as 2 in the present study. The isoelectric points of silica, alumina, HAP were reported to be 2 (Vandeventer et al.,2012), 9 (Polat et al, 2006) and 8 (Komulski ,2009) respectively. DNA is negatively charged above pH 2. Since silica surface is also negatively charged above pH 2 the adsorption of DNA should be due to hydrogen bonding, wan der Waals attractions between silica and DNA. Alumina and DNA had opposite surface charges between pH 2 and 9, thus ionic attractions play an important role on adsorption on alumina. The surface charge of HAP is positive up to pH 8. Thus ionic attractions between DNA and hydroxyapatite had a great contribution to the adsorption on HAP.
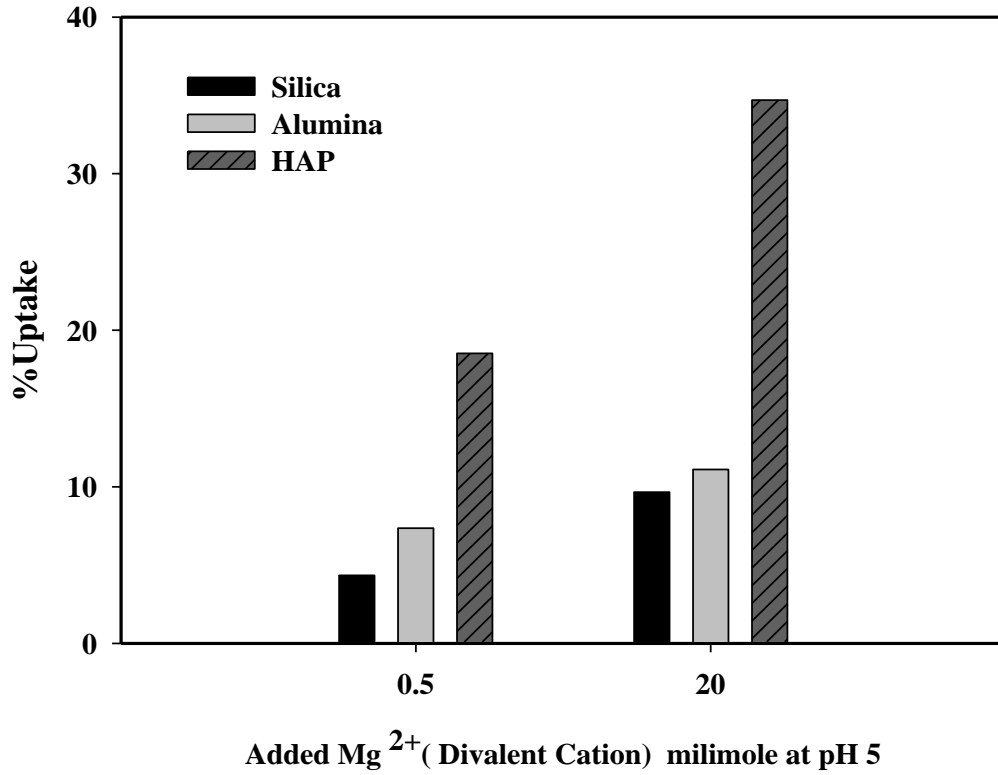
Figure 7. 50. Calf thymus DNA removal % by Silica Alumina and HAP versus divalent cation addition at pH 5 value
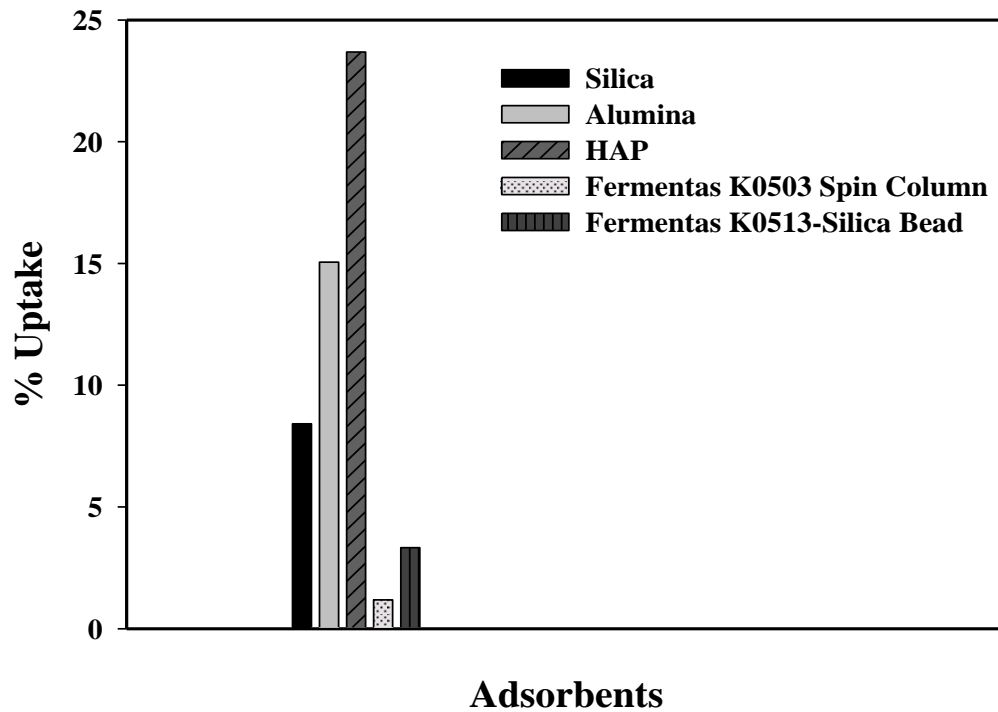

Figure 7. 51. Calf thymus DNA removal uptake % by Silica Alumina , HAP and the commercial kit DNA adsorbents (Fermantas K0503 GeneJET™ Spin Column, and Fermantas K0513 Silica Bead at pH 5 value

Smaller amount of DNA was adorbed by the commercial kit DNA adsorbents (Fermentas K0503 spin column and Fermentas K0513 Silica bead) compared to silica alumina and HAP as seen in Figure 7. 51.

Saeki and coworkers made DNA adsorption study with different solids. Their experimental conditions were "Solid weight: 10 mg, Solution volume: 1.0 cm3, Initial DNA concentration: 100 ng cm^{-3}.They had same initial DNA concentration (100 ng cm^{-3}) and the twice of the solid/liquid ratio (10 g/dm^3 versus 5 g/dm^3) of the present study. They found maximum 86.1% adsorption of available DNA in solution by goethite and 6.1% for montmorillinite at pH 7 . Our result indicated that silica adsorbed 1.3% at pH 7 while 8.4 and 3.35% at pH 5 and pH 6 respectively. At pH 7 HAP has the highest adsorption capacity as 5.57%. Additionaly it has highest adsorption uptake at pH 4 as 94.53% which is greater than Goethite adsorption average of 86.1% (see Table 3.2.)

Dubinin–Radushkevich model was also applied to obtained data. Parameters of qm K and Energy (E) (Eqn. 4.5) were defined and listed in Table 7.6 to Table 7.8. Regression coefficients of D–R isotherm models for silica alumina and HAP were lower than 0.92, 0.97 and 0.95 respectively. Model parameter could not be obtained at some pH values such as for silica at pH 8, alumina at pH 5, and HAP at pH ^{3} for. Furthermore no reliable data were obtained in the presence and absence of MgCl$_2$ at pH 5 for silica. It should be noted that D-R adsorption isotherm is the formulated for microporous materials. Silica has the highest micropore volume among to all adsorbents. All energy values were lower than 8 kj/mol therefore DNA adsorption on silica, alumina and HAP were physical.

Table 7. 6. Dubinin–Radushkevich parameters of calf thymus DNA for Silica at 25 °C

	pH value	Qm (ng/mg)	K (mol^2/kj^2)	R^2	E (kj/mol)
Silica	2	1.36E+10	2.440	0.92	0.453
	4	4.49E+02	0.057	0.86	2.972
	5	5.18E+03	0.304	0.23	1.282
	6	6.06E+03	0.432	0.74	1.076
	8				
	9	1.22E+07	1.929	0.65	0.509
	0.5 mM				
	20 mM	9.19E+06	1.504	0.91	0.577

Table 7.7.Dubinin–Radushkevich parameters of calf thymus DNA for Alumina at 25 °C

	pH value	Qm (ng/mg)	K (mol^2/kj^2)	R^2	E (kj/mol)
Alumina	2	2.30E+08	1.741	0.97	0.536
	4	1.31E+05	0.455	0.80	1.048
	5				
	6	2.44E+04	0.631	0.87	0.890
	7	6.32E+03	0.780	0.88	0.801
	8	8.39E+03	0.611	0.97	0.904
	9	4.12E+05	0.631	0.91	0.890
	0.5 mM MgCl$_2$	4.84E+03	0.234	0.79	1.463
	20 mM MgCl$_2$	1.91E+04	0.444	0.60	1.061

Table 7. 8 Dubinin–Radushkevich parameters of calf thymus DNA for HAP at 25 °C

	pH value	Qm (ng/mg)	K(mol^2/kj^2)	R^2	E (kj/mol)
	2	4.80E+06	1.075	0.95	0.682
	3				
	4	5.45E+04	0.135	0.94	1.925
	5	5.27E+03	0.138	0.95	1.903
	6	1.08E+10	2.509	0.95	0.446
	7	3.39E+03	0.222	0.73	1.499
HAP	8	1.65E+04	0.377	0.86	1.151
	9	1.17E+04	0.374	0.82	1.156
	0.5 mM MgCl$_2$	9.12E+03	0.210	0.83	1.544

7.3.2. Sorption Kinetics

Experimental data show the adsorption of DNA took place in a short time interval. Figure 7.52. to Figure 7.54. summarized sorption kinetic analysis for silica alumina and HAP respectively. Equilibrium was generally achieved within 15 minutes. Based on these results to investigate adsorption kinetics, pseudo first-order and pseudo second-order models were tested with experimental adsorbed DNA concentration in solid (q_t) versus time (t) data. The pseudo first-order kinetic (eqn 4.6) and second order equation (eqn 4.8) were analyzed by nonlinear regression. These figures also include plots of the amount of adsorbed, q_t, against the square root of time, $t^{0.5}$ based on Equation 4.12. These plots did not give a straight line. R^2 values range obtained between 0.62 to 0.93 for Silica, 0.47 to 0.84 for Alumina and 0.15 to 0.84 for HAP. Therefore none of the straight lines pass the origin. However intraparticle diffusion has effect on silica more than alumina and HAP. It should be noted that Weber Morris model (eqn 4.12) often suffer from some uncertainties caused by the multi-linear nature of their plots (Malash and El-Khaiary 2010). This tendency to multilinearty can be expressed film-diffusion controls the rate of adsorption only in the initial time period. Furthermore these plots show several linear segments.
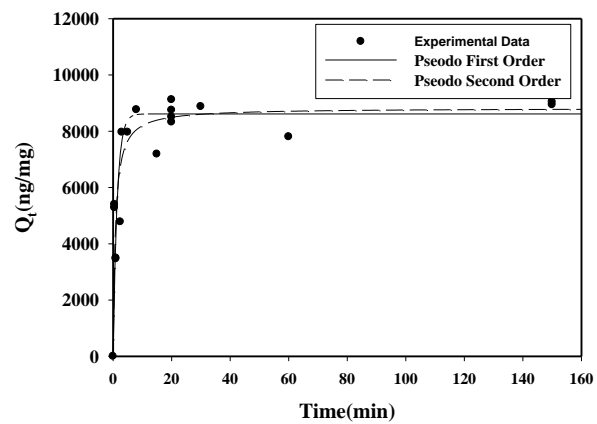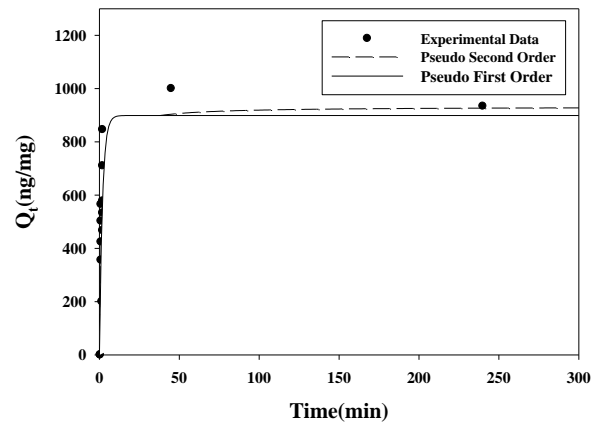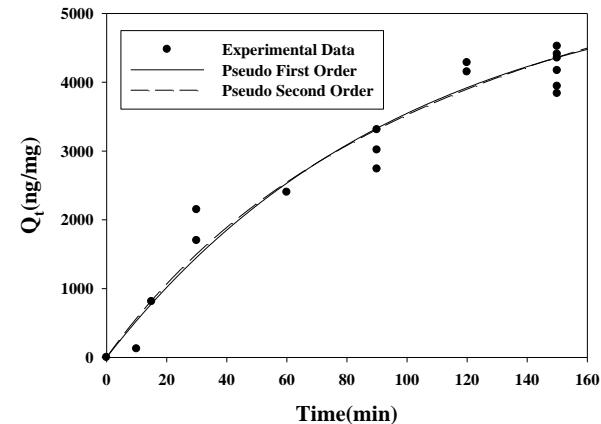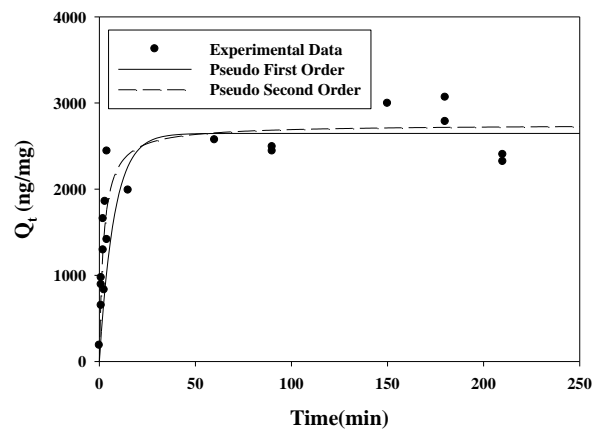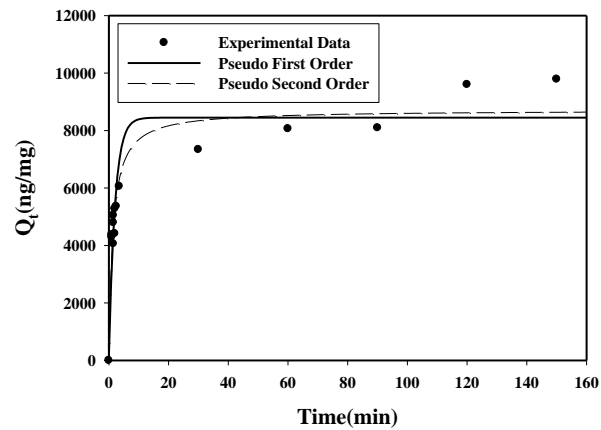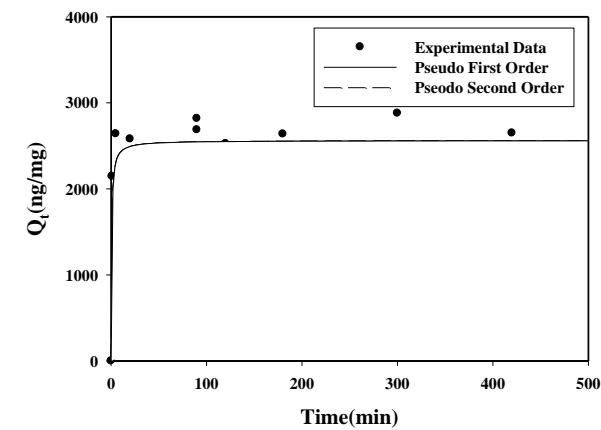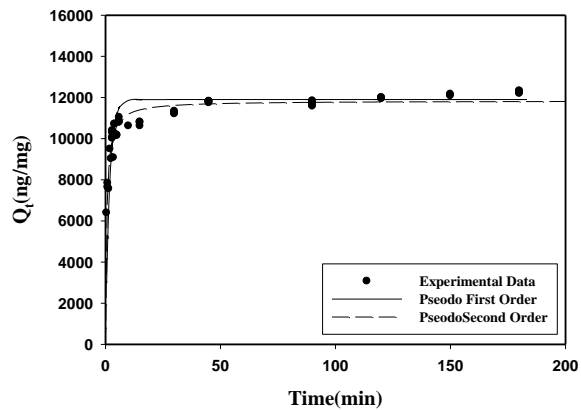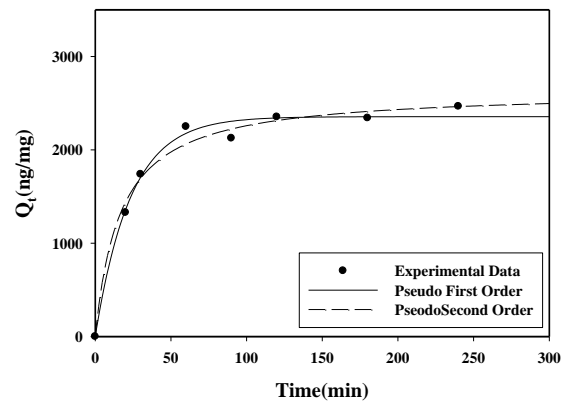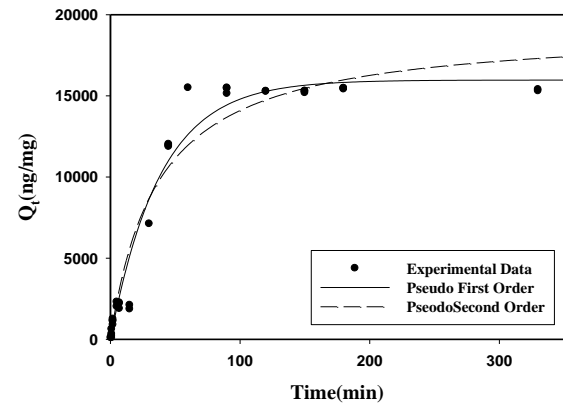
Figure 7. 52. Kinetics plots for DNA adsorption on Silica (a) pH 2, (b)pH 3, (c) pH 4 (d) pH 5 (e) pH 7.4 (f) pH 8

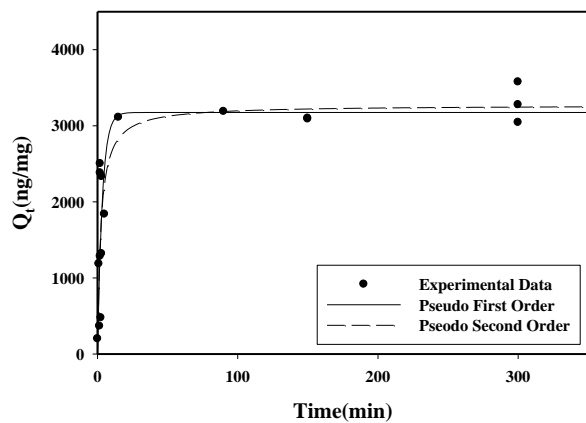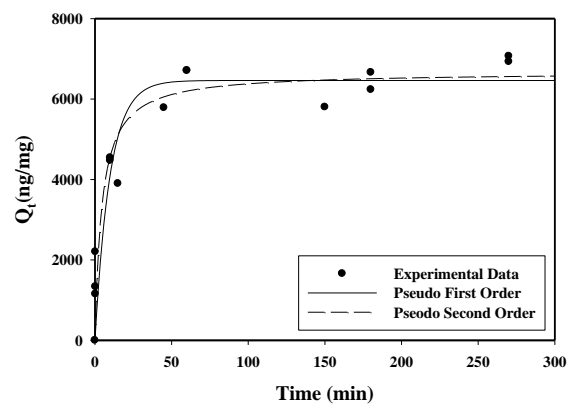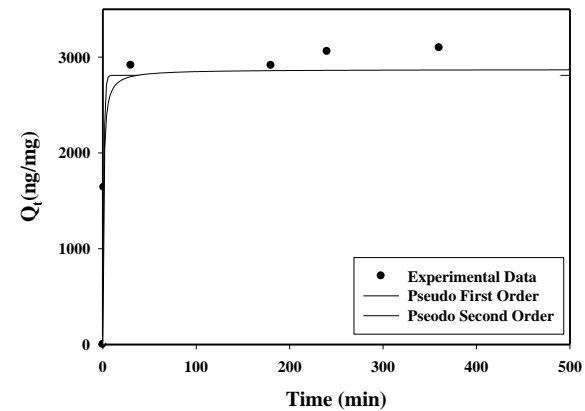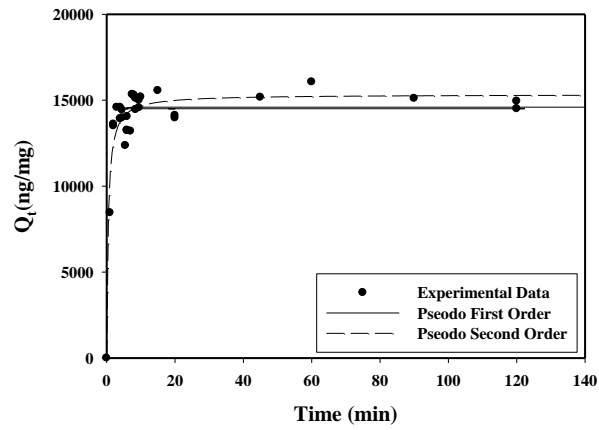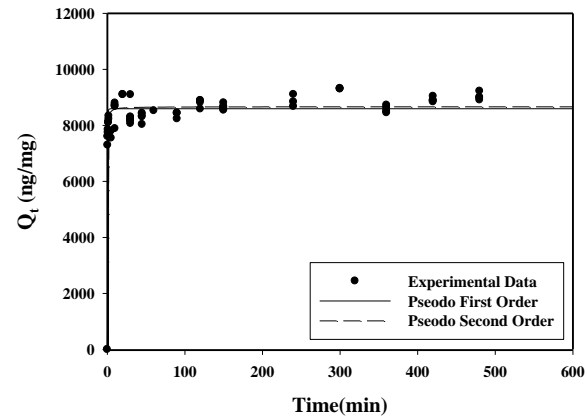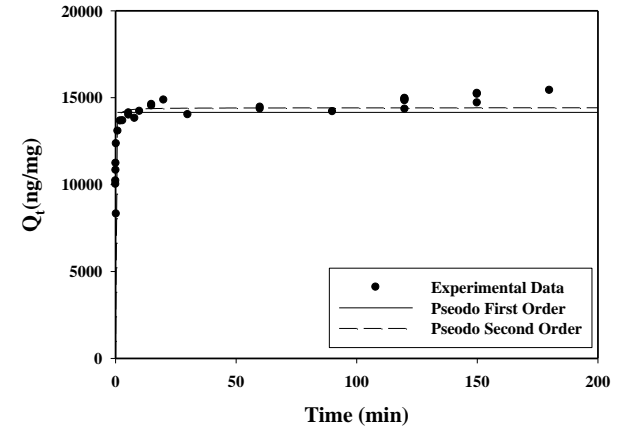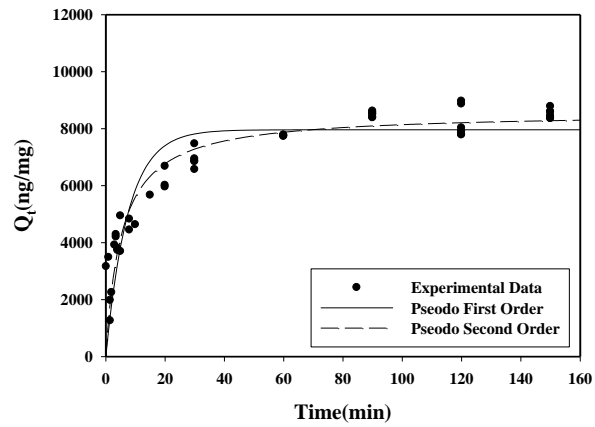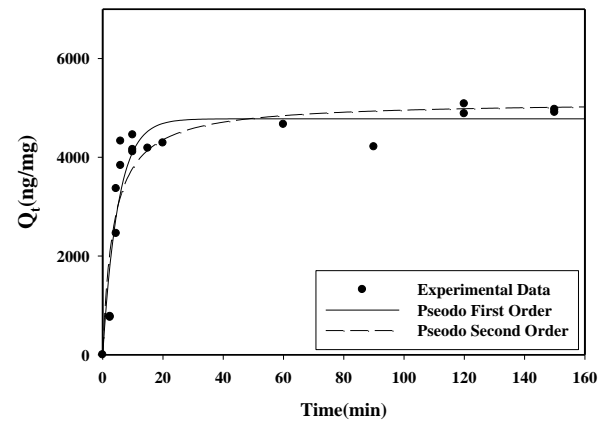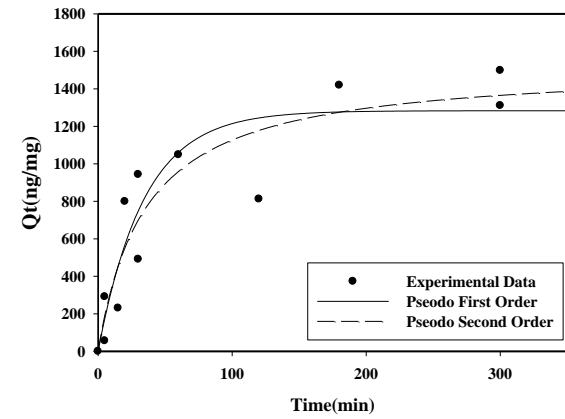Figure 7. 53. Kinetics plots for DNA adsorption on Alumina (a) pH 2, (b)pH 3, (c) pH 4 (d) pH 5 (e) pH 7.4 (f) pH 8

Figure 7. 54. Kinetics plots for DNA adsorption on HAP (a) pH 2, (b)pH 3, (c) pH 4 (d) pH 5 (e) pH 7.4 (f) pH 8

Reaction model parameters which were analysed by nonlinear regression for silica, alumina and HAP were listed in the Table 7. 9, Table 7. 10 and Table 7. 11 respectively. High correlation coefficients were obtained with pseudo second order reaction than the pseudo first order reaction model.

Table 7. 9 The reaction model parameters of calf Thyus DNA on Silica at 25 °C.

	pH	Pseudo First Order			Pseudo Second Order		
		R^2	q_e (ng/mg)	k_1 (1/min)	R^2	qe (ng/mg)	k_2 (g/mg min)
Silica	2	0.78	8615	0.731	0.83	8821.0	0.000148
	3	0.74	899	0.529	0.72	932.1	0.000765
	4	0.94	5605	0.010	0.94	8270.2	8.95E-07
	5	0.48	2647	0.130	0.86	2750.1	0.000166
	7.4	0.89	8449	0.495	0.93	8713.6	8.54E-05
	8	0.59	2483	1.992	0.63	2561.2	0.00071

Table 7. 10 The reaction model parameters of calf thymus DNA on Alumina at 25 oC.

|	pH	Pseudo First Order			Pseudo Second Order		
		R^2	qe	k	R^2	qe	k_2
Alumina	2	0.87	11420	0.876	0.96	11839.4	0.000147
	3	0.99	2356	0.043	0.99	2635.2	2.28E-05
	4	0.98	15973	0.026	0.96	19184.5	1.44E-06
	5	0.77	3175	0.297	0.78	3270.8	0.000131
	7.4	0.88	6461	0.102	0.91	6672.0	3.27E-05
	8	0.94	2810	0.876	0.96	2871.6	0.00043

Table 7. 11 The reaction model parameters of calf thymus DNA on HAP at 25 °C.

|	pH	Pseudo First Order			Pseudo Second Order		
		R^2	qe	k	R^2	qe	k_2
HAP	2	0.92	14592	1.045	0.91	15333.9	0.000142
	3	0.89	8594	3.673	0.91	8664.7	0.001182
	4	0.82	14157	11.051	0.91	14422.1	0.001352
	5	0.84	7961	0.133	0.91	8574.7	2.19E-05
	7.4	0.88	4779	0.197	0.83	5132.4	5.45E-05
	8	0.72	1283	0.029	0.86	1524.7	1.85E-05

The initial stage of DNA adsorption was defined as very fast kinetically and completed within about 15 minutes. After that mechanism of intraparticle diffusion become dominant. This conclusion was evaluated long time diffusion assumption. Diffusion models intraparticle diffusion coefficient and kf calculated from external film transfer model (eqn 4.10). The intercept and the slope of the Figure 7.55, Figure 7.56 and 7.57 plots for silica, alumina and HAP respectively were used to calculate diffusion coefficients. Data were tabulated in Table 7.12. Long time diffusion coeffcient –in other word intraparticle diffusion rate was decreased significantly in the order of alumina, silica and HAP. In Table 7. 4 average pore diameter of alumina was greater than silica. Diffusion coeffient of DNA in alumina was determined to be nearly 10 times fold than in silica. HAP has the highest average pore diameter value and on the contrary the smallest particle size (100 nm) in all adsorbents. Therefore diffusion is not expected in HAP thus the diffusivity 10^{-20}m^2/s is very low.
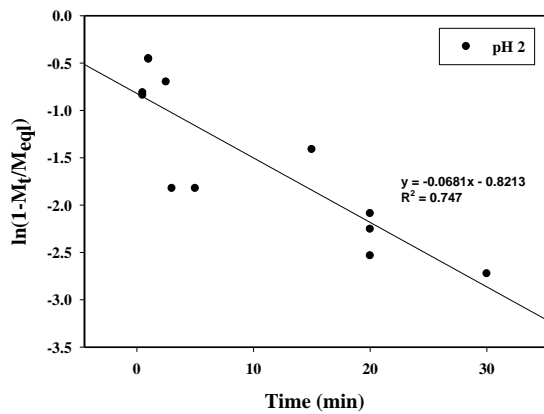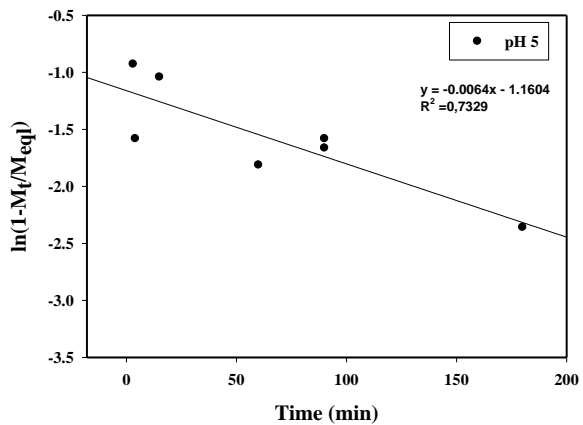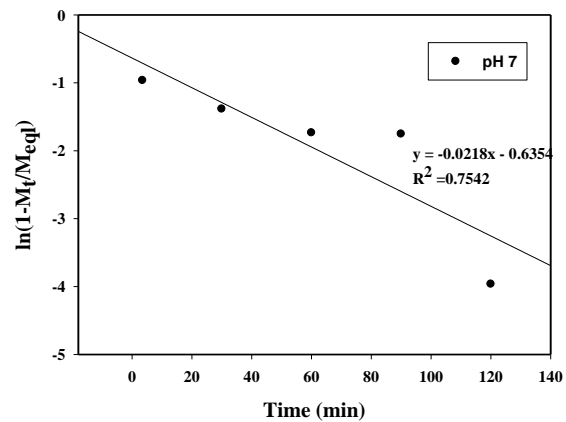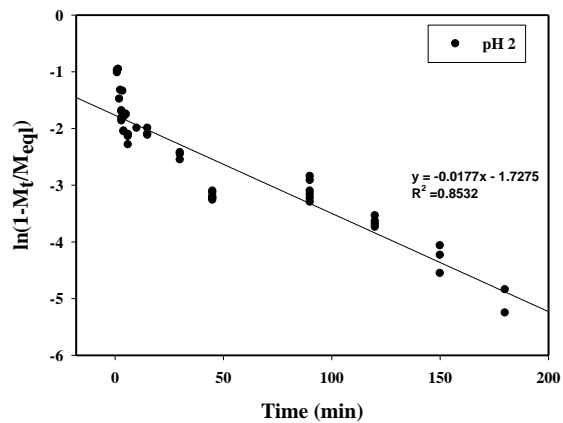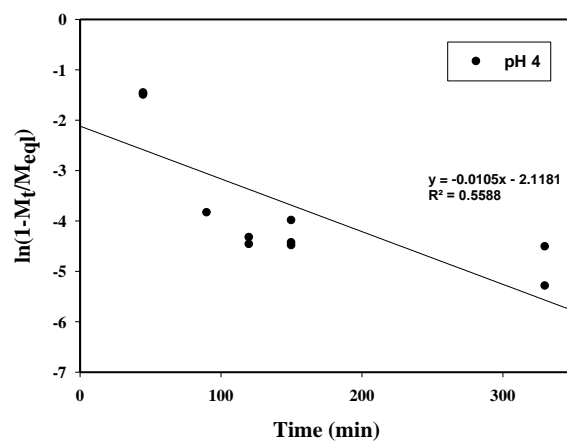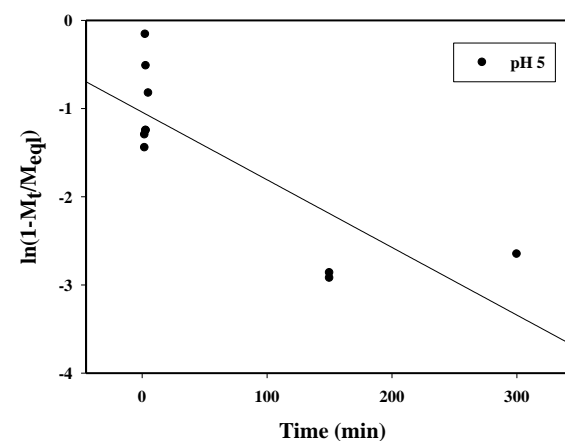
(a)
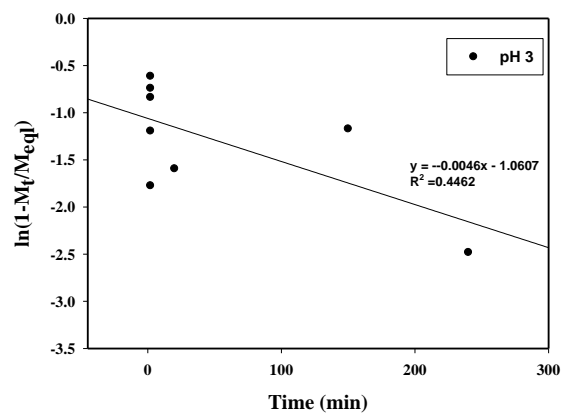
(b)
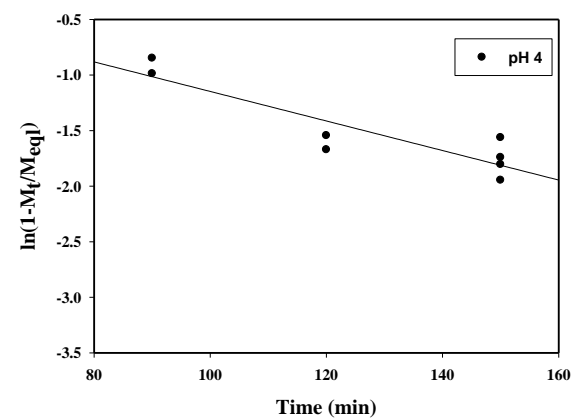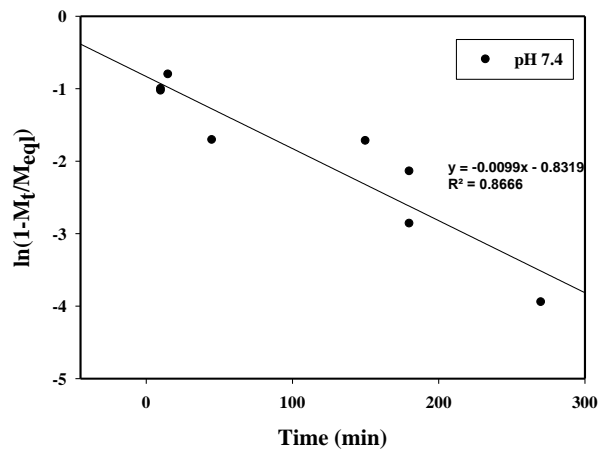
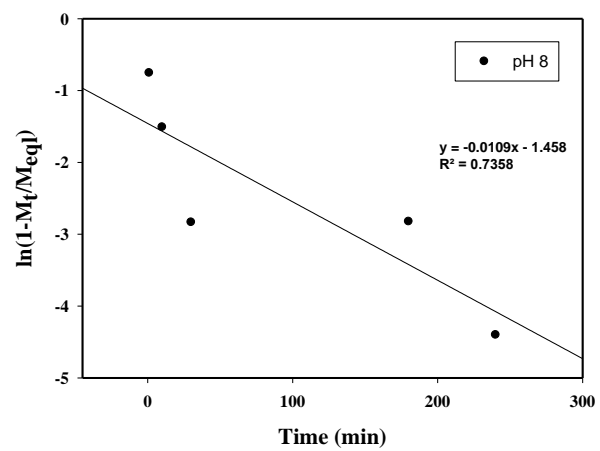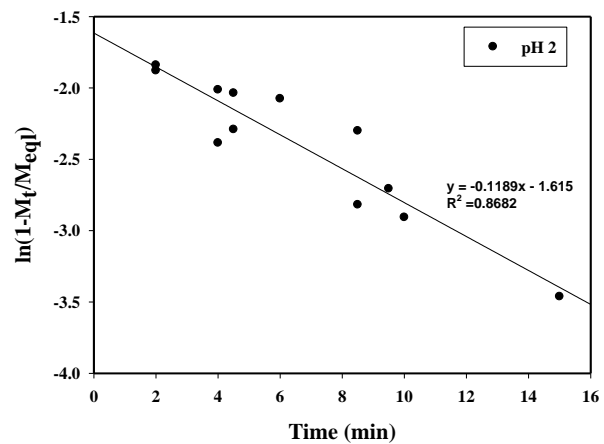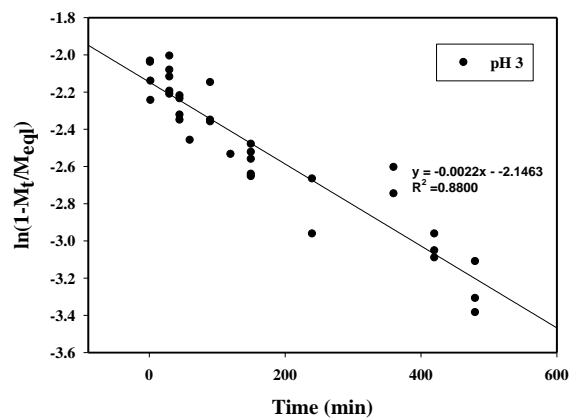(c)

(d)

(e)

Figure 7. 55. Diffusion Kinetics of Silica

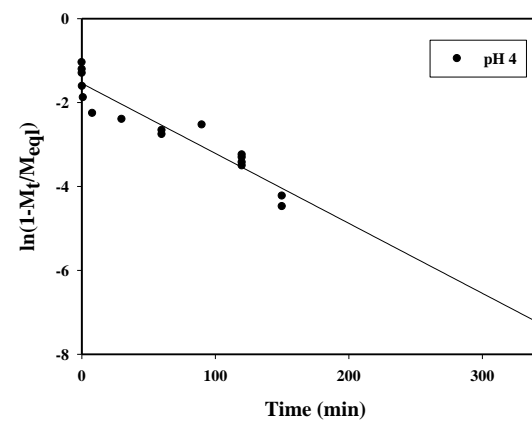(a)

(b)

(c)

(d)

(e)

Figure 7. 56. Diffusion Kinetics of Alumina

(a)　　　　　　　　　　　　　(b)　　　　　　　　　　　　　(c)
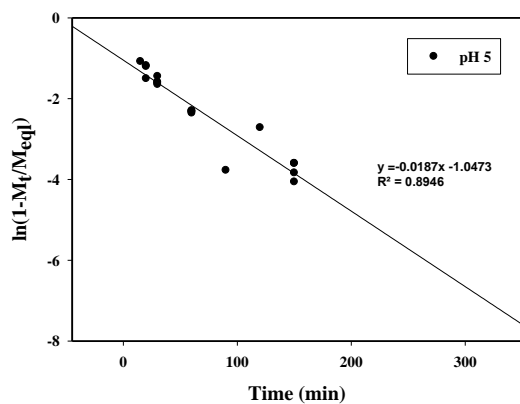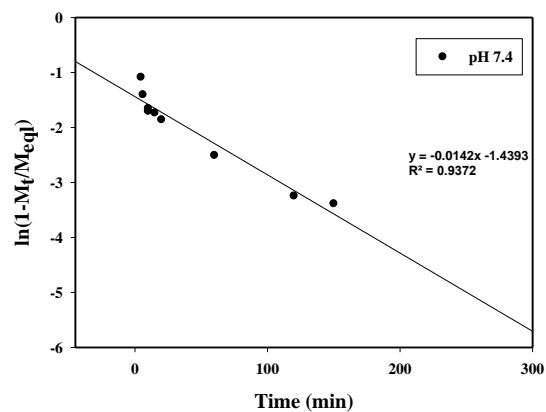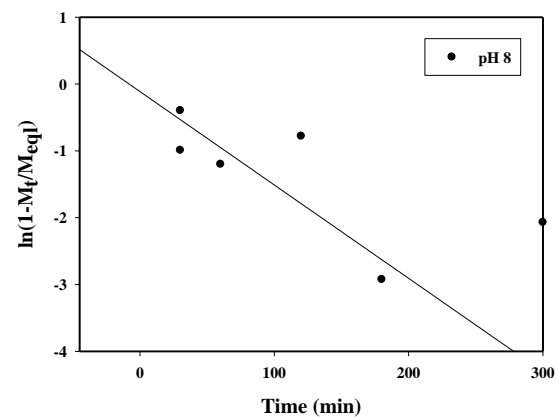
(d)　　　　　　　　　　　　　(e)　　　　　　　　　　　　　(f)

Figure 7. 57. Diffusion Kinetics of HAP

Table 7. 12 Long Time DNA Diffusion Coefficients at 25 °C

	pH values	R^2	a	y_o	$Dc(m^2/s)$	p values	
						Slope	intercept
Silica	2	0.75	-0.0681	-0.82	7.84E-15	0.0003	0.0009
	3	0.45	-0.0046	-1.06	5.29E-16	0.0702	0.0022
	4	0.82	-0.0133	0.18	1.53E-15	0.0021	0.6083
	5	0.73	-0.0064	-1.16	7.36E-16	0.0139	0.0006
	7.4	0.75	-0.0218	-0.64	2.51E-15	0.0561	0.3158
Alumina	2	0.86	-0.0173	-1.77	2.54E-14	<0.0001	<0.0001
	4	0.56	-0.0105	-2.12	1.54E-14	0.0082	0.0033
	5	0.66	-0.0077	-1.04	1.13E-14	0.0043	0.0017
	7.4	0.87	-0.0099	-0.83	1.46E-14	0.0008	0.0105
	8	0.74	-0.0109	-1.46	1.60E-14	0.0630	0.0644
HAP	2	0.87	-0.1189	-1.62	5.23E-19	<0.0001	<0.0001
	3	0.88	-0.0022	-2.15	9.67E-21	<0.0001	<0.0001
	4	0.90	-0.0167	-1.54	7.34E-20	<0.0001	<0.0001
	5	0.89	-0.0187	-1.05	8.22E-20	<0.0001	<0.0001
	7.4	0.94	-0.0142	-1.44	6.24E-20	<0.0001	<0.0001
	8	0.57	-0.0140	-0.11	6.16E-20	0.0482	0.9120

Morphology of DNA on Powders

Adsorbents after DNA adsorption experiment were examined by SEM. The liquid over the solid phase were separated by micropipette. The adsorbent was let to be dried under atmospheric conditions. DNA was detected in HAP surface as shown in Figure 7.58. Images were taken in different part of the sample. It is concluded that calf thymus DNA was surrounded by nanosized HAP particle. DNA sizes were comparable to the size of pure DNA already measured based on SEM picture (Figure 7.26.). However images in Figure 7. 58 (c) and (d) showed that DNA adsorbed was in agglomerated form not as single molecules. Small fibers of DNA can be seen at the surface of a large agglomerate of DNA in Figure 7. 58. (d).

(a)　　　　　　　　　　　　　(b)

(c)　　　　　　　　　　　　　(d)
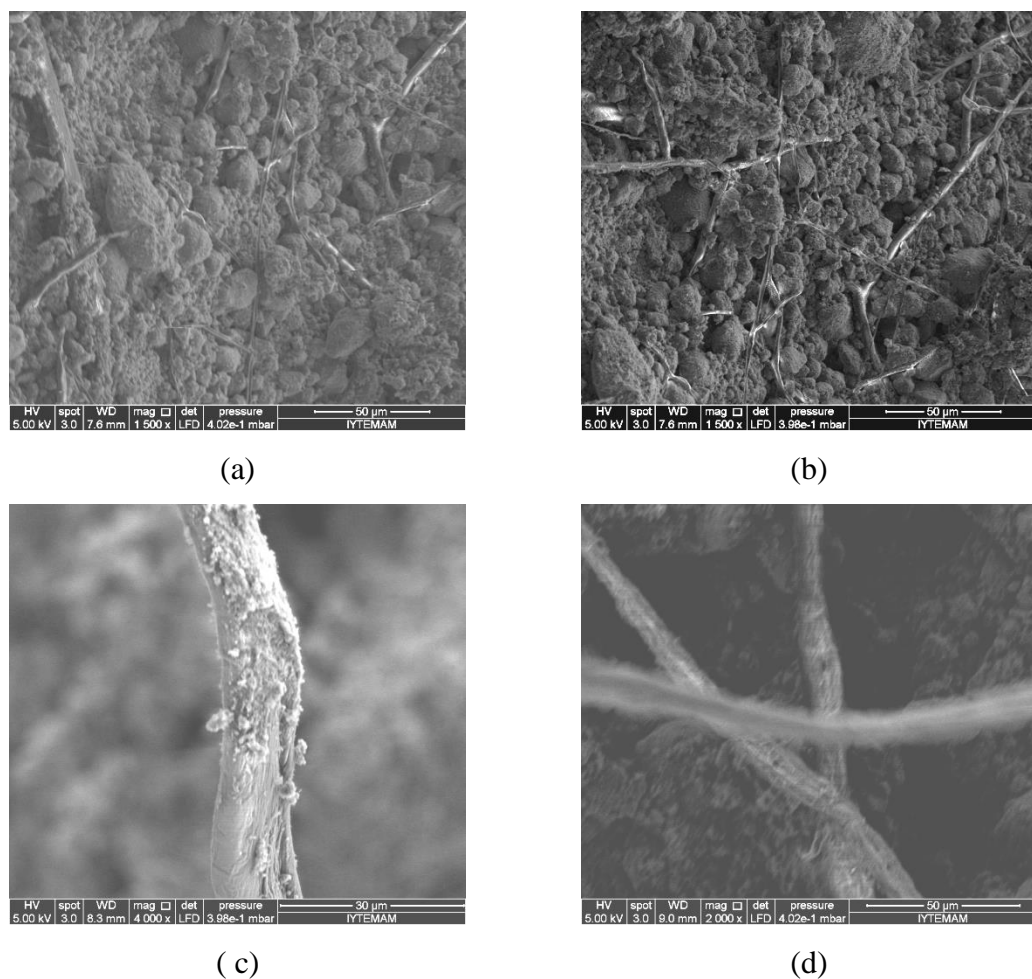
Figure 7. 58. Electron Microscopy (SEM) micrograhs of DNA adsorbed HAP

This is an important constraint of the adsorption process. If DNA does not dissolve successfully in aqueous soluitons in molecular level, its adsorption on solids could not be explained by models based on single molecules.

DNA adsorbed onto both silica and alumina adsorbents were not observed in SEM photographs. Although alumina has both lower surface area and pore size than silica its adsorption capacity was found to be greater than the silica. Silica's total pore volume and micropore volume also greater than the others. It might be caused by just pore diameter, but it is not expected that only 0.2 nm difference caused this much difference. To increase the external surface area of silica it was ground to a smaller particle size. Morphology of silica after this procedure was obtained by SEM. Images are represented in Figure 7.59 . All of the experiments for DNA adsorption on silica was made on these ground particles. .The average size of the particles was reduced to 10 μm.

| (a) | (b) |

Figure 7. 59. Silica morphology before (a) and after (b) grinding

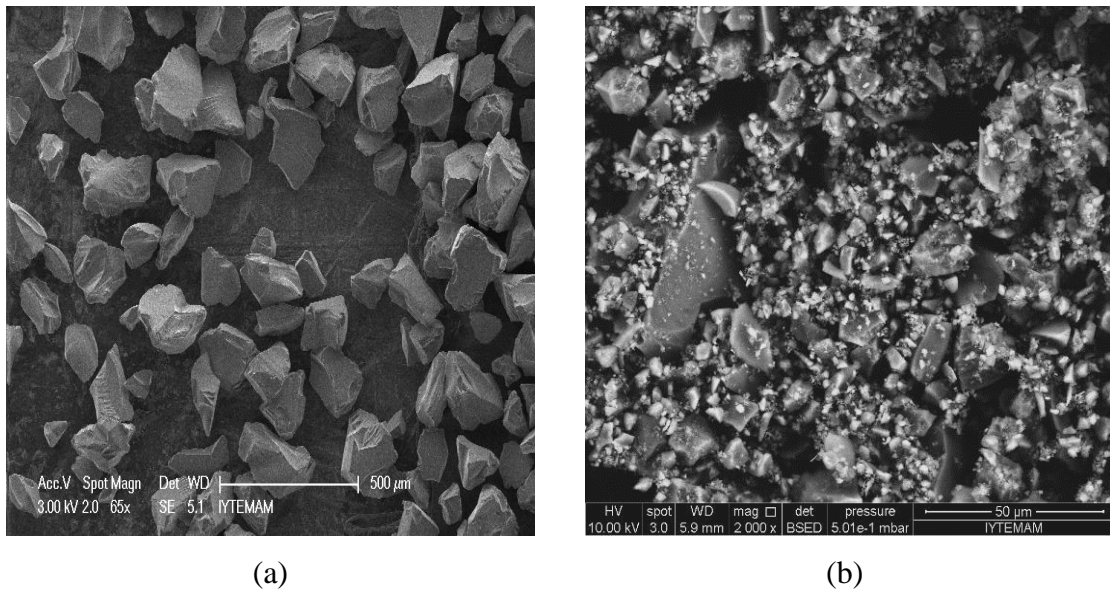### 7.3.3. Adsorption of DNA to Silica Aerogel

Moreover synthesis of bigger pore size of silica was considered. Therefore supercritical dried silica gel production has been investigated.

Silica aerogel was prepared by two steps sol gel method. The details of the method developed by Brinker and co-workers have been described by Ru et al.(Ru et al. 2010).

7.4. Supercritical Ethanol Drying Process

Supercritical ethanol drying method was chosen not only increase the surface areas but also increase the pore diameter of the silica sorbent. Supercritical ethanol drying experiment was started with 5.0g of alcogel mixed with 110 cm3 ethanol in PARR 5500 Series Compact Reactor seen in Figure 7.60.
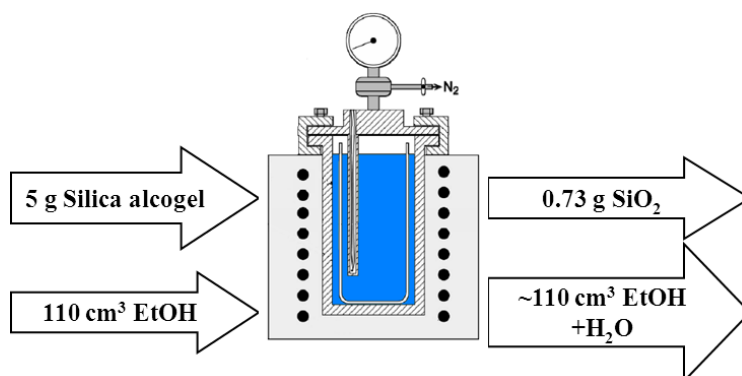
Figure 7. 60. Schematic representation of ethanol SCD experimental setup

Silica aerogel is collected dry in reactor while ethanol mixed with water in second reactor (Figure 6. 2). The weight of the dry sample obtained was 0.73g (silica aerogel). The material balance around the reactor is listed in Table 7. 13. Alcogel (wet gel) initial composition, after SCD sample composition and extracted ethanol phase composition are reported in this table.

Table 7. 13. Composition of the streams in supercritical ethanol extraction assuming the solid phase is pure SiO_2

Chemicals	Initial Composition of the sample, mass %	Composition of the sample after supercritical ethanol drying, mass %	Composition of ethanol phase after supercritical ethanol extraction, mass %
SiO_2	14.6	100	-
Ethanol	84.3	-	99.93
Water	1.1	-	0.07

Diffusion of Water in Silica Alcogel:

Hydrolysis reaction was started mixing water with starting alkoxide. According to Table 7. 14 mixture contained excess water which was not reacted during hydrolysis. Water was removed from wet gel structure by repeated washing with ethanol.

Table 7. 14 Time and washing amount ethanol values with respect to transferred water amount

Time (day)	Ethanol amount for washing process (cm^3)	Transferred water amount through Ethanol during washing (cm^3/g SiO_2)
0	0	0
5	40	0.035
7	40	0.015
9	40	0.025
12	40	0.021
39	40	0.047
total	200	0.143

7.4.1. Water Content of Silica Alcogel

Silica alcogel was washed nearly 5 times with 40 cm^3 ethanol to extract water. After each washing step water content of supernatant was measured and then water diffusion coefficient was calculated based with given data in Table 7. 14 by Equation (7.1). If there is diffusion controlled mass transfer, graph of the fraction of water diffused (Mt/M$_\infty$) versus square root of time (t) should be linear. Where L is the layer thickness of the alcogel.

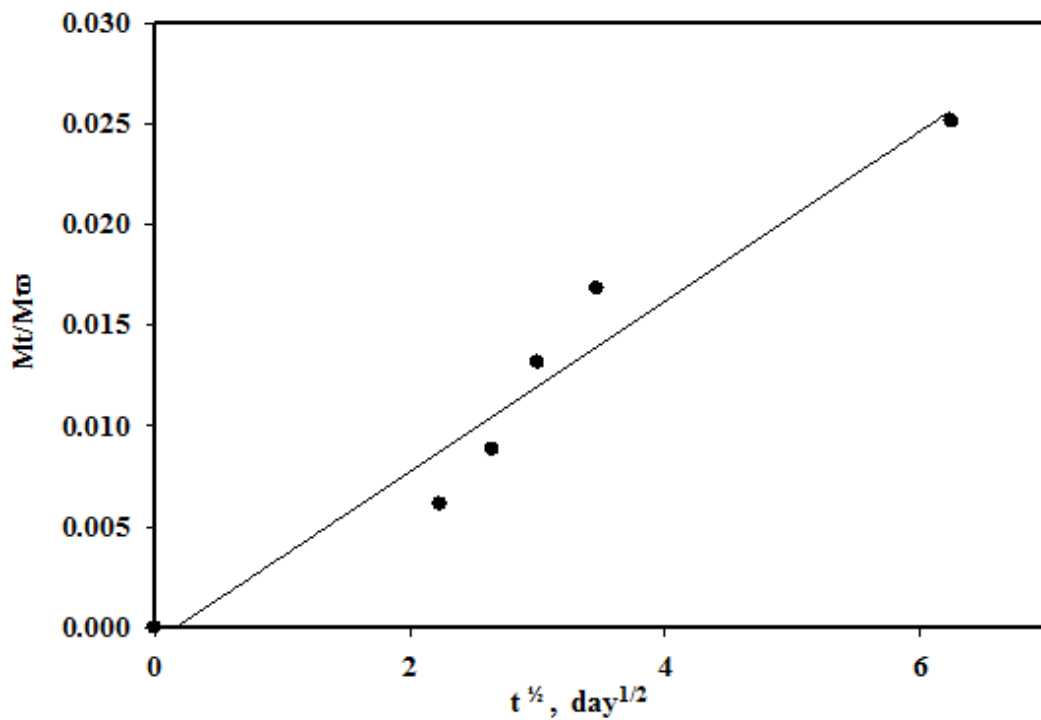$$\frac{M_t}{M_\infty} = \frac{4}{L}\sqrt{\frac{D_{AB}t}{\pi}} \qquad (7.1)$$

Figure 7. 61. Mass transfer of water through wet gel

The diffusion coefficient of water in wet gel was found to be 4×10^{-11} m^2/s which is lower then self diffusion coefficient of water reported nearly as 1×10^{-9} m^2/s at normal conditions (Yu and Gao 2001).

7.4.2. Silica Aerogel Characterization Results

7.4.2.1. Chemical Characterization

As can be seen in Figure 7.62. prepared silica aerogel has characteristics of silica. The peak band at 3400 cm^{-1} is related to the νO–H mode of residual silanol (Si–OH) groups and of adsorbed water hydrogen bonds (Fidalgo and Ilharco 2007). Another silanol band, assigned to the Si-O (H) stretching mode become visible at 950 cm^{-1}. The strongest band, with maximum absorption at ~1100 cm^{-1}, is assigned to the asymmetric Si-O-Si stretching mod. The xerogel obtained by conventional drying of silica alcogel had the same FTIR peaks of silica aerogel as seen in Figure 7.63 .
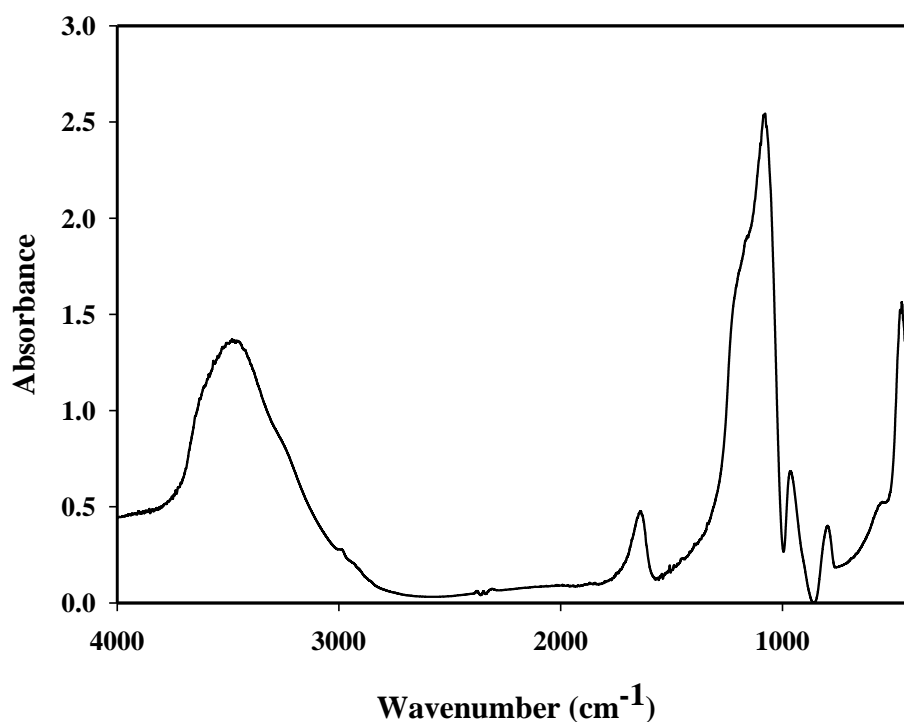
Figure 7. 62. FTIR spectrum of Silica Aerogel
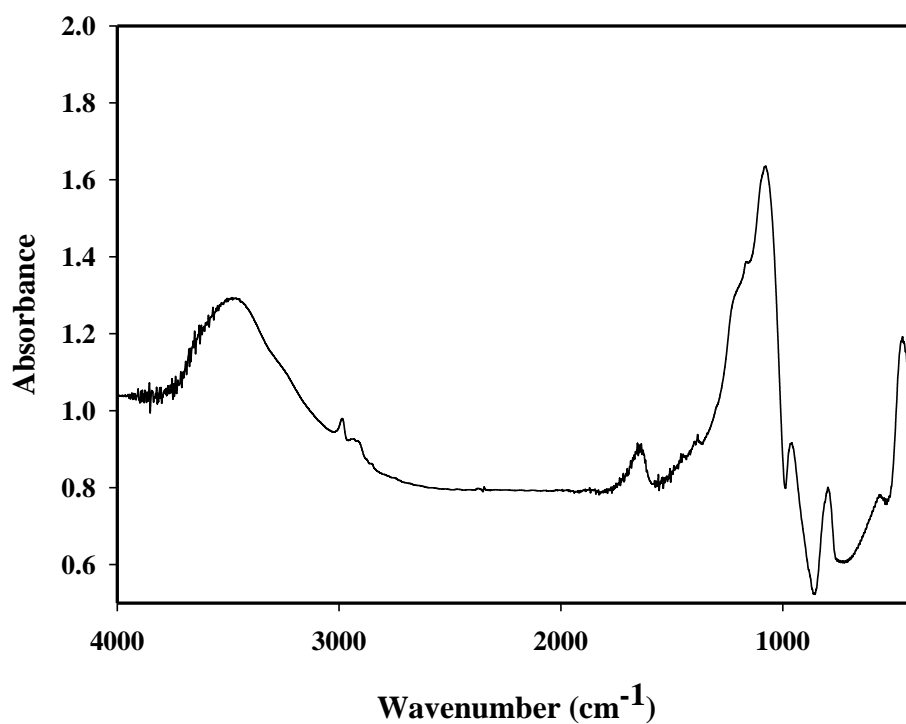
Figure 7. 63. FTIR spectrum of Conventional Dried Silica gel (Xerogel)

7.4.2.2. Nitrogen Adsorption

Hysteresis loop formed by adsorption/desorption isotherms due to condensation and evaporation of liquid nitrogen from mesopores depends upon the shape and size of pores (Sing et al., 1982). Hysteresis cycle was commonly observed for materials with interrelated pore networks with different size and shape. According to these data single point, BET and Langmuir surface areas, average pore diameter, total pore volume, micropore volume of the adsorbents have been listed in Table 7. 15.

Figure 7. 64. Nitrogen adsorption and desorption isotherms (1)as prepared aerogel . (2) after 2 months.(3) after 3 months aerogel (4) as prepared xreogel

Silica aerogel was tested several times for surface area; first one was done after SCD was completed, the second one was performed after one mo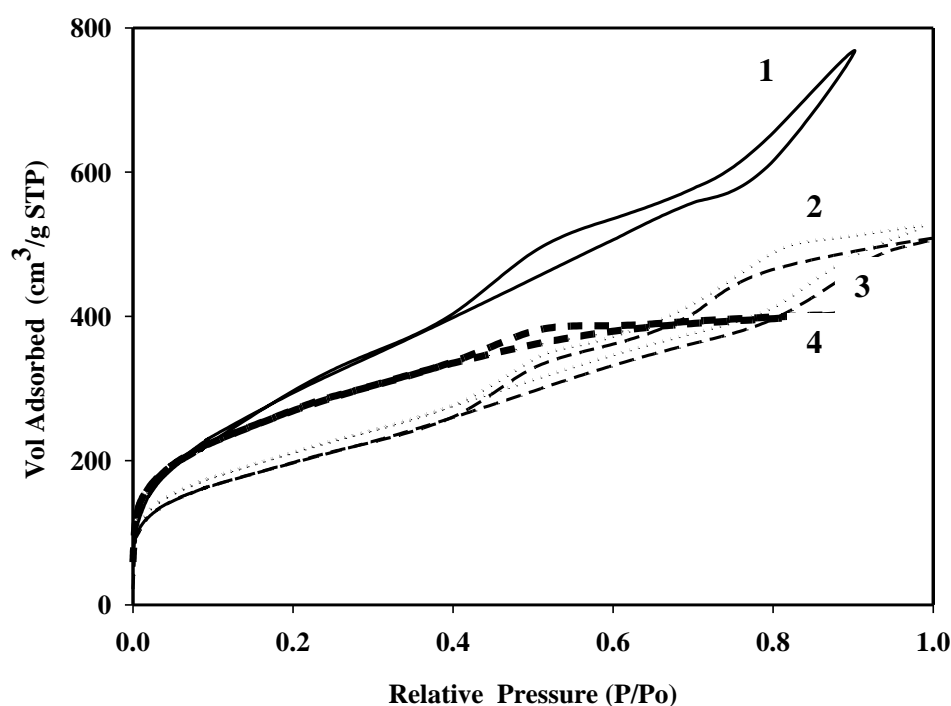nth ageing and the third one was done after two months ageing in a desiccator. Sample codes 1, 2 and 3 in Figure 7. 64 and Table 7. 15 referred to supercritical dried silica aerogel. (1), (2) and (3) for as prepared aerogel, 2 months aged and 3 months aged aerogel respectively. Curve (4) represents demonstrates the silica which was dried conventionally (xerogel). The total pore volume of prepared aerogel was 1.19 cm^3/g and it decreased to 0.81 cm^3/g and 0.79 cm^3/g on one month and 2 months ageing time. BET surface area of the aerogel was also decreased for ageing period of 1 mount and 2 months from 1549 m^2/g to 1012 and 981 m^2/g respectively. It was concluded mesoporpus structure were collapsed with time. However it is obvious that SCD has an advantageous method to gain high surface area then conventional dried silica (xerogel) structure.

Table 7. 15. Surface Characteristics of of the Aerogel and Xerogel

Properties	Sigma Aldrich-Silicagel	Aerogel (1)	Aerogel (2)	Aerogel (3)	Xerogel (4)
Single Point Surface Area (m^2/g)	556	1055	740	691	922
BET Surface Area (m^2/g)	571	1107	756	708	945
Langmuir Surface Area (m^2/g)	787	1549	1012	981	1390
Average Pore Diameter (nm) (4V/A by BET)	5.5	4.2	4.3	4.4	2.6
Single Point Total Pore Volume (cm^3/g)	0.79	1.19	0.81	0.79	0.62
Max Micropore Volume (cm^3/g)	0.20	0.36	0.28	0.26	0.35

7.4.2.3. Morphological Characterization

Produced silica aerogel and xerogel morphology were also investigated by scanning electron microscopy technique. According to obtained micro picture SCD silica aerogel has smaller particles then conventional dried xerogel as seen in Figure 7.65.
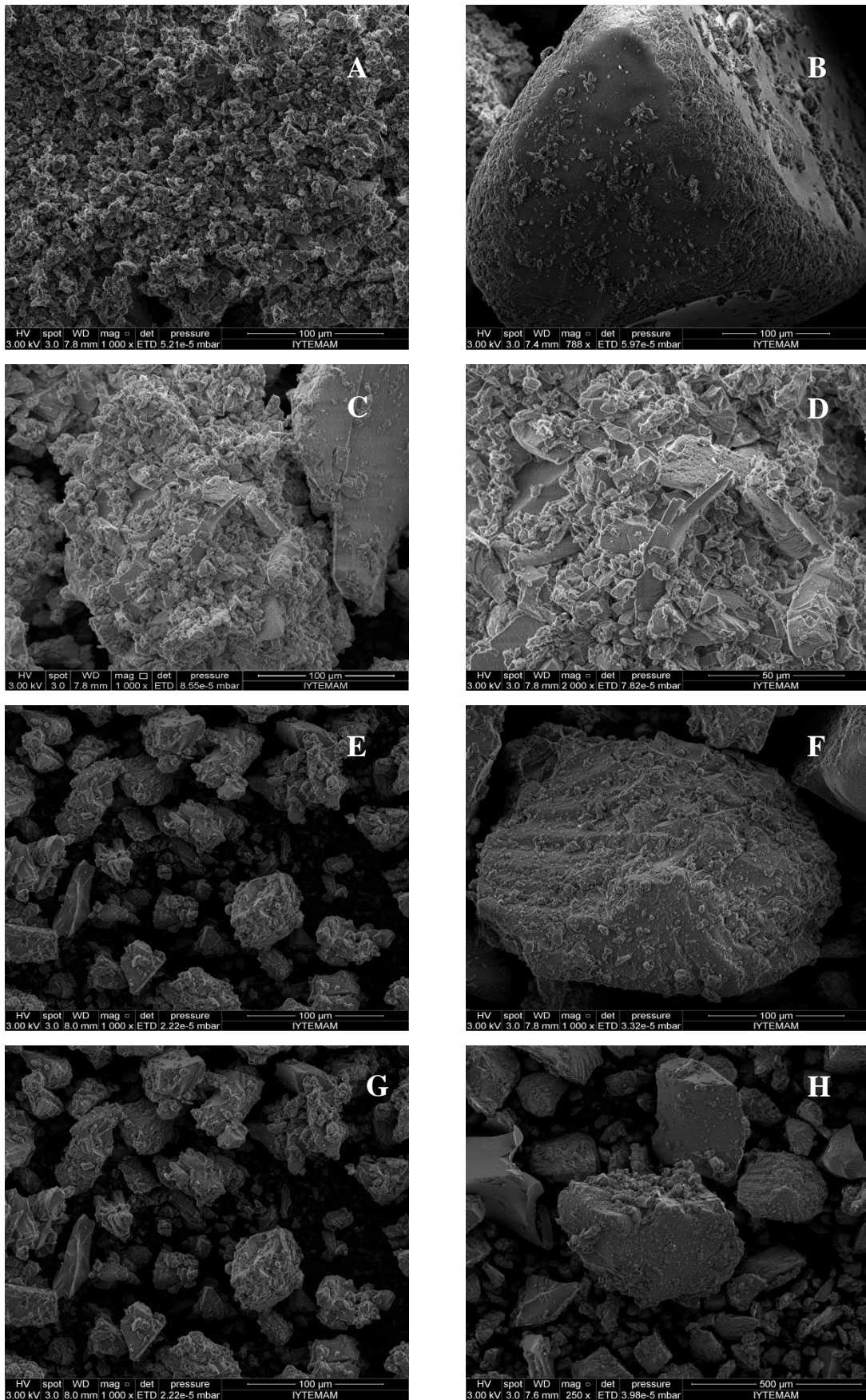
Figure 7. 65. SEM images for Aerogel (A) (B) (C) and (D) and for conventinaly dried
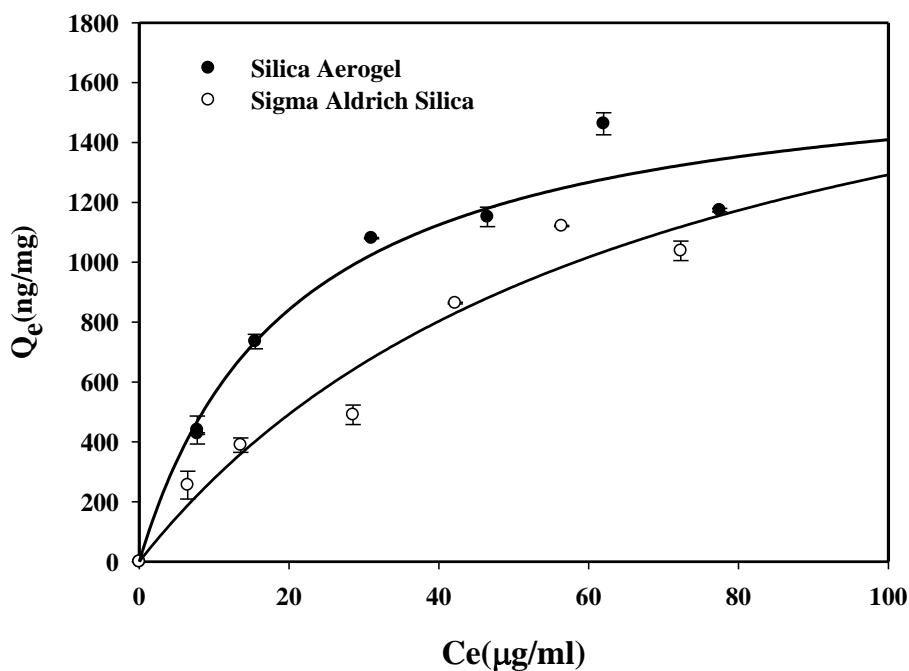Xerogel (E) (F) (G) (H)

Figure 7. 66. Adsorption isotherm of DNA on Silica Aerogel and Silica gel

Sorption isotherms of DNA on silica aerogel and silica gel are shown in Figure 7.66. Comparison of silica aerogel and previously used silica adsorbent adsorption capacity indicated that the adsorption capacity was higher for silica aerogel. However it should be emphasised that calf thymus DNA adsorption increase was not so high as expected from higher surface area of the aerogel due to its lower pore diameter than commercial silica as listed in Table 7.15.

The linear Langmuir plot as shown in Figure 7.67 can be obtained by plotting $1/q_e$ versus $1/Ce$ in given Equation4. 5. The coefficients Q_o and b can be evaluated from the intercept and slope, as 169.5 and 0.051 respectively for DNA adsorbed in silicaaerogel. From the Freundlich isotherm plot in Figure 7.68 the Freundlich isotherm constants Kf and n are found as 211 and 2.3 respectively.
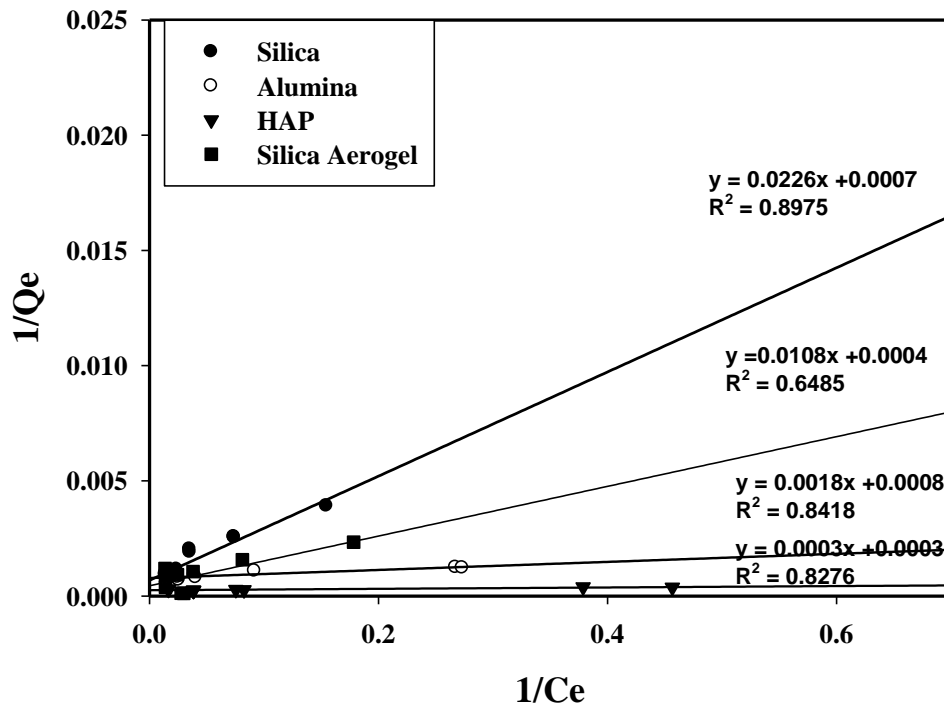
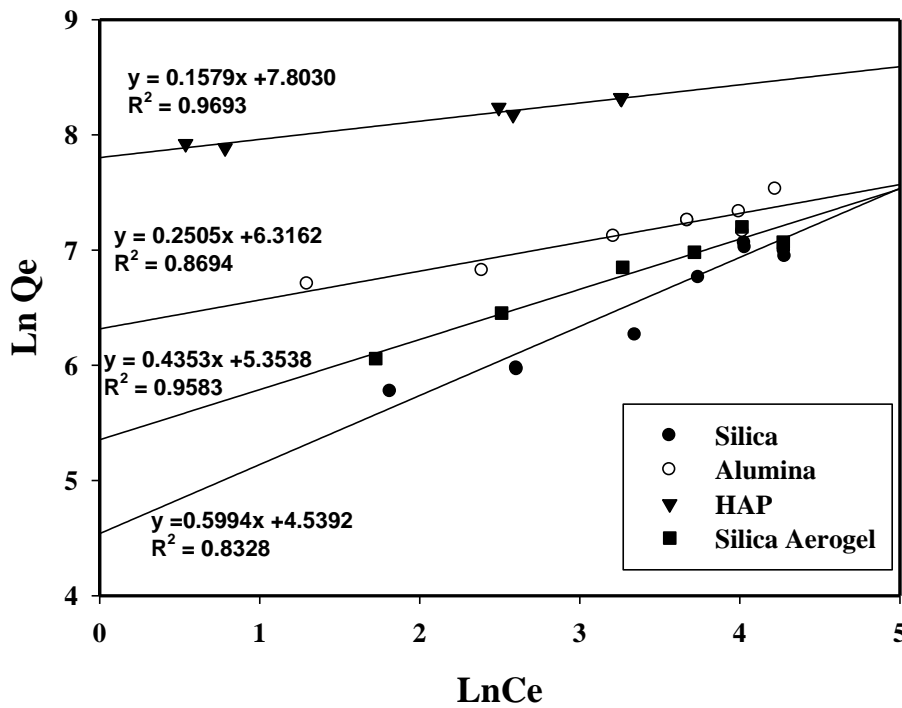Figure 7. 67. Langmuir isotherm at pH 5 all adsorbents and Silica aerogel

Figure 7. 68. Freundlich isotherm at pH 5 all adsorbents and Silica aerogel

7.5. DNA Visualization by Atomic Force Microscopy (AFM)

7.5.1. Substrates Used in AFM Experiments

Silica, alumina, HAP coated thin film glass cover, HAP pellet and mica are the essential substrates on this study to image calf thymus DNA. Alumina ceramic and silica wafer were purchased from CS analytic company and their surface topologies were investigated by AFM. 2 dimensional scans of the surfaces of the substrates of silica and alumina wafers by AFM are seen in Figure 7.69. Figure 7.71. According to these images silica wafer (Figure 7.71.) has better surface property with roughness ratio of 9.8 nm then that of alumina (152 nm) received from CS analytic (Figure 7.69.). However alumina, which is received from MIT Corporation has a tolerable (10.5 nm) roughness (Figure 7.71.). Therefore DNA on alumina surface image studies were carried out with this alumina wafer.
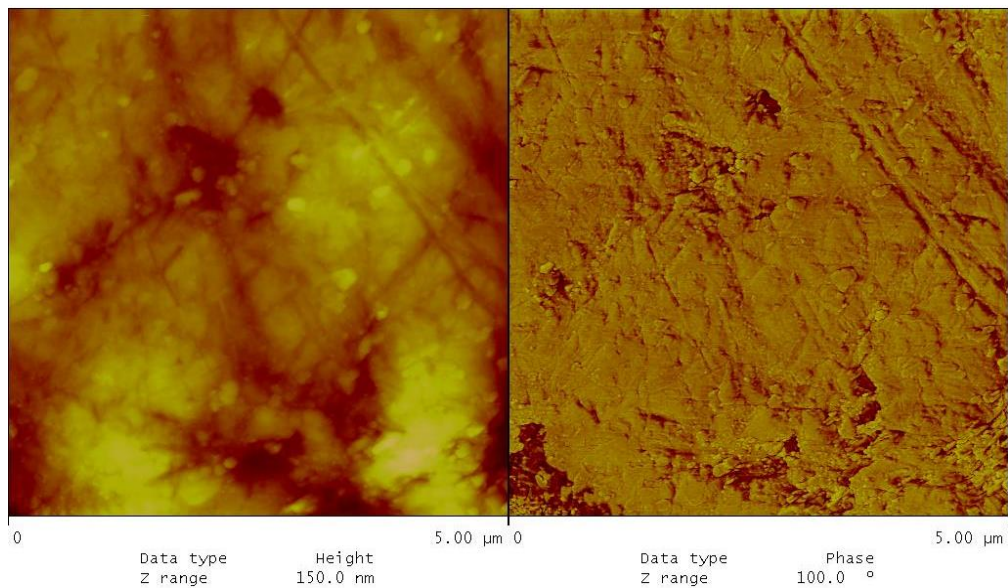
Figure 7. 69 The AFM images of Alumina wafer received from CS analytic company
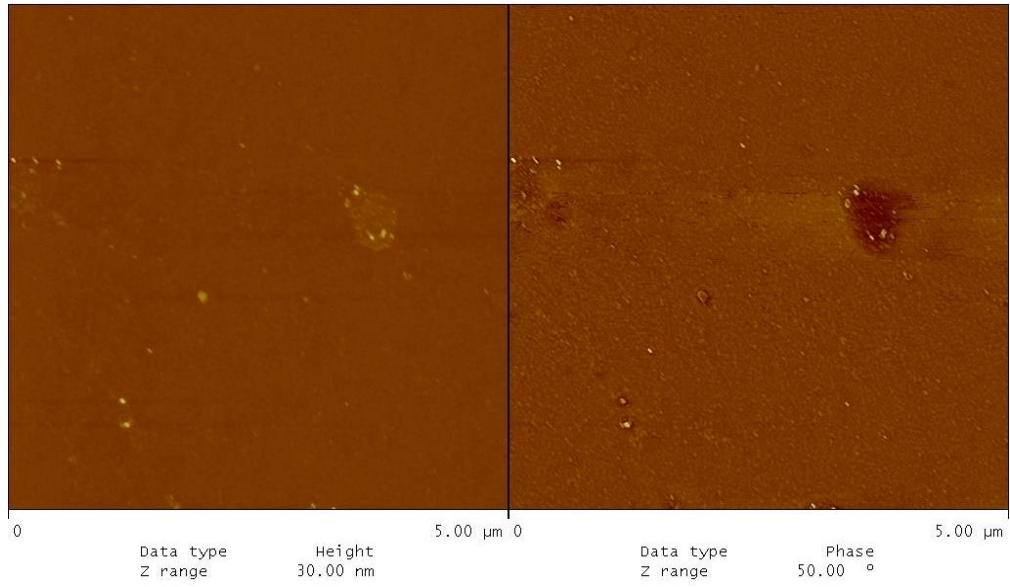
Figure 7. 70. The AFM images of Alumina wafer received from MTI Corporation
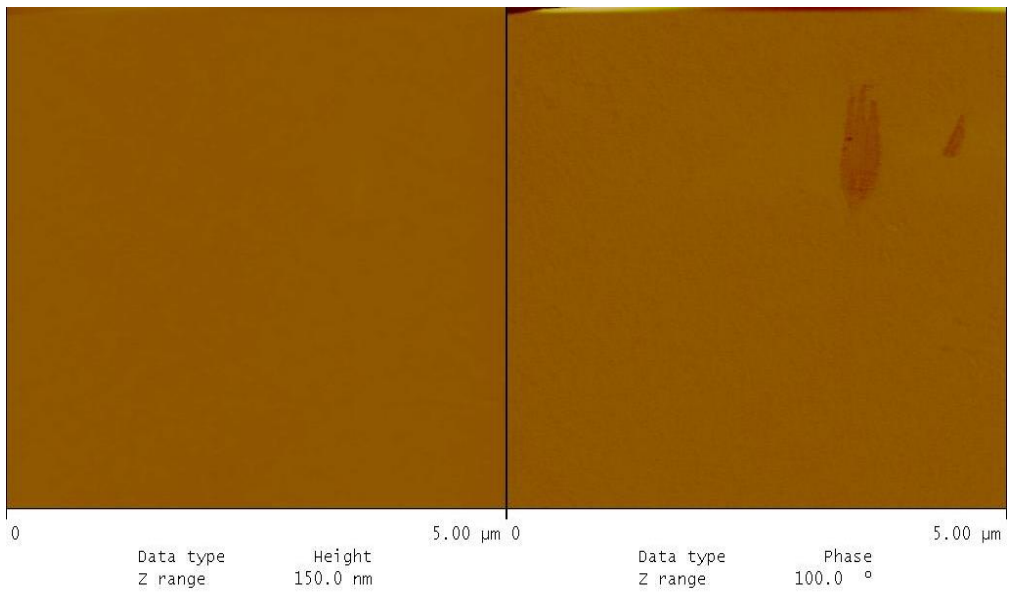
Figure 7. 71. The AFM images of Silica wafer

AFM images at HAP coated on glass substrates by dip coating and drying are seen in Figure 7.72 to Figure 7.74.
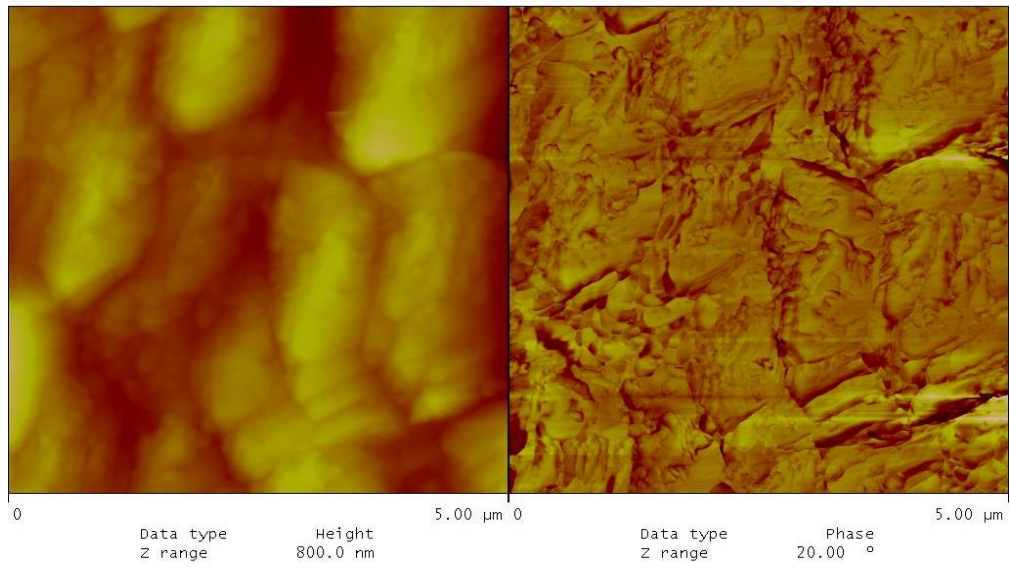
Figure 7. 72. AFM images 2-dim. topographical and phase images 5x5 µm of 5 times HAP coated glass substrate in air
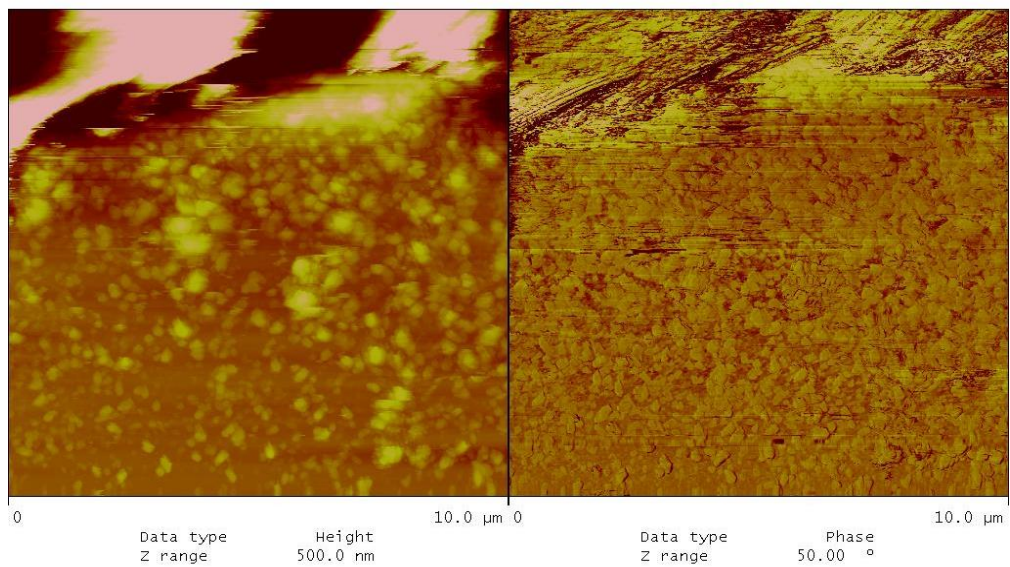
Figure 7. 73. AFM images of 2 times HAP coated glass substrate in air

2 times coating with HAP resulted in a smoother surface on glass substrate as seen in Figure 7.73 and Figure 7.74.
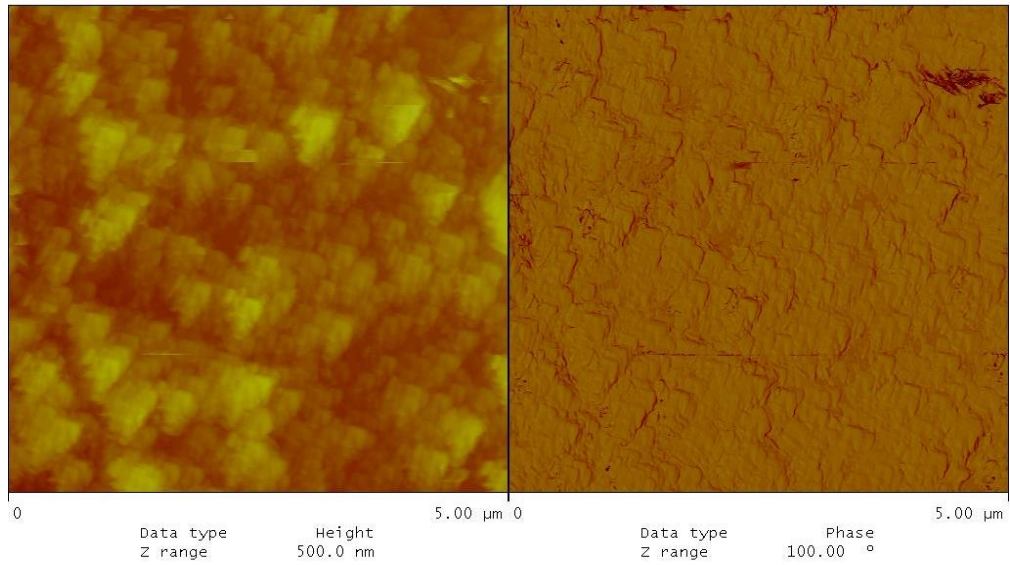
Figure 7. 74. AFM images of 2 times HAP coated glass substrate in air
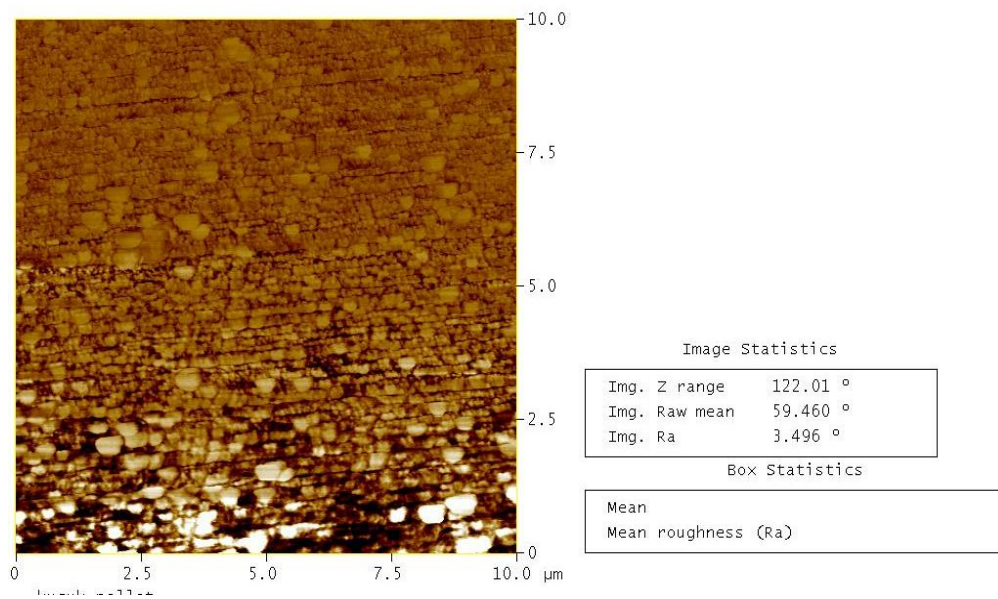
Figure 7. 75. Roughness Analysis of HAP pellet

The AFM image of HAP pellet obtained by fusion of HAP powder at 1300 °C is seen in Figure 7.75.

7.5.2. DNA Image on a Substrate with Different Drying Methods

7.5.2.1. Drying in Ambient Air

7.5.2.1.1 DNA on Mica:

Calf thymus DNA solution (100ng/µl) was dropped onto suitable substrate as a size of 2 µl and then dried with different methods such as in ambient air condition, under N_2 flow regime, and by freeze drying.

In literature studies emphases that after dropping DNA solution onto a surface, washing with deionized water eliminates the buffer salt effect. Therefore our mica surface was washed with three times with 1 cm^3 water after drying DNA droplet and then dried for very long time approximately 3 days. However no DNA structure was detected after this washing step on mica surface as seen in Figure 7.76 . However the water droplets on the surface were present as seen in Figure 7.76. It was not possible to dry the surface washed with large amount of water even for 3 days drying period.
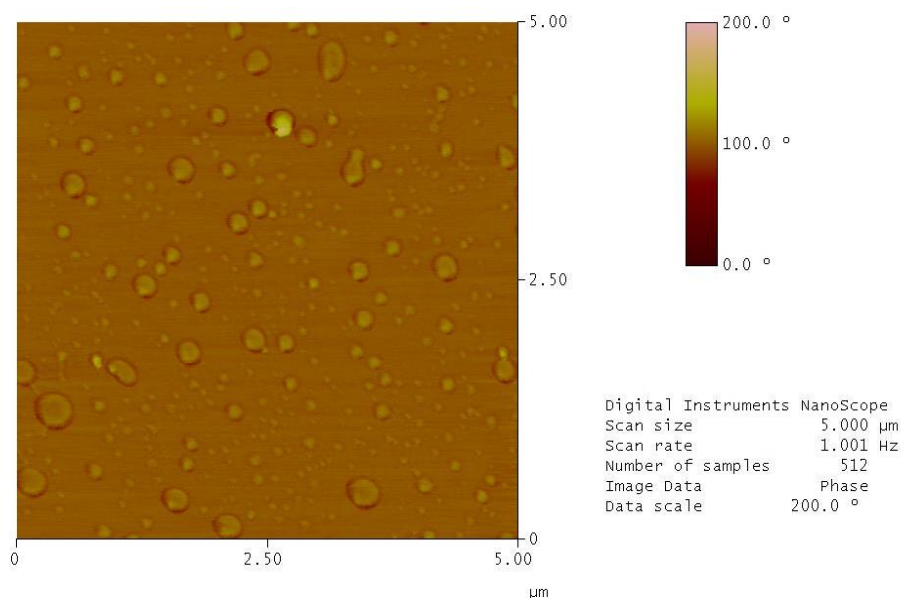
Figure 7. 76. Mica surface after washing dried DNA droplet with water and redrying.

AFM images were taken for two different DNA solutions, one was in TE buffer and the other was in just ultrapure water. DNA average particle size were determined to be 500 nm in solution assuming their shape as spherical by zeta sizer. This indicated the dissolution of DNA in water was not at molecular level. The AFM studies also confirmed this. Figure 7. 77. and Figure 7.78. 3D image of display this considiration The AFM images obtained in TE buffer showed that DNA molecules were self assembled into fibers having 5 µm length and 200 nm diameter fibers. AFM results indicated that DNA was observed in rod like structure in TE buffer.
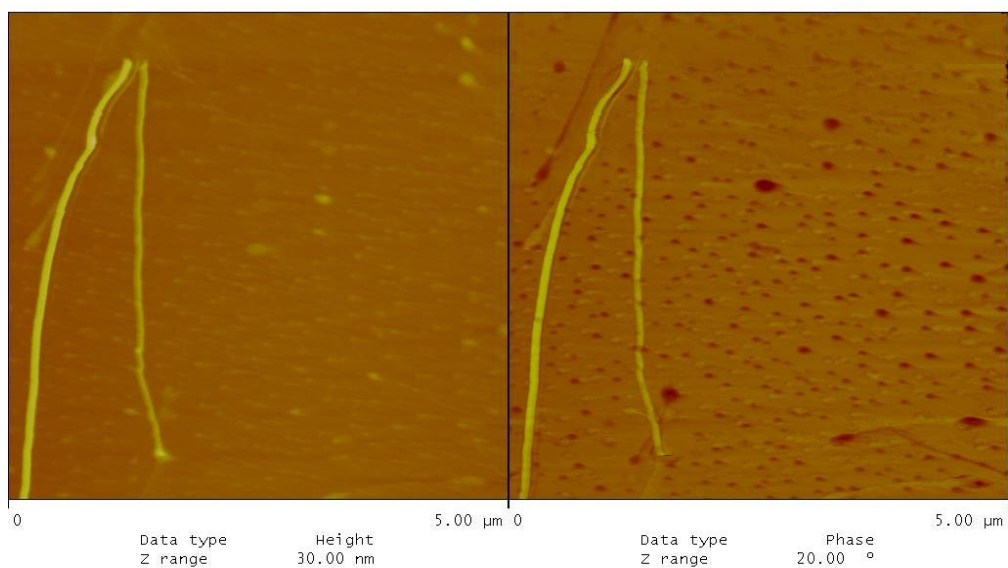
Figure 7. 77. AFM image of 100 ng/µl DNA dissolved in TE buffer on mica surface

Scan size   5.000 µm
Scan rate   1.001 Hz
Number of samples   512
Image Data   Height
Data scale   100.0 nm
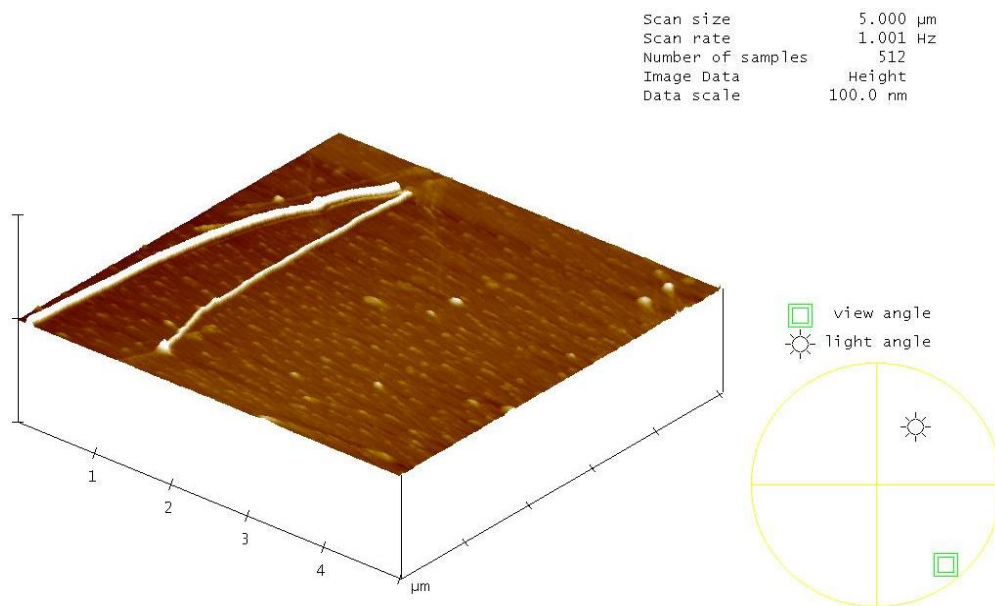
Figure 7. 78. 3D at 100 ng/µl DNAdissolved in TE on mica imaged in ambient air in the tapping mode of an AFM

On the other hand a network structure seen in Figure 7. 79. a,b,c and d was observed at different magnification ratios, for DNA dissolved in pure water. The rootmean square, Rms and average surface roughness, Ra were 0.630 nm and 0.536 nm respectively. Average of the height of DNA strands in 90 different domains was determined to be 1.4 ± 0.34 nm. The average thickness of the fibers was 60 nm and the average distance between the fibers was 240 nm. Gaussian distribution of DNA strands is seen in Figure 7.80. According to this DNA cover the mica surface homogenously.
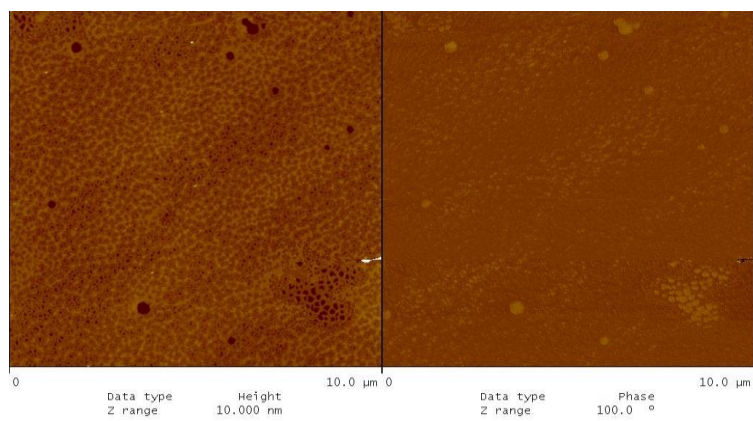
(a)
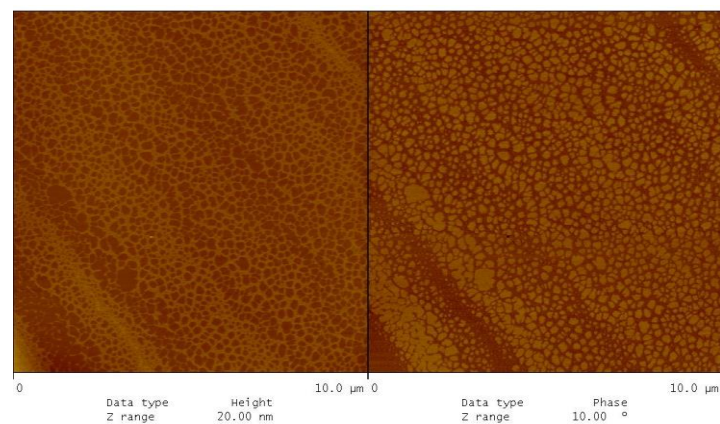
(b)
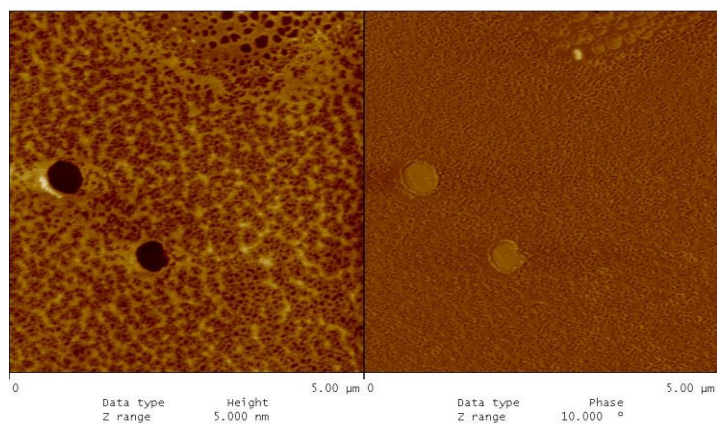
(c)
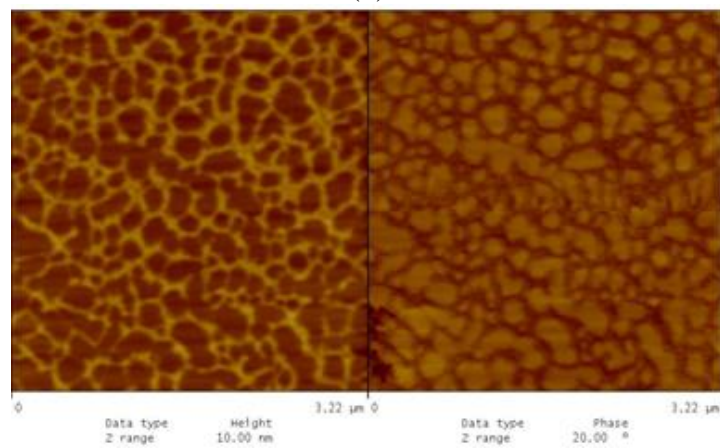
(d)

Figure 7. 79. AFM image of at 100 ng/µDNA dissolved in pure water on mica imaged in ambient air in the tapping mode of an AFM (a) ,(b) 10×10 µm^2 (c) 5×5 µm^2 (d) 3×3 µm^2 scans

The DNA molecules appeared to have crosslinks between them due to intermolecular attractions. Zeta potential measurement showed that calf thymus DNA isoelectric point is at nearly pH 2.2. Mica is a layered mineral with point of zero charge of pH 2. Thus at the pH of the adsorption, pH 7 both mica surface and DNA are negatively charged. However DNA was adsorbed on mica surface since there were attractive forces due to sharing of the counter ions of the mica with DNA.

Buffer also played an important role in DNA structure. It was in a network structure when the DNA dissolved in water was dried on mica surface. However DNA dissolved in TE buffer had rodlike structure on mica.
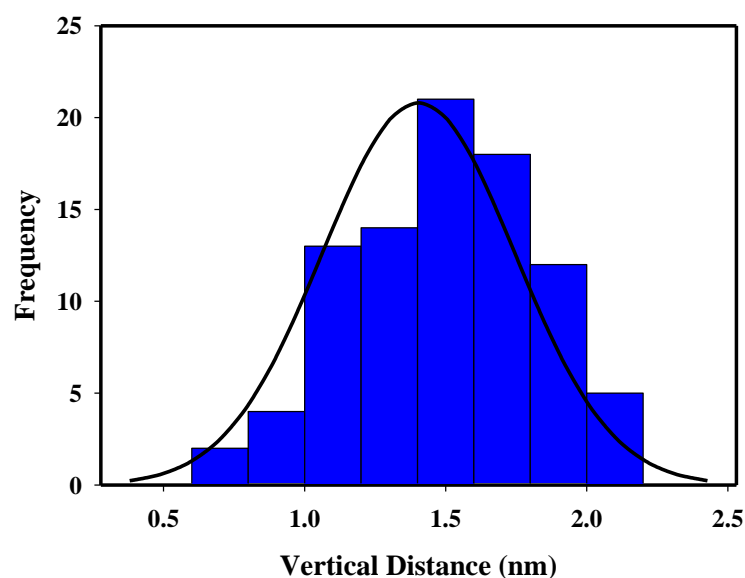
Figure 7. 80. Gaussian Distribution of AFM image DNA dissolved in pure water on mica

7.5.2.1.2 DNA on Alumina:

DNA has high density on the alumina surface as seen in Figure 7.81. DNA structure is different from DNA on mica surface (Figure 7.79). The average vertical distance of DNA on alumina was determined to be 4.6 nm as seen in its Gaussian distribution in Figure 7. 82.

Figure 7. 81. AFM image of at 100 ng/µDNA dissolved in pure water on alumina
imaged in ambient air in the tapping mode of an AFM
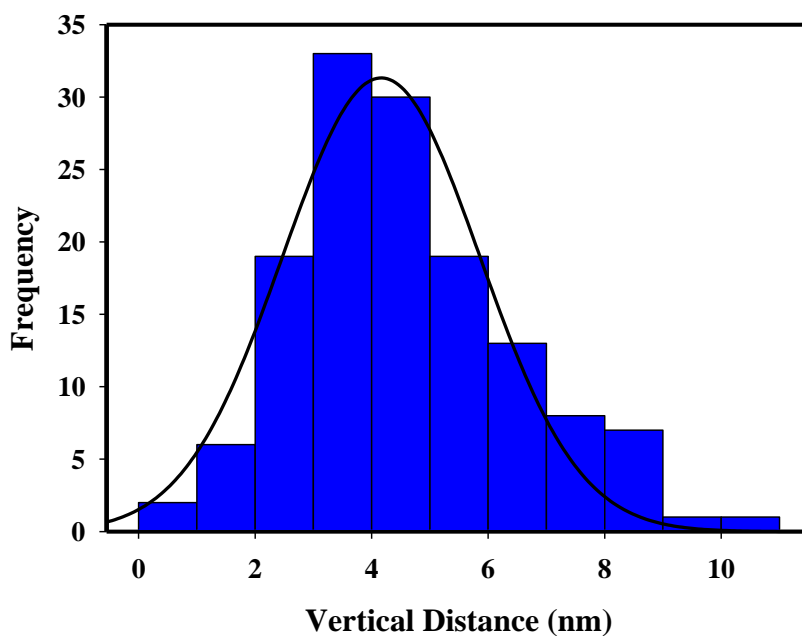
Figure 7. 82. Gaussian Distribution of AFM image of at 100 ng/µl DNA dissolved in
pure water on alumina

DNA Solution Concentration Effect On Mica And Alumina :

Diluted DNA solutions of 10 ng/µl were also analysed to figure out the concentration effect on DNA adsorption onto surfaces of mica and alumina. Images of DNA from dilute solutions on mica and alumina surfaces are shown in Figure 7.84, Figure 7.85. and Figure 7.86. respectively. The surface coverage was decreased with decrease of calf thymus concentration as expected. On the other hand Gaussian distribution of section analysis shown in Figure 7.86. indicated that the average height of DNA on the alumina surface decreased to 2 nm for 10 ng/ µl DNA as compared to 4.6 nm for the case for 100 ng/µl solution. Some other images obtained for DNA on mica surface are shown in Appendix C.
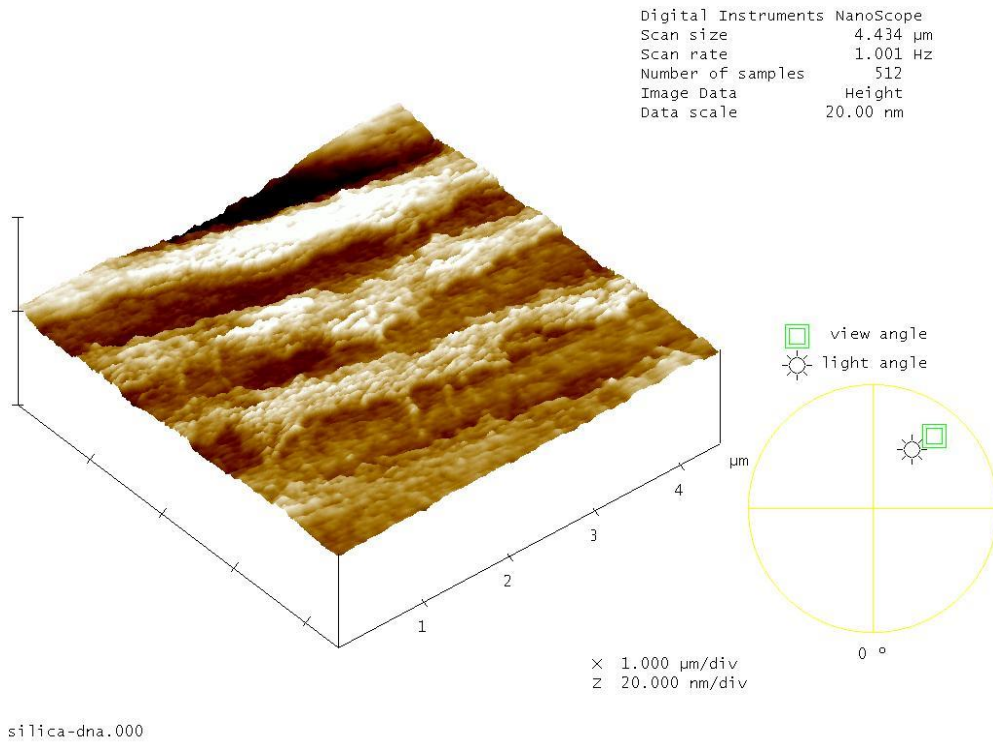
(a)
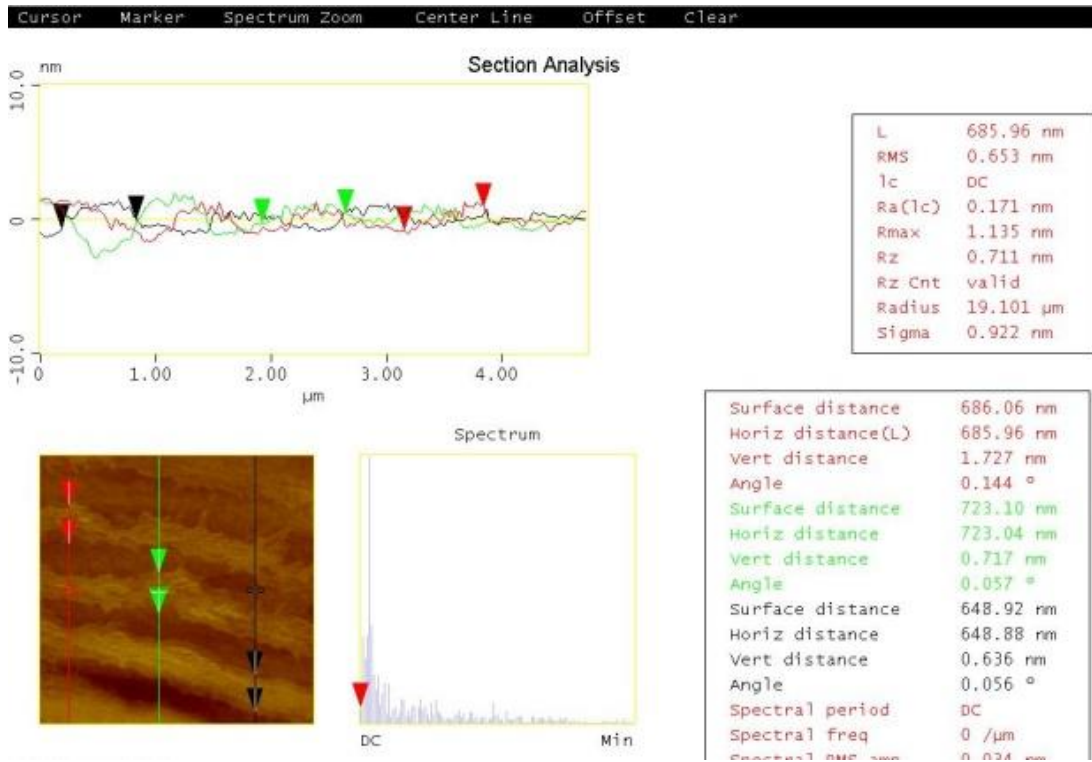
(b)

Figure 7. 83 AFM image of 100 ng/µl DNA dissolved in pure water on silica surface (a)
Surface Plot (b) section analysis

7.5.2.1.3 DNA on Silica:

DNA dissolved in pure water and dried on silica surface is seen in Figure 7.83.Section analysis and surface plot from 5×5 μm^2 scans was determined. Figure 7. 83 AFM image of 100 ng/μl DNA dissolved in pure water on silica surface (a) Surface Plot (b) section analysis (a) and (b) illustrated analysis results. According to these two figures highly polymerized DNA was assembled in rod like shape on the silica surface like it was on mica surface. The average distance between the fibers is 686 nm and average height of the selected three lines is 1.8 nm. However average height of the DNA is higher than obtained average value of mica surface, which was 1.4 ± 0.34 nm.

It is suggested that if the surface is rough enough DNA form crosslinked more easily and closely packed on silica surface (Jo et al., 2003) network, so that more DNA strands can be closely packed together. This suggestion may explain the roles of SiO_2 surface on the DNA network formation.
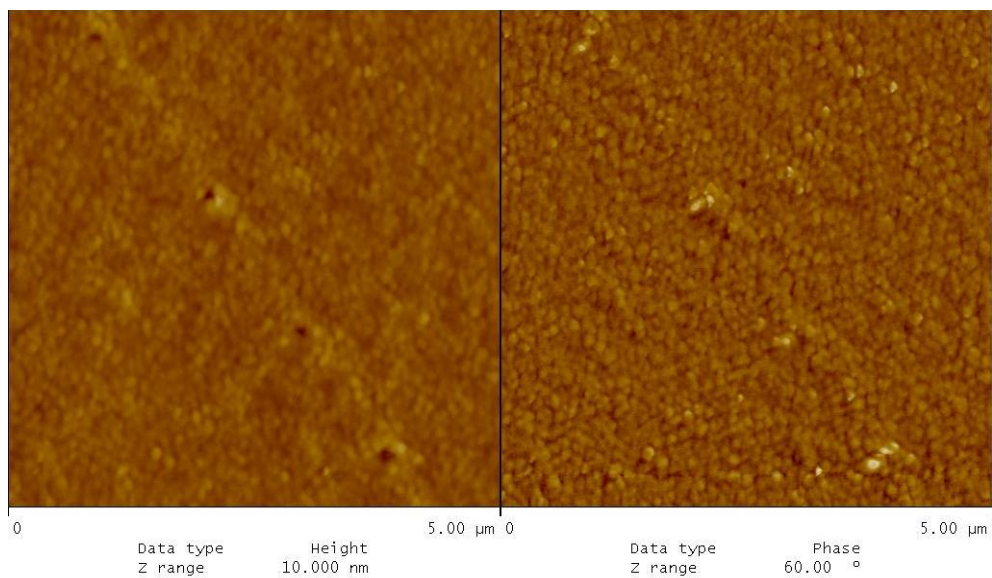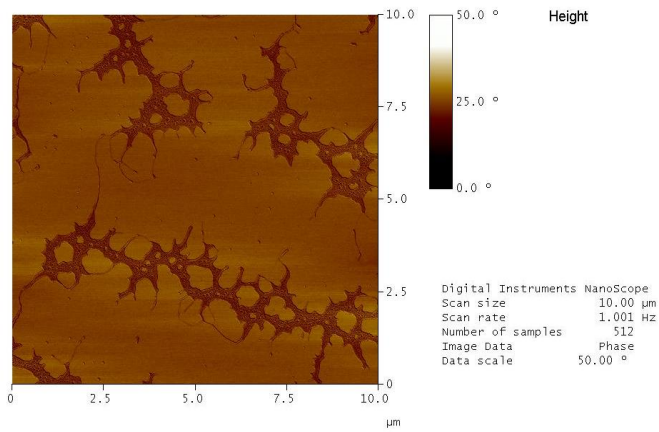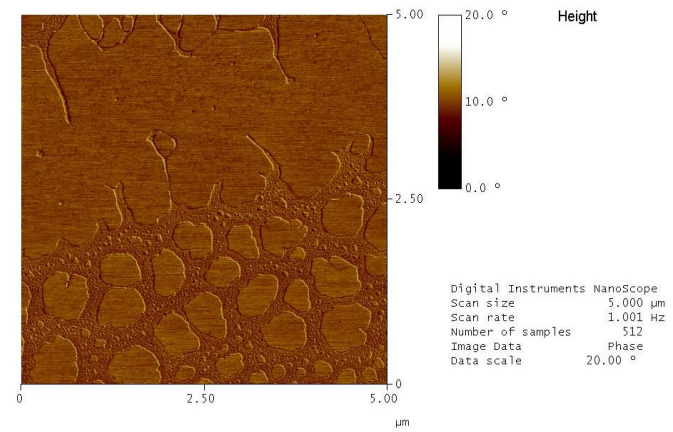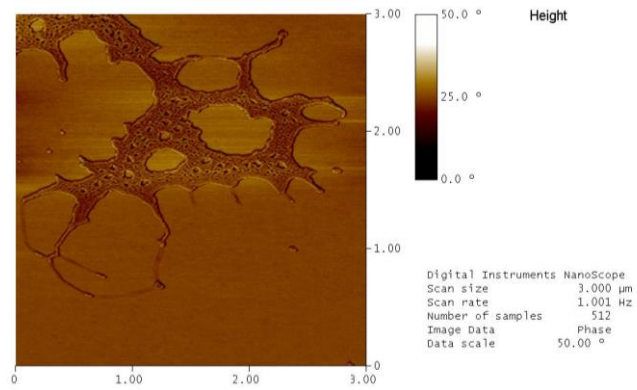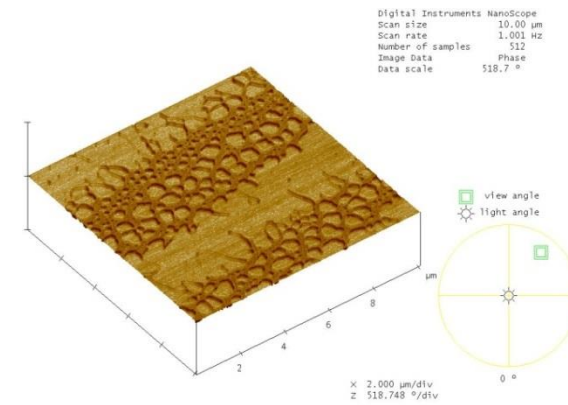
Figure 7. 84. AFM image of DNA dissolved in pure water at 10 ng/µl on mica imaged in ambient air in the tapping mode of an AFM (a) 10×10µm^2 scan (b) section analysis (c) 3D surface plot (d) Gaussian Distribution
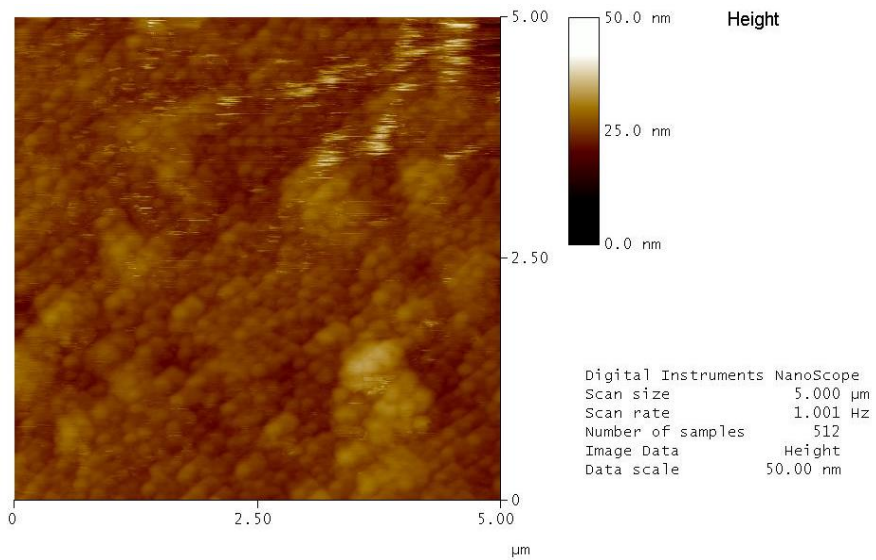
Figure 7. 85 AFM image of DNA dissolved in pure water at 10 ng/µl on alumina imaged in ambient air in the tapping mode of an AFM

.
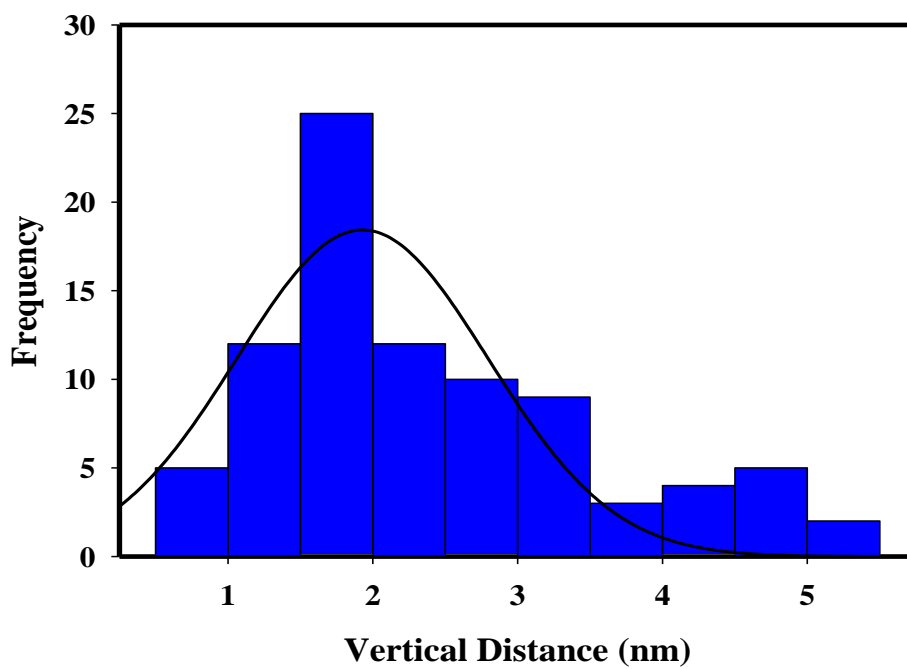
Figure 7. 86. Gaussian Distribution of AFM image of at 10 ng/µl DNA dissolved in pure water on alumina

7.5.2.1.4 DNA on Hydroxyapatite:

It is the first time DNA can be detected on HAP surface. DNA has the rod like form as indicated inside the regtangle in Figure 7.87. DNA with 345 nm length was imaged on HAP pellet.
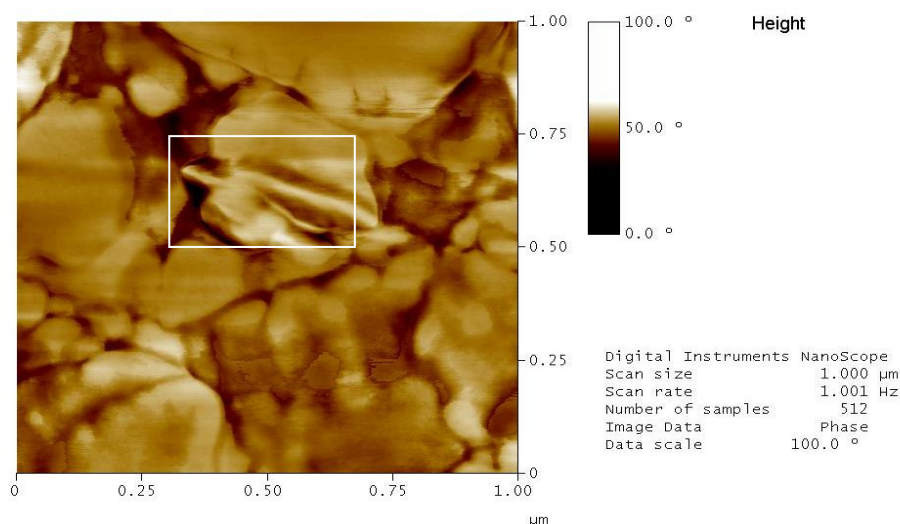
Figure 7. 87. AFM image of 100 ng/µl DNA dissolved in pure water on HAP pellet surface

7.5.2.1.5 DNA Dissolved in Ethanol -Drying in Ambient Air

DNA dissolved in ethanol and dried in air on mica surface. Figure 7.88. illustrates calf thymus DNA image on mica with pure ethanol used as solvent. An average height of DNA taken with least 50 domains is 6 nm. DNA conformational change B to A is obtained in the presence of ethanol.

7.5.2.2. Drying with N_2 Flow Regime

DNA droplet on mica surface was dried under nitrogen flow at room temperature and AFM images was taken. Figure 7. 89. is belong to DNA on the mica surface. The image Figure 7.89. of DNA taken on mica surface dried with nitrogen has a compact structure. Construction of supercoiled DNA occurred. Two-dimensional

network of DNA structures was obtained. There were crosslinks between DNA molecules forming a network structure on the surface of mica. Distance between the fibers is 154.5 nm for Figure 7.89. This is less than the value of 240 nm which was evaluated before for ambient air dried sample. Consequently quick evaporation of water from the dropped surface causes less tension through the edge of the ring. Laminar N_2 flow regime has great influence on the morphology of DNA on the surface.
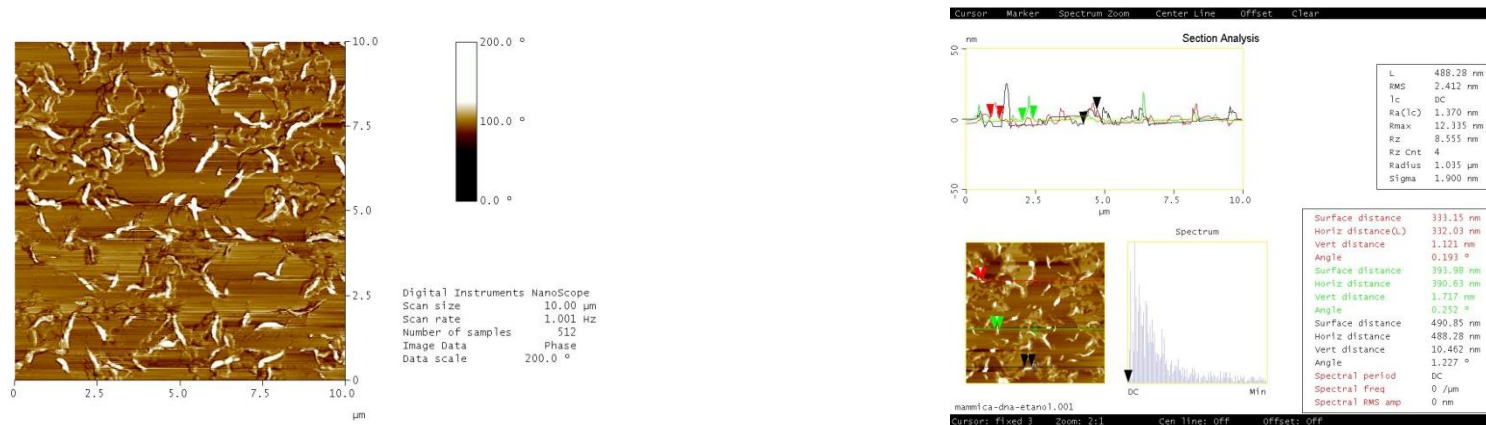
(a)

(b)
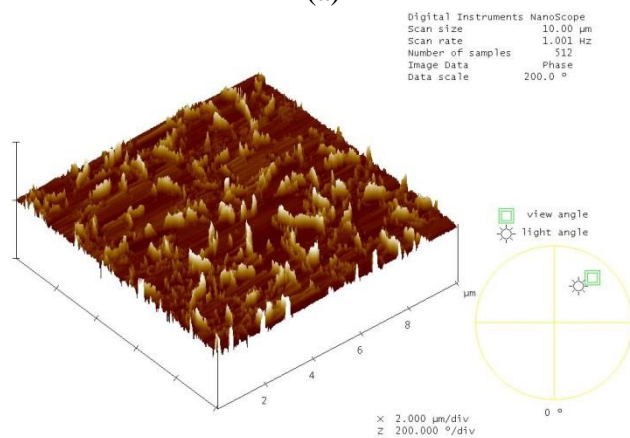
(c)
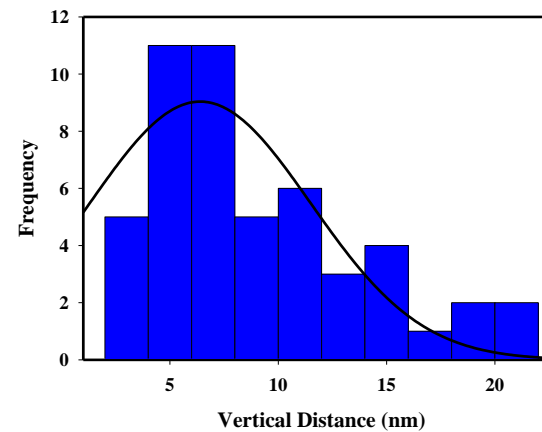
(d)

Figure 7. 88. AFM image of DNA dissolved in pure EtOH at 10o ng/µl on mica imaged in ambient air in the tapping mode of an AFM (a) 10×10 µm^2 scan (b) section analysis (c) 3D surface plot (d) Gaussian Distribution
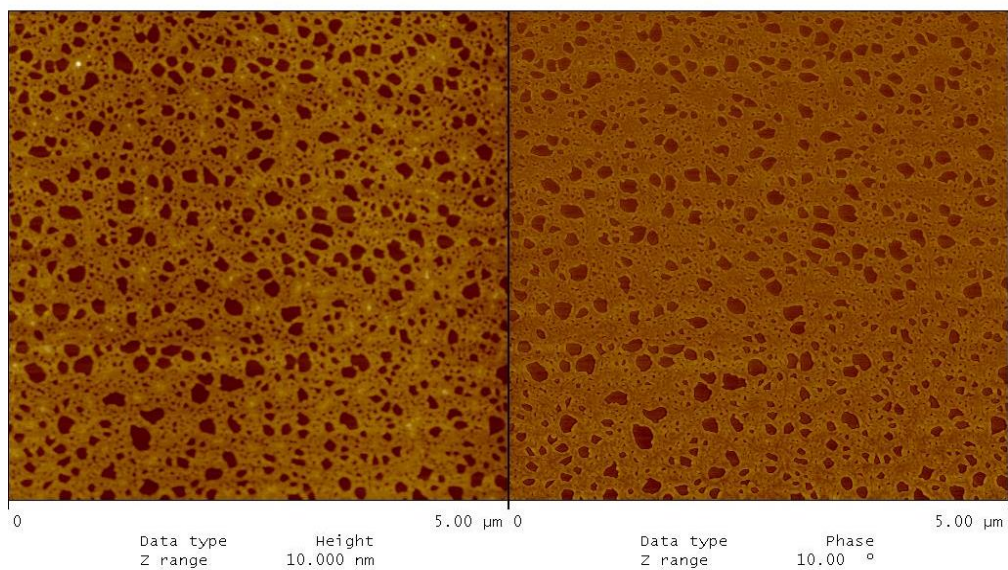
Figure 7. 89. AFM image of at 100 ng/µDNA dissolved in pure water on mica and dried in N$_2$ flow
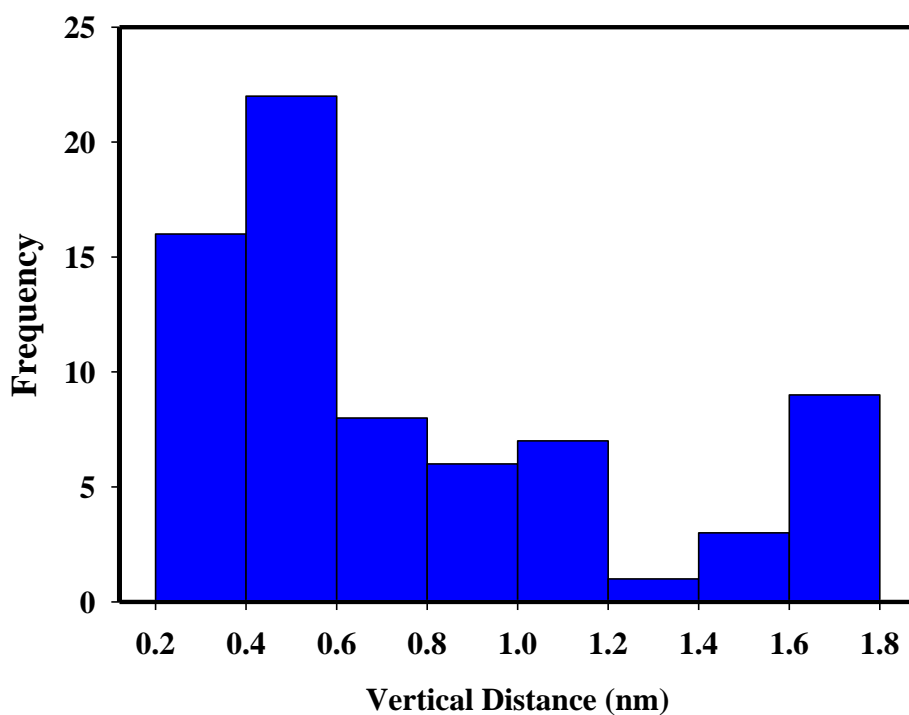
Figure 7. 90. Gaussian Distribution of AFM image of at 100 ng/µl DNA dissolved in pure water on mica and dried in N$_2$ flow

The average vertical distanceies of the domain are mainly obtained between 0.2 and 1.2 nm.

180
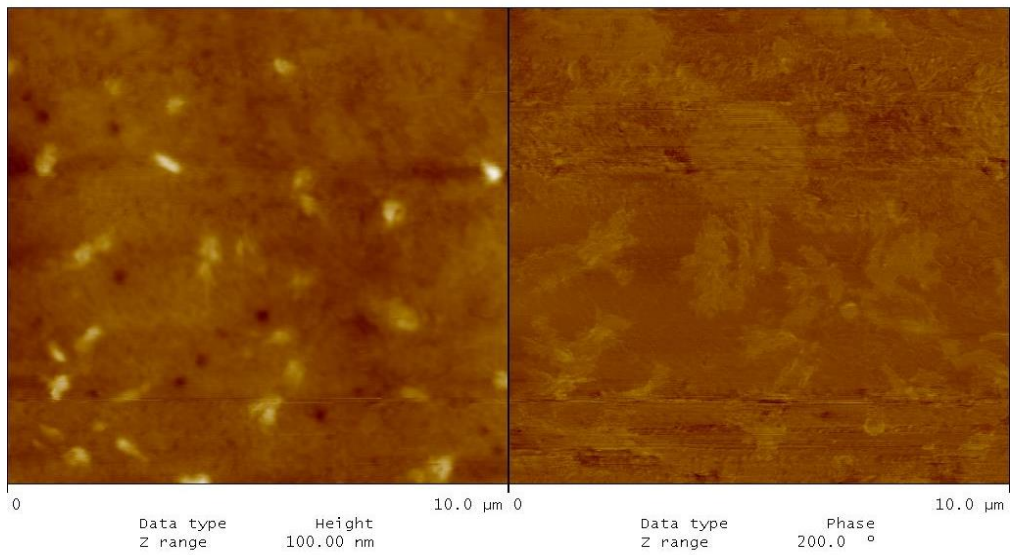
Figure 7. 91. AFM image of DNA dissolved in pure water at 100 ng/µl on alumina dried in N$_2$ flow
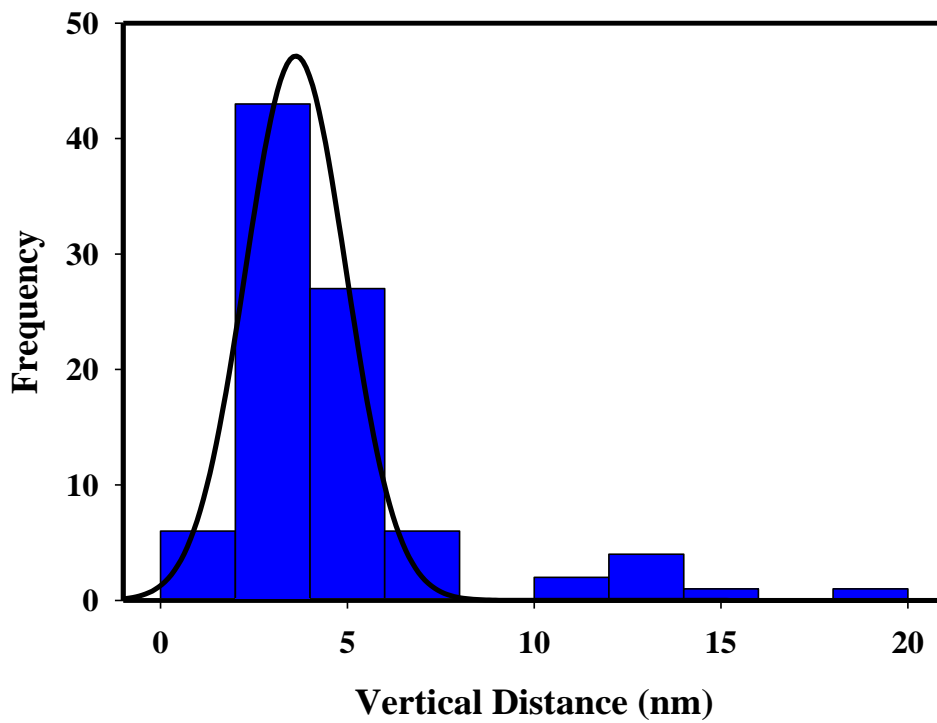
Figure 7. 92. Gaussian Distribution of AFM image of at 100 ng/µl DNA dissolved in pure water on alumina and dried in N$_2$ flow
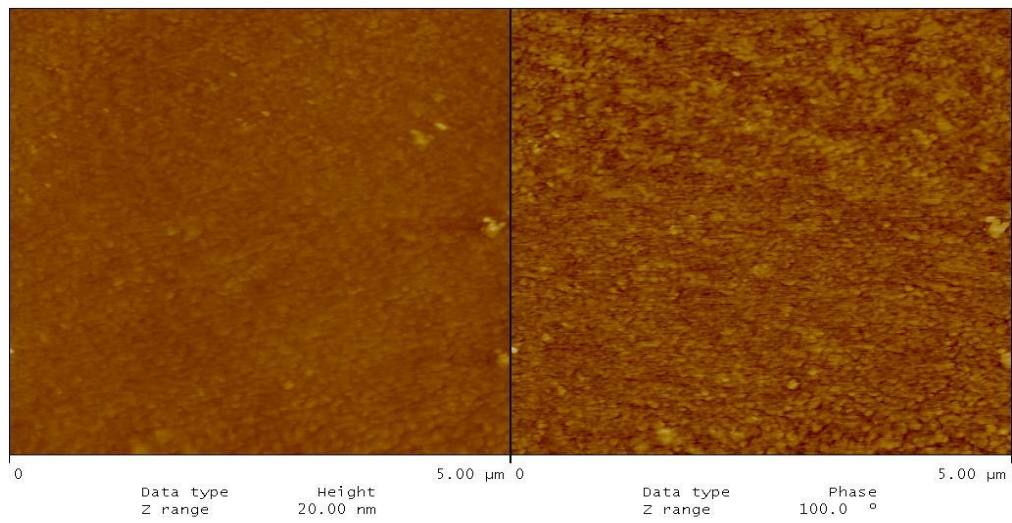
Figure 7. 93. AFM image of DNA dissolved in pure water at 100 ng/µl on silica and dried in N_2 flow
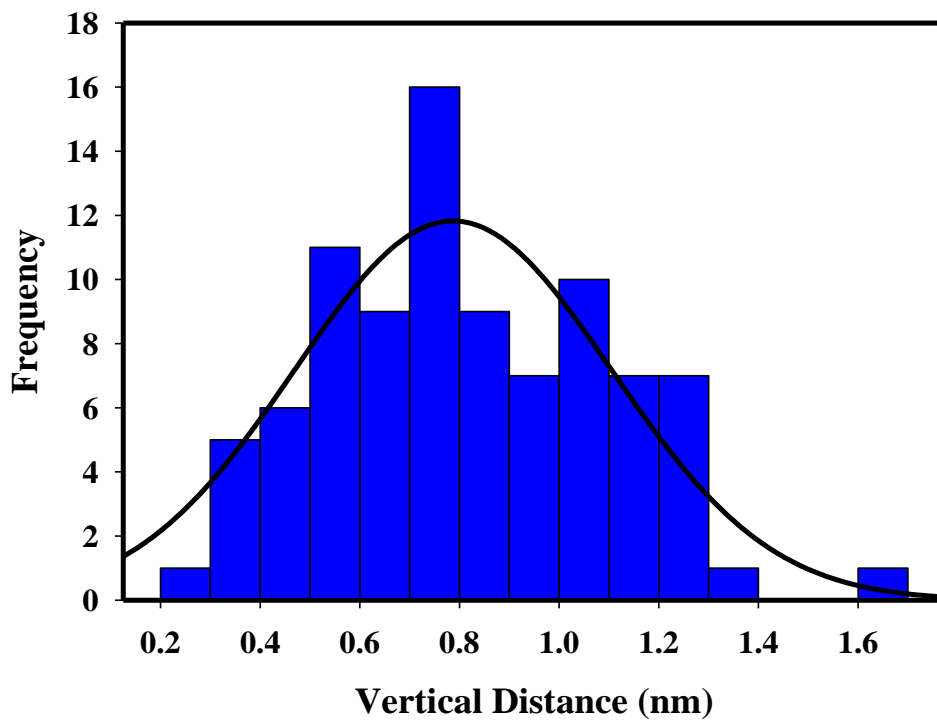
Figure 7. 94. Gaussian Distribution of AFM image of at 100 ng/µl DNA dissolved in pure water on silica and N_2 flow dried

N$_2$ flow regime was also applied to silica and alumina surfaces. In addition to mica DNA supercoils were constructed on these surfaces. They showed homogenously distributed DNA supercoil structures in Figure 7.91 and Figure 7.93. Average vertical distances of least 90 domains were 0.8 and 4.6 nm for silica and alumina respectively. DNA was self-assembled perfectly on silica surface. N$_2$ flow regime on alumina did not change the average vertical distance of DNA. However vertical distance distribution of DNA on alumina surface dried in N$_2$ flow in Figure 7.92 is narrower when compared to Figure 7. 86 for ambient air drying on alumina.

7.5.2.3. Drying with Freeze Dryer
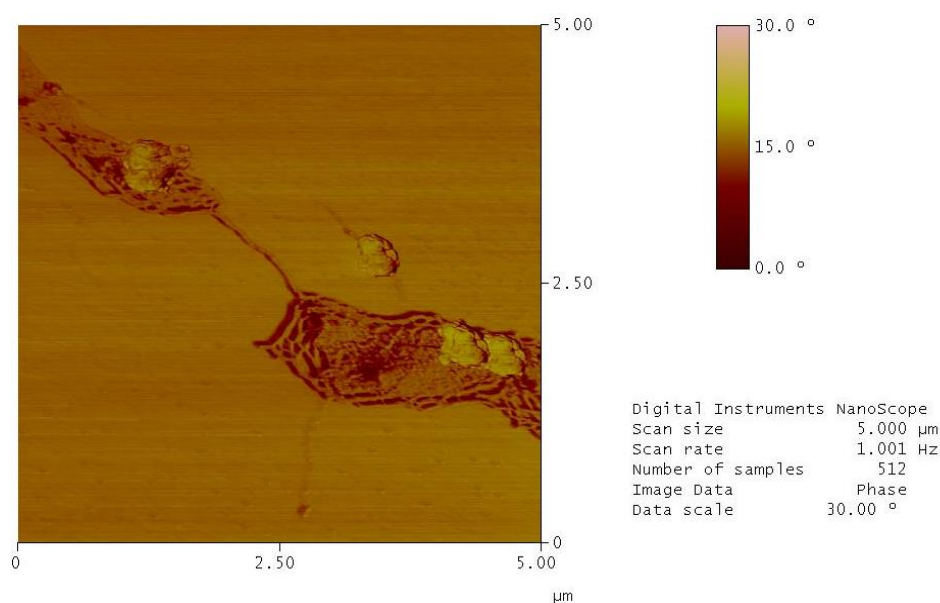
Figure 7. 95. AFM image of DNA dissolved in pure water at 100 ng/µl on mica and freeze dried
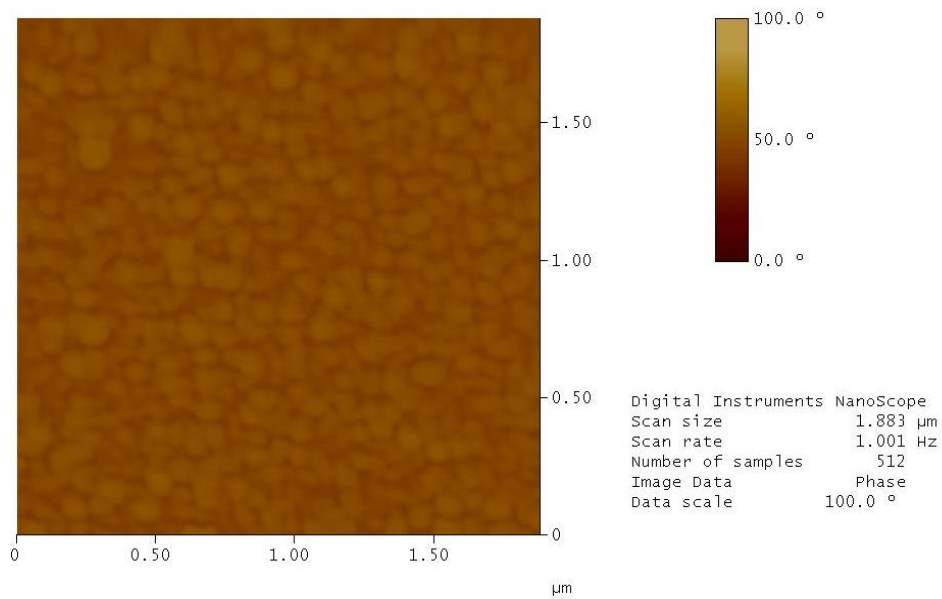
Figure 7. 96. AFM image of DNA dissolved in pure water at 100 ng/µl on alumina and
freeze dried
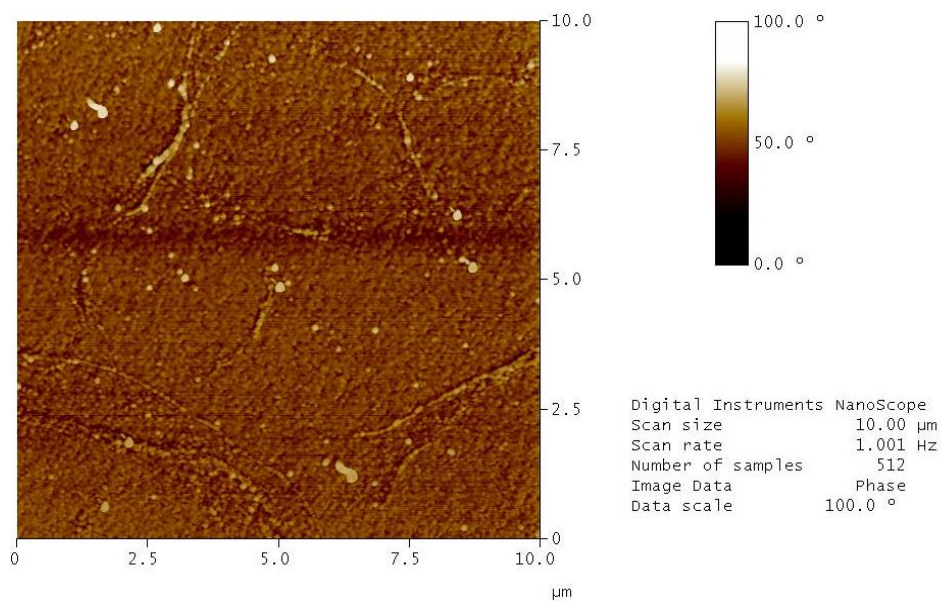
Figure 7. 97. AFM image of DNA dissolved in pure water at 100 ng/µl on silica-and
freeze dried
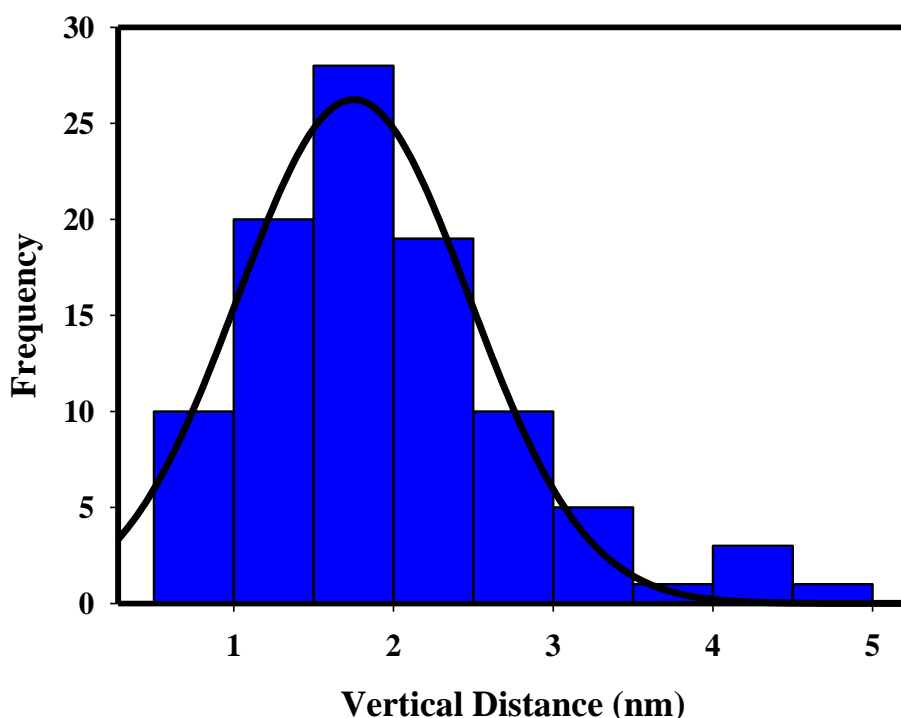
Figure 7. 98. Gaussian Distribution of AFM image of at 100 ng/μl DNA dissolved in
            pure water on alumina freeze dried

Tapping mode AFM investigation of influence of freeze drying process was applied on DNA dropped surfaces which are mica, alumina and silica. Figure 7.95 to Figure 7.98 display the related images. Gaussian distribution of freeze dried DNA on alumina surface is shown in the Figure 7.98. It is indicated that freezing causes the DNA structure become compact. Freeze drying is known the most efficient method for avoiding deconstruction but conformation of calf thymus DNA was changed. DNA was imaged as individual fibers with height higher than previous images. Table 7. 16 shows average vertical distance and variance of Gaussian distribution of DNA on mica, silica and alumina for different drying methods. Concequently alumina has lower variance values than mica and silica surface. Nitrogen flow regime does not show significant effet on mica and alumina surfaces except quick drying. Other freeze dried DNA images are shown in Appendix C.

Table 7. 16 Average vertical distance values taken by least 90 domains for different drying method for mica, silica and alumina surfaces

Subtrate (Average vertical distance)	Ambient Air				N$_2$ flow		Freeze Drying	
	Concentrated DNA solution		Diluted DNA Solution					
	average	σ	average	σ	average	σ	average	σ
Mica (nm)	1.4	0.125	-		1.6	0.135	-	
Silica(nm)	-		-		0.8	0.212	-	
Alumina(nm)	4.6	0.08	2.4	0.136	4.6	0.05	1.99	0.095

CHAPTER 8

CONCLUSIONS

The purpose of this study was to evaluate the potential of the promising adsorbent powders like alumina, hydroxyapatite (HAP), silica and silica aerogel for DNA purification. The adsorbents and solids in DNA purification kits were well characterized by SEM, x-ray fluorescence, EDX and x-ray diffraction, nitrogen gas adsorption and FTIR techniques. Silica and alumina were mesoporous powders with 59 and 162 μm sizes respectively and HAP had mesoporous nanoparticles. Silica powders were ground to 10 μm size was used in adsorption experiments. It was found that the commercial DNA kits had adsorbents of glass fibers and quartz powders. Highly polymerized calf thymus DNA dissolved in water had 600 nm size as indicated by its particle size analysis. The adsorption capacities of the studied adsorbents were much higher than that of DNA adsorbents present in commercial kits. Nano sized hydroxyapatite had the highest DNA adsorption capacity among all the adsorbents studied.

Another aim of this research is to investigate the improvement in the adsorption capacity of silica. Thus silica aerogel having 1055 m^2/g surface area was synthesized by the supercritical ethanol drying method. Its DNA adsorption capacity was found to be greater than the commercial silica due to its high surface area.

It is known that DNA adsorption is possible because DNA has negative charge due to the phosphate backbone above its isoelectric point, it can make hydrogen bond with the solid surfaces and there are Van der Waals attractions between DNA and the surfaces. Calf thymus DNA's isoelectric point was found to be less than pH 2.2 in the present study. The isoelectric points of silica, alumina, and HAP were reported to be 2, 9 and 8 respectively. DNA was negatively charged above pH 2. Since the silica surface was also negatively charged above pH 2, the adsorption of DNA on silica should be due to hydrogen bonding and Vander Waals attractions. Alumina and DNA had opposite surface charges between pH 2 and 9, thus ionic attractions play an important role on adsorption of DNA on alumina. The surface charge of HAP was positive up to pH 8.

Thus ionic attractions between DNA and hydroxyapatite had a great contribution to the adsorption of DNA on HAP.

Enhancements of the adsorption capacities of adsorbents were obtained with the addition of $MgCl_2$. The adsorption capacity of DNA on adsorbents increased when divalent cation molarity was changed from 0.5mM to 20 mM.

The adsorption isotherms of DNA on silica, alumina and HAP were fitted to Langmuir model better than Freundlich model and Dubinin Astokovich model. Higher correlation coefficients were obtained with pseudo second order model than the pseudo first order reaction model in adsorption kinetics of DNA. The DNA adsorption to the external surface of the particles was very fast kinetically and accomplished within about 15 min. After that intraparticle diffusion mechanism become dominant. Intraparticle diffusion rate constant, ki, decreased significantly in the order of alumina, silica and HAP. The kinetic models, reaction and diffusion models showed that, adsorption at the external surface was dominant at initial stages of the DNA adsorption and it was followed by a slower intraparticle diffusion.

DNA adsorbed on the flat surfaces mica, alumina, silica and HAP was examined with AFM to define highly polymerized calf thymus DNA morphology. DNA dispersed in water was adsorbed on the surfaces not as single molecules but as supercoils consisting of many molecules. Buffer also played an important role in DNA structure. DNA had a network structure when the DNA dissolved in water was dried on mica surface. However, the structure was rodlike when DNA dissolved in TE buffer was dried on mica.

Adsorbed DNA was imaged in ambient air on flat surfaces of mica, silica and alumina wafers and HAP particles coated glass surfaces and a HAP pellet surface by AFM. The effects of the ambient air, nitrogen flow and freeze drying methods on DNA morphology on the related surfaces were also investigated. DNA assemblies having a vertical distance in the range of 0.8 to 4.6 nm on different surfaces were achieved by using AFM imaging process. A supercoil of DNA with 345 nm length and 9.8 nm width was imaged on the surface of the HAP pellet.

Freeze drying was determined to be the most effective method to achieve a clear image of DNA by AFM. Drying under N_2 flow regime resulted in a narrower distribution of the vertical distance of DNA on mica and alumina surfaces.

The study can be extended by investigating the effects of different types of proteins in DNA solution. New and more efficient DNA purification kits can be

developed by using the thermodynamic and kinetic data obtained on DNA adsorption in the present study. Adsorption behaviour of DNA from aqueous solutions could further be investigated by using liquid flow cell of AFM. Fabrication of large scale DNA nanostructures, pattern transfer from DNA nanostructure to an inorganic substrate and directed assembly of DNA nanostructures on flat surfaces could furher be investigated by AFM technique Nanofabrication of Au and Ag nanofibers on flat surfaces by metallizing highly polymerized calf thymus DNA adsorbed on the surfaces could be investigated. Calf thymus DNA mediated etching of silica by HF can also be performed for nanolithography.

REFERENCES

Albrecht T. R, Grütter P., Horne D., Rugar (1991). Frequency modulation detection using highQ cantilevers for enhanced force microscope sensitivity. *J. Appl. Phys.* 69, 668

Alie C.,Pirard R., Pirard J.P., (2002). The role of the main silica precursor and the additive in the preparation of low-density xerogels. *Journal of Non-Crystalline Solids ,* 311, 304–313

Allahverdyan A. E., Gevorkian Zh. S., Hu C.K, Nieuwenhuizen T. M., (2009). How adsorption influences DNA denaturation. *Physical Review E,* 79, 031903

Allemand J.-F, Bensimon D., Jullien L., Bensimon A., Croquette V. (1997). pH-Dependent Specific Binding and Combing of DNA. *Biophysical Journal,* 73, 2064-2070

Allen M. J., Bradbury E. M., Balhorn R. (1997). AFM analysis of DNA–protamine complexes bound to mica. *Nucleic Acids Research,* 25, (11), 2221–2226

Anastassopoulou J., (2003). Metal–DNA interactions. *Journal of Molecular Structure,* 651–653,.19–26

Anselmetti D, Luthi R, Meyert E, Richmond T, Dreier M, Frommer J E , Guntherodt H-J, (1994). Attractive-mode imaging of biological I materials with dynamic force microscopy. *Nanotechnology ,*5, 87-94.

Aslanoglu Mehmet, Andrew Houlton and Benjamin R. Horrocks, (1998). Functionalised monolayer for nucleic acid immobilisation on gold surfaces and metal complex binding studies. *Analyst,* 123, 753–757

Balköse D., Alp B., Ülkü S. (2008). Water Vapour Adsorptıon on DNA. *Journal of Thermal Analysis and Calorimetry,* 94, 695–698

Bensimon A., Simon A., Chiffaudel A., Croquette V., Heslot F., Bensimon D. (1994) Alignment and Sensitive Detection of DNA by a Moving. *Science,* 265, 2095

Biochem.2010. University of California, Biochemistry and Molecular Biology (BMB) Web   site:

http://www.biochemistry.ucla.edu/biochem/Faculty/Martinson/Chime/abz_dna/abz_master.html, (acsessed June 28, 2010)

Bisson A, Rigacci A, Lecomte D, Rodier E, Achard P (2003). Drying of Silica Gels to Obtain Aerogels :Phenomenology and Basic Techniques. *Progress in Drying Technologies,* 21,(4): 593–628

Bixon, M., Giese B., Wessely S., Langenbacher T., Michel-Beyerle M. E., Jortner J.. (1999). Long-range charge hopping in DNA. *Proc. Natl. Acad. Sci. USA.* 96, 11713–11716.

Boom, R., Sol C. J. A., M. M. M. Salimans, C. L. Jansen, P. M. E. Wertheim-van, noordaa j. Van der, (1990). Rapid and Simple Method for Purification of Nucleic Acids. *Journal of Clinical Microbiology,* 28, (3), 495-503

Breadmore M. C.; Wolfe, K. A.; Arcibal, I. G.; Leung, W. K.; Dickson, D.; Giordano, B. C.; Power, M. E.; Ferrance, J. P.; Feldman, S. H.; Norris, P. M.; Landers, J. P. (2003). Microchip-Based Purification of DNA from Biological Samples. *Anal. Chem.,*75,1880-1886.

Brinker, C. J.; Scherer G.W. 1990. Sol-Gel Science: *The Physics and Chemistry of Sol-Gel Processing*. Academic Press: Boston,.

Brun A. M. and Harriman A., (1992). Dynamics of Electron Transfer between Intercalated Polycyclic Molecules: Effect of Interspersed Bases. *J. Am. Chem. Soc.* 114, 3656

Buffone G. J., Demmter G. J., Schimbor C. M., Greer J.,(1991). Improved Amplification of Cytomegalovirus DNA from Urine after Purification of DNA with Glass Beads. *Clinical Chemistry,* 37, (11), 1945

Bussiek M, Mucke N., Langowski Joerg (2003). Polylysine-Coated Mica Can Be Used to Observe Systematic Changes in The Supercoiled DNA Conformation by Scanning Force Microscopy In Solution. *Nucleic Acids Research,.* 31, (22*),* e137

Bustamante C., Keller D. (1995). Scanning Force Microscopy in Biology. *Phys. Today,* 48, .32

Bustamante C., Rivetti C., (1996). Visualizing Interactions on a Large Scale with the Scanning Force Microscope. *Annu. Rev. Biophys. Biomol. Struct.,* 25,.395-429

Bustamante C., Vesenka J., Tang C.L., Rees W., Guthold M., Kellers R., (1992). Circular DNA Molecules Imaged in Air by Scanning Force Microscopy. *Biochemistry,* 31, 22-26

Cai P., Huang Q, Jiang D., Rong X., Liang W. (2006). Microcalorimetric studies on the adsorption of DNA by soil colloidal particles. *Colloids and Surfaces B Biointerfaces* , 49, 49–54

Caruso Frank, Elke Rodda, and D. Neil Furlong (1997). Quartz Crystal Microbalance Study of DNA Immobilization and Hybridization for Nucleic Acid Sensor Development. *Anal. Chem.* 69, 2043-2049

Chao Z.Z.,Cui Y., HongW.Q., (2007). Surface Modification of Magnetic Silica Microspheres and Its Application to the Isolation of Plant Genomic Nucleic Acids. *Chin J Anal Chem,* 35, (1),.31–36.

Chargaff E. and J. N. Davıdson, (1955). *The Nucleic Acids- Chemistry and Biology*. Academic Press Inc, Publishers -New York

Chattoraj D. K.and Mitra A. (2009). Adsorption of DNA at solid–water interfaces and DNA–surfactant binding interaction in aqueous media. *Current Scıence,* 97,(10), 1430-1438

Chen W.Y. ,Lin S.M., Lin P.S., Tasi S.P., Chang Y., Yamamoto S., (2007). Studies of the interaction mechanism between single strand and double-strand DNA with hydroxyapatite by microcalorimetry and isotherm measurements. *Colloids and Surfaces A: Physicochem. Eng. Aspects*, 295, .274–283

Clemente A.V. and Gloystein K., (2008). *Principles of Atomic Force Microscopy (*AFM). Physics of Advanced Materials Winter School Retrieved January 05, 2013 from project founded by EC Web site: http://www.mansic.eu/documents/PAM1/Frangis.pdf

Delain E., Fourcade A., Poulin J.C., Barbin A., Coulaud D., Cam E. L., Paris E. (1992). Comparative Observations of Biological Specimens, Especially DNA and Filamentous Actin Molecules in Atomic Force, Tunnelling and Electron Microscopes. *Microsc. Microanal Microstruct* ,3 ,457-470

Dias R.S, Lindman B. (2008). *DNA Interactions with Polymers and Surfactants*" John Wiley & Sons

Do, D.D. (1998). *Adsorption Analysis: Equilibria and Kinetics*. Imperial College Press, London

Dorcheh A. S., Abbasi M.H. (2008). Silica aerogel; synthesis, properties and characterization. *Journal of Materials Processing Technology* , 199, 10–26

Douarche C., Robert Cortes, Steven J. Roser, Jean-Louis Sikorav, Alan Braslau, (2008). DNA Adsorption at Liquid/Solid Interfaces. *J. Phys. Chem. B*, 112, (44), 13676–13679

Dunlap D.D., Maggi A., Soria M. R., Monaco L.(1997). Nanoscopic structure of DNA condensed for gene Delivery. *Nucleic Acids Research*, 25, (15), 3095– 3101

Eaton P. and West P. (2010). *Atomic Force Microscopy*. Oxford University press.

Engel A. (1991). Biological Applications of Scanning Probe Microscopes. *Annu. Rev. Biophys. Biophys. Chern*, 20, 79-108

Erdoğan B.C.,Ülkü S.(2012). Cr(VI) Sorption By Using Clinoptilolite and Bacteria Loaded Clinoptilolite Rich Mineral" *Microporous and Mesoporous Materials*, 152, 253–261

Estella J., Echeverrıa J. C., Julian M.L., Garrido J., (2008). Effect of Supercritical Drying Conditions in Ethanol on The Structural and Textural Properties of Silica Aerogels. *J Porous Mater*, 15, 705–713

Fang X., Li B., Petersen E., Seo Y.S., Samuilov V. A., Chen Y.,. Sokolov J. C, Shew.Y.C., Rafailovich M. H. (2006). Drying of DNA Droplets. *Langmuir,* 22, (14), 6308–6312

Fang Y., Spisz T. S.,. Hoh J. H. (1999). Ethanol-Induced Structural Transitions of DNA on Mica. *Nucleic Acids Research*, 27,(8) 1943–1949

Fang Y. and Hoh J. H. (1998). Surface-Directed DNA Condensation in the Absence of Soluble Multivalent Cations.*Nucleic Acids Research*, 26, (2), 588–593

Fasman D. G. (1992). *Practical Handbook of Biochemistry and Molecular Biology*. CRC Press

Fawcett, N.C., Craven, R.D., Zhang, P., Evans, J.A., (1998). Quartz Crystal Microbalance Response to Solvated Macromolecules. *Anal. Chem*. 70 (14), 2876–2880

Feng Z.,Jingkun X., Shufeng L. (2008). Atomic Force Microscopy Visualization of The DNA Network and Molecular Morphological Transition on a Mica Surface. *Thin Solid Films*, 516, 7555–7559

Fidalgo A, Farinha JPS, Martinho JMG, Rosa ME, Ilharco LM. (2005). The Influence of The Wet Gels Processing on The Structure and Properties of Silica Xerogels. *Microporous and Mesoporous Materials*, 84, 229–235

Fidalgo A., Ilharco L.M., (2001). The Defect Structure of Sol-Gel Derived Silica/Polytetrahydrofuran Hybrid Films By FTIR. *J. Non-Cryst. Solids*, 283, 144

Fidalgo A.,Rosa M.E., Ilharco M. (2003). Chemical Control of Highly Porous Silica Xerogels: Physical Properties and Morphology. *Chem. Mater.*, 15, 2186-2192

Fitzgerald-Hayes and Reichsman. (2010). *DNA and Biotechnology.* Third Edition Academic Press is an imprint of Elsevier Web site: http://www.knovel.com/web/portal/basic_search/display?_EXT_KNOVEL_DISPLAY_bookid=3194

Fowler B.O. (1974). Infrared Studies of Apatites. I. Vibrational Assignments for Calcium, Strontium, and Barium Hydroxyapatites Utilizing Isotopic Substitution. *Inorg. Chem*, 13, 194

Franchi M., Ferris J.P., Gallori E. (2003). Cations as Mediators of The Adsorption of Nucleic Acids on Clay Surfaces in Prebiotic Environments. *Origins of Life and Evolution of the Biosphere*, 33, 1–16

Franchis S.M., Stephens W.E., Richardson N. V. (2009). X-Ray Photoelectron and Infrared Spectroscopies of Quartz Samples. *Environmental Health*, 8, 1

Fujiwara M, Yamamoto F, Okamoto K.,, Shiokawa K., Nomura R. (2005). Adsorption of Duplex DNA on Mesoporous Silicas: Possibility of Inclusion of DNA into Their Mesopores. *Anal. Chem.*, 77, 8138-8145

Gad M., Mizutani W., Machida M., Ishikawa M. (2000). Method For Stretching DNA Molecules on Mica Surface in One Direction For AFM Imaging. *Nucleic Acids Symposium Series*, 44, 215-216

Gadgil H.,. Oak S.A., Jarrett H.W. (2001). Affinity Purification of DNA-Binding Proteins. *J. Biochem. Biophys. Methods*, 49, 607–624

Giglio S., Monis P.T. , Saint C.P. (2003). Demonstration of Preferential Binding of SYBR Green I to Specific DNA Fragments in Real-Time Multiple. *Nucleic Acids Research*, 31, 22

Greeg S.J. and Sing K.S.W. (1982). *Adsorption, Surface Area and Porosity*. Academic Press London

Grosberg A. and Khokhlov A. (1994). *Statistical Physics of Macromolecules*. AIP Press, New York

Hadjiliadis N.and Sletten E. (2009). *Metal Complex–DNA Interactions*" A John Wiley & Sons, Ltd., Publication Blackwell Publishing Ltd.

Hamon L, Pastre D., Dupaigne P., Breton C.L., Cam E.L., Pie trement O. (2007). High-Resolution AFM Imaging of Single-Stranded DNA-Binding (SSB) Protein—DNA Complexes. *Nucleic Acids Research*, 35, 8, e58

Hansma, H. G., and Laney D. E. (1996). DNA Binding to Mica Correlates with Cationic Radius: Assay by Atomic Force Microscopy. *Biophys. J.*,70, 1933–1939.

Hansma, H. G., Revenko I., Kim K., Laney D. E. (1996). Atomic Force Microscopy of Long And Short Double-Stranded, Single-Stranded and Triple-Stranded Nucleic Acids. *Nucleic Acids Research*, 24, 713-720

Hansma, H. G. (2001). Surface Biology of DNA By Atomic Force Microscopy. *Annu. Rev. Phys. Chem.*, 52, 71–92

Hench, L. L. (1991). Bioceramics: From Concept to Clinic. *J. Am. Ceramic. Soc.*, 74, 7, 1487 -1510

Hench, L. L. (1998). Bioceramics. *J. Am. Ceramic. Soc*. 81, 7,1705 -1728

Ho Y. S. and Mckay G. (1999). Research Note the Sorption of Lead (Ii) Ions on Peat. *Wat. Res.*,33, 2, 578-584,

Ho Y. S., J.C.Y. Ng, Mckay G. (2000). Kinetics of Pollutant Sorption by Biosorbents" Review. *Separation and Purification Methods*, 29, 2, 189–232

Hui W. C., Yobas L., Samper V.D., Heng C.K., Liw S., Ji H., Chen Y.,Cong L., Li J., Lim T.M. (2007). Microfluidic Systems For Extracting Nucleic Acids for DNA and RNA Analysis. *Sensors and Actuators A*, 133, 335–339

Jo Y.S Lee Y., Roh Y. (2003). Roles of Buffer Solution and Substrate Surface on the Characteristic of DNA Network Formed on SiO_2. *Materials Science and Engineering C,* 23, 851–855

Kanno S., Tanaka H.,Miyoshi N., Kawai T. (2000). A New Self Fabrication of Large Scale Deoxyribonucleic Acid Network on Mica Surface" *Jpn J. Applied Physics*, 39. L269-L270

Karlsson M., Palsg E. , Wilshaw P.R., Silvio L.Di. (2003). Initial in Vitro Interaction of Osteoblasts with Nano-Porous Alumina. *Biomaterials*, 24, 3039–3046

Kasumov, A.Y., M. Kociak, S. Gueron, B. Reulet, V.T. Volkov, D.V. Klinov, H. Bouchiat. (2001). Proximity-Induced Superconductivity in DNA. *Science,* 291, 280.

Khanna M. and Stotzky G. (1992). Transformation of Bacillus subtilis by DNA Bound on Montmorillonite and Effect of DNase on the Transforming Ability of Bound DNA. *Applied and Environmental Microbiology*, 58, 1930-1939

Khanna M., Yoder M., Calamai L., Stotzky G. (1998). X-Ray Diffractometry and Electron Microscopy of DNA from Bacillus Subtilis Bound on Clay Minerals. *Sciences of Soils*, 3, 1

Kim J., Mauk M., Chen D., Qiu X., Kim J., Galeb B., Baua H. H. (2010) . A PCR Reactor with an Integrated Alumina Membrane for Nucleic Acid Isolation. *Analyst*, 135, 2408–2414

Kistner C., André A. Fischer T, Thoma A., Janke C., Bartels A., Gisler T., Maret G.,. Dekorsyb T. (2007). Hydration Dynamics of Oriented DNA Films Investigated by Time-Domain Terahertz Spectroscopy. *Applied Physics Letters*, 90, 233902

Klinov D., Dwir B., Kapon E., Borovok N., Molotsky T., Kotlyar A. (2007). High-Resolution Atomic Force Microscopy of Duplex and Triplex DNA Molecules. *Nanotechnology*, 18, 225102

Komlev V.S., S.M. Barinov, E.V. Koplik. (2002). Method To Fabricate Porous Spherical Hydroxyapatite Granules Intended For Time-Controlled Drug Release. *Biomaterials*, 23, 3449.

Komulski M. (2009). pH Dependent Surface Charging and Points of Zero Charge IV. Update and New Approach. *Journal of Colloid and Interphase Science*, 337, 439

Kumar MA., Jung S.,Ji T. (2011). Protein Biosensors Based on Polymer Nanowires, Carbon Nanotubes and Zinc Oxide Nanorods. *Sensors*, 11, 5087-5111

Lagergren, S. (1898) "About the Theory of So-Called Adsorption of Soluble Substances". Kungliga Svenska Vetenskapsakademiens. Handlingar, 24(4):1-39.

Land V. D, Harris T. M., Teeters D. C. (2001). Processing of Low density Silica Gel by Critical Point Drying or Ambiant Pressure Drying. *Journal of Non-Crystalline Solids*,. 283, (1-3), 11-17

Levin I.,and Brandon D. (1998). Metastable Alumina Polymorphs: Crystal Structures and Transition Sequences. *J. Am. Ceram. Soc*.,81, 8,1995–2012

Li J, Bai C, Wang C, Zhu C, Lin Z, Li Q, Cao E. (1998). A Convenient Method of Aligning Large DNA Molecules on Bare Mica Surfaces for Atomic Force Microscopy. *Nucleic Acids Res.*, 26, 20, 4785-6.

Lorenz M.G.,and Wackermagel (1987). Adsorption of DNA to Sand and Variable Degradation Rates of Adsorbed DNA. *Appl.Enviromental Microbiol*., 53, .2948-2952

Lorenz M.G., Wackernagel W. (1994). Bacterial Gene Transfer by Natural Genetic Transformation in the Environment. *Microbiological Reviews*, 58, 3, 563-602

Lyubchenko, Y. L., Oden P. I., Lampner D., Lindsay S. M., Dunker K. A. (1993). Atomic Force Microscopy of DNA and Bacteriophage in Air, Water and Propanol: the Role Of Adhesion Forces. *Nucleic Acids Res*.,21, 5, 1117-1123.

Lyubchenko, Y. L. (2011). Review: Preparation of DNA and Nucleoprotein Samples for AFM Imaging. *Micron*, 42, 196–206

Maier, B.; Radler, J. O. (2000). DNA on Fluid Membranes: a Model Polymer in Two Dimensions. *Macromolecules*, 33, 7185–7194.

Malash Gihan F.,. El-Khaiary Mohammad I. (2010). Piecewise linear regression: A statistical Method for the Analysis of Experimental Adsorption Data by the Intraparticle-diffusion Models" *Chemical Engineering Journal*, 163, 256–263

Mao Y., Daniel L. Y., Whittaker N., Saffiottil U. (1994). DNA Binding to Crystalline Silica Characterized by Fourier-Transform Infrared Spectroscopy. *Environ Health Perspectives*, 102 ,165-171

Marx K.A., Lim J.O., Minehan D, Pande R., Kamath M, TripathyS.K., Kaplan D.L. (1994). Intelligent Materials Properties of DNA and Strategies for Its Incorporation into Electroactive Polymeric Thin Film Systems. *Journal of Intelligent Material Systems and Structures,* 54, 47-454

Mathews A. P. and Weber W. J. (1976). Effects of External Mass Transfer and Inter-particle Diffusion on Adsorption. *Physical Chemical Waste Water Treatment AIChE Symp. Ser. 7*, 3, 91-98

Melzak K. A., Sherwood, C. S., Turner, R. B. F., and Haynes, C. A. (1996). Driving Forces for DNA Adsorption to Silica in Perchlorate Solutions. *J. Colloid Interface Sci.*,181, 635

Miller S.A., Dykes D.D., Polesky H.F. (1988). A Simple Salting out Procedure for Extracting DNA from Human Nucleated Cells. *Nucleic Acids Research*, 16, 3, 1253

Möller C., Allen M., Elings V., Engel A, Möller D.J. (1999). Tapping-Mode Atomic Force Microscopy Produces Faithful High-Resolution Images of Protein Surfaces. *Biophysical Journal*, 77, 1150–1158

Muramatsu H., Kim J.M.,·Chang S.M. (2002). Quartz-crystal Sensors for Biosensing and Chemical Analysis. *Anal.Bioanal.Chem.*, 372, 314-321

Murphy, C. J. Arkin M. R., Jenkins Y., Ghatlia N. D., Bossmann S. H., Turro N. J, Barton J. K. (1993). Long range photoinduced Electron Transfer through a DNA Helix. *Science*, 262, 1025

Nawrocki, J. (1997). The Silanol Group And Its Role in Liquid Chromatography. *J. Chromatogr. A*, 779, (1−2), 29−71

Nguyen T.H., and Chen K. (2007). Role of Divalent Cations in Plasmid DNA Adsorption to Natural OrganicMatter-Coated Silica Surface. *Environ. Sci. Technol*, 41, 5370-5375

Nguyen T.H, and Elimelech M. (2007). Adsorption of Plasmid DNA to a Natural Organic Matter-Coated Silica Surface: Kinetics, Conformation, and Reversibility. *Biomacromolecules,* 8, 24-32

Nguyen, T. H.; Elimelech, M. (2007). Adsorption of Plasmid DNA to A Natural Organic Matter-Coated Silica Surface: Kinetics, Conformation and Reversibility. *Langmuir*, 23, 6, 3273-3279.

Ohgushi, H. A.I. Caplan. (1999). Stem Cell Technology and Bioceramics: From Cell to Gene Engineering. *J. Biomed. Mater. Res*. 48, 913.

O'Sullivan C.K., Guilbaul G.G. (1999). Commercial Quartz Crystal Microbalances – Theory and Applications. *Biosensors & Bioelectronics*, 14, 663–670

Ozcan and Çiftçioğlu. (2010). Particulate Sol Route Hydroxyapatite Thin Film-Silk Protein Interface Interactions. *Gazi University Journal of Science GU J Sci* , 23 (4), 475-485

Pablo P. J., Herrero F. M., Colchero J., Herrero J. G., Herrero P., Baró A. M., Ordejón P., Soler J. M., Artacho E. (2000). Absence of dc-Conductivity in λ-DNA. *Physical Review Letters*, 85, 23, 4492-4995

Paget E., Monroziera L.J., Simonet P. (1992). Adsorption of DNA on Clay Minerals: Protection Against DNaseI and Influence on Gene Transfer. *FEMS Microbiology Letters*, 97, 31-39

Paget E., Simonet P. (1994). On The Track of Natural Transformation in Soil. *FEMS Microbiol. Ecol*., 15, 109-118

Palecek,E. (1960). Oscillographic Polarography of Highly Polymerized Deoxyribonucleic Acid. *Nature* 188, 656–657

Parida S. K., Dash, S., Patel S., Mishra B.K. (2006). Adsorption of Organic Molecules on Silica Surface. *Advances in Colloid and Interface Science*, 121, 77–110

Pastre D. Pietrement O., Zozime1 A., Cam E. L. (2005). Study of the DNA/Ethidium Bromide Interactions on Mica Surface by Atomic Force Microscope: Influence of the Surface Friction. *Biopolymers*, 77, 53–62

Paulo A. S, Garcia R. (2000). High-Resolution Imaging of Antibodies by Tapping-Mode Atomic Force Microscopy: Attractive and Repulsive Tip-Sample Interaction Regimes. *Biophysical Journal*, 78 , 5, 1599–1605

Peroos, S., Z. Du and N.H. de Leeuw. (2006). A Computer Modeling Study of the Uptake, Structure and Distribution of Carbonate Defects in Hydroxyapatite. *Biomaterials*, 27, 2150-2161.

Pierre, A.C. (1998). *Introduction to Sol-Gel Processing*" Kluwer Academic Publisher: Boston

Pierre A. C., Pajonk G. M. (2002). Chemistry of Aerogels and Their Applications. *Chem. Rev*., 102, 4243-4265

Pietramellara G., Franchi M. Gallori E., Nannipieri P. (2001). Effect of Molecular Characteristics of DNA on Its Adsorption and Binding on Homoionic Montmorillonite and Kaolinite. *Biol Fertil Soils*, 33, 402–409

Pie´trement, O.; Pastre´, D.; Fusil, S.; Jeusset, J.; David, M.-O.; Landousy, F.; Hamon, L.; Zozime, A.; Le Cam E. (2003). Reversible Binding of DNA on $NiCl_2$-Treated Mica by Varying the Ionic Strength. *Langmuir*, 19, 2536–2539.

Platero M.M., Valdivia E., Maqueda M,, -Bueno M.B. (2007). Fast, Convenient, And Economical Method for Isolating Genomic DNA From Lactic Acid Bacteria Using a Modification of the Protein ''Salting-Out'' Procedure. *Analytical Biochemistry*, Vol. 366, 102–104

Polat M., Sato K., Nagaoka T. , Watari K. (2006). Effect of pH and Hydration on The Normal and Lateral Interaction Forces between Alumina Surfaces. *Journal of Colloid and Interface Science*, 304, 2, 378 - 387

Porsch B., Laga R.,Horsky J., Konak C., Ulbrich K. (2009). Molecular Weight and Polydispersity of Calf-Thymus DNA: Static Light-Scattering and Size-Exclusion Chromatography with Dual Detection. *Biomacromolecules*, 10, 3148–3150

Price C.W., Leslie D.C., Landers J.P. (2009). Nucleic Acid Extraction Techniques and Application to the Microchip. *Lab Chip*, 9, 2484–2494

Profio P. D., Germani R., Goracci L., Grilli R., Savelli G., Tiecco. (2010). Interaction between DNA and Cationic Amphiphiles: A Multi-Technique Study. *Langmuir*, 26, 11, 7885–7892

Psifidi A, Dovas I C., Banos G. (2010). A Comparison of Six Methods for Genomic DNA Extraction Suitable for PCR-Based Genotyping Applications Using Ovine Milk Samples. *Molecular and Cellular Probes*, 24, 93-98

Qiu H., LV L., Pan B., Zhang Q.J., Zhang W., Zhang Q. (2009). Critical Review in Adsorption Kinetic Models. *J Zhejiang Univ Sci A.*, 10, 5, 716-724

Ricci D.and Braga P. C. (2004). *Atomic Force Microscopy Atomic Force Microscopy Biomedical Methods and Applications. Atomic Force Microscopy*" Humana Press

Rippe K., Mücke N., Langowski J. (1997). Superhelix Dimensions of a 1868 Base Pair Plasmid Determined by Scanning Force Microscopy in Air and in Aqueous Solution. *Nucleic Acids Research*, 25, 9, 1736–1744

Rivero E.R.C.,Neves A.C., Valenzuela M.G.S., Sousa S.O.M.,Nunes F.D. (2006). Simple Salting-o Method for DNA Extraction from Formalin-Fixed, Paraffin-Embedded Tissues. *Pathology – Research and Practice*, 202, 523–529

Romanowski G., Lorenz M.G., Wackernagel W. (1991). Adsorption of Plasmid DNA to Mineral Surfaces and Protection against DNase I. *Applied and Environmental Microbiology*, 7, 4, 1057-1061

Ru Y., Guoqiang L., Min L. (2010). Analysis of The Effect of Drying Conditions on the Structural and Surface Heterogeneity of Silica Aerogels and Xerogel by Using Cryogenic Nitrogen Adsorption Characterization. *Microporous and Mesoporous Materials*, 129, 1–10,

Ruthven D. (1984). Principles of Adsorption and Adsorption Processes. John Wiley and Sons

Saeki K., and Sakai M. (2009). The Influence of Soil Organic matter on DNA Adsorption on Andosols. *Microbes Environ.*, 24, 2, 175-179

Saeki K.,Morisaki M., Sakai M. (2008). The Contribution of Soil Constituents to Absorption of Extracellular DNA by Soils. *Microbes Enviroment*, 23, 4, 353-355

Saeki K., Morisaki M., Sakai M., Wada S.I. (2010). DNA Adsorption on Synthetic and Natural Allophanes. *Applied Clay Science*, 50, 493–497

Safinya C. R, Koltover I., Raedler J. (1998). DNA at Membrane Surfaces: an Experimental Overview. *Colloid & Interface Scie*nce, 3, 1, 69-77

Saoudi B, Jammul N, Abel M.L., Chehimi M.M., Dodin G. (1997). DNA Adsorption onto Conducting Polypyrrole. *Synthetic Metals*, 87, 97–103

Saoudi B, Jammul N, Chehimi MM,McCarthy GP, Armes SP. (1997). Adsorption of DNA onto Polypyrrole-Silica Nanocomposites. *J Colloid Interface Sci.* 192, (1), 269-73.

Schmoeger E., Paril_C.,Tscheliessnig R.,Jungbauer A. (2010). Research Article Adsorption of Plasmid DNA on Ceramic Hydroxyapatite Chromatographic Materials. *J. Sep. Sci.*, 33, 3125–3136

Shlyakhtenko L. S.. Gall A. A, Weimer J. J., Hawn D.D, Lyubchenko Y. L. (1999). Atomic Force Microscopy Imaging of DNA Covalently Immobilized on a Functionalized Mica Substrate. *Biophysical Journa*l, 77, 568–576

Slosarczyk A., Paluszkiewiczb C., Gawlicki M., Paszkiewicf Z. (1996). The FTIR Spectroscopy and QXRD Studies of Calcium Phosphate Based Materials Produced from the Powder Precursors with Different Ca/P Ratios. *Ceramics International*, 23, 297-304

Smith, D. E.; Perkins, T. T.; Chu, S. (1996). Dynamical Scaling of DNA DiffusionCoefficients. *Macromolecules*, 29, 1, 372–1373.

Song Y., Wang L, Zhao S., Lian W.,Li Z. (2009). Disassembly of DNA–ligand on Mica surface: Atomic Force Microscopy Studies. *Journal of Microscopy*, 234, 130–136

Souza K.C., Mohallem, N.D.S., Sousa E.B.M. (2010). Mesoporous Silica-Magnetite Nanocomposite: Facile Synthesis Route for Application in Hyperthermia. *J Sol-Gel Sci Technol*, 53, 418–427

Stoliar P., Bystrenova E., Quiroga S.D., Annibale P., Facchini M. , Spijkman M., Setayesh S., Leeuw D. de, Biscarini F. (2009). DNA Adsorption Measured with Ultra-Thin Film Organic Field Effect Transistors. *Biosensors and Bioelectronics*, 24, 2935–2938

Sundaresan N., Suresh H. C., Thomas T., Thomas T. J., Pillai C. K. S, (2008).Liquid Crystalline Phase Behavior of High Molecular Weight DNA: A Comparative Study of the Influence of Metal Ions of Different Size, Charge and Binding Mode. *Biomacromolecules*, 9, 1860–1869

Şahin E. 2006, Synthesis and Characterization of Hydroxyapatite-Alumina-Zirconia Biocomposites. Master Thesis, İzmir Institute of Technology, Materials Science and Engineering, Izmir,

Şenel S., Bayramoglu G., Arıca M.Y. (2003). DNA adsorption on a poly-L-lysine-Immobilized poly(2-hydroxyethyl methacrylate) Membrane. *Polym Int*, 52, 1169–1174

Şimşek D., 2002, Preparation and Characterization of HA Powders – Dense and Porous HA Based Composite Materials. Master Thesis Izmir Institute of Technology, Materials Science and Engineering, Izmir,

Tabata H., Cai L.T., Gu J.-H., Tanaka S., Otsuka Y., Sacho Y., Taniguchi M., Kawai T. (2003). Toward the DNA Electronics. *Synthetic Metals*, 133–134, 469–472

Tanigawa M., Suzuto M., Fukudome K., Yamaoka K. (1996). Changes in Molecular Weights and Molecular Weight Distributions of Differently Stranded Nucleic Acids after Sonication: Gel Permeation Chromatography/Low Angle Laser Light Scattering Evaluation and Computer Simulation. *Macromolecules* 29, 7418-7425

Thundat T, Allison DP, Warmack RJ, Brown GM, Jacobson KB, Schrick JJ, Ferrell TL. (1992). Atomic force microscopy of DNA on Mica and Chemically Modified Mica. *Scanning Microscopy*, 6, 4, 911-918

Tian H.. Huhmer A. F. R., Landers J. P. (2000). Evaluation of Silica Resins for Direct and Efficient Extraction of DNA from Complex Biological Matrices in a Miniaturized Format. *Anal. Biochem*, 283, 175–191.

Tran P., B. Alavi, G. Gruner. (2000). Charge Transport Along the l-DNA Double Helix. *Phys. Rev. Lett*., 85, 1564.

Tseng S.H., JangJian P.C., Tsai M.C., Cheng T., Chu L.H., Chang Y.C., Chung H.W., Chang C.C. (2011). Ni $^{2+}$ Enhanced Charge Transport via p-p Stacking Corridor in Metallic DNA. *Biophysical Journal*, 100, 1042–1048

Umemura K., Ishikawa M., Kuroda R. (2001). Controlled Immobilization of DNA Molecules Using Chemical Modification of Mica Surfaces for Atomic Force Microscopy: Characterization in Air. *Analytical Biochemistry*, 290, 232–237

Vallet-Regi, M., Gonzalez-Calbet, J.M. (2004). Calcium Phosphates as Substitution of Bone Tissues. *Progress in Solid State Chemistry*, 32, 1-2, 1-31

Van der Merwe, P. A. (2003). Surface Plasmon Resonance. Web site: http://users.path.ox.ac.uk/~vdmerwe/internal/spr.pdf (acsessed January 10, 2013)

Vandeventer, P. E ,. Lin J. S., Zwang T. J.,, Nadim A.,. Johal M. S, Niemz A. (2012). Multiphasic DNA Adsorption to Silica Surfaces under Varying Buffer, pH, and Ionic Strength Conditions. *Journal of Physical Chemistry B*, 116, 19, 5661-5670

Vogelstein B and D. Gillespie. (1979). Preparative and Analytical Purification of DNA from Agarose. *Proc. Natl. Acad. Sci. U. S. A*., 76, 615–619.

Watson J. D., Crick F.H.C. (1953). Molecular Structure of Nucleic Acids a Structure for Deoxyribose Nucleic Acid. *Reprinted from Nature*, 171,.737-738

Weisenhorn, A. L., P. K. Hansma, T. R. Albrecht, and C. F. Quate. (1989). Forces in Atomic Force Microscopy in Air and Water. *Appl. Phys. Lett*., 54, 2651-2653.

Wettig S.D, Li C.Z, Long Y.T, Kraatz H.B, Lee J.S. (2003). M-DNA: a Self-Assembling Molecular Wire for Nanoelectronics and Biosensing. *Anal Sci:*, 1923-6

Wu A.,Li Z.,Wang E. (2004). DNA Network Structures on Various Solid Substance Investigated by AFM. *Analytical Science*, 20, 1083-1086

Wu C. H., Wang, T.W., Sun J.S., Wang W.H., F.H Lin. (2007). .A Novel Biomagnetic Nanoparticle Based on Hydroxyapatite. *Nanotechnology*, 18, 165601

Xu, K., P.G. Cao, and J.R. Heath. (2010). Graphene Visualizes the First Water Adlayers on Mica at Ambient Conditions. *Science*, 329, 1188-1191.

Ye J. Y., Umemura K., Ishikawa M,. Kuroda R. (2000). Atomic Force Microscopy of DNA Molecules Stretched by Spin-Coating Technique. *Analytical Biochemistry* 281, 21–25

Yu S., Geng J., Zhou P., Wang J., Chen X., Hu J. (2008). New Hydroxyapatite Monolithic Column for DNA Extraction and Its Application in the Purification of Bacillus Subtilis Crude Lysate. *Journal of Chromatography A*, 183, 29–37

Zhao X. and Johnson J. Karl. (2007). Simulation of Adsorption of DNA on Carbon Nanotubes. *Journal of. American Chem. Soc*. 129, 10438-10445
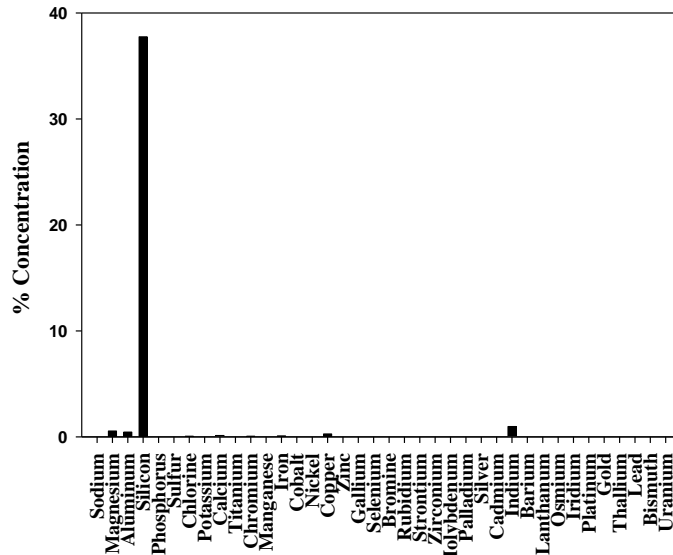
APPENDIX A

XRF ANALYSIS GRAPHS

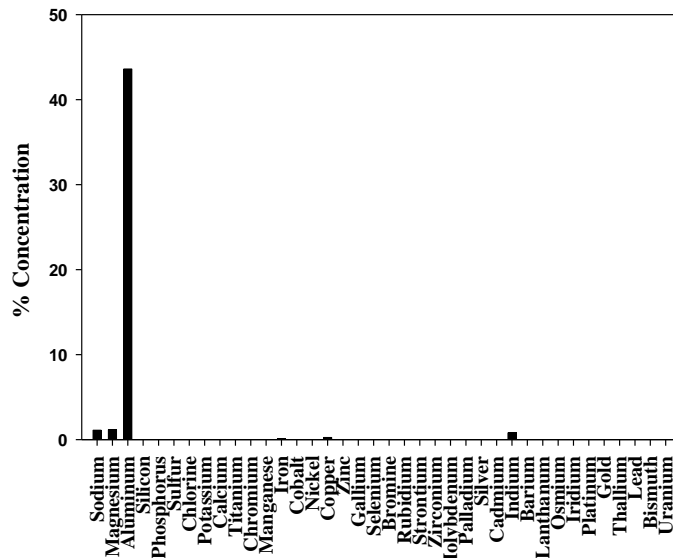Figure A. 1Elemental analysis of Silica
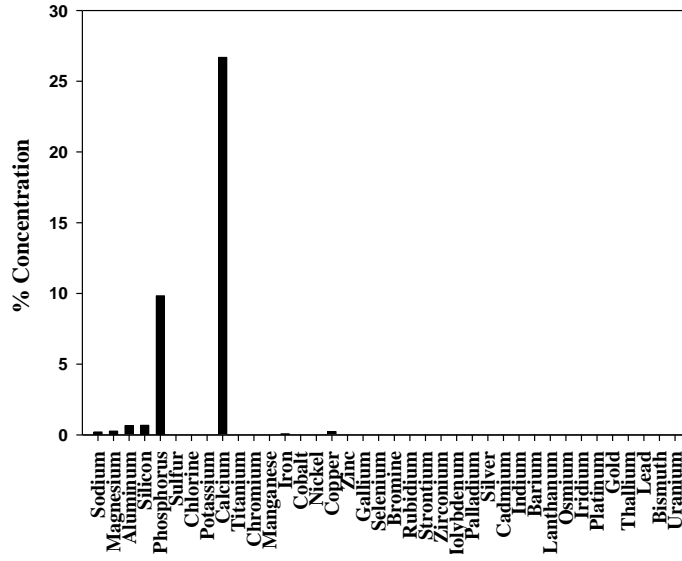

Figure A. 2 Elemental analysis of Alumina

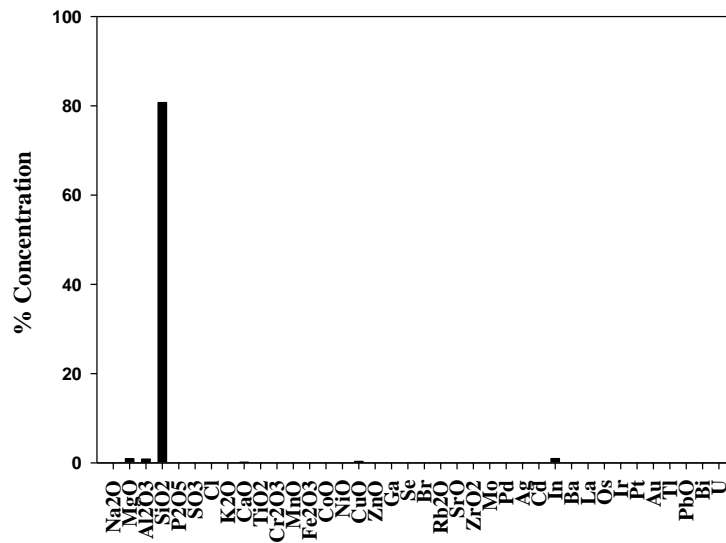Figure A. 3 Elemental analysis of HAP

Figure A. 4 Composition of Silica reported in Oxide Form
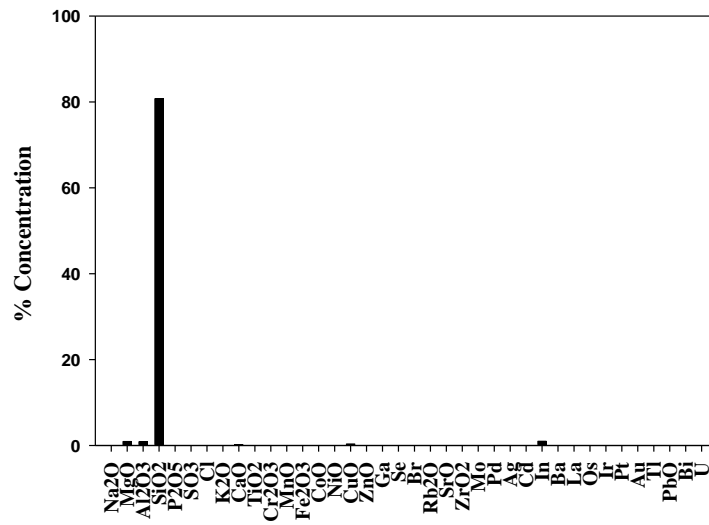
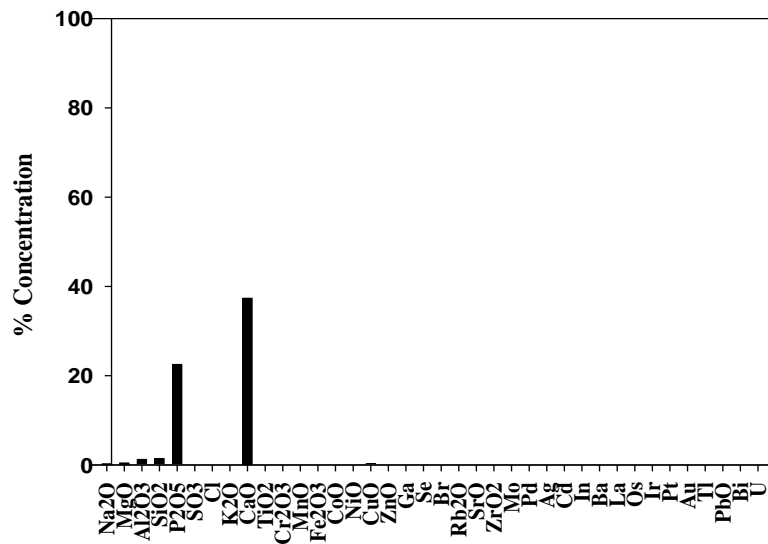Figure A. 5 Composition of Alumina reported in Oxide Form

Figure A. 6 Composition of HA reported in Oxide Form
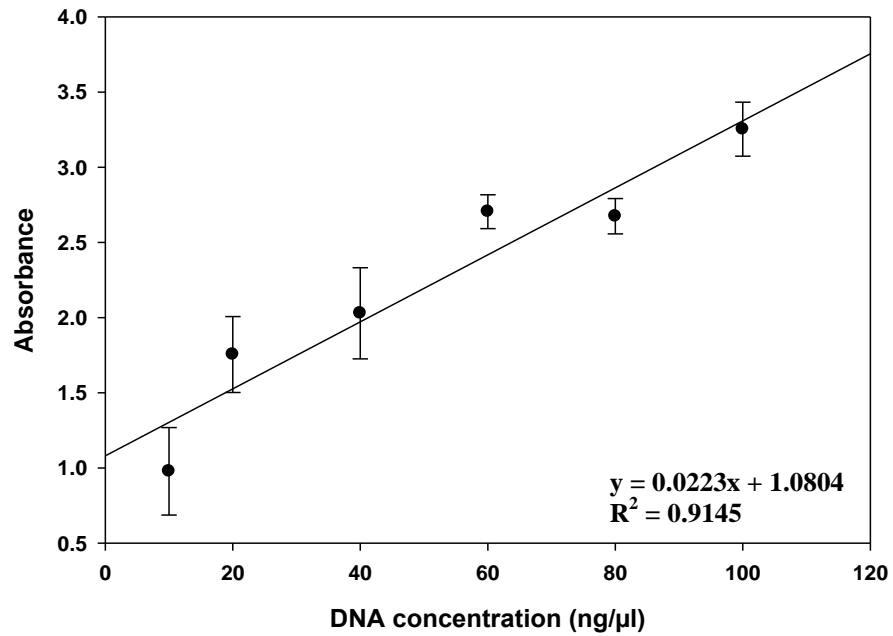
APPENDIX B

CALIBRATION CURVES

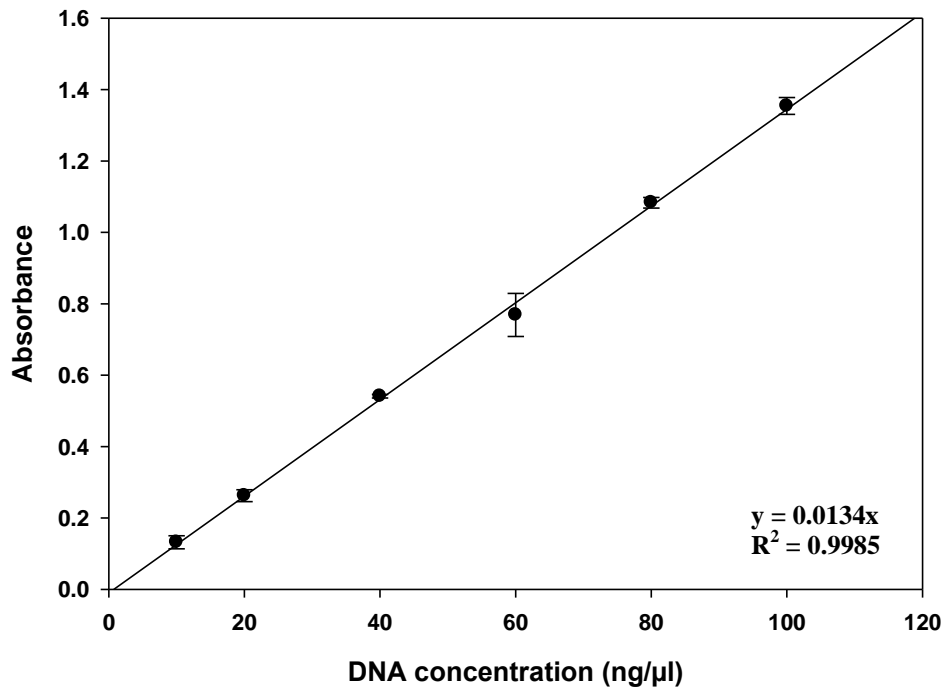

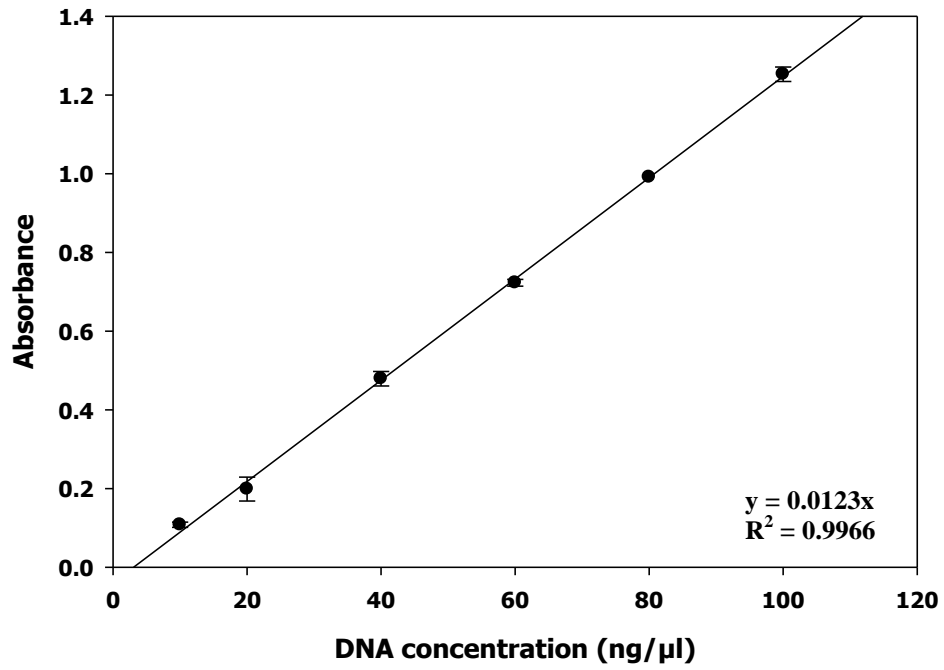Figure B. 1 Calf Thymus DNA calibration graph at pH 2

Figure B. 2. Calf Thymus DNA calibration graph at pH 4

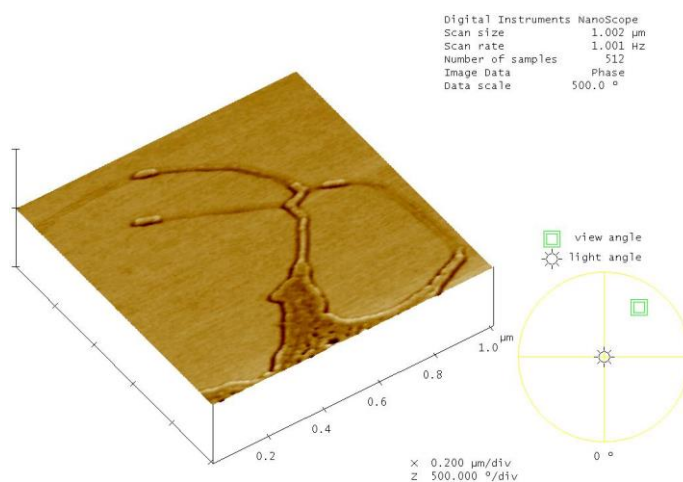Figure B.3 Calf Thymus DNA calibration graph pH 5
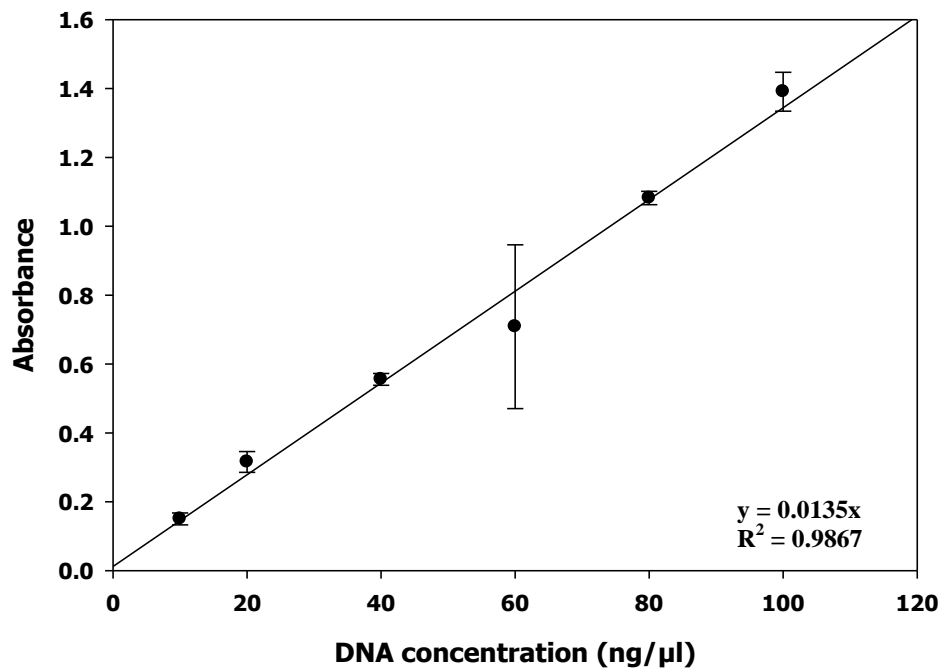
Figure B. 4 Calf Thymus DNA calibration graph pH 6

APPENDIX C

AFM IMAGES
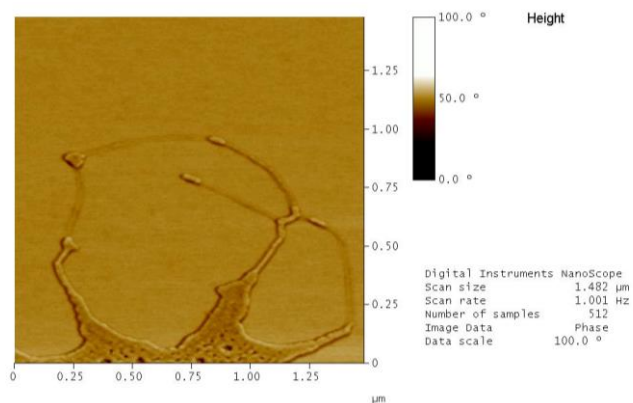
(a)

(b)

Figure C. 1 AFM image of DNA dissolved in pure water at 10 ng/µl on mica imaged in ambient air in the tapping mode (a) top view (b) 3 D image
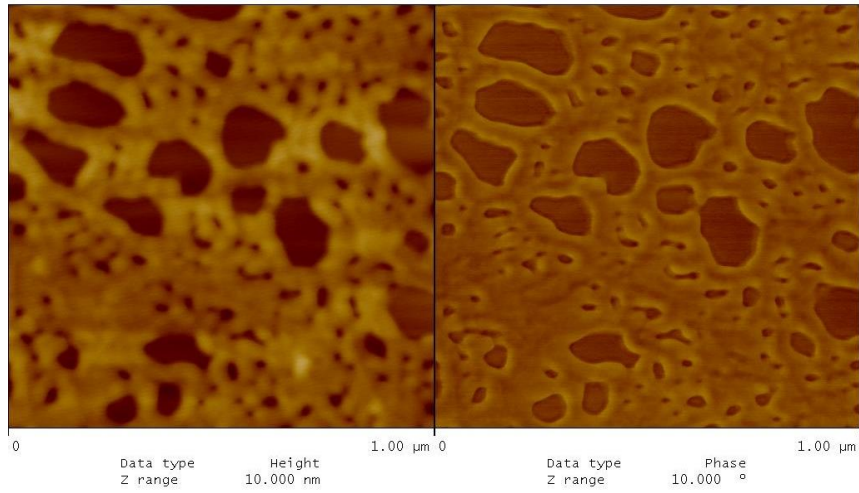
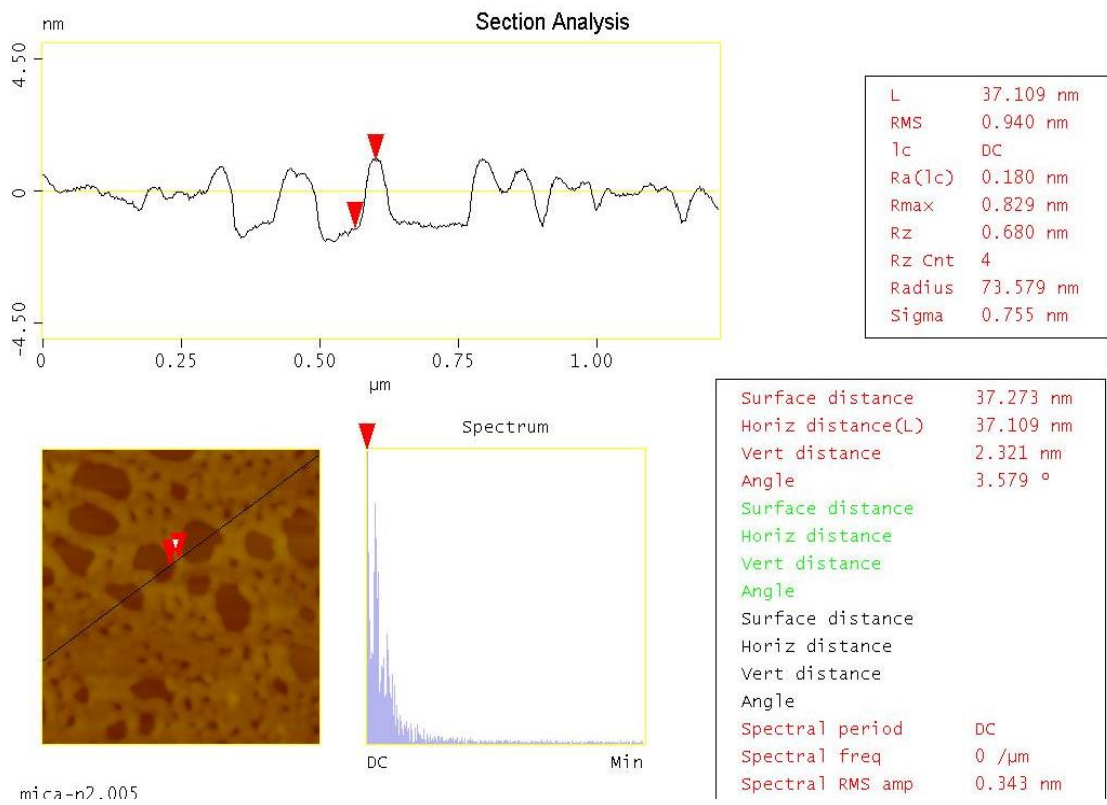Figure C. 2 AFM image of DNA dissolved in pure water at 100 ng/µl on mica dried by N$_2$ flow regime

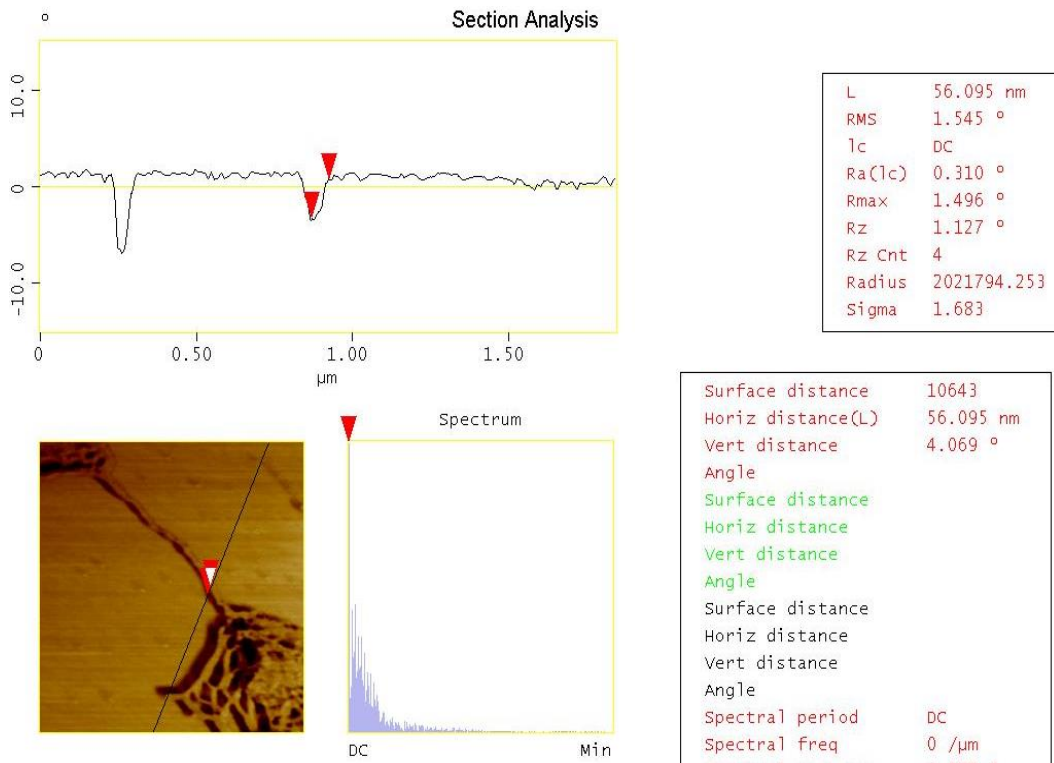Figure C. 3 Section analysis of Figure C 2

Figure C. 4.AFM image of DNA dissolved in pure water at 100 ng/µl on mica-freeze dried
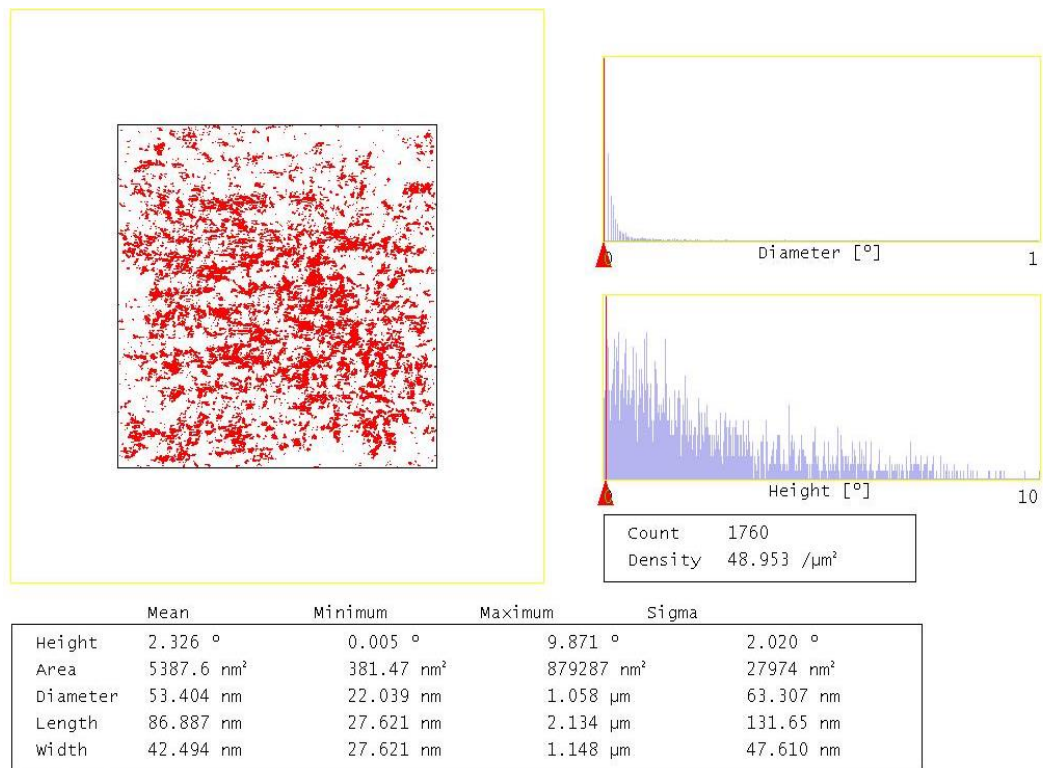

Figure C. 5 Particle Size Analysis of HAP pellet by AFM

VITA

Name: Senem YETGİN

Place and Date of Birth: Ahlat, 05 April 1980

EDUCATION

2007 – Present   Ph. D. (Chemical Engineering) IZTECH

Thesis: DNA Adsorption on Silica Alumina and Hydroxyapatite and DNA Imaging DNA by Atomic Force Microscopy
Advisor: Prof.Dr.Devrim BALKÖSE

2004 – 2007   M.Sc. (Chemical Engineering) IZTECH
Thesis: Investigation of Fuel Oxygenate Adsorption on Clinoptilolite Rich Natural Zeolite,
Advisor: Doç Dr.Fikret İnal

- 1997 – 2002   B.Sc. (Chemical Engineering) Inonu University, Malatya Turkey

- 1994 – 1997   Erzurum Science High School, Erzurum Turkey

- Reserach Subjects: Adsorption, DNA, Sol-Gel, Polymer Science, Poly Vinyl Chloride (PVC), Artificial Neural Networks (ANN) ,AFM, Supercitical Drying

- PUBLICATIONS

- •Inal, F., Yetgin, S., Aksu G.T., Simsek, S., Sofuoglu, A., Sofuoglu, S.C.,(2009) "Activated Carbon Adsorption of Fuel Oxygenates MTBE and ETBE from water" Water Air Soil Pollution, Vol. 204, pp. 155-163,. doi:10.1007/s11270-009-0034-8

- Sahin E., Yaşar Mahlıçlı F., Yetgin S., Balköse D.,(2012.) "Preparation and Characterization of Flexible Poly (vinyl chloride) Foam Films" Journal of Applied Polymer ScienceVolume 125, Issue 2, pages 1448–1455,

- Kurt E, Özçelik C.Y., Yetgin S., Ömürlü F.O, Balköse D. 2013 "Preparation and Characterization of Flexible Polyvinylchloride-Copper omposite Films" Polymers & Polymer Composites Volume 21 No. 3 page 139

- Ulutan S., Yetgin S., Balkose D., "Flexible PVC-Silica Composites as an Adsorptive Material for Water Soluble Dyes" Polymers & Polymer Composites Volume 21 No. 3 page 177

- Yetgin S., Ulutan S., Balkose D., "Methylene Blue Adsorption from Aqueous Solutions to Flexible PVC-Silica Composites" Journal of Vinyl and Additive Technology,in Press